OPTIMIZATION OF PROCESS PARAMETERS OF WELDED JOINT PRODUCED BY COMPOUND CASTING

THESIS

Submitted in fulfillment of the requirement of the degree of

DOCTOR OF PHILOSOPHY

to

J.C. BOSE UNIVERSITY OF SCIENCE & TECHNOLOGY, YMCA, FARIDABAD

by

RAJENDER KUMAR

(Registration No. YMCAUST/Ph 41/2011)

Under the supervision of

DR. VIKRAM SINGH
Professor, Mechanical Engg.
J.C. Bose University of Science & Tech., YMCA, Faridabad (HR)

DR. SUDHIR KUMAR
Professor, Mechanical Engg.
Greater Noida Institute of Tech., Greater Noida (UP)

Department of Mechanical Engineering

Faculty of Engineering and Technology

J.C. Bose University of Science & Technology, YMCA,

Sector-6, Mathura Road, Faridabad, Haryana, India

NOVEMBER, 2019

Dedicated

to

My Family

CANDIDATE'S DECLARATION

I hereby declare that this thesis entitled **OPTIMIZATION OF PROCESS PARAMETERS OF WELDED JOINT PRODUCED BY COMPOUND CASTING** by **RAJENDER KUMAR**, being submitted in fulfillment of the requirements for the Degree of Doctor of Philosophy in Mechanical Engineering under Faculty of Engineering and Technology of J.C. Bose University of Science & Technology, YMCA, Faridabad during the academic year 2019, is a bonafide record of my original work carried out under guidance and supervision of **Dr. VIKRAM SINGH, Professor, Mechanical Engineering**, J.C. Bose University of Science & Technology, YMCA, Faridabad and **Dr. SUDHIR KUMAR, Professor, Mechanical Engineering**, Greater Noida Institute of Technology, Greater Noida and has not been presented elsewhere.

I further declare that the thesis does not contain any part of any work which has been submitted for the award of any degree either in this university or in any other university.

Rajender Kumar

Registration No.YMCAUST/Ph 41/2011

CERTIFICATE OF THE SUPERVISOR

We hereby declare that this thesis entitled **OPTIMIZATION OF PROCESS PARAMETERS OF WELDED JOINT PRODUCED BY COMPOUND CASTING** by **RAJENDER KUMAR**, being submitted in fulfillment of the requirements for the Degree of Doctor of Philosophy in Mechanical Engineering under Faculty of Engineering and Technology of J.C. Bose University of Science & Technology, YMCA, Faridabad during the academic year 2019 is a bonafide record of work carried out under our guidance and supervision.

We further declare that to the best of my knowledge, the thesis does not contain any part of any work which has been submitted for the award of any degree either in this university or in any other university.

Dr. Vikram Singh
Professor,
Department of Mechanical Engineering,
Faculty of Engineering and Technology,
J.C. Bose University of Science & Technology,
YMCA, Faridabad-121106

Dated:

Dr. Sudhir Kumar
Professor,
Department of Mechanical Engineering,
Greater Noida Institute of Technology,
Greater Noida-201310

Dated:

Ph. D. viva-voce examination of Mr. Rajender Kumar, Research Scholar was done on dated……………………….

Signature of Supervisors

Signature of External Examiner

ACKNOWLEDGEMENT

All praise is just for **Baba Bajrang Bali**, the Almighty deity, who is the only source of knowledge.

While bringing out this research work to its final form, I came across a number of people whose contributions and concerned efforts have helped me successfully shape and complete this work. They deserve special thanks. It is a pleasure to convey my gratitude to all of them.

It gives me great pleasure to express my heartfelt gratitude towards my esteemed supervisor **Dr. Vikram Singh,** Professor, Mechanical Engineering Department, J.C. Bose University of Science & Technology, YMCA, Faridabad. His supervision indeed helped me to overcome arising problems throughout this research. Without his continuous motivation, constant monitoring and constructive criticism this would not have been possible.

I would like to express my sincere and great appreciation to my esteemed supervisor, teacher and mentor **Dr. Sudhir Kumar**, Professor, Mechanical Engineering Department, Greater Noida Institute of Technology, Greater Noida. His invaluable continued guidance, motivation, constant inspiration and above all for his ever co-operating attitude that enabled culmination of this huge task possible. His suggestions and attention to the minutest details made it possible to give this study its present form. He has been the primary guiding force and inspiration behind this study. I feel privileged on being associated with such an esteemed research supervisor.

I am highly grateful to **Dr. Dinesh Kumar,** Vice Chancellor, J.C. Bose University of Science & Technology, YMCA, Faridabad for giving me the opportunity to conduct this study.

I am extremely thankful to **Prof. Tilak Raj,** Chairperson, Mechanical Engineering Department, J.C. Bose University of Science & Technology, YMCA, Faridabad for providing all kinds of possible help and advice during the course of this work.

I cannot forget to thank **Prof. Sandeep Grover, Prof. M. L. Aggarwal, Prof. Hari Om, Dr. Rajiv Saha, Dr. Nikhil Dev, Dr. Rohit Garg, Dr. Anand Kumar, Dr. Anju Gupta, Dr. Deepa Ujjawal** and **Mr. Mandeep Chahal** for valuable discussions and suggestions.

I would like to thank **Er. Sudhir Kumar Gilhotra**, Principal, Government Polytechnic, Sirsa to allow me to prepare the experimental setup and for the use of facilities available at the institution workshop.

Assistance from my colleagues, workshop instructors as well as the students of the Government Polytechnic, Sirsa is gratefully acknowledged.

This work would not have seen light of the day without the kind co-operation of my friend **Er. Subhash Chander**, Lecturer, Govt. Polytechnic, Sirsa. I am highly grateful to him for the invaluable help, guidance and constant encouragement. His suggestions became an important part for the completion of this work. His excellent writing skill became an invaluable inspiration for me. I would fail in my duty to appreciate his support if any word could be found suitable to explain it.

A word of special thanks to my ex-students **Mr. Amit Jangra** and **Mr. Ankur** for their support and help during my experimental work.

Still remain many whose names do not feature above. But their anonymity, however in no way suggests that their contribution has gone unacknowledged.

Hand that rocks the cradle rules the world. I bow my head to my beloved parents **Sh. Satyanarain Tayal** and **Smt. Snehlata Tayal** whose love and care have been the keys to my success. No words can express what their undemanding love, sacrifices, dedication and prayers have done to help me become what I am today. I thank them for always being there to support me.

I also express deep gratitude to my brother, **Dr. Bajrang Gupta**, his wife **Dr. Hemlata Gupta,** his daughter **Teesha** and his son **Takshay** for their constant love, and care, and being there to support me.

A special thanks to my dear wife, **Varsha Tayal,** and my little champs **Hiti** and **Gourav** for supporting me in every step of my life, encouraging me, trusting me, conducting me through my troubles and always being my best allies.

Finally, I remember and thank the all-powerful **ALMIGHTY GOD**, who gave me energy, skill and enthusiasm to complete the task. I pray to him to empower me to scale new heights, to kindle my mind with knowledge, to dispel the darkness of ignorance and to lead the life gifted by him fruitfully.

Rajender Kumar

Registration No.YMCAUST/Ph 41/2011

ABSTRACT

The current need of aerospace and automobile industry arise the demand of parts with minimum weight while achieving similar or even superior properties. Sometimes, a single light metal may not be effective as per the market demand, then multi-material configuration is required. Al-Mg compound structures seem to be a promising solution for present industrial applications. Compound casting is a unique metal casting process by which similar/dissimilar metals are joined properly. This process has drawn great attention, as it is associated with high efficiency and lower manufacturing cost. It is employed to join a variety of similar/dissimilar metallic materials such as Al-Al, Al-Mg, Al-steel, Al-brass, Al-Cu, Cu-steel, Mg-steel, etc.

In the present experimental investigation, vacuum assisted sand mold compound casting process employed to join A356 alloy and pure Mg by pouring molten Mg around solid A356 insert. Planning of experiments done by using design of experiment approach by considering four significant process parameters i.e., pouring temperature, vacuum pressure, insert temperature and grit size of sand paper. Investigated the mechanism of joint interface formation, micro-structural characteristics and mechanical properties. Studied the microstructure using optical microscopy, SEM, EDS and XRD. The results indicated that a relatively uniform joint interface obtained. The joint interface composed of three distinct layers containing Mg_2Al_3 on aluminum side, $Mg_{17}Al_{12}$ +δ eutectic structure on magnesium side and $Mg_{17}Al_{12}$ as middle layer. The mechanical properties such as shear strength, impact strength and microhardness of joint interface measured and utilized to formulate second-order regression models. The models so developed validated the accuracy and reliability of experimental values.

Optimization of process parameters; pouring temperature, vacuum pressure, insert temperature and grit size of sand paper carried out with reference to the mechanical properties; shear strength, impact strength and microhardness. Optimization accomplished by response surface methodology, desirability analysis and genetic algorithm. The results indicated that genetic algorithm proved an effective approach in finding the better solution in terms of optimal values of mechanical properties.

Genetic algorithm increased shear strength, impact strength and microhardness by 14.21, 17.05 and 1.35% respectively with respect to the experimental results. The optimal values of shear strength, impact strength and microhardness obtained as 37.85 MPa, 12.29 J and 326.51 HV respectively.

Joint strength of A356/Mg interface evaluated by applying graph theoretic approach. Results revealed that shear strength has maximum influence on joint strength followed by microhardness and impact strength. Executed multiobjective optimization to predict the optimal process parameters by choosing two or more output characteristics simultaneously. A range of optimal solutions obtained for the possible combinations of shear strength, impact strength and microhardness.

TABLE OF CONTENTS

LIST OF TABLES

LIST OF FIGURES

ABBREVIATIONS

Symbol	**Description**
ANOVA	Analysis of Variance
CCD	Central Composite Design
DA	Desirability Analysis
DOE	Design of Experiments
EDS	Energy Dispersive X-ray Spectroscopy
GA	Genetic Algorithm
GS	Grit Size of Sand Paper
GTA	Graph Theoretic Approach
IS	Impact Strength
IT	Insert Temperature
MH	Microhardness
PR	Pouring Rate
PT	Pouring Temperature
RSM	Response Surface Methodology
SEM	Scanning Electron Microscope
SS	Shear Strength
VASMCC	Vacuum Assisted Sand Mold Compound Casting
VC	Vacuum Pressure
XRD	X-ray Diffractometer

CHAPTER 1

INTRODUCTION

1.1 INTRODUCTION

Die casting is an effective method for the bulk production of light metal components. The parts with complicated shape and high degree of precision can be fabricated with this method which finds a large number of applications in industrial sector [1-3]. Aluminium and magnesium, the lightest engineering metals, are preferred in aerospace, automobile, computers and electronics industry, navigation and military affairs owing to their unique properties [4]. These metals possess remarkable castability with low weight to strength ratio and high corrosion resistance [5-7]. Aluminium possesses high ductility and able to maintain the strength at elevated temperature. Aluminium alloys as an alternative to steel and cast iron exhibit the improved energy efficiency and performance of vehicles. On the other hand, the use of magnesium alloys has increased significantly in automobile sector in order to reduce the weight of vehicle and hence CO_2 emissions. Weight of magnesium is nearly two third of aluminium while having the similar melting points [8]. Magnesium exhibits higher creep resistance, excellent castability, and better noise and vibration dampening properties than aluminium [9].

Aerospace and automobile industry arise the demand of parts with minimum weight while achieving similar or even superior parts properties. At the same time, the parts must be produced at lower cost. Sometimes, single material is not able to complete the demand of market then compound configuration is required because it provides desired properties [10-12]. A feasible solution arises with the use of multi-materials. Joining techniques of multi-material plays a vital role in manufacturing of such lightweight structures. The combined configuration proves to be quite effective to meet the requirement for lightweight and high performance parts. Al-Mg compound structures seem to be a promising solution for present industrial applications. Joining of aluminium and magnesium provides the benefits of combined properties of both the materials. These metals can be joined together by different fusion and diffusion processes such as spot welding [13-14], tungsten inert gas welding [15], laser welding [16-18], gas metal arc welding [19], friction stir welding [20-23], and vacuum diffusion bonding [24-25]. The joining of Al/Mg by these processes leads to the formation of hard and brittle intermetallic compounds at the joint interface, which are undesirable as far as the mechanical properties are concerned. Compound casting process provides a better solution to this problem. Preference of using the compound casting process over other dissimilar joining processes is due to the formation of a uniform interfacial zone. At this zone, liquid metal diffuses into the solid metal by the formation of reaction phases and solid solutions. [11].

1.2 COMPOUND CASTING PROCESS

Compound casting is a unique metal casting process employed to join similar or dissimilar metals. In this process, joint of two metallic materials is achieved through direct casting in which one metal is kept in solid state while the other in liquid state. Solid insert is placed in the mold cavity and liquid metal is allowed to pour around it. A diffusion process is initiated at the solid-liquid interface, resulting in the formation of a uniform transition zone sandwiched between the two metals. This zone is obtained by the formation of solid solutions and reaction phases. The transition zone consists of intermetallic compounds, which possesses the combined properties of parent metals [26-28]. This process has drawn great attention, as it is associated with high efficiency and lower manufacturing cost. It is employed to join a variety of similar or dissimilar metals/alloys such as aluminium and aluminium, magnesium and magnesium, aluminium and magnesium, aluminium and cast iron, aluminium and copper, aluminium and brass, aluminium and titanium, steel and aluminium, steel and copper, iron and aluminium, and mild steel and magnesium [29-39]. Schematic of compound casting process is shown in Figure 1.1.

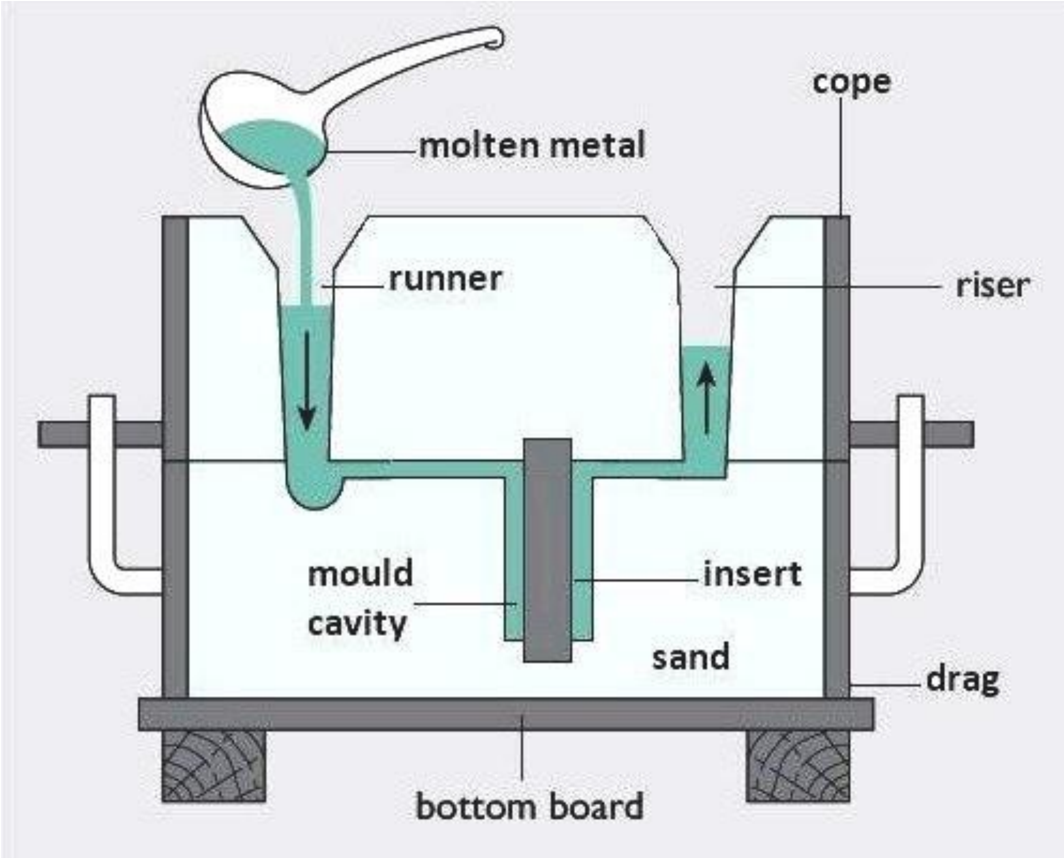

Figure 1.1 Compound casting process

1.3 ADVANTAGES OF COMPOUND CASTING PROCESS

The main advantages of compound casting process are:

- It is a quite simple process to execute as it involves simply pouring a molten metal onto a solid insert placed in the mold cavity.
- It is an economical process which involves minimum operating cost.
- It could join semi-finished parts with complex structures thus eliminating the long processing time and high operating cost.
- The process is suitable for the mass production of components.
- It involves lower energy consumption.
- A good metallurgical bond between similar or dissimilar metallic materials can be achieved by this process.
- In this process, metallurgical bonding is created by casting and therefore, separate hot or cold bonding/jointing processes are not required. This, in turn reduces the number of production steps needed in the manufacturing process.

1.4 DISADVANTAGES OF COMPOUND CASTING

In comparison to the conventional joining or welding processes, fabrication of a compound cast components require additional handling, manipulation of inserts and pre-treatment of the surfaces, if desired.

1.5 APPLICATIONS OF COMPOUND CASTING

This process finds a wide range of application in automobile and aerospace industry. The specific applications include:

- Parts of the chassis
- Connection supports
- Dashboard mounts in the interior
- Automotive door frames
- Bodywork components
- Shock strut supports [40]
- Flanges and bearing carriers [40]
- Gearbox casing [40]
- Al-Si automobile suspension part with cast iron insert [41]
- 6-cylinder magnesium engine with aluminium insert from BMW [42-43]
- Hammer of high chromium cast iron - high manganese steel [44]
- Ductile iron and aluminium truck wheel hub [45]
- Magnesium-aluminium crankcase of BMW's inline 6 cylinder engine [46]
- Engine block as it is made up of several individual parts which are joined to one another. Compound casting makes it feasible to produce as a single piece.

Figure 1.2 to Figure 1.8 depicts applications of compound casting.

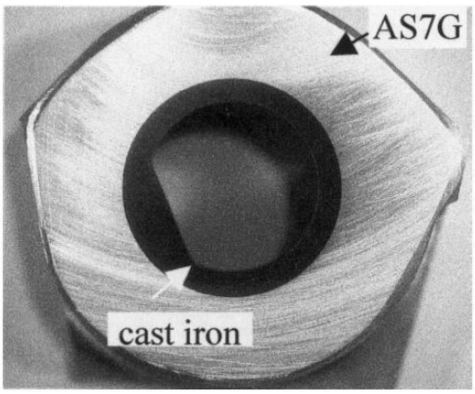

Figure 1.2 Automobile suspension part [41]

Figure 1.3 Shock strut support [47]

Figure 1.4 Bearing carriers [48]

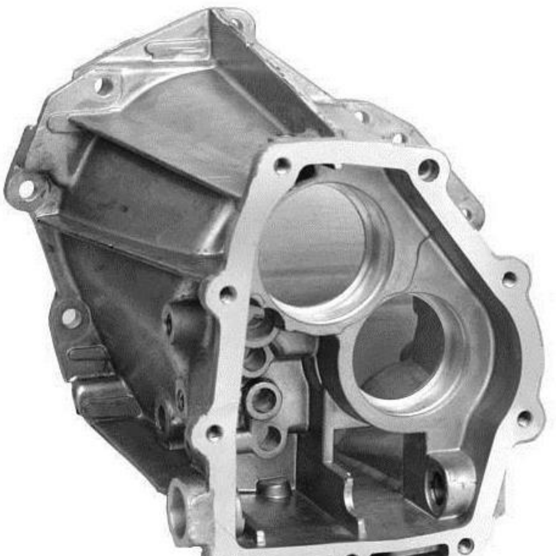

Figure 1.5 Gear box casing [49]

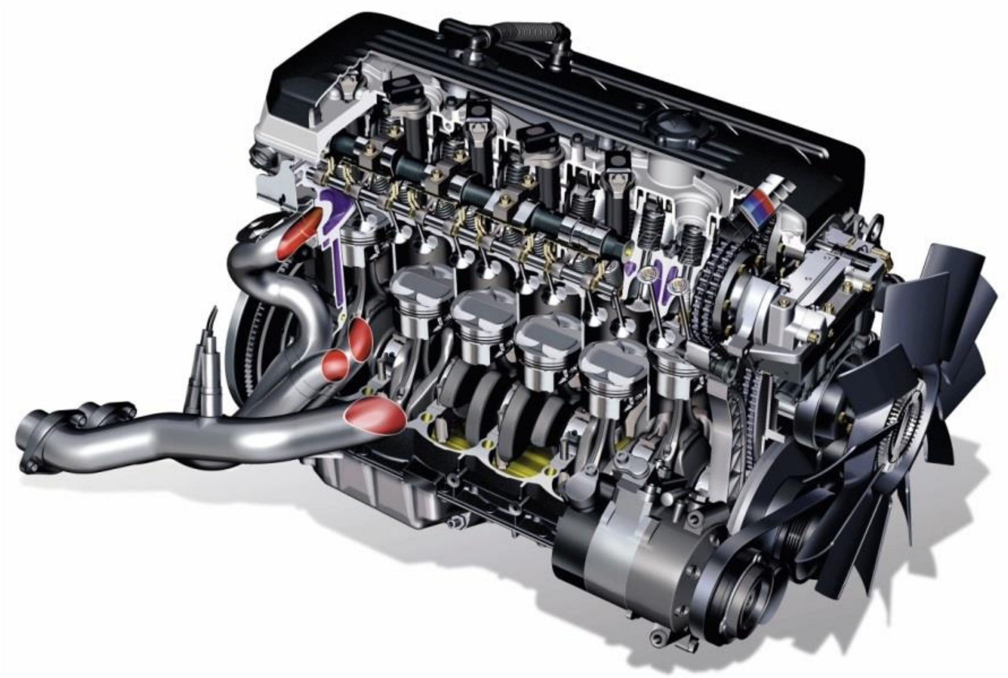

Figure 1.6 BMW six-cylinder magnesium engine with aluminium insert [50]

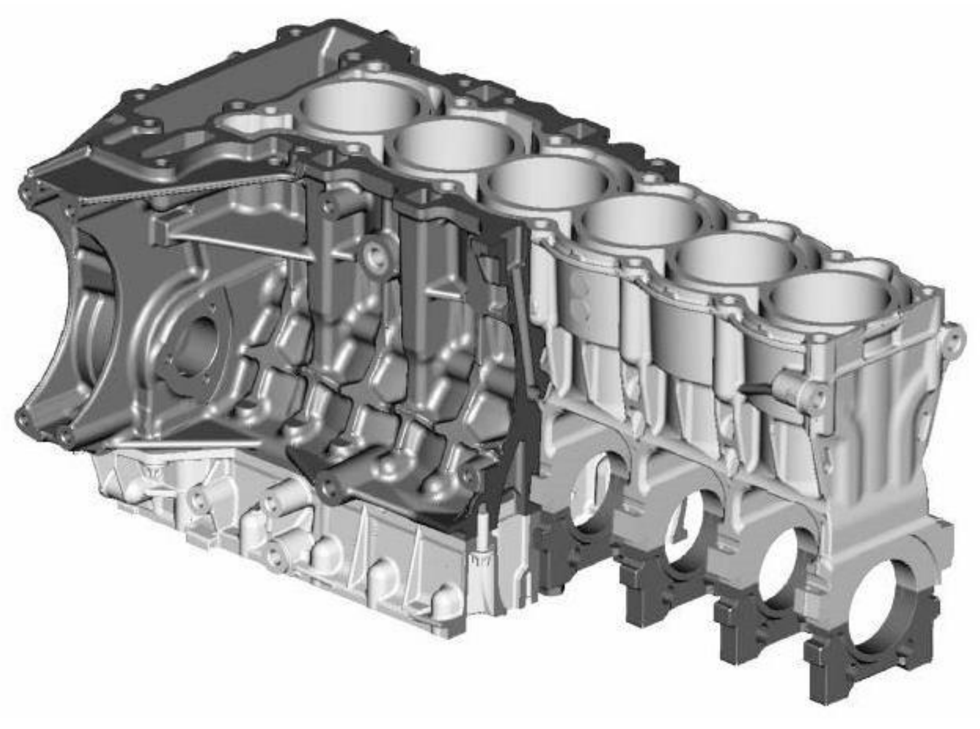

Figure 1.7 BMW magnesium-aluminium crankcase [51]

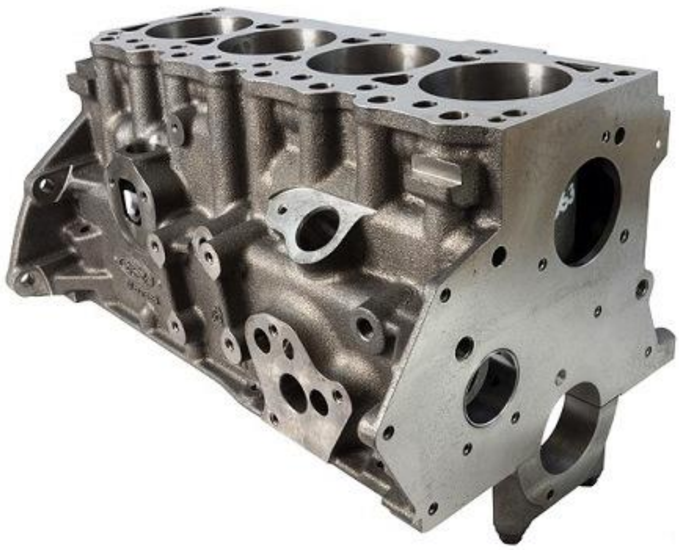

Figure 1.8 Engine block [52]

1.6 ORGANIZATION OF THESIS

The present research work is organized in seven chapters in this thesis. Each chapter provides a platform for achieving the proposed objectives as well as a proper direction for completion of research work. A brief outline of these chapters is as follows:

CHAPTER – 1. INTRODUCTION

This chapter deals with the introduction to compound casting process, its advantages, disadvantages and applications. It provides the outline of the thesis also.

CHAPTER – 2. LITERATURE REVIEW

This chapter presents the relevant literature about the compound casting process and other similar processes published in reputed journals. It deals with the materials used, fabrication methods, characterization, mechanical properties, modeling and optimization related to the compound casting process. Gaps are identified in the literature and objectives of current study are presented.

CHAPTER – 3. EXPERIMENTAL SETUP AND PROCEDURE

In this chapter, the experimental setup for vacuum assisted sand mold compound casting process is elaborated. Materials used, selection of process parameters, design of experiments and procedure for production of compound cast parts are explained.

CHAPTER – 4. RESULTS AND DISCUSSION

This chapter deals with the characterization of A356/Mg joint interface by means of optical microscope, scanning electron microscope, energy dispersive X-ray spectroscopy and identification of the phase constitutions by X-ray diffractometer. Mechanism of interface formation is explained. Preparation of test specimens and the methods used for measurement of mechanical properties like shear strength, impact strength and microhardness of joint interface are discussed. RSM models for the shear strength, impact strength and microhardness are discussed. ANOVA is carried out for designated process parameters. The predicted values of shear strength, impact strength and microhardness are tabulated and effect of process parameters on the mechanical properties of joint interface is discussed in details.

CHAPTER – 5. OPTIMIZATION OF PROCESS PARAMETERS USING DESIRABILITY ANALYSIS, GENETIC ALGORITHM AND GRAPH THEORETIC APPROACH

This chapter presents the optimization of process parameters by desirability analysis and genetic algorithm for shear strength, impact strength and microhardness. The joint strength evaluation by graph theoretic approach is discussed in details. Multi objective optimization is also included.

CHAPTER – 6. CONCLUSION AND SCOPE FOR FUTURE WORK

This chapter concludes the present research work along with its significant contribution to the industrial applications dealing with dissimilar joining by compound casting. Scope for the future work is spelt out.

CHAPTER 2

LITERATURE REVIEW

2.1 INTRODUCTION

Technological advancements have imparted an increased use of light metals having high strength and serviceability. Selection of a light metal depends upon its properties and processing methods. There exist a number of techniques through which the light metals can be processed. Die casting is an effective casting method for the bulk production of light metal components. Sometimes, a single metal may not be effective as per the market demand, then multi-metal configuration with desired properties is required. Joining techniques play a vital role in the fabrication of multi-metal structures. Compound casting is a unique metal casting process by which similar or dissimilar metallic materials can be joined properly. Preference is given to the compound casting process over other dissimilar joining processes as it results into the formation of a more uniform joint interface.

Various research works on the joining of multi-materials are carried out by researchers and scientists. This chapter presents the relevant literature about the compound casting and other similar processes published in reputed journals. The research work on joining of similar or dissimilar metallic materials, characterization, mechanical properties, modeling and optimization related to the compound casting process is discussed. Gaps are identified in the literature and objectives of current study are presented.

2.2 COMPOUND CASTING PROCESS

Compound casting is a metal casting process used to join similar or dissimilar metals. Figure 2.1 illustrates the schematic of process. In this process, two metals get diffused when brought in contact with each other, provided that one metal being in liquid state while keeping the other in solid. As a result, a consistent metallic transition is formed between the two [11]. The process is employed to join semi-finished components having the complicated shapes merely by pouring a liquid metal around a solid shaped insert. A few researchers have adopted this method to join dissimilar materials.

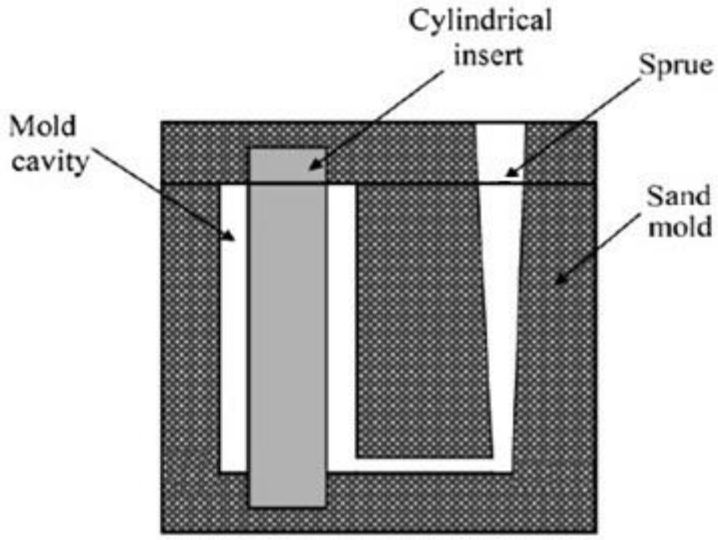

Figure 2.1 Schematic of basic compound casting process

Hajjari et al. [11] studied the microstructure and mechanical characterization of Al/Mg cast pieces produced by compound casting process. Two types of Al/Mg couples were prepared; firstly by pouring Al melt around Mg insert and secondly by pouring Mg melt around Al insert. The results indicated that joining of Al and Mg by this process is feasible only by casting the Mg melt around solid Al insert. This was due to the fact that by casting Al melt around Mg insert, a large gap was formed at the interface except few local interactions. While by casting the Mg melt around solid Al insert, a relatively uniform interface was observed without any macroscopic crack at the joint. The authors explained that by pouring Mg melt around Al insert, aluminium oxide layer present on the surface of Al insert was reduced due to the interaction with Mg melt. This resulted in direct contact between fresh Al surface and Mg melt leading to the formation of a uniform joint between them. Whereas, by pouring Al melt around solid Mg insert, the oxide layer on Mg surface was not reduced. This resulted a gap between Al and Mg. Also, the higher coefficient of thermal expansion of Mg leads to the loosening of interface. The minimum and maximum interface thickness was measured as 50 and 190 µm corresponding to the top and bottom of the joint respectively. Shear strength of joint interface was observed as 39.9 MPa at the top and 20.2 MPa at the bottom depending upon interface thickness. The microhardness at the joint interface varied between 152 to 221 HV, whereas the base metals aluminium and magnesium indicated the average hardness of 25 and 28 HV respectively. Hardness value of interfacial zone indicated the formation of higher hardness Al/Mg intermetallic compounds.

Papis et al. [12] investigated the wettability behavior of Al/Al and Al/Mg compound cast pieces. The wettability problem of Al insert surface was solved by replacing the natural oxide layer with zinc layer. The Al/Al and Al/Mg couples prepared by this process reflected the absence of imperfections like contraction, oxides inclusion and surface cracks. The results revealed the formation of a continuous metallic transition zone and heat-treatable microstructure of Al/Al cast pieces due to the diffusion of alloying elements in the vicinity of joint interface. The formation of low melting intermetallic compounds such as $Al_{12}Mg_{17}$ and Al_3Mg_2 at Al/Mg interface was prevented by applying a protective coating upon the insert surface without scarifying its wettability.

Rubner et al. [28] examined the development of Al/Al couples prepared by placing Al insert in die casting mold and Al alloy was embedded into it under the impact of vacuum. Before this, the natural oxide layer on Al surface was removed and zinc coatings of different thickness were applied. Authors reported that during the casting process, zinc layer got dissolved and a transition zone between casting alloy and insert was formed with prominent zinc content. The Al insert surfaces were activated by employing the zincate treatment and zinc galvanizing. The Zn layer reacted during the casting process and a continuous transition zone was formed. The microstructure and thickness of this zone varied with varying the initial layer thickness.

Papis et al. [29] analyzed the wettability behavior, microstructure and hardening behavior of Al/Al compound cast interface. The insufficient wettability was caused due to the presence of natural oxide layers on Al surface which create difficulty in joining Al/Al. The wettability of Al surface was enhanced significantly by applying the pre-treatment processes and Zn coating which produced a defect-free joint interface. A metallurgical reaction was initiated by applying zincate process and a Zn layer deposited by electrochemical process. This resulted in the formation of a continuous metallurgical bond and a joint interface with no imperfections. This offered the vital advantages in comparison to the other techniques of joining the light metals together.

Papis et al. [30] studied the interface formation of Mg/Mg compound cast pieces. Pure Mg as well as AJ62 was cast around solid AZ31 insert. The oxide layer on AZ31 insert was removed and replaced by Zn/$MgZn_2$ coating. It was reported that the present method of joining reduced the shortcomings of conventional method by adopting the galvanization and welding depth. The wettability behavior of AZ31 insert towards Mg melt was drastically enhanced by applying Zn/$MgZn_2$ coating. A continuous and defect free metallurgical transition zone was obtained between AZ31 insert and AJ62 alloy as well as pure magnesium.

Akbarifar and Divandari [34] investigated the interface layer formed between brass and aluminium couples. Molten aluminium was poured around solid cylindrical brass insert at a temperature of 700 and 750 °C with melt/solid insert volume ratio of 3 and 5. It was reported by the authors that due to the increase in temperature and melt/solid insert volume ratio; the heat content increased which activated the diffusion process. SEM microscopy and XRD analyses revealed the formation of three different layers in which intermetallic compounds such as Al_2Cu, CuZn, Al_4Cu_3Zn, and α-Al/Al_2Cu eutectic and Al dendrites were present. Traces of existence of Cu_4Al_9 in the interface were not observed as Al_2Cu and Al_4Cu_3Zn stalled the molten pool to be saturated by copper. In dendritic and eutectic zone, bubble entrapment near the surface of insert resulted in the formation of pores. Hardness values of 650, 477 and 513 HV were measured from solidified aluminium towards brass insert.

Ho et al. [37] accessed the bonding properties of S45C steel insert and copper joint prepared by compound casting. Continuous cooling heat treatment was applied using water quenching, oil quenching, air cooling and furnace cooling. It was concluded that joint interface consisted of three layers i.e., a cast welding layer near S45C steel matrix, an irregular layer near to copper matrix and a layer in between these two layers. Plentiful iron atoms were diffused in the copper matrix whereas diffusion of copper atoms in the iron matrix was limited. Maximum interfacial shear strength was obtained by furnace cooling while minimum in case of water quenching. Fracture surfaces in the cast welding layer were observed near the S45C steel matrix.

Tavassoli et al. [53] prepared the Al/Cu couples by casting aluminium melt around solid copper tubes using compound casting process. The interface formation was studied by varying the temperature of molten aluminium and preheating the copper tubes. Results revealed the formation of a uniform interface composed of three distinctive layers i.e., α-Al/Al_2Cu eutectic structure, intermetallic phases of Al_2Cu and a layer containing intermetallic phases like Al_4Cu_9, Al_3Cu_4, Al_2Cu_3 and AlCu. The thickness of transition zone was increased with increase in the temperature of molten aluminium and preheating of solid copper tubes. As a result, the specific electrical resistance was increased and aluminium/copper bond strength was decreased.

Akbarifar and Divandari [54] investigated the interface behavior of cast iron and aluminium bimetallic joints that were prepared using compound casting at different melt temperatures and melt/solid insert volume ratios. Molten aluminium was poured around solid cylindrical cast iron insert at a temperature of 700 and 750 °C with melt/solid insert volume ratio of 3, 5 and 8. It was concluded that interfacial layer thickness varied from 5 to 20 μm when the bimetallic joints were prepared at a temperature of 700 to 750 °C with melt/solid insert volume ratio of 3 to 8 respectively and a defect free transition zone was obtained. Authors proposed that the thickness of interfacial layer was possible to control by varying the process parameters like shape of casting, altering the pouring mechanism and making the provision for controlled solidification of casting. A transition layer containing Fe_2Al_5 intermetallic compound was identified in the interface which was produced as a result of interaction of cast iron with molten aluminium. Thickness of this layer was increased by increasing the temperature and melt/solid insert volume ratio.

Liu et al. [55] studied the mechanism of interface development, tensile strength, hardness and fracture surfaces of bimetallic couples made up of aluminium alloys, A356 as melt and A6101 as solid substrate. It was reported that a good metallurgical joint between A356 and A6101 alloys was achieved after applying zinc coating on solid substrate. The microstructure of A356 alloy was composed of α -dendritic aluminium phase and evenly distributed eutectic Si particles while the microstructure of A6101 alloy revealed a typical fine-grained wrought Al alloy structure. A transition layer between the two alloys showed fine-grain structure and eutectic Si structure at grain boundaries with a thickness of 100 μm. A localized diffusion between A356 and

A6101 alloys was observed due to the partial melting of A6101 alloy insert. The hardness of interfacial zone was measured lower than A356 alloy but higher than A6101 alloy. Tensile fracture occurred in as cast A356 alloy side with an ultimate tensile strength of 145 MPa. It indicated that over cast joint was associated with high strength than as cast A356 alloy. The fractured surfaces at the transition layer showed inter-granular fracture morphology along with obvious cleavage planes.

Hajjari et al. [56] examined the interfacial microstructure of Al/Mg joints fabricated by using compound casting process. Authors reported that joint interface consisted of three different layers. The interfacial zone adjacent to the Al and Mg base metals composed of Al_3Mg_2 and $Al_{12}Mg_{17}$ + δ eutectic structure respectively, while the middle zone composed of $Al_{12}Mg_{17}$ intermetallic compounds. Due to the deviation from stoichiometric proportion; antiphase domains and antiphase boundaries were generated within $Al_{12}Mg_{17}$ compound. The size of antiphase domains was increased whereas the density of the antiphase boundaries was decreased with increase in deviation from stoichiometric proportion.

Emami et al. [57] analyzed the effect of melt/solid insert volume ratio on Mg/Al joints prepared by compound casting process. In this process, magnesium melt was casted around the aluminium insert at different melt/solid insert volume ratios. Authors concluded that Mg/Al interface was formed due to the diffusion reaction at lower melt/solid insert volume ratio, while diffusion solidification at higher melt/solid insert volume ratio. The maximum hardness value of 252, 257 and 232 HV was observed corresponding to the melt/solid insert volume ratio as 1.25, 3 and 5.25, respectively. This indicated the formation of an interface with highest hardness corresponding to the intermediate value of melt/solid insert volume ratio. Thickness of interfacial zone increased with increase in melt/solid insert volume ratio. The average shear strength of interface decreased by increasing the melt/solid insert volume ratio.

Mola et al. [58] carried out the characterization of AZ91/AlSi17 joint interface prepared by pouring liquid AZ91 magnesium alloy around AlSi17 aluminium alloy insert. In this process steel mold was used to complete the casting process. The influence of pouring temperature was investigated on the formation of bonding zone.

It was reported that the formation of bonding zone between AZ91 magnesium alloy and AlSi17 aluminium alloy was affected by the temperature of AZ91 melt. At 650^{o}C pouring temperature, a continuous joint interface was constituted at AZ91/AlSi17 interface while such transition zone was not achieved at higher temperatures. The intermetallic compounds constituting the interfacial zone adjacent to AlSi17 alloy were observed as fine Mg_2Si compounds, primary Si particles enclosed by Mg_2Si compounds and an Al_3Mg_2 intermetallic phase. The interfacial zone adjoining AZ91 alloy was composed of a solid solution of Al and Si in Mg and $Mg_{17}Al_{12}$ eutectic structure.

Ren et al. [59] examined the microstructural behavior and mechanical properties of Al/Mg couples of ZL105 aluminium alloy and AZ91D magnesium alloy prepared by compound casting process. The transition zone was composed of three different layers having α-Al, β-$Al_{12}Mg_{17}$, γ-Al_3Mg_2, δ-Mg and Mg_2Si as the intermetallic compounds. Maximum bending strength of 23.06 MPa was observed at 680 °C of pouring temperature.

Zhang et al. [60] prepared the Al-0.08Ga/Mg bimetallic couples using compound casting process and investigated the effect of electro polishing and anodizing surface treatment of insert on interfacial microstructure and mechanical properties. Results indicated the major enhancement in metallic diffusion with Ga alloying, electro polishing and anodizing of insert. It was concluded that preheating of insert influenced the shear strength of castings. It increased up to the maximum value of 41.79 MPa when the preheat temperature was increased to 500 °C. Thereafter, the shear strength started decreasing as a result of excessive melting of aluminium and formation of hard and brittle intermetallic compounds at the interface.

Zare et al. [61] studied the microstructure and hardness of transition layer formed between aluminium and copper couples produced by compound casting process. Molten aluminium was casted around cylindrical copper substrate in order to prepare the Al/Cu joint. Authors reported that the transition zone was composed of five distinct layers containing the eutectic α-Al dendritic layer, eutectic layer and AlCu, Al_2Cu and Cu_9Al_4 intermetallic compounds. Maximum hardness of transition zone was measured as 300 HV due to the existence of hard and brittle intermetallic compounds whereas the base metals aluminium and copper indicated the hardness value less than 50 HV. Hardness was increased from aluminium to copper side across the transition zone.

Akbarifar and Divandari [62] characterized the interfacial microstructure of aluminium and cast iron couples. Aluminium melt was poured around the cast iron bars at a temperature of 700 and 750 °C with different melt/solid insert volume ratios. Results confirmed the formation of a transition layer at the interface having Fe_2Al_5 intermetallic compound. Fe_2Al_5 initially formed at the surface of insert due to the interaction with molten aluminium. A more uniform and thicker transition layer was observed when temperature and melt/solid insert volume ratio was increased. Transition layer thickness varied from 5 to 20 µm when the samples were prepared at a temperature of 700 and 750 °C with melt/solid insert volume ratio of 3 and 8 respectively.

Salimi et al. [63] fabricated the aluminium/steel bimetals by pouring molten aluminium around solid steel insert using compound casting process. The aluminizing and copper electroplating of steel insert was executed ahead of the casting. The influence of aluminizing and copper electroplating on the microstructure and mechanical properties of joint interface was examined. It was reported that metallurgical bonding of aluminium and steel matrix was significantly improved as a result of aluminizing and copper electroplating of steel insert. In case of copper coated insert, thicker and more uniform transition zone was observed as compared to aluminized steel insert. Shear strength of aluminium/steel bimetal with copper coated insert was observed higher despite its more thickness.

Lin et al. [64] examined the effect of continuous cooling heat treatment on the interfacial characteristics of SK3 steel insert and copper couples produced by compound casting process. Results indicated the formation of cast welding layer in between SK3 steel and copper. The shear strength at joint interface was obtained as 8.33, 13.43, 12.29 and 18.74 MPa corresponding to furnace cooling, air cooling, oil quenching and water quenching respectively. Fracture surfaces in cast welding layer were observed near SK3 steel matrix. Hardness of SK3 steel matrix was enhanced due to water quenching with simultaneous improvement in shear strength of joint interface.

Feng et al. [65] performed the comparative study of interfacial microstructure, hardness and tensile strength of A356/A6061 and A6061/A6061 bimetallic couples prepared using compound casting process where A6061 alloy was used as insert material. The effect of coating materials and casting processes were evaluated. It was concluded that nickel coating proved to be superior to copper coating for the joint between aluminium alloys. Maximum thickness of interface was measured as 5 and 150 µm for nickel and copper coating respectively. Due to the better thermal stability of nickel than copper, aggressive reaction with liquid aluminium alloy was taken place to form a transition zone. In gravity casting, mechanical properties of the joints were degraded due to the presence of coarse and cracked Al_3Ni phases distributed at the interfacial zone. In squeeze casting, metallurgical bonding of the joints was improved due to the presence of fine and uniformly distributed nickel-rich phases across the interfacial zone.

Hajjari et al. [66] studied the microstructure characterization and mechanical properties of Al 413/Mg couples produced by the compound casting process. It was concluded that $Al_{12}Mg_{17} + \delta$ eutectic structure adjacent to base metal magnesium showed the presence of magnesium oxide films. The initiation of longitudinal cracks and joint failure occurred due to the accumulated magnesium oxide within the interface consisted of $Al_{12}Mg_{17} + \delta$ eutectic structure. The thickness of joint interface ranges from 80 to 470 µm depending upon melt/solid insert volume ratio. It increased with increase in melt/solid insert volume ratio. The shear strength of the joint interface was more or less same at melt/solid insert volume ratio of 1.25 and 3.

Liu et al. [67] examined the impact of pressure and ambient temperature on diffusion behavior of Al/Mg couples fabricated by compound casting process. Results indicated that the diffusion between liquid magnesium and solid aluminium was dominantly influenced by the pressure and system temperature. The atomic diffusion was observed unidirectional as aluminium atoms participated more actively than magnesium atoms when the system temperature was kept lower than melting point of aluminium. Diffusion depth of aluminium was observed higher than the magnesium.

When the system temperature increased; more prominent diffusion of aluminium and magnesium atoms was observed which resulted in the formation of a uniform diffusion layer. Similarly, by increasing the pressure, both aluminium and magnesium atoms participated actively in the formation of joint interface.

Jiang et al. [68] joined Al/Cu bimetal by compound casting method. The interface of the Al/Cu bimetal displayed a defect-free and uniform morphology. Joint interface composed of α(Al)+Al_2Cu eutectic, Al_2Cu, AlCu, Al_4Cu_9, and Si phases. It showed much higher hardness in comparison to Al and Cu substrates, and Al_4Cu_9 phase in the interface layer had highest hardness. Bonding strength was achieved up to 28.5 MPa. Al/Cu bimetal represented brittle fracture morphology.

2.3 IMMERSION METHOD

It is a compound casting method which involves the insertion of solid insert into a molten bath. Figure 2.2 depicts the schematic of this method. In this process, the insert surface is cleansed and degreased by grinding with silicon carbide papers and then treated by alkaline cleaning, acid pickling or ultrasonically degreasing with acetone. The selected metal/alloy ingots are melted in a crucible located in an electrical resistance furnace. Melt is regularly stirred and the dross floating on the surface is removed. A thermocouple is used to measure the temperature of insertion bath. The bottom of the crucible containing insertion bath is machined and a device put on its top so that the insert remains perfectly vertical. The substrate is, then, inserted in the molten bath at a constant temperature and maintained for a particular time period. The power supply is turned off and the insertion bath is allowed to cool and solidify around the insert [69]. After solidification, the bimetallic sample is drawn. A few researchers have adopted this method to join dissimilar metallic materials.

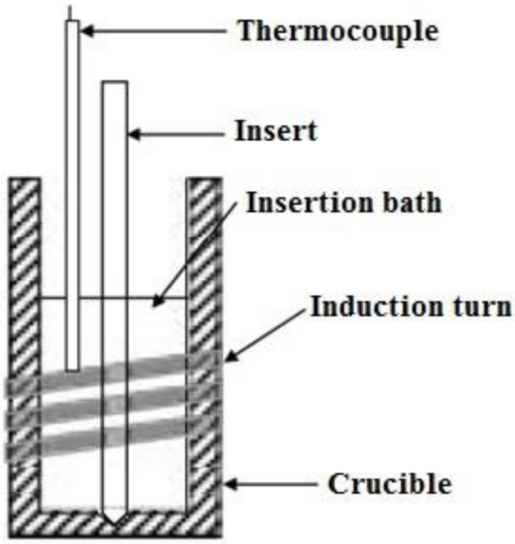

Figure 2.2 Schematic of immersion method of compound casting [62]

Hajjari et al. [31] investigated the interfacial heat flux for pure Al/Mg and Al413/Mg couples prepared by immersion method. Magnesium was used as melt material, and Al and Al413 as solid insert. It was concluded that interfacial heat flux serves as a method of assessing the wettability of solidifying metal and insert. It depends upon the surface roughness of solid insert. The interfacial heat flux was first increased up to a maximum level due to increase in surface roughness of solid insert, and thereafter started decreasing, for both Al/Mg and Al413/Mg couples. The maximum interfacial heat flux for Al413/Mg couple was observed higher than Al/Mg couple due to the superior wettability at almost all ranges of insert surface roughness.

Peronnet et al. [39] premeditated the significance of push out test to illustrate the interface bonding between E24 mild steel insert and GA6Z1 magnesium alloy melt. Immersion method was used to prepare E24 mild steel/GA6Z1 assemblies by using discrete processing conditions. The samples with partial and complete bonding were produced due to the chemical interaction between mild steel insert and GA6Z1 alloy melt. Authors concluded that the load displacement response and de-bonding load were strictly related with nature and extent of bonding formed at the joint interface.

Dezellus et al. [69] carried out the push out testing of mild steel/AS-13 bimetallic couples prepared by immersing mild steel bar in AS-13 alloy melt. The failure mode was investigated at different load levels till complete de-bonding of joint interface. It was reported by the authors that brittle failure was not detected at joint interface of mild steel/AS-13 bimetallic couples. The destruction mechanism accomplished in three stages started from crack initiation that happened in the interfacial zone near bottom face of the specimen, followed by propagation of crack in interfacial zone, deviation of crack towards AS-13 matrix and then plastic flow of AS-13 matrix, before failure. Authors also felt the requirement of accessing pushout tests in a more comprehensive manner so as to consider the distribution of shear stress along the interface in order to analyze the interfacial crack growth.

Bouayad et al. [70] studied the mechanism of interface formation and growth kinetics of solid iron/aluminium melt assemblies prepared by immersion process. Results indicated the formation of two intermetallic layers consisted of $FeAl_3$ and Fe_2Al_5 as main constituents. Growth kinetics of these intermetallic layers was recognized as a function of temperature and time. It was measured experimentally between 700 to 900 °C temperatures. Growth of intermetallic phases $FeAl_3$ and Fe_2Al_5 were controlled by kinetic regime and diffusion regime respectively for a moderate interaction time of less than 45 min. The growth of $FeAl_3$ phase followed a linear curve whereas the growth of Fe_2Al_5 phase was a parabolic curve.

Dezellus et al. [71] assessed the mechanical properties of Ti/A356.2 joints fabricated using immersion method. Authors revealed that chemical bonding between Ti and A356.2 enhanced the mechanical properties of joint interface. The shear strength of chemically bonded specimens was measured as 120 MPa while it was considerably low i.e., 48 MPa for simply fussed specimens. Due to the chemical reaction, a thick $Al_3Ti(Si)$ layer was formed on A356.2 side and a thin TiSi layer was formed on Ti side which improved the mechanical properties of joint interface. It was proposed by the authors that joint failure occurred in three stages beginning from crack initiation at the bottom face of specimen in A356.2 matrix or in the interfacial zone due to the tensile stresses. In second stage, crack propagation occurred towards top face and then deviated from interfacial zone to bulk A356.2 matrix. Lastly, the failure occurred when the yield stress of A356.2 matrix was exceeded by the huge value of equivalent von Mises Stress.

Zhao et al. [72] optimized the process parameters of insert molding method by analyzing the interface formation and mechanical behavior of AZ31/AZ91 bimetallic couples. The couples were prepared by inserting AZ31 alloy rod into AZ91 alloy melt at the insert temperature of 650, 675 and 700 °C with melt to solid insert volume ratio as 1 and 2. It was concluded that a proper interfacial bond attained at an insert temperature of 675 °C and melt to solid insert volume ratio as 2. Melt to solid insert interaction period was 90 to 120 s for proper metallurgical bonding. However, at high interaction period i.e., more than 300 s, the solid insert got melted and lost its shape. Average tensile strength of AZ31/AZ91 couples was measured as 98 MPa that approaches the as cast AZ91 tensile strength. Initiation of crack occurred in the weak part of casted AZ91 alloy.

Li et al [73] analyzed the mechanical properties and microstructure of joint interface of Ti-6Al-4V/Al7050 bimetallic prepared using insert molding method. Authors reported that an interfacial zone with good metallurgical bond having 90 μm thicknesses was achieved at 750 °C temperature. The interfacial zone consisted of $TiAl_3$ intermetallic and Al matrix. The microhardness of Ti-6Al-4V/Al7050 joint interface was measured between 180 and 210 HV. The compressive strength, tensile strength and shear strength of joint interface was achieved as 283, 215 and 154 MPa respectively. It was revealed that Ti-6Al-4V/Al7050 couples produced using insert molding method indicated better mechanical properties than the joints prepared by other joining methods like transient liquid phase bonding, ultrasonic assisted brazing and liquid state diffusion bonding.

Nie et al. [74] carried out the comparative study of Ti/Al and Ti–6Al–4V/Al joint interface by assessing the microstructural characteristics, interfacial thickness, distribution of elements and mechanical properties. The couples were prepared by insert molding method. Results revealed that interface reaction rate and shear strength of Ti/Al was higher than Ti–6Al–4V/Al joints. Considerably thin layer was observed at the joint interface of Ti–6Al–4V/Al couples having different morphology from that of Ti/Al joint interface.

Dezellus et al. [75] studied the mechanical behavior of T6 heat treated Ti/Al-7Si couples prepared using insert molding method. Classical push-out and circular bending tests were performed for this purpose. For T6 heat treatment of chemically bonded Ti/Al-7Si couples, the samples were reheated for 10 hours at a temperature of 540 °C, quenched in cold water and subsequently aged for 6 hours at a temperature of 170 °C. Authors reported improvement in the mechanical properties of T6 heat treated samples. Favorable effect of T6 heat treatment was caused due to change of silicon particles from angular to spherical, as these particles made superior nucleation sites for ductile tearing and voids creation in Al-7Si matrix. Furthermore, formation of silicon rich intermetallic compounds in joint interface was achieved by the solid state diffusion of silicon atoms from Al-7Si matrix toward the Ti insert. Due to this migration, the number and size of silicon particles decreased considerably in the surrounding area of interfacial zone of Ti insert and Al-7Si alloy matrix.

2.4 ROTATING DISC TECHNIQUE

It is a type of compound casting method in which flux is used to protect the melt from oxidation and to pre-heat the solid insert to the required temperature. The flux is first melted in an alumina crucible. Pieces of melt material are then melted under the flux. When the required temperature has reached, the rotating solid insert is lowered from position I into position II as shown in Figure 2.3 near the middle of the flux layer. The pre-heating of insert takes place in this manner. When the temperature reaches to the equilibrium, the insert rotating at the required speed is lowered from position II into position III in the molten metal. The disc is allowed to rotate in the melt for a pre-determined period of time. The temperature of the liquid phase is measured by a thermocouple. The crucible, together with the melt, the flux and the solid insert, is allowed to cool in a water bath [76]. Figure 2.3 shows the schematic of the process.

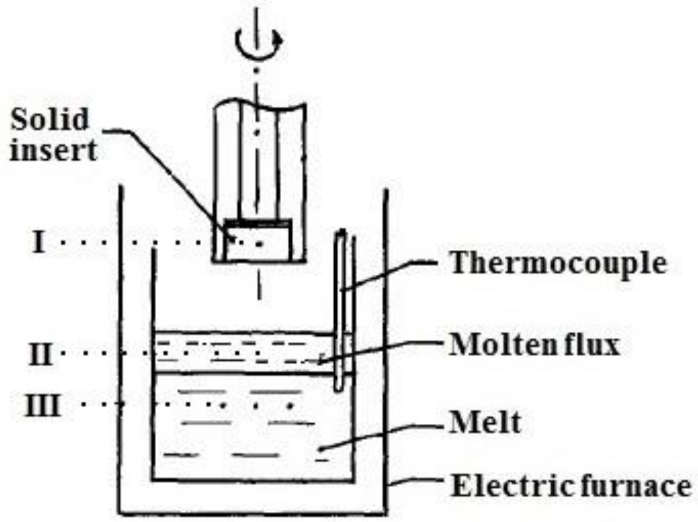

Figure 2.3 Schematic of rotating disc method

Dybkov [76] investigated the rotating disc method by the interaction of liquid aluminium with 18Cr-10Ni stainless steel. The author reported that steel/Al joints with good mechanical properties can be produced by the interaction of solid steel and liquid Al melt under pre-controlled process parameters. During dissolution, the elements of steel pass into the Al melt. In an unsaturated Al melt, a single intermetallic layer was formed at the steel /Al interface whereas in saturated Al melt, two intermetallic phases were detected between Al melt and steel at the temperature of 700 °C. The layer next to steel was possibly a solid solution of Fe_2Al_5 intermetallic compound. The porous layer adjacent to the Al melt was probably a solid solution based upon $FeAl_3$ compound. The growth phenomenon of this compound was para-linear. Thickness of this layer was increased by increasing the dipping time. The growth phenomenon of layer adjacent to Al melt became linear after some duration of non-linear growth.

Barmak and Dybkov [77] analyzed the intermetallic phases produced by the interaction of Fe-Cr alloy with aluminium melt by rotating-disc method. The experiments were conducted by taking the composition of Cr in Fe-Cr alloy as 10 and 20%. The results revealed that joint of iron-chromium alloys and aluminium can be successfully achieved by the dissolution of Fe-Cr alloy into liquid aluminium followed by cooling up to the crystallization. The interface was composed of two intermetallic layers between Fe-Cr alloys and liquid aluminium that consisted of

Fe_2Al_5 along alloy base side and Fe_2Al_7 along aluminium side. The layer on alloy side was uniform and dense while the other was non-uniform and spongy. Other intermetallic compounds such as $Cr_{0.67}Fe_{0.33}Al_{13}$, $CrAl_7$, $FeAl_6$ and $FeAl_3$ were also detected in Al matrix near joint interface. These compounds were formed due to the crystallization of melt. Tensile tests revealed that joint strength of intermediate zone was lower than the pure aluminium.

Dybkov [78] studied the interaction of iron-nickel alloys containing 5-90% iron with aluminium melt by using rotating disc method. Experimental and test results reported a good interaction of iron and nickel in Al melt. The interaction was more dominated in the alloy containing more than 50% nickel. The value of dissolution rate constant was decreased by increasing the dipping time, and nickel and iron concentrations in aluminium melt. The magnitude of diffusion coefficient of Fe and Ni across the diffusion boundary was decreased nearly 25 to 40% with increase in Fe and Ni concentration in Al melt. For Fe-Ni (90%-10%) alloy, the diffusion coefficient was increased with increasing iron and nickel concentration in Al melt, up to the diffusion coefficient value of pure iron in aluminium melt. For other Fe-Ni alloys under investigation, the values of diffusion coefficient were obtained less than or close to the diffusion coefficient of nickel.

Dybkov [79] examined the phenomenon of dissolution of iron-nickel alloys in aluminium melt by a non-selective and diffusion controlled rotating-disc technique. It was concluded that Fe_2Al_7 and $FeAl_3$ intermetallic compounds were detected at the intermediate layer between iron-nickel alloy and aluminium melt at a temperature of 700 °C when the percentage of iron in iron-nickel alloy was less than 50%. In case, the percentage of iron was more than 50%, $FeNiAl_9$, $NiAl_2$ and $NiAl_3$ intermetallic compounds were detected at the intermediate layer between iron-nickel alloy and aluminium melt having FeNiAl9 as chief constituent. Iron-nickel proportion of intermetallic compounds at joint interface was dependent upon the percentage of iron or nickel in the alloys. The dissolution of iron-nickel alloy with aluminium melt tends to decrease the interface thickness in comparison to the saturated melt. Therefore, the extent of saturation of a molten metal with the alloy constituents was considered.

2.5 LOST FOAM COMPOUND CASTING

In this process, the foam (polystyrene) pattern is first prepared having a cavity to mount insert in it. This foam patterns together with the solid inserts is placed into a sand mold. A sprue cup was placed on the sprue for pouring of molten metal. The molten metal was poured through it. Heat of the molten metal evaporates the foam pattern and melt takes the shape of pattern around the solid insert. The cast piece is being removed after solidification [80]. Figure 2.4 depicts schematic of the process. The process can be executed by applying vacuum for faster removal of gases produced due to the evaporation of foam pattern.

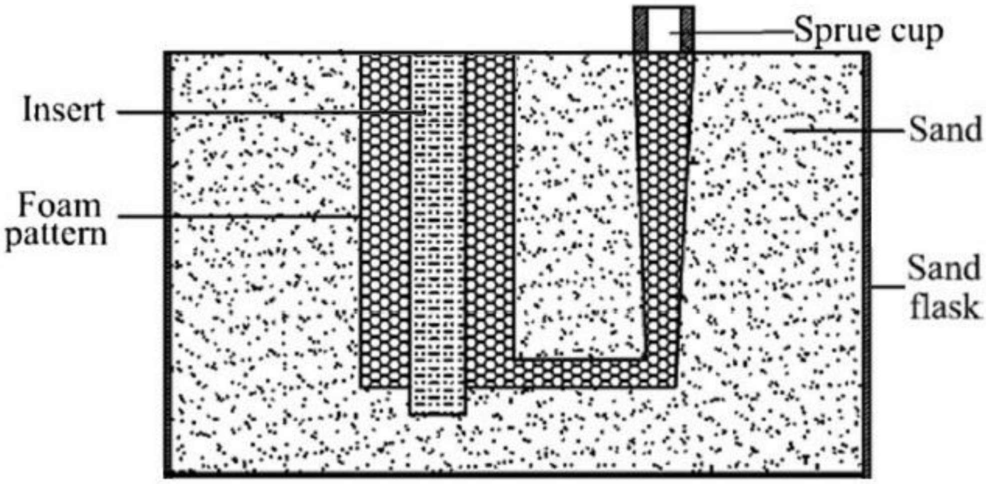

Figure 2.4 Schematic of lost foam compound casting process

Jiang et al. [80] studied the influence of melt/solid insert volume ratio on the microstructural characteristics and mechanical behavior of A356/AZ91D assemblies produced by vacuum assisted lost foam compound casting method. Solid insert was made up of A356 alloy and AZ91D alloy was used as melt material. It was observed by the authors that interfacial zone composed of $Al_{12}Mg_{17}$ + δ eutectic intermetallic in the vicinity of AZ91D matrix, $Al_{12}Mg_{17}$ and Mg_2Si intermetallic in the middle portion, and Al_3Mg_2 and Mg_2Si intermetallic in the vicinity of A356 base metal for all the assemblies produced by using different melt/solid insert volume ratio. The thickness of transition zone between A356 and AZ91D increased considerably due to increase in melt/solid insert volume ratio. A uniform and dense interfacial zone was achieved at 14.6 melt/solid insert volume ratio. The microhardness of interfacial zone was significantly higher than A356 and AZ91D base metals for all the melt/solid insert volume ratios. Al_3Mg_2 intermetallic showed the highest microhardness followed by $Al_{12}Mg_{17}$ and $Al_{12}Mg_{17}$ + δ eutectic intermetallic. The maximum shear strength was achieved at 14.6 melt/solid insert volume ratio. Fractured surfaces of push out specimens revealed that increase in melt/solid insert volume ratio changed the mixed ductile and brittle fracture morphology into brittle fracture morphology.

Li et al. [81] analyzed the effect of pouring temperature on interfacial microstructure, shear strength, microhardness and fracture behavior of A356/AZ91D couples prepared using lost foam compound casting process. The process was executed under vacuum condition by pouring AZ91D magnesium melt around A356 alloy solid insert. It was concluded that thickness of transition zone increased with increase in pouring temperature of magnesium alloy melt. A uniform and dense interfacial zone was achieved at 730 °C pouring temperature. Interfacial portion of A356/AZ91D joint showed higher microhardness than that of parent metals for different pouring temperatures. Maximum shear strength was attained at 730 °C pouring temperature displaying an optimal bonding between Al and Mg. Brittle fracture morphology was obtained in interfacial zone while a partial plastic deformation in $Al_{12}Mg_{17}$ + δ-Mg eutectic phase.

Divandari and Golpayegani [82] examined the Cu/A356 joints produced by lost foam compound casting process. In this study, A356 alloy melt was poured around Cu wire inserted in polystyrene pattern. It was reported that joint interface of Cu and A356 matrix was composed of copper rich phases like Al_2Cu and AlCu, Fe containing intermetallic and Si particles. The copper wire of 1.2, 0.8 and 0.4 mm diameter showed no melting, partial melting and complete melting of the wire, respectively when A356 melt was casted around it. A wire affected zone was made around the inserted Cu wire by the formation of cooling affected zone and composition affected zone. The cooling affected zone was caused during solidification due to the cooling effect of wire whereas; the composition affected zone was resulted due to the partial or complete dissolution of Cu wire into A356 melt. The size of wire affected zone was influenced by wire diameter or size of test bar cross section, temperature and type of alloy used.

Dongfeng et al. [83] optimized the process parameters of lost foam casting process by fabricating a composite layer on AZ91D insert. Authors concluded that development of composite layer was affected by mold filling method and pouring temperature of melt, vacuum degree, and pre coating thickness. Experiments showed that an outstanding composite layer was achieved with the optimal process parameters setting as 0.4 mm pre coating layer thickness, 0.06 MPa vacuum pressure and 800 ^oC pouring temperature.

Hejazi et al. [84] fabricated the Cu/gray iron bimetals using lost foam casting process. The couples were prepared by pouring of molten gray iron around 0.4, 1 and 2 mm diameter Cu wires inserted in polystyrene pattern at 1230 and 1370 ^oC temperature. Influence of pouring temperature of gray iron and diameter of Cu wires on the microstructural characteristics of joint interface was investigated. Results reflected that dissolution of Cu wire was achieved up to 0.9 wt.% in gray iron matrix. Cu surpassing the limits of solubility was separated out at the bottom of the melt or disseminated all over the matrix. Graphite morphology without Cu wire was type A flakes while it was changed to B, D or E flakes for the specimens having Cu wire. Type D or E graphite flakes were generated as a result of high undercooling at the time of eutectic solidification when Cu wire melted fully. The cooling rate increased because of chilling effect of Cu wire when it got partially melted or not melted. This resulted in the formation of a wire affected zone around Cu wire with type B graphite flakes. Size of wire affected zone was influenced by pouring temperature, wire diameter and specific heat capacity of Cu insert and gray iron matrix.

Fan et al. [85] studied the microstructure characterization of Al/Mg joints prepared using lost foam compound casting process. Aluminium alloy, A356 was used as insert material and magnesium alloy, AZ91D was poured around the solid insert to accomplish the joint. It was reported by the authors that thickness of joint interface was maximum at the bottom cross section of Al/Mg joint and then it gradually reduced from bottom to top. The joint interface was observed uniform and dense at the mid of the specimen while it was observed uneven at top cross section. Joint interface composed of intermetallic compounds occurred in three distinct layers containing Al_3Mg_2 + Mg_2Si, $Al_{12}Mg_{17}$ + Mg_2Si and $Al_{12}Mg_{17}$ + δ-Mg constituents.

Emami et al. [86] performed the comparative study of two variants of compound casting process i.e., lost foam compound casting and conventional compound casting. Bimetallic couples of aluminium and magnesium metals were prepared separately using these techniques by pouring molten magnesium onto the solid aluminium substrate. The joint formed composed of three distinct layers. It was concluded by the authors that microhardness values (200 to 250 HV) at the joint interface was measured higher than the hardness of parent metals. In case of lost foam compound casting process, the thickness of joint interface was reduced due to reduction in speed and temperature of magnesium melt.

Tayal et al. [87] joined aluminum alloys AA6063 and AA6351 by vacuum-assisted lost foam compound casting process. Results revealed formation of uniform and defect-free joint interface between AA6063 and AA6351. Pouring temperature was the most dominating process parameter that influenced shear stress, microhardness and impact strength. It had the maximum contribution (69.6 to 85.06%) followed by the size of sand particles (9.39 to 21.27%) and vacuum pressure (3.26 to 8.69%).

Li et al. [88] prepared A356/AZ91D bimetallic by using lost foam casting compound process. Authors concluded that interface layer was composed of $Mg_2Si + Al_3Mg_2$, $Mg_2Si + Al_3Mg_2 + Al_{12}Mg_{17}$, $Mg_2Si + Al_{12}Mg_{17}$, and $Al_{12}Mg_{17} + \delta$-Mg eutectic + Mg_2Si. The interface layer of A356/AZ91D bimetallic composites had a higher hardness than the substrates, and the Mg_2Si phase obtained the highest hardness in the intermetallic phases. The shear strength and tensile strength of the A356/AZ91D bimetallic composites reached 47.67 and 48.17 MPa, respectively. The fracture surface of the bimetallic composites exhibited brittle fracture morphology with a partial plastic deformation.

It is reflected from the literature survey that compound casting process seems superior to other similar or dissimilar joining processes such as rotating disc method, immersion molding and lost foam casting. The execution of compound casting process is quite simple as it involves merely pouring a molten metal onto a solid insert placed in mold cavity. It is possible to fabricate complex shapes easily thus eliminating the long processing time and high operating cost. Owing to the simple handling and minimum operating cost, this process is useful for the mass production of components in comparison to the rotating disc and immersion molding method. The experimental set-up in case of rotating disc method and immersion molding is rather complex and therefore, it requires additional handling and frequent maintenance. While, in lost foam casting method, the extra cost for fabrication and handling of pattern is involved. Also, the thickness of joint interface gets reduced due to reduction in speed and temperature of molten metal [86].

2.6 OTHER DISSIMILAR JOINING METHODS

A number of researchers have investigated the joining of Al/Mg metals and their alloys using different fusion welding and solid-state joining methods. It include processes such as spot welding, tungsten inert gas welding, gas metal arc welding, laser welding, friction-stir welding and vacuum diffusion bonding etc. The major problem in these joining processes is the formation of high hard and brittle intermetallic compounds as an interlayer between Al and Mg. These compounds are undesirable as far as the mechanical properties of the joint interface are concerned [80, 87-91]. Solid-state joining processes such as friction-stir welding and vacuum diffusion bonding can achieve relatively higher joining strengths compared to fusion methods, due to elimination of defects like shrinkage, porosities and inclusions. But these processes include special equipment and tooling, and have complex procedures. Lengthy processing and high operating cost of vacuum diffusion bonding and specific requirements for the shape of the substrate in friction stir welding may render use of these solid state joining processes for practical and industrial applications [54, 60, 65, 66, 92-94].

2.7 GAPS OBSERVED IN LITERATURE

As per the available literature, it seems that

- Dissimilar joining of aluminium and magnesium can be possible by some fusion welding and solid-state joining methods such as tungsten inert gas welding, spot welding, laser welding, vacuum diffusion bonding and friction-stir welding etc. The formation of brittle intermetallic compounds at Al/Mg interface is accompanied in these processes due to which the interface turns out to be weaker.
- There is lack of literature available on compound casting process.

- Few studies have been published on dissimilar joining of Al/Mg by compound casting process. More research is still required in this field so that the process can be utilized effectively and efficiently at the shop floor. Evaluation of micro-structural characteristics, mechanical properties and mechanism of Al/Mg joint interface formation is not much reported in the literature.
- Joint strength in compound casting process dependent upon number of process parameters. An effective process planning can be achieved by controlling the process variables. The study over process controls in compound casting is yet to be carried out. Optimization of process parameters of compound casting w.r.t. mechanical properties such as shear strength, impact strength and microhardness is not reported in literature.

2.8 PROBLEM FORMULATION

The present research work is an attempt towards the improvement over compound casting process by analyzing the influence of significant process parameters. The available literature on this topic reveals that a lot more is to be carried out to explore the potential of compound casting process. This may lead towards the better solution for the problems associated with this process.

In the present experimental investigation, the following research work is executed:

- Dissimilar light materials, A356 alloy and pure magnesium are joined by vacuum assisted sand mold compound casting process. Mechanism of interface formation, micro-structural characteristics and mechanical properties of the joint interface is investigated. Microstructure of joint interface is analyzed by optical microscopy, SEM, EDS and XRD techniques.
- The optimization of four significant process parameters - pouring temperature, vacuum pressure, insert temperature and surface roughness of insert has been carried out w.r.t. mechanical properties - shear strength, impact strength and microhardness of joint interface. Optimization is accomplished by response surface methodology, desirability analysis and genetic algorithm.
- Graph theoretic approach is applied to evaluate the impact of mechanical properties on joint strength.

- Multiobjective optimization has also been carried out by considering two or more output characteristics simultaneously.

2.9 OBJECTIVES OF THE RESEARCH

The main objectives of this research are:

1. Fabrication of experimental setup of vacuum assisted sand mold compound casting process.
2. Selection of process parameters and their ranges.
3. Design of experiments.
4. Preparation of compound cast joints.
5. Characterization of joint interface by optical microscope, SEM, EDS and XRD.
6. Evaluations of mechanical properties i.e., shear strength, impact strength and microhardness.
7. Investigation and analysis of effect of process parameters on joint properties by response surface methodology.
8. Optimization of the process parameters by desirability analysis and genetic algorithm.
9. Evaluation and analysis of joint strength (shear strength, impact strength and microhardness) by graph theoretic approach.
10. Multiobjective optimization by desirability analysis and genetic algorithm.

CHAPTER 3

EXPERIMENTAL SET-UP AND PROCEDURE

3.1 INTRODUCTION

This chapter comprises the experimental set-up of vacuum assisted sand mold compound casting process by incorporating the schematic diagram and photographs. The materials used for the experimental work is described by providing the composition. The selection of process parameters, design of experiments and procedure for production of compound cast parts is presented.

3.2 EXPERIMENTAL SET-UP OF VASMCC PROCESS

The set-up for vacuum assisted sand mold compound casting process is fabricated as per the requirement of experimental work. It comprises of following three units in order to prepare the compound cast pieces:

3.2.1 Molding Box Unit

It consists of a double wall molding box as shown in Figure 3.1. The molding box is fabricated by using mild steel sheet with a provision to suck air from its chamber in order to create vacuum inside it. Nozzles are provided on both sides, which connect the molding box to the vacuum pump.

3.2.2 Vacuum Unit

It consists of a vacuum pump of 1 H.P. capacity fitted with a vacuum gauge of range 0-760 mm of Hg. It is connected to the molding box with the help of flexible rubber hoses. A pressure regulator is fitted near the molding box nozzle to adjust the vacuum pressure. An air filter is provided between molding box and vacuum pump to protect the vacuum pump from sand particles. Figure 3.2 depicts the vacuum unit.

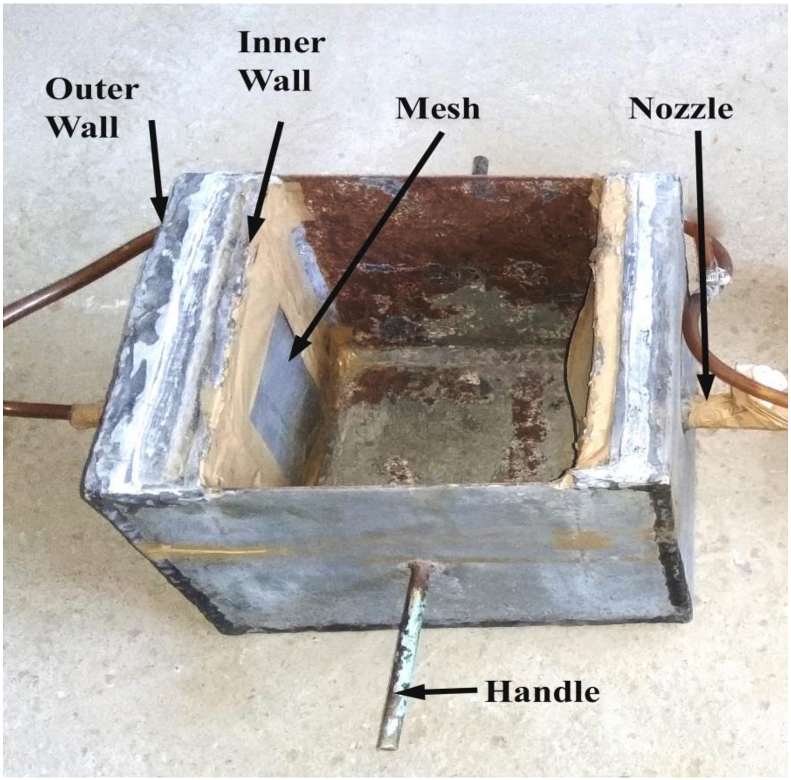

Figure 3.1 Double wall molding box

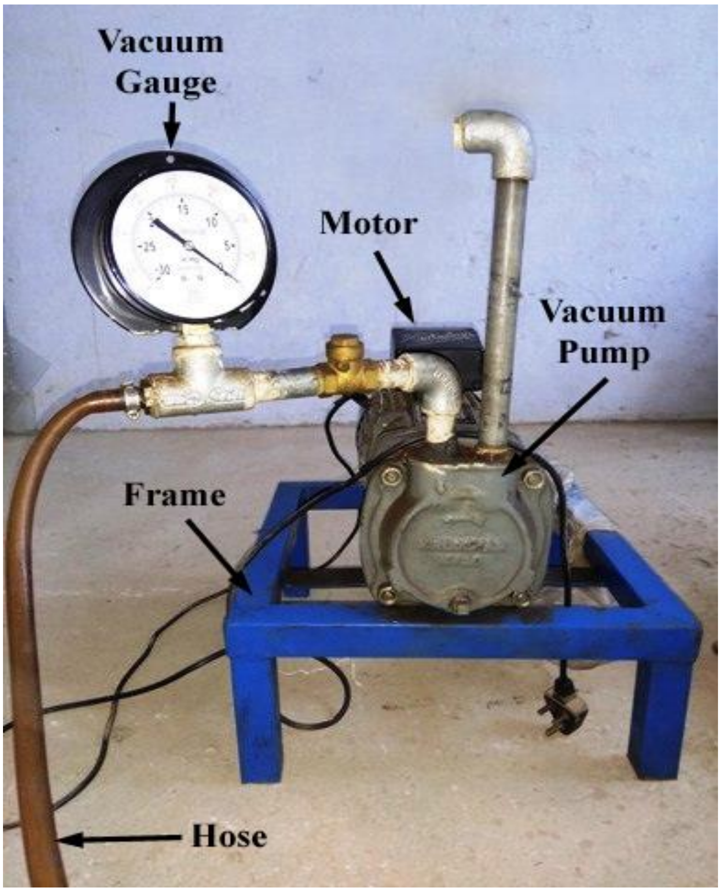

Figure 3.2 Vacuum unit

3.2.3 Heating and Melting Unit

It consists of one horizontal muffle furnace for preheating the solid A356 insert and one vertical muffle furnace for melting the pure magnesium. Figure 3.3 and Figure 3.4 depicts these furnaces.

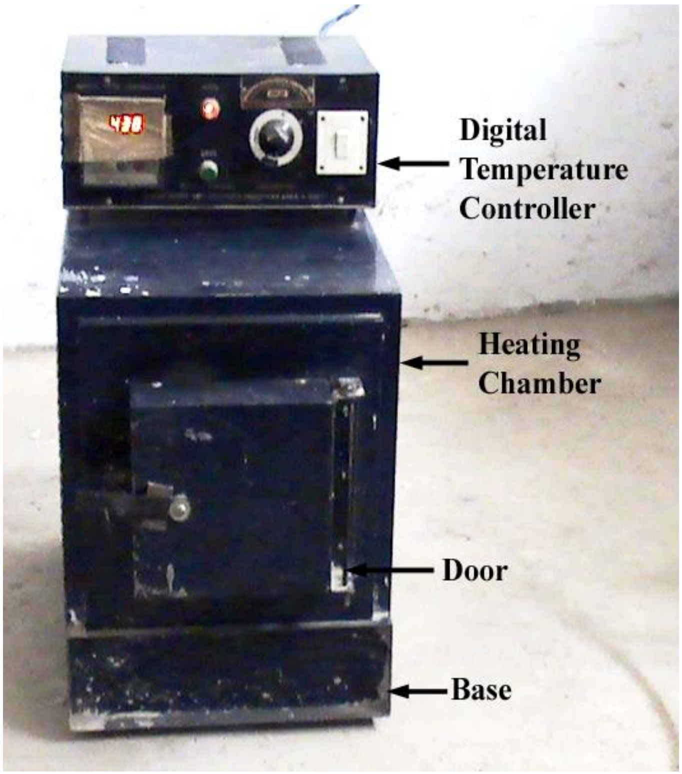

Figure 3.3 Horizontal muffle furnace

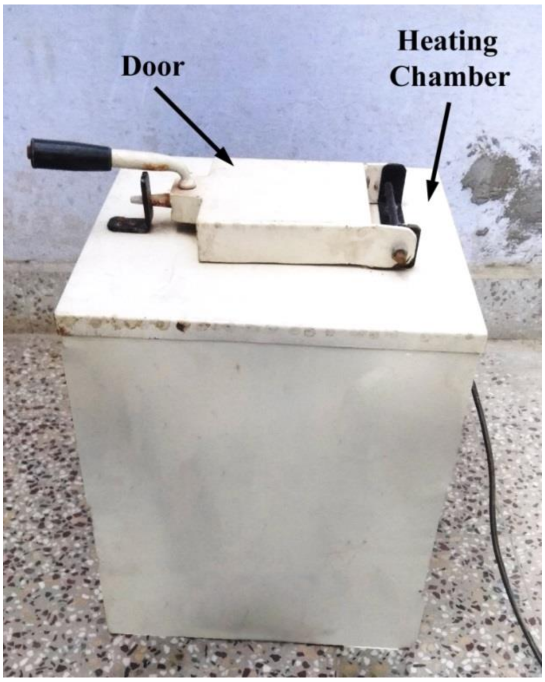

Figure 3.4 Vertical muffle furnace

The complete set-up for VASMCC process including connection of various units is shown in Figure 3.5

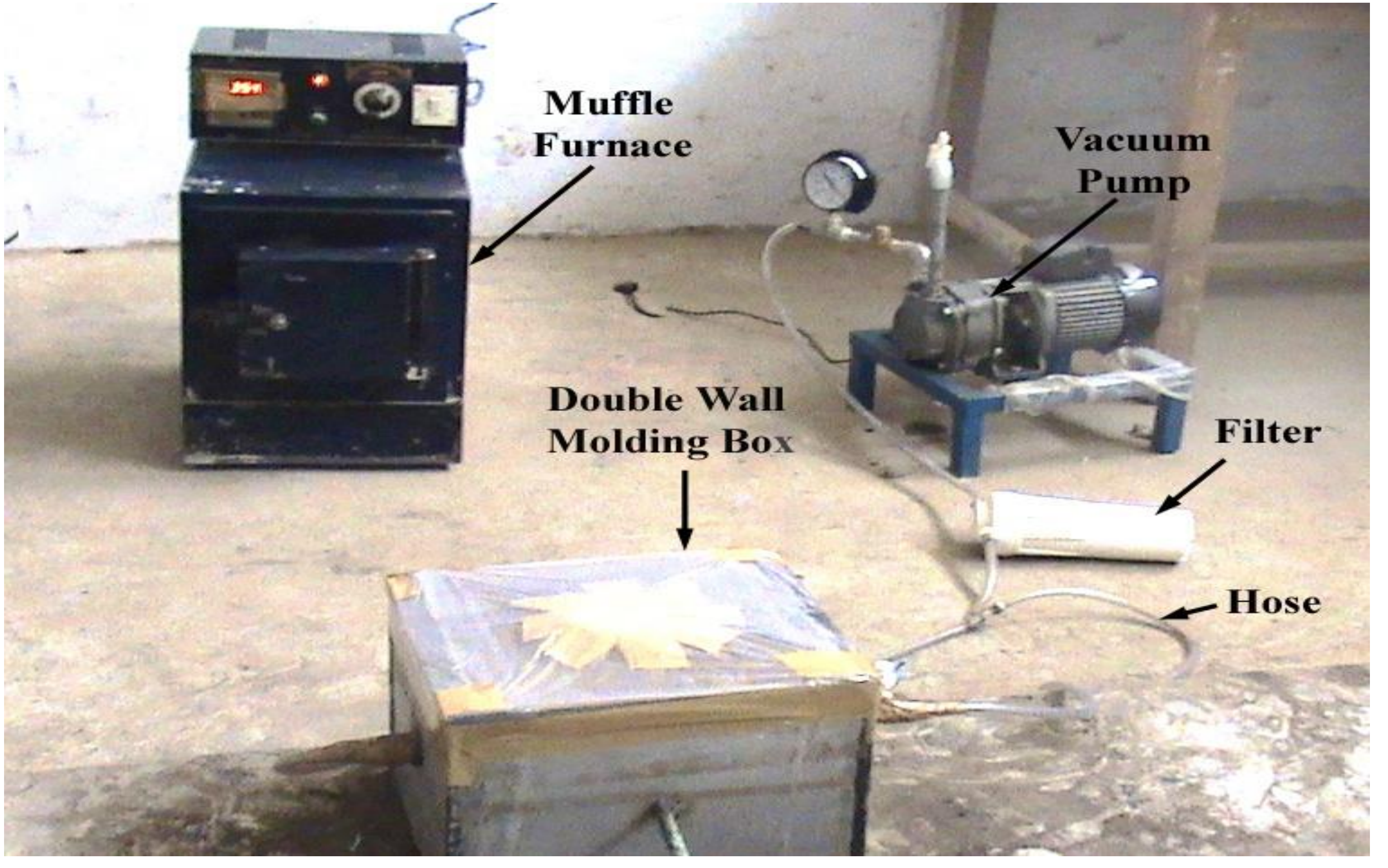

Figure 3.5 Experimental set-up of VASMCC process

3.3 MATERIALS USED

Aluminium alloy, A356 is used as an insert material and commercially available pure magnesium is used as molten metal to surround the insert. Table 3.1 represents the composition of materials. Ingots of A356 and pure magnesium used for producing compound cast pieces are shown in Figure 3.6 and Figure 3.7 respectively.

Table 3.1 Composition of materials (wt.%)

Material	Al	Si	Mg	Mn	Fe	Cu	Ni	Zn	Others
A356	91.834	7.28	0.378	0.064	0.114	0.06	0.003	0.026	0.241
Mg	0.02	0.03	99.861	0.048	0.002	0.017	0.002	-	0.02

Figure 3.6 Ingot of A356 alloy

Figure 3.7 Ingot of pure magnesium

3.4 SELECTION OF PROCESS PARAMETERS

The compound casting process is influenced by a numbers of parameters as shown in cause-and-effect diagram in Figure 3.8. These process parameters are as follows:

- Pouring temperature
- Pouring rate/time
- Insert Temperature
- Heating time of insert
- Surface roughness of insert
- Vacuum pressure
- Inert gas pressure
- Solidification time

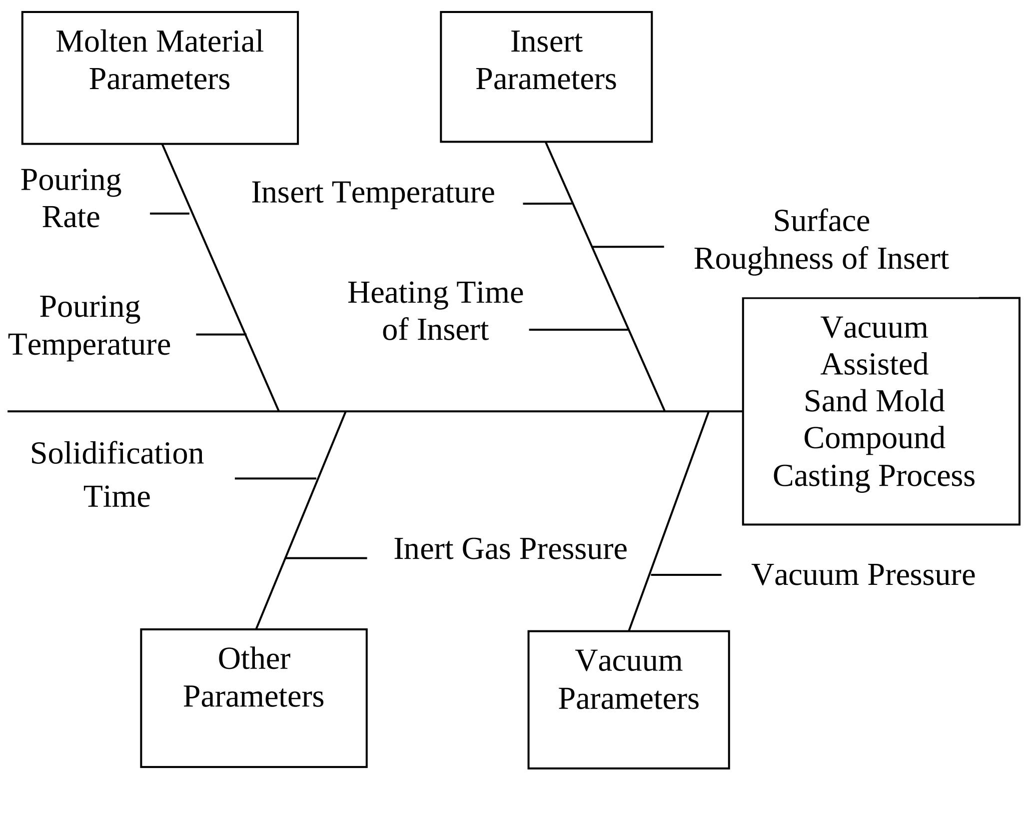

Figure 3.8 Cause-and-effect diagram of VASMCC process

Out of these, the pouring temperature, vacuum pressure, insert temperature and surface roughness of insert govern the process dominantly. The pouring rate is considered as constant parameter with a value of 20g/sec for all experiments. Range of these process parameters is determined by conducting the pilot experiments using one factor at a time approach. In this method one process parameter is varied while keeping other parameters as constant. Range of process parameters is obtained by variations in response characteristic; shear strength, impact strength and microhardness. Figure 3.9 to Figure 3.20 represents the results of pilot experiments.

3.4.1 Pouring Temperature

Pouring temperature refers to the temperature of molten metal when poured into the mold cavity. It has a significant effect on compound casting process. Variation of pouring temperature causes variation in mechanical properties of cast part. Values of shear strength, impact strength and microhardness varies with a variation of 650 to 750˚C of pouring temperature as shown in Figure 3.9 to Figure 3.11.

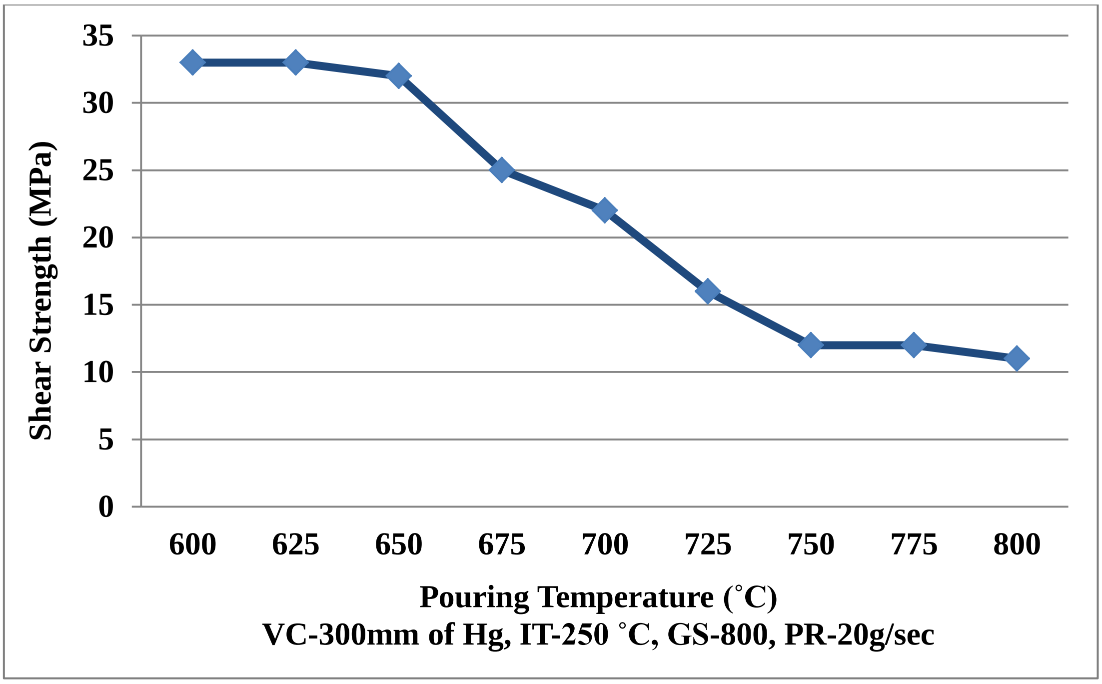

Figure 3.9 Plot of shear strength vs. pouring temperature

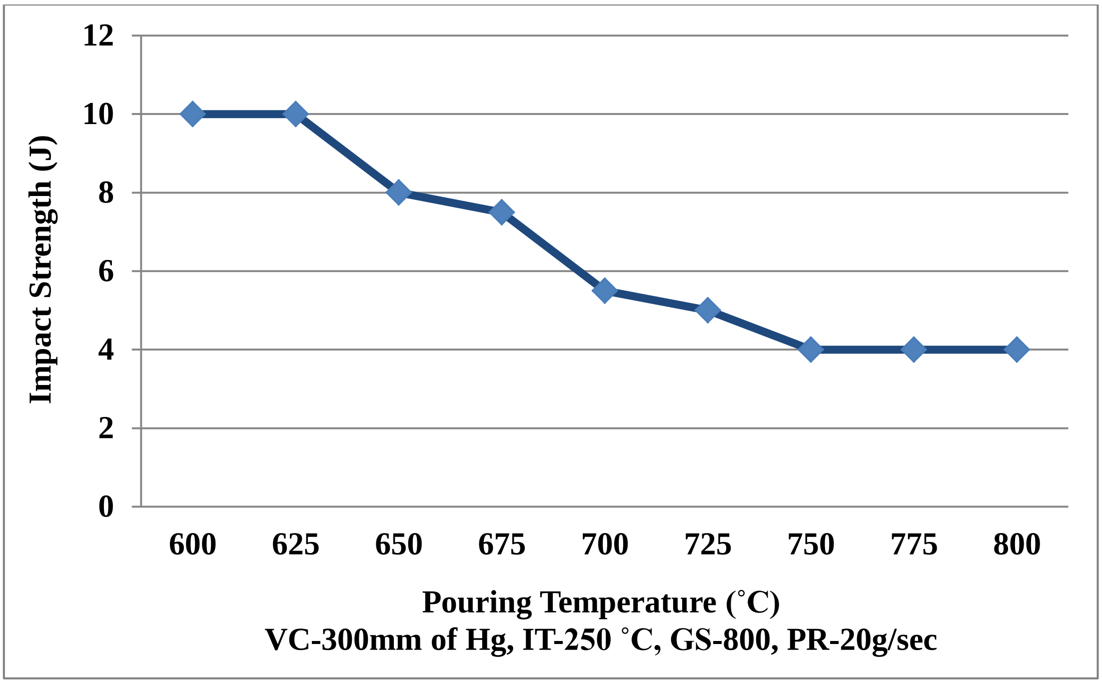

Figure 3.10 Plot of impact strength vs. pouring temperature

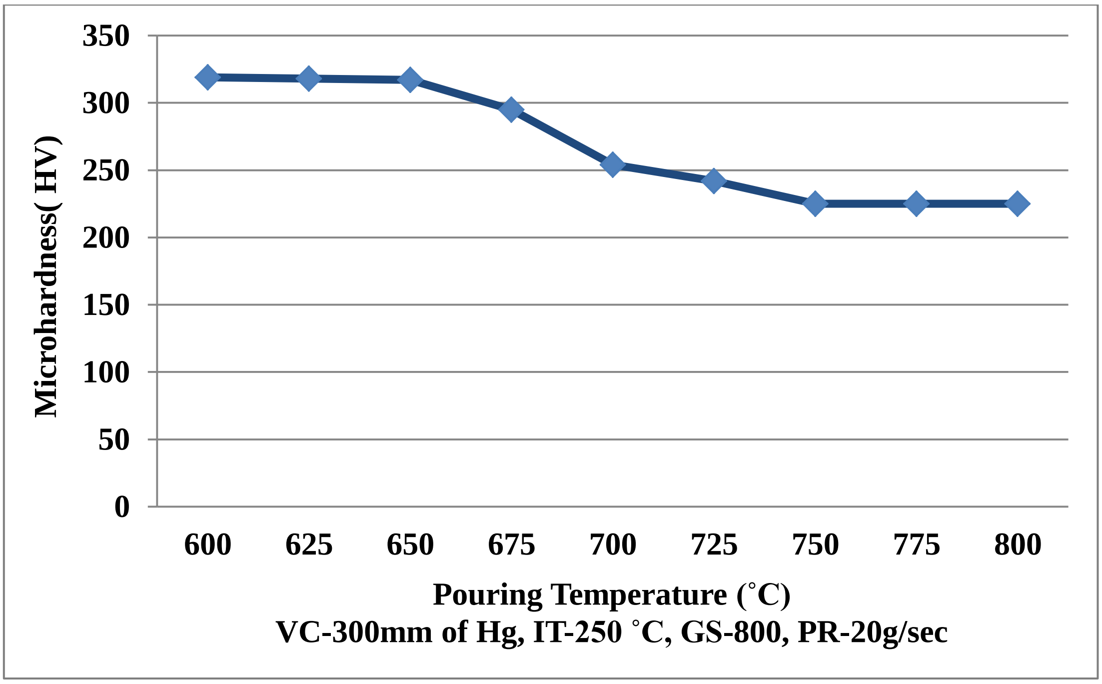

Figure 3.11 Plot of microhardness vs. pouring temperature

3.4.2 Vacuum Pressure

It refers to the degree of vacuum inside the molding box at the instance of pouring the molten metal into the mold cavity and during the solidification of casting. Vacuum is required to control the porosity defects and to eliminate the oxidation during interaction of molten metal and solid insert. Range of vacuum pressure is obtained as 200 to 400 mm of Hg by pilot experiments as shown in Figure 3.12 to Figure 3.14.

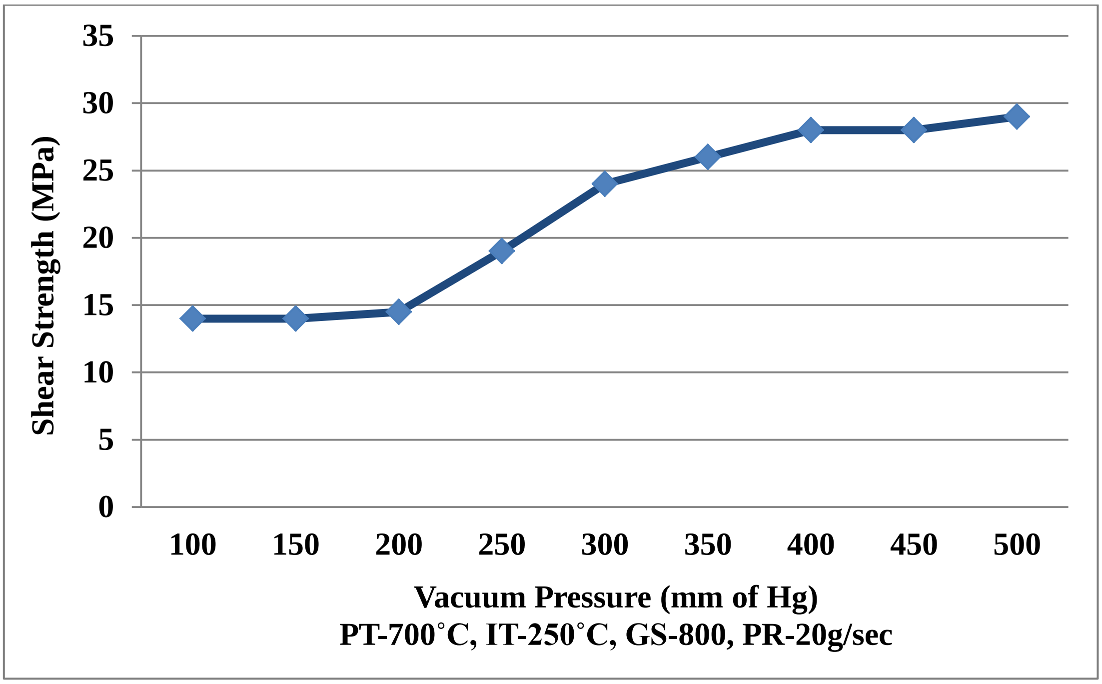

Figure 3.12 Plot of shear strength vs. vacuum pressure

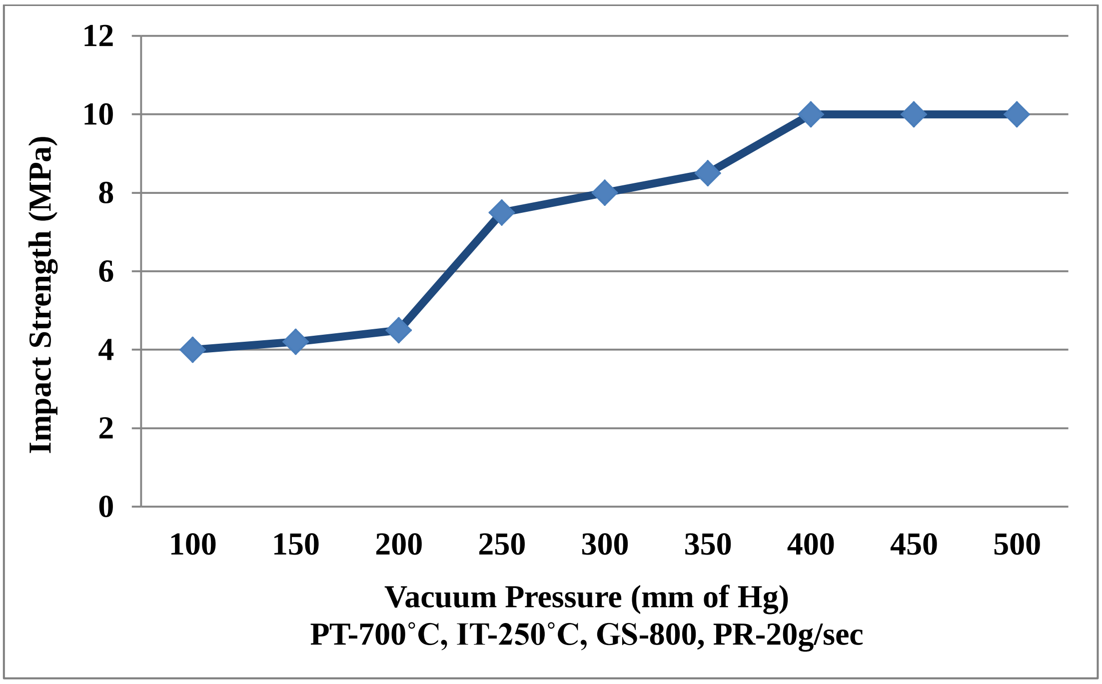

Figure 3.13 Plot of impact strength vs. vacuum pressure

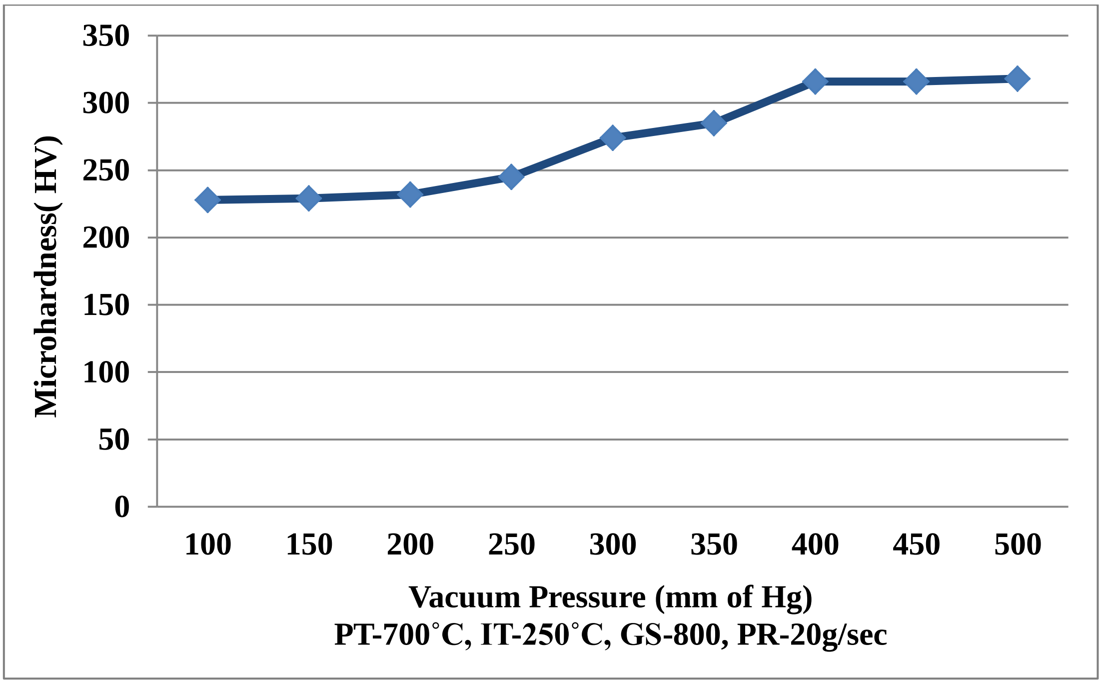

Figure 3.14 Plot of microhardness vs. vacuum pressure

3.4.3 Insert Temperature

It is the temperature up to which insert is heated before pouring of molten metal around it. Heating of insert is required in compound casting process for the smooth interaction of molten metal with solid insert. It reduces the temperature difference between molten metal and solid insert. Insert temperature range of 100 to 400 ˚C is predicted by pilot experiments as shown in Figure 3.15 to Figure 3.17.

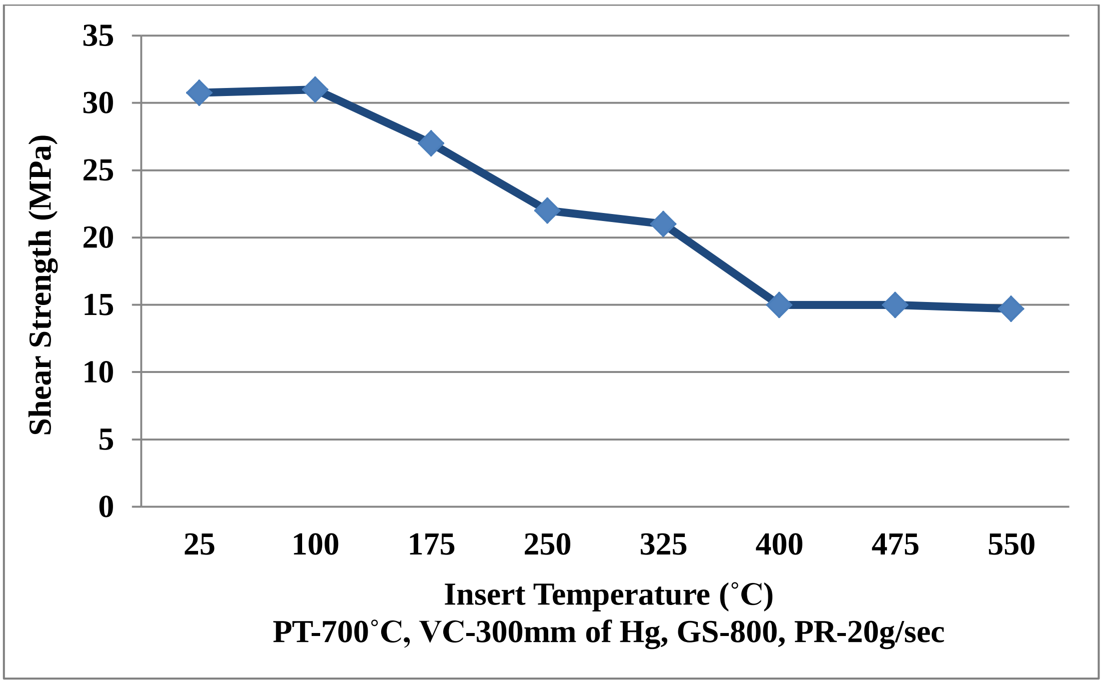

Figure 3.15 Plot of shear strength vs. insert temperature

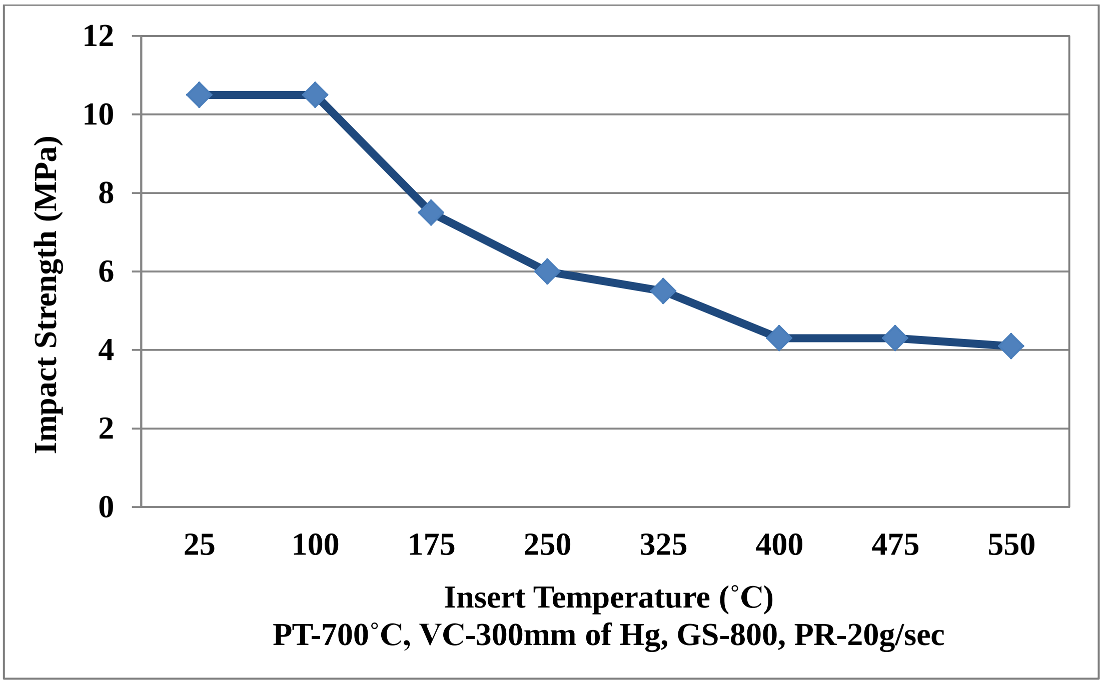

Figure 3.16 Plot of impact strength vs. insert temperature

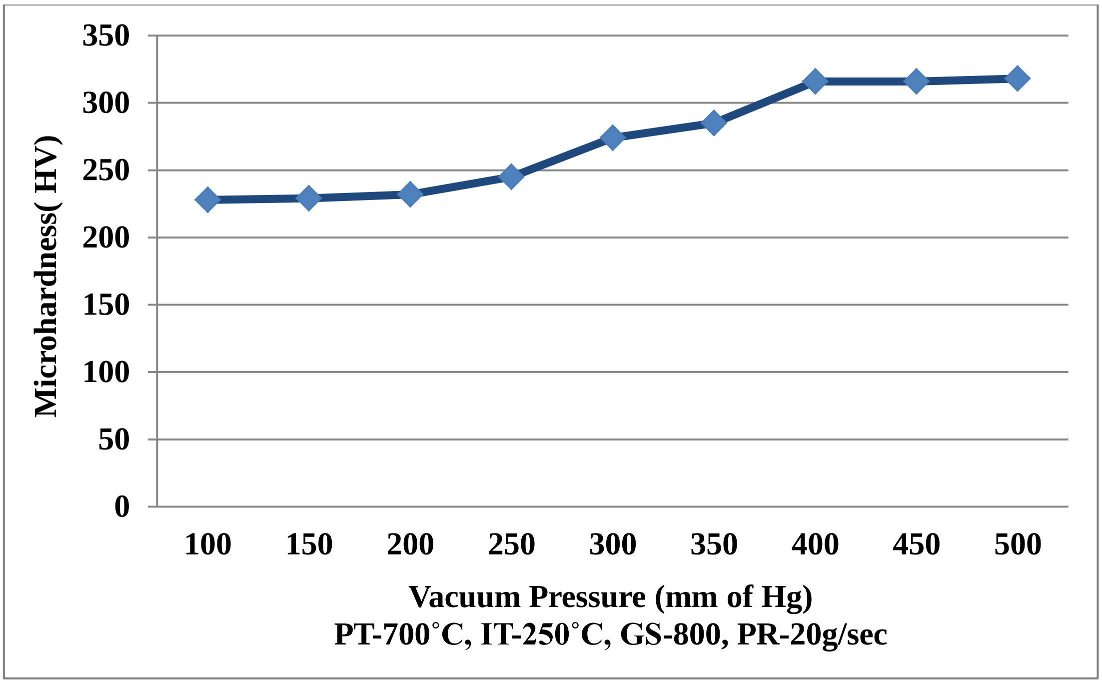

Figure 3.17 Plot of microhardness vs. insert temperature

3.4.4 Surface Roughness of Insert

The roughness of insert surface affects the diffusion between insert material and molten metal. Different roughness values can be obtained by grinding the insert with sand papers of different grit sizes. In the present wok, surface roughness of insert is measured in terms of the grit size of sand paper used for finishing the surface of insert. Values of shear strength, impact strength and microhardness varies with a variation of 400 to 1200 grit size of sand paper as shown in Figure 3.18 to Figure 3.20. Table 3.2 represents the chosen process parameters along with their ranges.

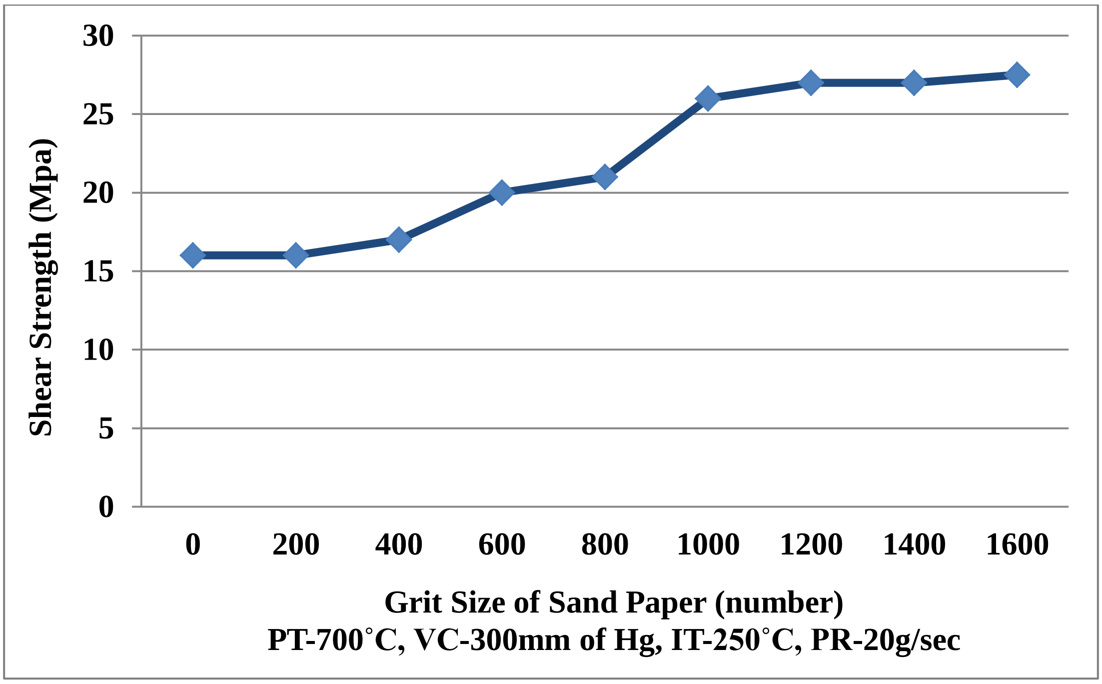

Figure 3.18 Plot of shear strength vs. grit size of sand paper

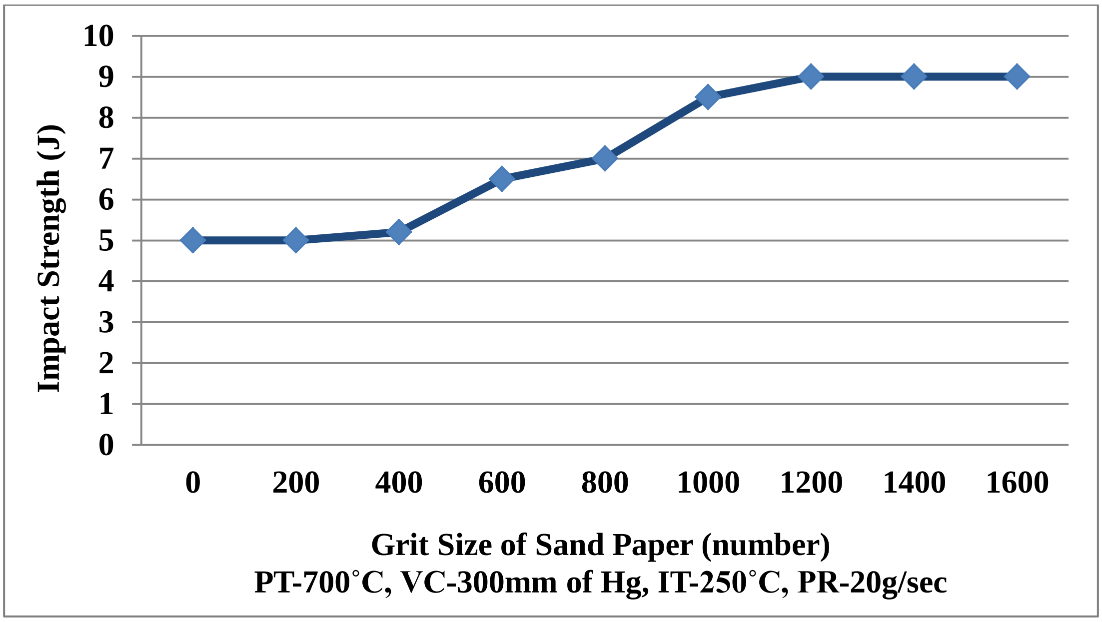

Figure 3.19 Plot of impact strength vs. grit size of sand paper

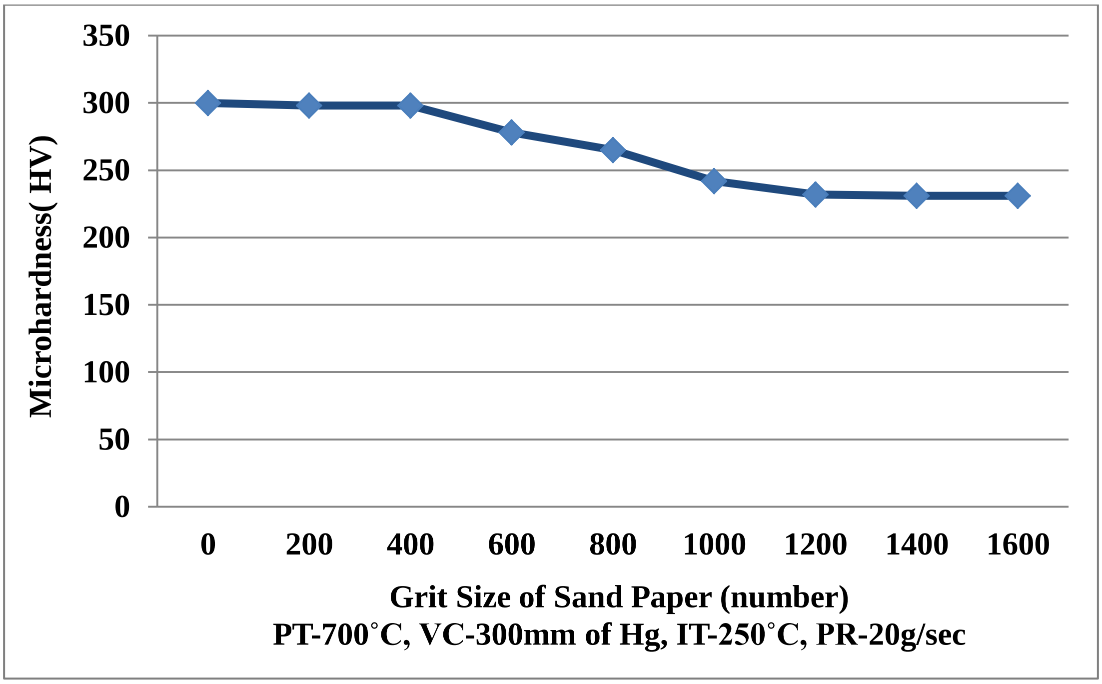

Figure 3.20 Plot of microhardness vs. grit size of sand paper

Table 3.2 Process parameters with their ranges

Parameter	Range	Level 1 Lowest -2	Level 2 Lower -1	Level 3 Medium 0	Level 4 Higher 1	Level 5 Highest 2
Pouring Temperature (˚C)	650-750	650	675	700	725	750
Vacuum Pressure (mm of Hg)	200-400	200	250	300	350	400
Insert Temperature (˚C)	100-400	100	175	250	325	400
Grit Size of Sand Paper (number) (Surface Roughness of Insert)	400-1200	400	600	800	1000	1200
Pouring Rate	Constant parameter – 20g/sec					

3.5 DESIGN OF EXPERIMENTS

Experimental runs are planned with the help of design of experiments method by considering the five levels of each process parameters. The central composite design approach of response surface methodology suggested the thirty experiments as represented in Table 3.3. Design expert software is used for this purpose.

Table 3.3 Design of experiments

Experiment No.	Pouring Temperature (^oC)	Vacuum Pressure (mm of Hg)	Insert Temperature (^oC)	Grit Size of Sand Paper (number)
1	675	250	175	600
2	725	250	175	600
3	675	350	175	600
4	725	350	175	600
5	675	250	325	600
6	725	250	325	600
7	675	350	325	600
8	725	350	325	600
9	675	250	175	1000
10	725	250	175	1000
11	675	350	175	1000
12	725	350	175	1000
13	675	250	325	1000
14	725	250	325	1000
15	675	350	325	1000
16	725	350	325	1000
17	650	300	250	800
18	750	300	250	800
19	700	200	250	800
20	700	400	250	800
21	700	300	100	800
22	700	300	400	800
23	700	300	250	400
24	700	300	250	1200
25	700	300	250	800
26	700	300	250	800
27	700	300	250	800
28	700	300	250	800
29	700	300	250	800
30	700	300	250	800

3.6 EXPERIMENTAL PROCEDURE OF VASMCC PROCESS

A356 alloy and pure magnesium are joined by vacuum assisted sand mold compound casting process. Figure 3.21 shows the schematic of VASMCC process. In this process, A356 alloy is used as insert material and pure magnesium as pouring metal. Cylindrical inserts having 20 mm diameter and 115 mm height are machined from A356 ingot. Silicon carbide sand papers of 400, 600, 800, 1000 or 1200 grit size are used to ground the lateral surface of insert. The insert is rinsed with acetone and placed in a horizontal muffle furnace for preheating. Mold cavity of 30 mm diameter and 100 mm height is prepared with the help of a wooden pattern in double wall molding box. Preheated insert is located into mold cavity and the cavity is covered with a circular sand disc of 50 mm diameter. The molding box is covered with a polyethylene film and vacuum is created with the help of a vacuum pump. Vertical muffle furnace is used to melt the magnesium up to the required temperature under MAGREX 36 covering flux. The molten magnesium is poured into the sprue cup to fill the mold cavity. Sufficient time is given to solidify the melt. After being cooled to the room temperature, the cast piece is removed from the mold. Flow process chart of VASMCC is shown in Figure 3.22. The prepared cast pieces (30 nos) are as shown in Figure 3.23 and close up of one of the cast pieces is shown in Figure 3.24.

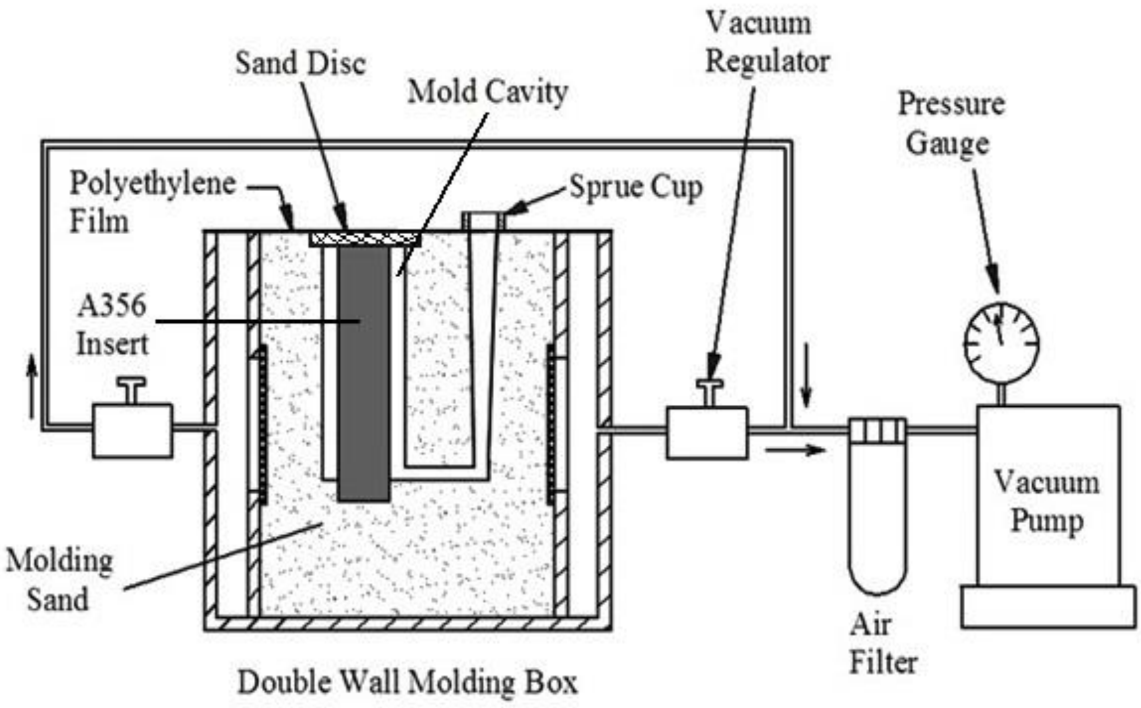

Figure 3.21 Schematic of vacuum assisted sand mold compound casting process

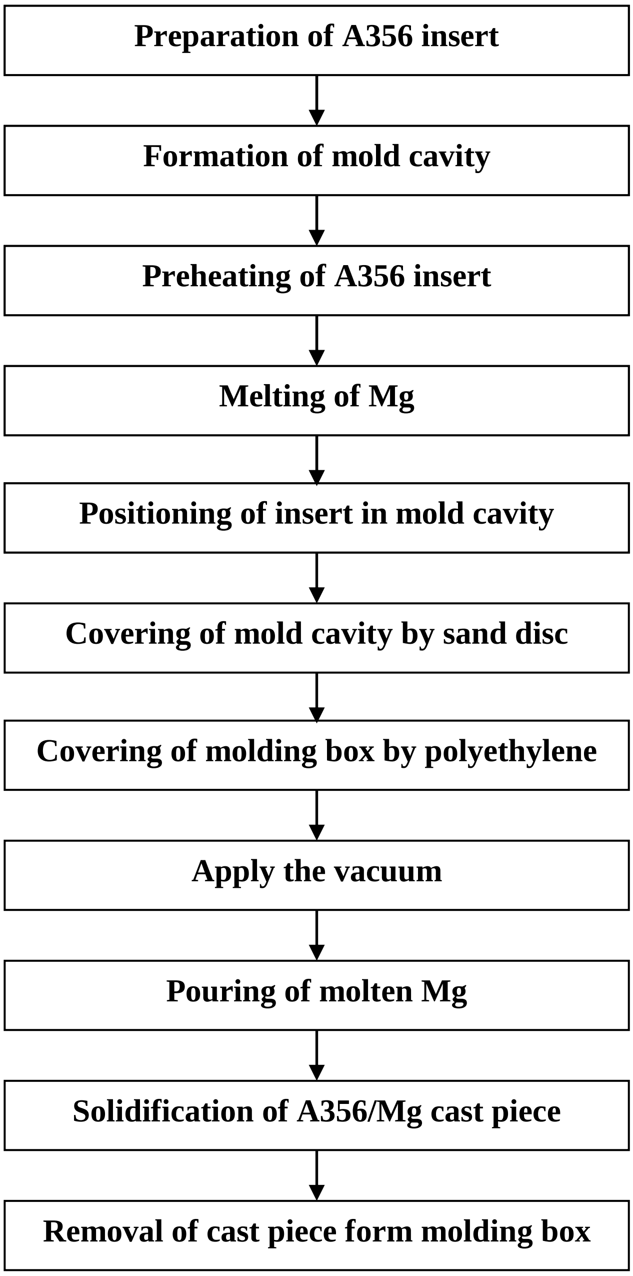

Figure 3.22 Flow process chart of vacuum assisted sand mold compound casting process

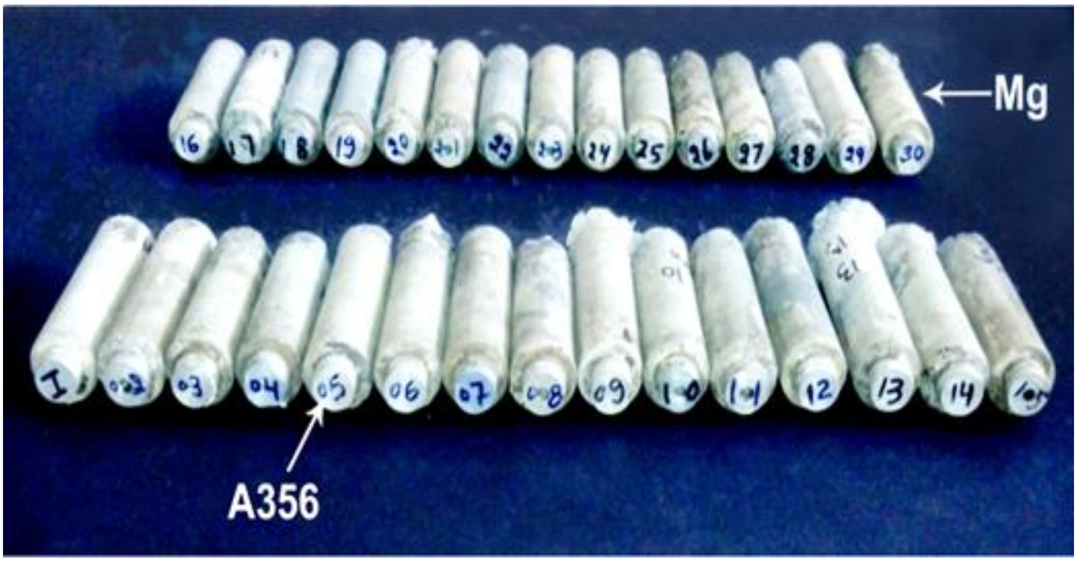

Figure 3.23 A356/Mg cast pieces produced by vacuum assisted sand mold compound casting process

Figure 3.24 Close up of one of the A356/Mg cast piece produced by vacuum assisted sand mold compound casting process

CHAPTER 4

RESULTS AND DISCUSSION

4.1 INTRODUCTION

This chapter deals with the characterization of A356/Mg joint interface by means of optical microscope, scanning electron microscope, energy dispersive X-ray spectroscopy and identification of the phase constitutions by X-ray diffractometer. Mechanism of interface formation is explained. Preparation of test specimens and the methods used for measurement of mechanical properties like shear strength, impact strength and microhardness of joint interface are discussed. RSM models for the shear strength, impact strength and microhardness are discussed. ANOVA is carried out for designated process parameters. The predicted values of shear strength, impact strength and microhardness are tabulated and effect of process parameters on the mechanical properties of joint interface is discussed in details.

4.2 CHARACTERIZATION OF JOINT INTERFACE

In order to characterize the microstructures of A356/Mg joint interface, the test specimens are cut and ground with SiC papers of 320, 600, 800, 1000, 1200 and 2000 grit size. The specimens are polished and etched with Keller's reagent. The interfacial microstructure is assessed by SEM and EDS. XRD is performed to identify the phase constitutions by taking a powdered sample from the joint interface. The sample is placed in a holder and illuminated with X-rays of fixed wavelength (1.54060 A°). Intensity of reflected radiation is recorded by goniometer. The compounds are identified by analyzing the peaks obtained.

4.2.1 Mechanism of A356/Mg Joint Interface Formation

In compound casting process, diffusion mechanism plays a vital role in mass transportation of the elements resulting in formation of layers with different composition. During this process, the surface layer of insert gets melted by the intense heat of molten metal. Due to which the elements are diffused together as a result of concentration gradient [95-97]. Figure 4.1 depicts the mechanism of joint formation between A356 alloy insert and Mg melt.

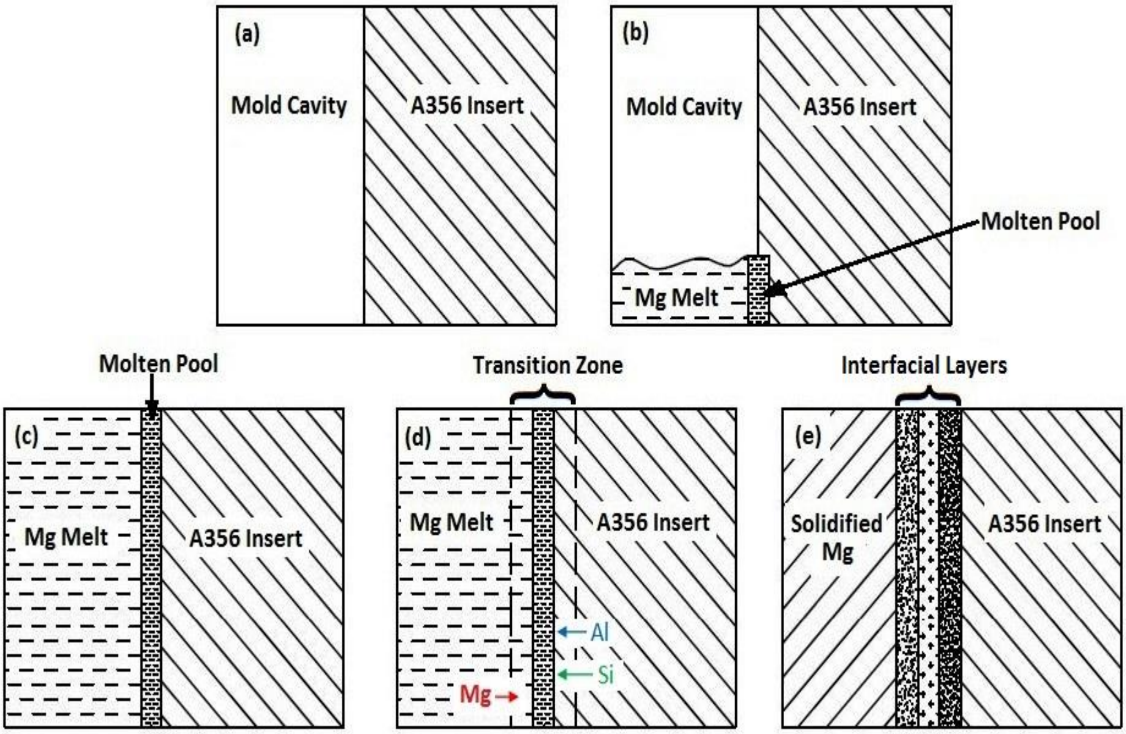

Figure 4.1 Mechanism of VASMCC process: (a) initial position, (b) pouring of Mg, (c) formation of molten pool, (d) diffusion of elements, and (e) solidification and interfacial layers formation

When magnesium melt is poured around A356 alloy insert, its surface gets melted due to the heat content of molten Mg. Molten pool is generated at the interface by mixing of A356 alloy and molten magnesium. Diffusion reaction takes place among the molten pool due to the concentration gradient of magnesium, aluminium and silicon elements. Consequently, a uniform joint interface consisting of three distinct layers formed after solidification as shown in optical micrograph Figure 4.2. The layer adjacent to A356 side composed of Mg_2Al_3, middle layer $Mg_{17}Al_{12}$ and the layer adjacent to Mg side composed of $Mg_{17}Al_{12} + \delta$ eutectic structure as shown in SEM micrograph Figure 4.3. The aluminium-magnesium binary phase diagram Figure 4.4 and XRD patterns Figure 4.5 to Figure 4.7 confirmed formation of these intermetallic compounds. Other researchers have also reported similar results in joining of Al/Mg by compound casting process [66, 80, 85, 98].

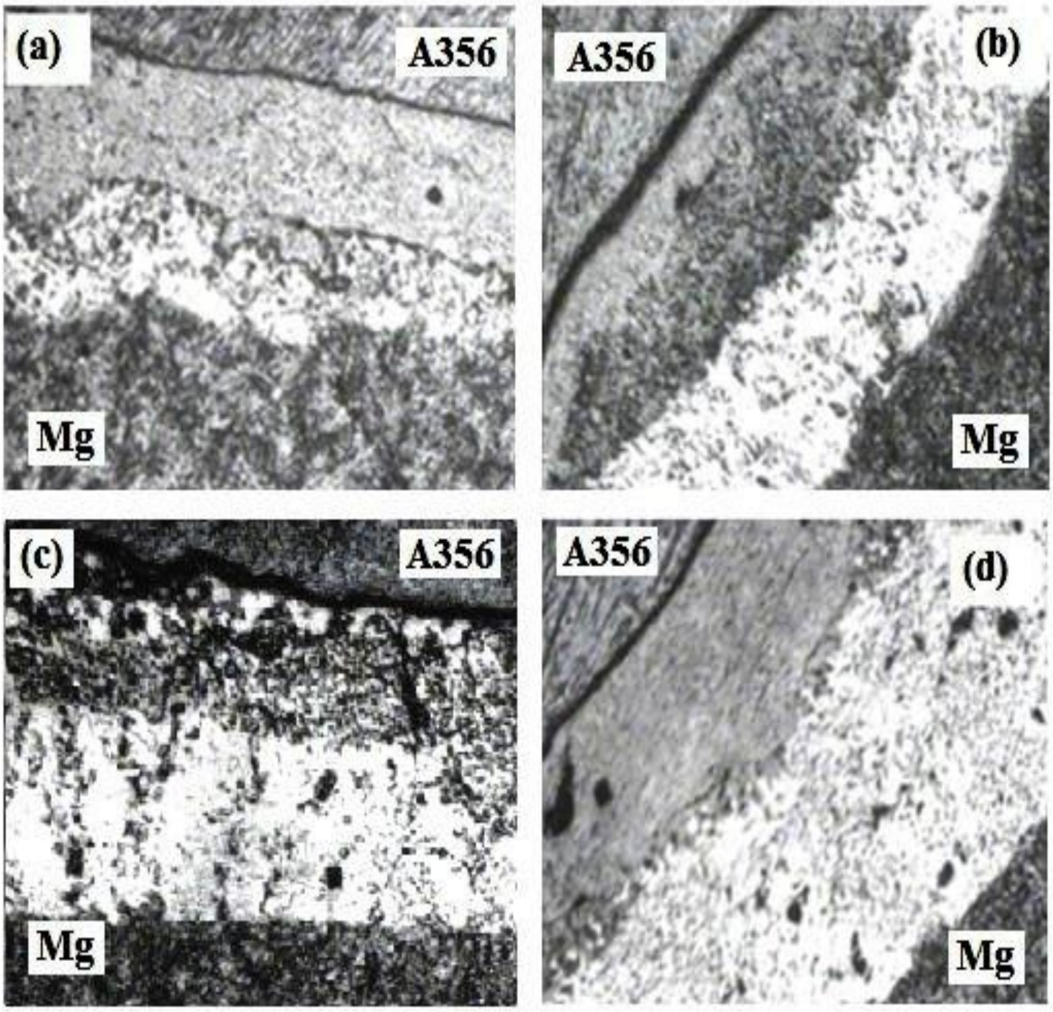

Figure 4.2 Optical micrographs of A356/Mg joint interfacial

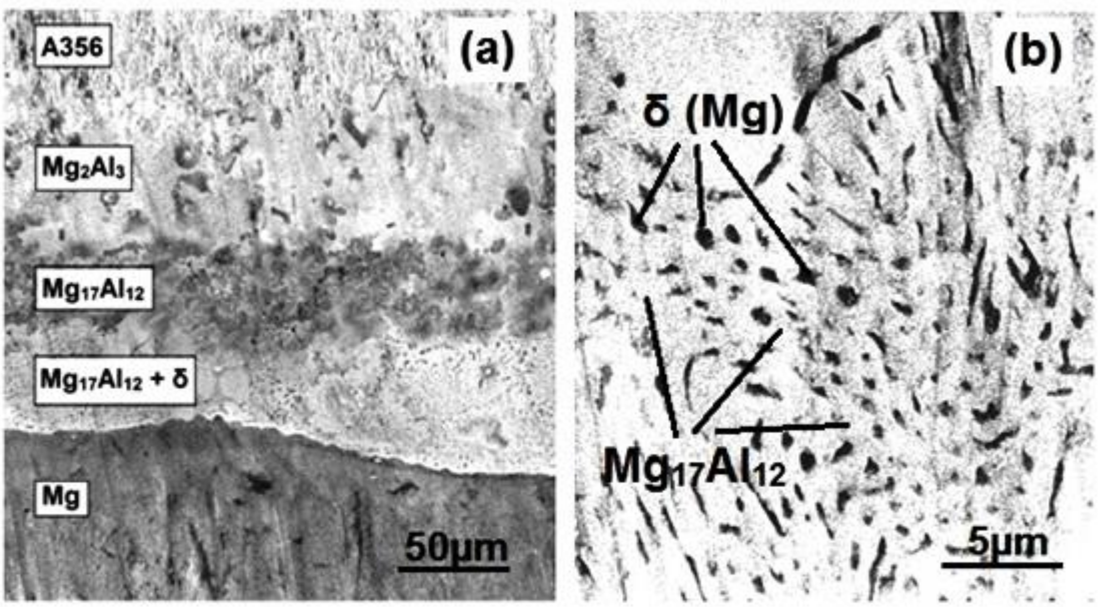

Figure 4.3 Interfacial microstructure of A356//Mg joint

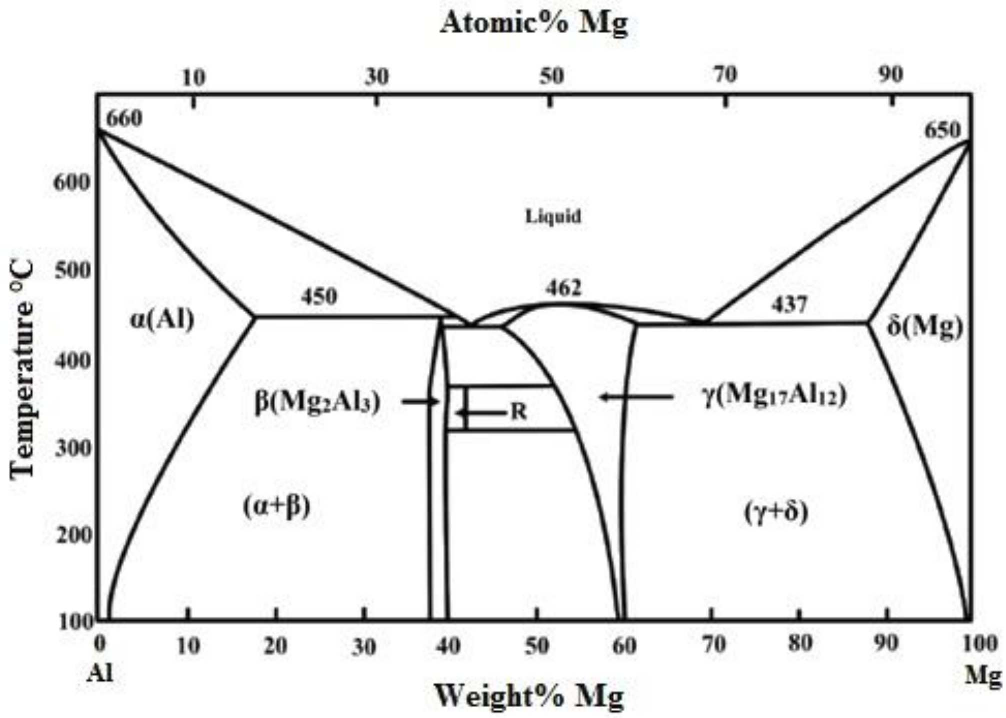

Figure 4.4 Al-Mg binary phase diagram [11]

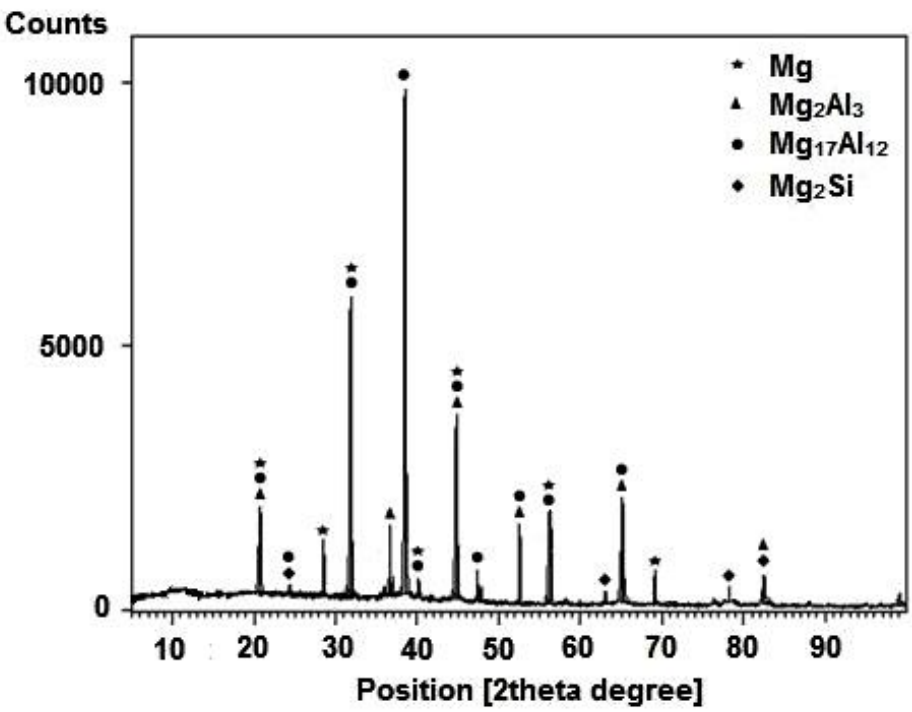

Figure 4.5 XRD pattern of A356/Mg joint interface produced by VASMCC process

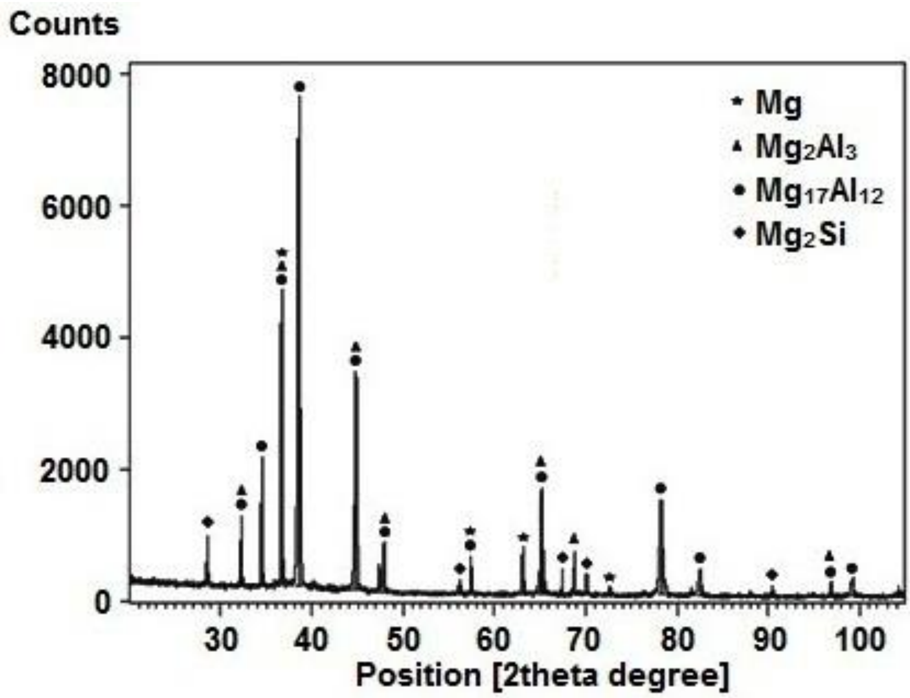

Figure 4.6 XRD pattern of A356/Mg joint interface produced by VASMCC process

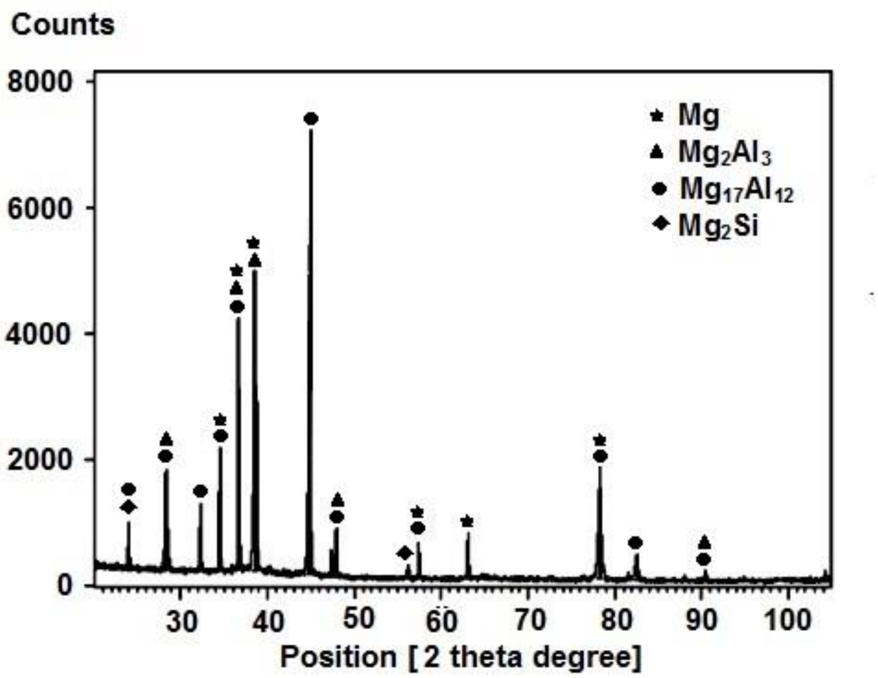

Figure 4.7 XRD pattern of A356/Mg joint interface produced by VASMCC process

A descriptive EDS map of Mg, Al, Si and O elements is shown in Figure 4.8 and Figure 4.9. As can be seen, the layers adjacent to magnesium and aluminium are rich in magnesium and aluminium respectively. At the middle layers, a concentration gradient of magnesium and aluminium elements exists. The magnesium content (green) gradually decreasing across the interface from bulk magnesium to aluminium and it is exactly vice versa for aluminium (blue). Moreover, it can be seen that silicon (yellow) is dispersed throughout the joint interface.

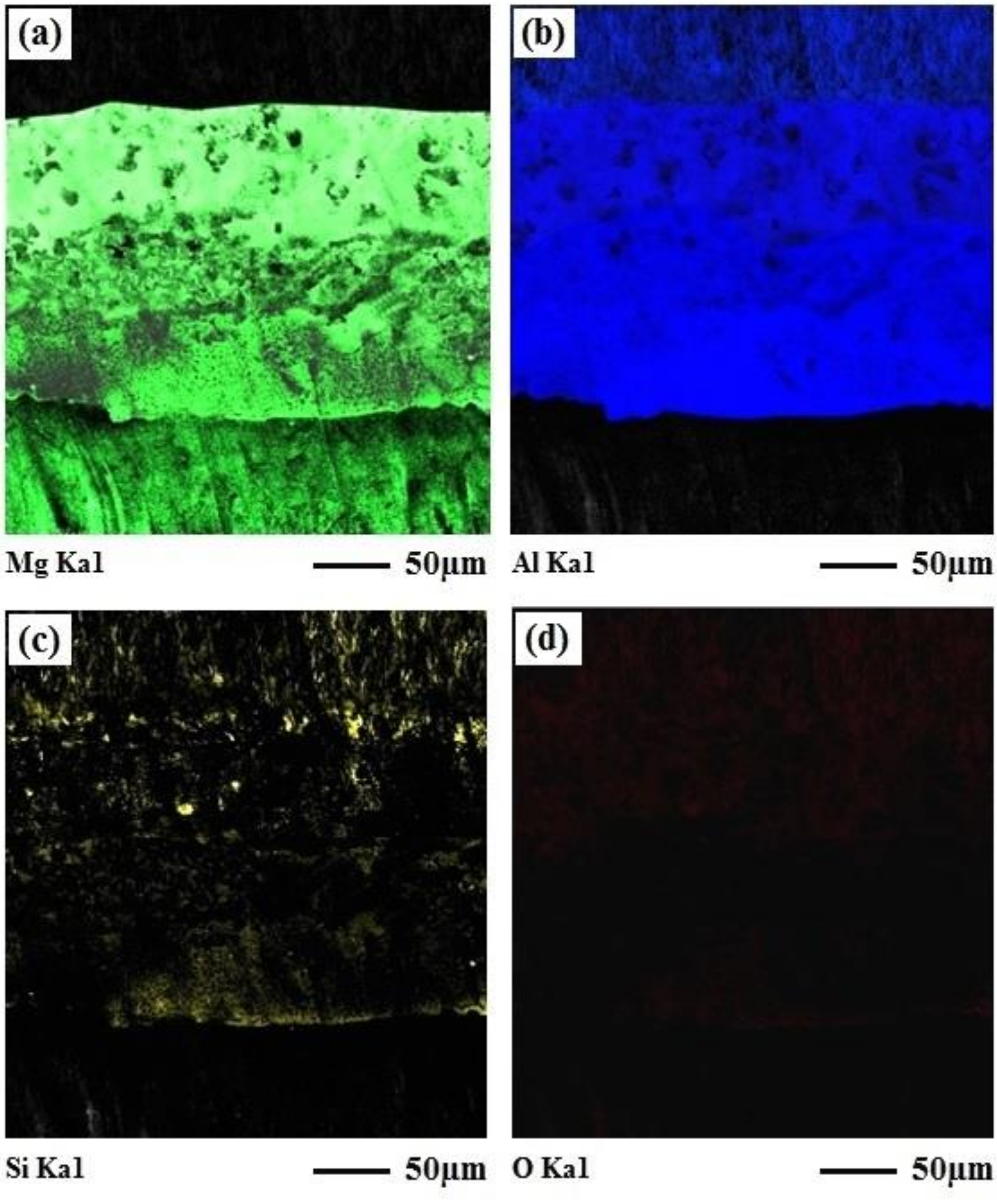

Fig. 4.8 EDS map of A356/Mg joint having distribution of (a) magnesium (b) aluminium, (c) silicon and (d) oxygen

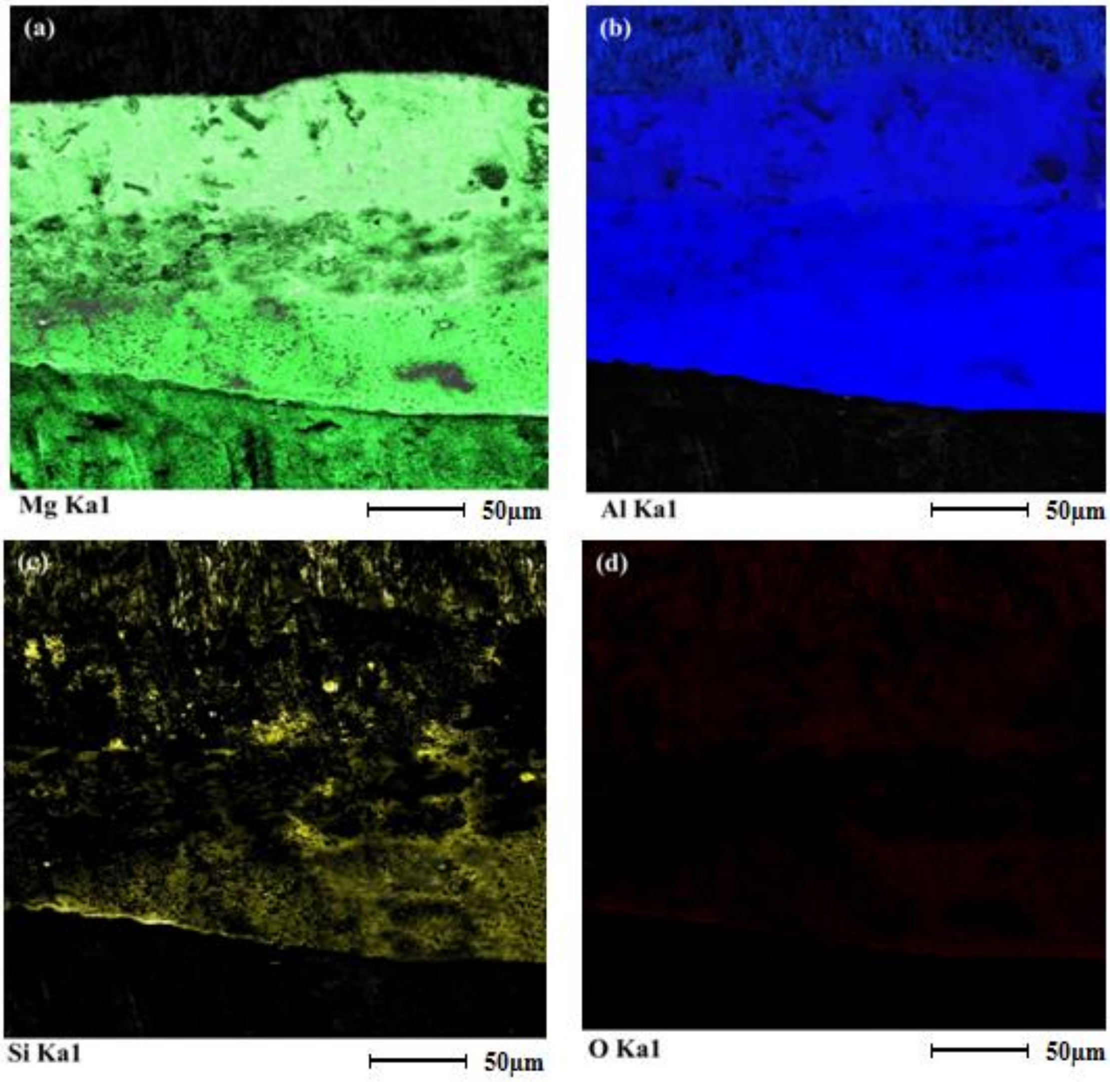

Fig. 4.9 EDS map of A356/Mg joint having distribution of (a) magnesium (b) aluminium, (c) silicon and (d) oxygen

4.3 MEASUREMENT OF MECHANICAL PROPERTIES

The mechanical properties of joint interface are measured experimentally by preparing the test specimen from A356/Mg compound cast pieces. Following properties are determined:

4.3.1 Shear Strength

Push out test is performed on A356/Mg compound cast pieces to measure the shear strength across the joint interface. Cylindrical test specimens of 10 mm thickness are cut from cast pieces perpendicular to their axis and finished with emery papers of 150-1200 grit size as shown in Figure 4.10. Test is carried out on electronics universal testing machine. The arrangement consists of a flat supporting die with a circular hole of 22 mm diameter and steel punch of 18 mm diameter. The specimens are placed on supporting die in such a way that the axis of punch, insert and circular hole of die are collinear as shown in Figure 4.11. The insert is pushed by the punch at a displacement rate of 0.5 mm/min. The following equation is used to determine the shear strength (SS) of joint interface [70].

$$SS = P_{max}/\pi.d.t \tag{4.1}$$

Where, P_{max} is the maximum load in N, d is the diameter of insert (20mm) and t is the thickness of specimen (10 mm). Calculated values of shear strength are represented in Table 4.1.

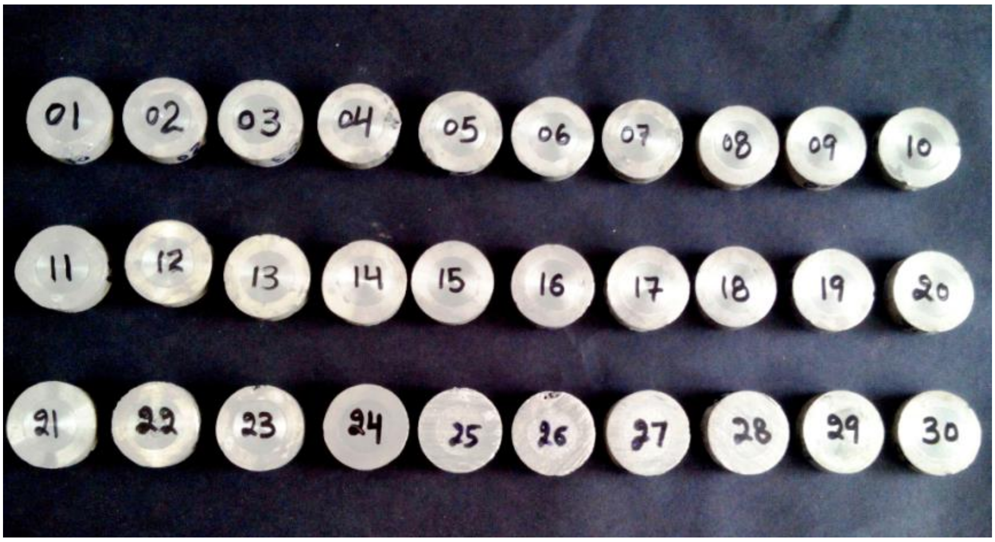

Fig. 4.10 Specimens for push out test

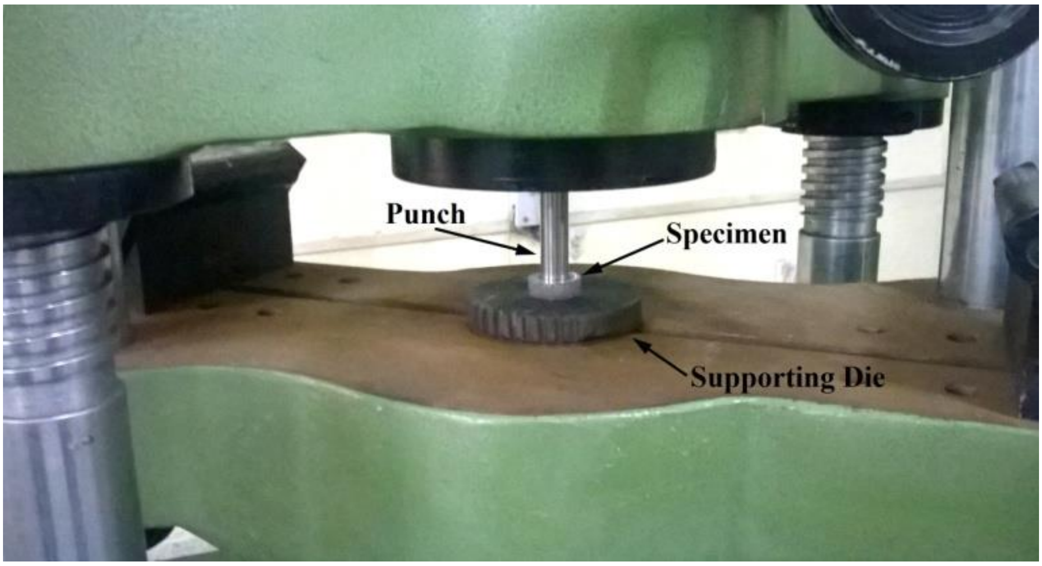

Fig. 4.11 Push out test arrangement

Table 4.1 Experimental values of shear strength

Exp. No.	Process Parameters				Ultimate Load of Push Out Test 'P_{max}' (KN)	Diameter of Insert 'd' (mm)	Thickness of Specimen 't' (mm)	Experimental Shear Strength $P_{max}/\pi.d.t$ (MPa)
	Pouring Temp. (˚C)	Vacuum Pressure (mm of Hg)	Insert Temp. (˚C)	Grit size of Sand paper (number)				
1	675	250	175	600	17.87	20	10	28.45
2	725	250	175	600	12.28	20	10	19.56
3	675	350	175	600	18.29	20	10	29.12
4	725	350	175	600	10.94	20	10	17.42
5	675	250	325	600	13.99	20	10	22.27
6	725	250	325	600	11.23	20	10	17.89
7	675	350	325	600	11.53	20	10	18.36
8	725	350	325	600	8.94	20	10	14.23
9	675	250	175	1000	15.19	20	10	24.19
10	725	250	175	1000	9.91	20	10	15.78
11	675	350	175	1000	20.81	20	10	33.14
12	725	350	175	1000	13.93	20	10	22.18
13	675	250	325	1000	11.78	20	10	18.76
14	725	250	325	1000	8.87	20	10	14.12
15	675	350	325	1000	16.38	20	10	26.09
16	725	350	325	1000	11.99	20	10	19.1
17	650	300	250	800	16.46	20	10	26.21
18	750	300	250	800	7.40	20	10	11.78
19	700	200	250	800	15.17	20	10	24.16
20	700	400	250	800	15.94	20	10	25.39
21	700	300	100	800	17.41	20	10	27.72
22	700	300	400	800	13.85	20	10	22.06
23	700	300	250	400	9.44	20	10	15.03
24	700	300	250	1200	10.81	20	10	17.21
25	700	300	250	800	15.15	20	10	24.12
26	700	300	250	800	15.20	20	10	24.21
27	700	300	250	800	15.93	20	10	25.36
28	700	300	250	800	15.19	20	10	24.19
29	700	300	250	800	14.71	20	10	23.42
30	700	300	250	800	15.23	20	10	24.25

4.3.2 Impact Strength

Charpy test is employed to measure the impact strength of cast pieces. Test specimens of 10x10 mm section having a length of 55 mm are cut from A356/Mg cast pieces as per ASTM E23 standard. The joint interface lies on the longitudinal axis of the specimen. A V-notch having 2 mm depth at 45^{o} angle with a tip radius of 0.25 mm is made at the middle of specimen perpendicular to the joint interface. The schematic of test specimen is shown in Figure 4.12. The prepared specimens are shown in Figure 4.13. Impact tests are performed on a pendulum type Charpy impact testing machine (Figure 4.14) having the capacity of 300 J. The determined values of impact strength for test specimens are shown in Table 4.2.

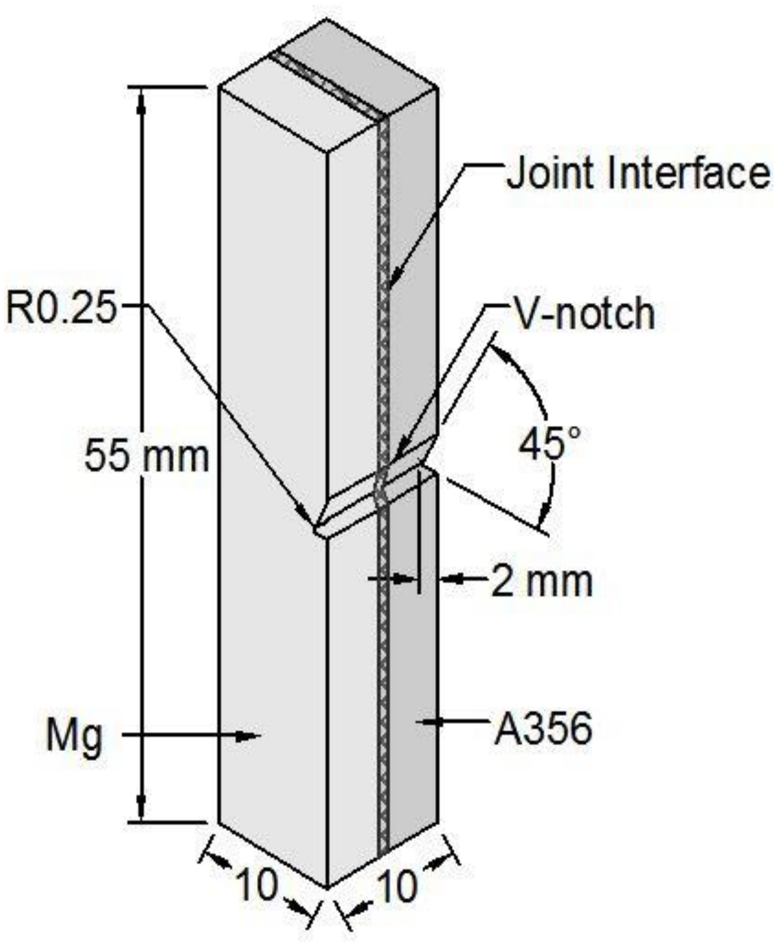

Figure 4.12 Schematic of Charpy impact test specimen

Figure 4.13 Specimens for Charpy impact test

Figure 4.14 Charpy impact testing machine

Table 4.2 Experimental values of impact strength

Exp. No.	Process Parameters				Experimental Impact Strength (J)
	Pouring Temperature (˚C)	Vacuum Pressure (mm of Hg)	Insert Temperature (˚C)	Grit size of Sand paper (number)	
1	675	250	175	600	7.5
2	725	250	175	600	6.5
3	675	350	175	600	8.0
4	725	350	175	600	6.0
5	675	250	325	600	8.0
6	725	250	325	600	4.5
7	675	350	325	600	8.0
8	725	350	325	600	4.0
9	675	250	175	1000	8.0
10	725	250	175	1000	7.5
11	675	350	175	1000	9.0
12	725	350	175	1000	7.5
13	675	250	325	1000	9.0
14	725	250	325	1000	6.5
15	675	350	325	1000	10.5
16	725	350	325	1000	6.0
17	650	300	250	800	8.5
18	750	300	250	800	4.5
19	700	200	250	800	10.0
20	700	400	250	800	10.5
21	700	300	100	800	7.0
22	700	300	400	800	5.5
23	700	300	250	400	4.0
24	700	300	250	1200	6.5
25	700	300	250	800	6.5
26	700	300	250	800	6.0
27	700	300	250	800	6.5
28	700	300	250	800	6.0
29	700	300	250	800	6.5
30	700	300	250	800	6.5

4.3.3 Microhardness

In order to measure the microhardness of A356/Mg compound cast pieces across the joint interface, the cylindrical test specimens of 10 mm thickness are cut perpendicular to their axis. The test specimens are ground with emery papers of grit size 150, 320, 600, 800, 1200, 1500, 2000 & 2500 and then finished on polishing machine by using aluminium-oxide powder. The prepared specimens are shown in Figure 4.15. Vickers microhardness at joint interface is determined by using ‘Mitutoyo’ hardness tester with 50g test load and 20 sec holding time. Determined values are represented in Table 4.3.

Figure 4.15 Specimens for microhardness testing

Table 4.3 Experimental values of microhardness

Exp. No.	Process Parameters				Experimental Microhardness (HV)
	Pouring Temperature (˚C)	Vacuum Pressure (mm of Hg)	Insert Temperature (˚C)	Grit size of Sand paper (number)	
1	675	250	175	600	303.54
2	725	250	175	600	276.86
3	675	350	175	600	300.02
4	725	350	175	600	245.36
5	675	250	325	600	281.68
6	725	250	325	600	251.23
7	675	350	325	600	322.15
8	725	350	325	600	267.06
9	675	250	175	1000	279.63
10	725	250	175	1000	263.35
11	675	350	175	1000	276.12
12	725	350	175	1000	231.86
13	675	250	325	1000	258.63
14	725	250	325	1000	240.16
15	675	350	325	1000	300.56
16	725	350	325	1000	254.79
17	650	300	250	800	284.03
18	750	300	250	800	217.56
19	700	200	250	800	269.85
20	700	400	250	800	280.13
21	700	300	100	800	279.15
22	700	300	400	800	281.41
23	700	300	250	400	299.19
24	700	300	250	1200	263.34
25	700	300	250	800	281.96
26	700	300	250	800	280.98
27	700	300	250	800	281.42
28	700	300	250	800	280.76
29	700	300	250	800	280.89
30	700	300	250	800	280.12

4.4 RESPONSE SURFACE METHODOLOGY

RSM is a widely accepted tool in the field of quality engineering. It includes the collection of statistical and mathematical techniques, which can be adopted for empirical modeling, analysis and optimization of the process. Its objective is to optimize the output variable (response) which is exaggerated by a number of independent input variables [99-101]. It is employed to solve and determine the multi-parameter equation by taking exact quantitative experimental data simultaneously. During the execution of RSM, a series of experiments are performed by varying the input variables and the reasons for change in output response are identified and analyzed [102-105]. Model formation in RSM is elaborated in appendix-II

The RSM models are developed separately for the response characteristics i.e., shear strength (SS), impact strength (IS) and microhardness (MH). These models are represented by a second-order response surface which could be expressed as a function of vacuum assisted sand mold compound casting process parameters i.e., pouring temperature (PT), vacuum pressure (VC), insert temperature (IT) and grit size of sand paper (GS). The correlation between response characteristic (output) and the input process parameters is symbolized as:

$$\begin{aligned} SS \text{ or } IS \text{ or } MH = {} & \beta_0 + \beta_1 (PT) + \beta_2 (VC) + \beta_3 (IT) + \beta_4 (GS) + \beta_5 (PT)^\wedge 2 + \beta_6 \\ & (VC)^\wedge 2 + \beta_7 (IT)^\wedge 2 + \beta_8 (GS)^\wedge 2 + \beta_9 (PT*VC) + \beta_{10} (VC*IT) + \beta_{11} \\ & (IT*GS) + \beta_{12} (GS*PT) + \beta_{13} (PT*IT) + \beta_{14} (VC*GS) + \varepsilon \end{aligned} \tag{4.2}$$

In RSM, the generated model is either significant or non-significant. A significant model validates the reliability of conducted experiments. Analysis of variance (ANOVA) is performed for this purpose. ANOVA identify the parameters that are statistically significant. It validates the model results and check that conducted experiments are accurate and the adopted experimental method is reliable. In present research, separate RSM models for output characteristics; shear strength, impact strength and microhardness is generated and ANOVA is carried out by considering process parameters.

4.5 RSM MODEL FOR SHEAR STRENGTH

The coefficients of second-order regression equation are determined from experimental data. The regression equation obtained by response surface methodology as a function of four input process parameters (pouring temperature, vacuum pressure, insert temperature and grit size of sand paper) subjected to the response characteristic, shear strength is represented as:

$$SS = -769.45144 + 2.63608*PT - 0.148586*VC - 0.44473*IT + 0.000660667*PT*IT - 0.000152333*VC*IT + 0.000255295*VC*GS - 0.00210*(PT)^2 - 0.000046601*(GS)^2 \quad (4.3)$$

The results of second-order response surface quadric model fitting in the form of ANOVA after neglecting the insignificant parameters for impact strength of compound casting are mentioned in Table 4.4.

Table 4.4 Analysis of variance for shear strength – values of coded and real coefficients with F ratio for significant terms

Source	Sum of Squares	Degree of freedom	Mean Square	F Value	P Value (Prob. > F)	
Model	723.87	8	90.48	73.62	< 0.0001	Significant
A - PT	329.75	1	329.75	268.27	< 0.0001	
B - VC	18.52	1	18.52	15.06	0.0009	
C - IT	105.59	1	105.59	85.9	< 0.0001	
AC - PT * IT	24.55	1	24.55	19.97	0.0002	
BC - VC * IT	5.22	1	5.22	4.25	0.0519	
BD - VC * GS	84.18	1	84.18	68.49	< 0.0001	
A^2 – PT^2	51.05	1	51.05	41.53	< 0.0001	
D^2 – GS^	120.52	1	120.52	98.06	< 0.0001	
Residual	25.81	21	1.23			
Lack of Fit	23.87	16	1.49	3.84	0.0719	Not Significant
Pure Error	1.94	5	0.39	-		
Cor Total	749.68	29	-			
Standard deviation	1.11	R-Squared			0.9656	
Mean	21.86	Adjusted R-Squared			0.9525	
Co-eff. of variation%	5.07	Predicted R-Squared			0.9259	
PRESS	55.52	Adequate Precision			33.200	
Significant at 95% confidence level.						

P-value (“Prob. > F’’) less than 0.05 indicates that model terms are statistically significant at 95% confidence level. It is desirable as it indicates that the terms in model have the significant effect on the response. In the present model, pouring temperature (PT), vacuum (VC), and insert temperature (IT); interaction effect of pouring temperature and insert temperature (PT.IT), vacuum pressure and insert temperature (VC.IT), vacuum pressure and grit size of sand paper (VC.GS), and second order term of pouring temperature (PT^2) and grit size of sand paper (GS^2) have the significant effect. The rest of the terms are insignificant. The lack-of-fit is not significant relative to the pure error, as it is desired.

The R^2 is the ratio of variability explained by the model to the total variability in actual data. This is used to measure the goodness of fit. The value of R^2 as unity indicates the best result in terms of model. The calculated value of R^2 (0.9656) verifies that the relationship between the selected process parameters and response (shear strength) can be adequately described by the model. The adjusted R^2 value is particularly useful when comparing models with different number of terms. This comparison is, however, done in the background when model reduction is taking place. The value of adjusted R^2 (0.9525) is also high, which indicates a high level of accuracy of model. The value of predicted R^2 (0.9259) indicates a reasonable agreement with that of adjusted R^2. Adequate precision compares the range of predicted values at the design points to the average prediction error. It indicates the signal to noise (S/N) ratio. The value of S/N ratio greater than 4 implies that the model is fit to proceed further. Adequate precision (33.20) indicates an adequate signal in compound casting process. At the same condition, relatively lower value of standard deviation (1.11) and coefficient of variation (5.07%) indicates better precision and reliability of the conducted experiments. The normal probability plot of the residuals as shown in Figure 4.16 for shear strength reveals that the residuals are falling on the straight line, which means the errors, are distributed normally.

The experimental values of shear strength obtained by push out test and regression model values obtained from Equation 4.3 are represented in Table 4.5. Figure 4.17 represents the relationship between predicted and actual value of shear strength. Comparison between experimental and regression results of shear strength is elaborated in Figure 4.18. It indicates that regression model and experimental values of shear strength follow a similar pattern. Further, the results predicted by regression model are quite closer to the experimental results.

Table 4.5 Shear strength values by experimentation and regression model

Exp. No.	Process Parameters				Shear Strength by Experiment (MPa)	Shear Strength by Regression Model (MPa)
	Pouring Temp. (˚C)	Vacuum Pressure (mm of Hg)	Insert Temp. (˚C)	Grit size of Sand paper (number)		
1	675	250	175	600	28.45	31.02
2	725	250	175	600	19.56	21.60
3	675	350	175	600	29.12	28.81
4	725	350	175	600	17.42	19.40
5	675	250	325	600	22.27	25.49
6	725	250	325	600	17.89	21.03
7	675	350	325	600	18.36	21.00
8	725	350	325	600	14.23	16.54
9	675	250	175	1000	24.19	26.72
10	725	250	175	1000	15.78	17.31
11	675	350	175	1000	33.14	34.73
12	725	350	175	1000	22.18	25.31
13	675	250	325	1000	18.76	21.19
14	725	250	325	1000	14.12	16.73
15	675	350	325	1000	26.09	26.92
16	725	350	325	1000	19.1	22.45
17	650	300	250	800	26.21	28.38
18	750	300	250	800	11.78	14.50
19	700	200	250	800	24.16	24.93
20	700	400	250	800	25.39	28.45
21	700	300	100	800	27.72	30.89
22	700	300	400	800	22.06	22.50
23	700	300	250	400	15.03	18.43
24	700	300	250	1200	17.21	20.05
25	700	300	250	800	24.12	26.69
26	700	300	250	800	24.21	26.69
27	700	300	250	800	25.36	26.69
28	700	300	250	800	24.19	26.69
29	700	300	250	800	23.42	26.69
30	700	300	250	800	24.25	26.69

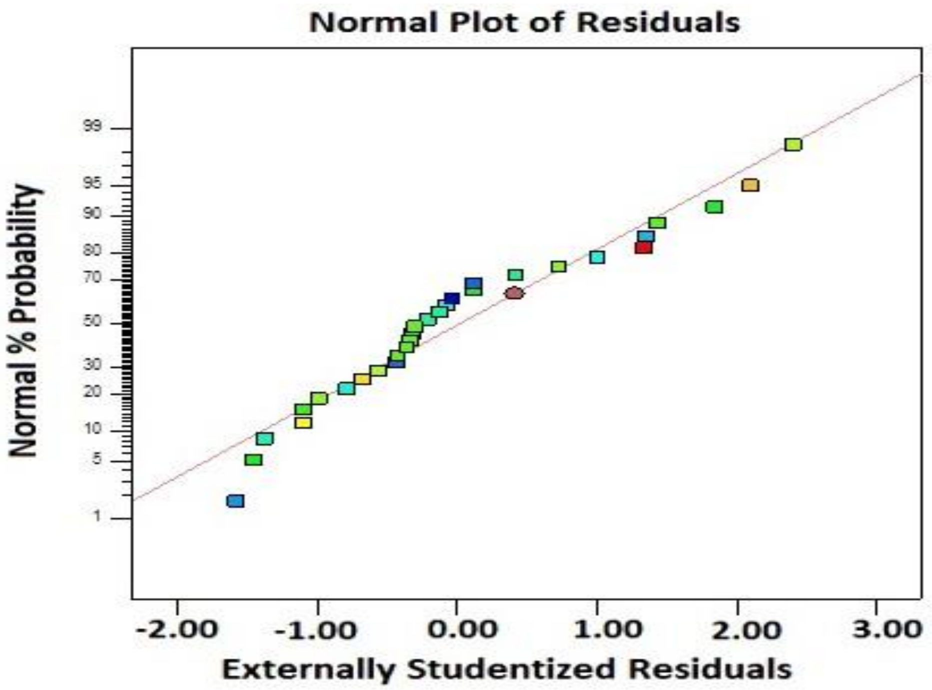

Figure 4.16 Plot of normal probability of residuals for shear strength

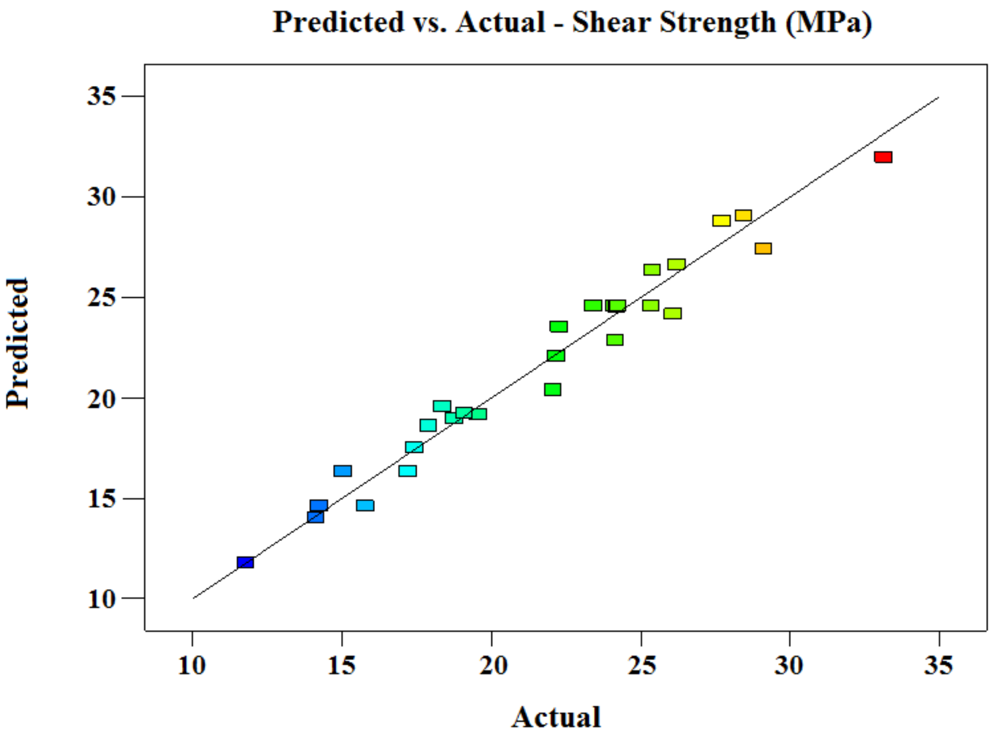

Figure 4.17 Plot of predicted vs. actual for shear strength

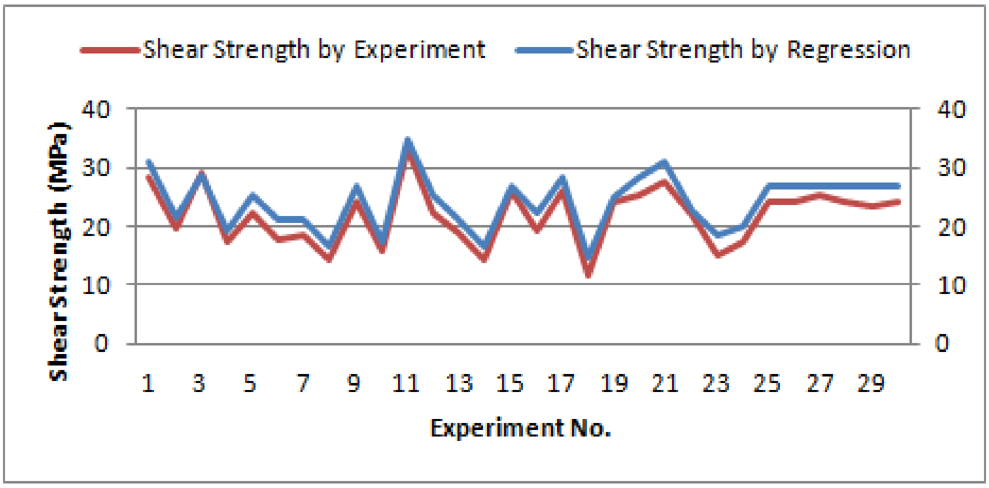

Figure 4.18 Comparison of experimental and regression model values of shear strength

4.6 EFFECT OF PROCESS PARAMETERS ON SHEAR STRENGTH

The 3D surface plots as shown in Figure 4.19 (a-c) indicates the combined effect of process parameters on shear strength of joint interface. Figure 4.19 (a and b) shows that by increasing the pouring and insert temperature, shear strength decreased. This may be due to the effect that increase in pouring and insert temperature, increases the solidification time. A coarse grain structure is obtained with longer solidification time which implies a low value of shear strength [106]. Figure 4.19 (b) reperesents that shear strength is increased with increase in vacuum pressure. This may be due to the fact that increase in the degree of vacuum increases the degree of compaction of sand aggregates. Higher degree of compaction implies the effective contact area of sand particles to be more. This results in increased cooling rate and hence decreases the dendritic arm spacing. Dendritic arm spacing has the opposite relationship with mechanical properties. Consequently, the shear strength is increased. Figure 4.19 (c) reflects that grit size of sand paper (surface roughness of insert) doesn’t have a significant effect on shear strength in existence of other parameters (pouring temperature, degree of vacuum and insert temperature). Moreover, at the high value of vacuum (350 mm of Hg), the shear strength tends to increase with increase in grit size of sand paper whereas at the low value of vacuum pressure (250 mm of Hg), shear strength tends to decrease with increase in grit size of sand paper.

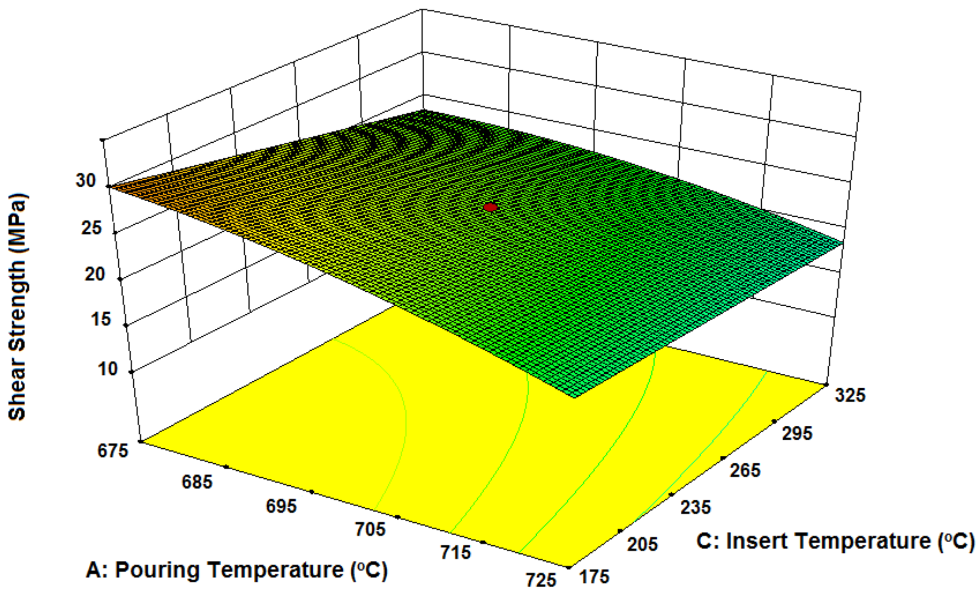

Figure 4.19 (a) Effect of pouring and insert temperature on shear strength

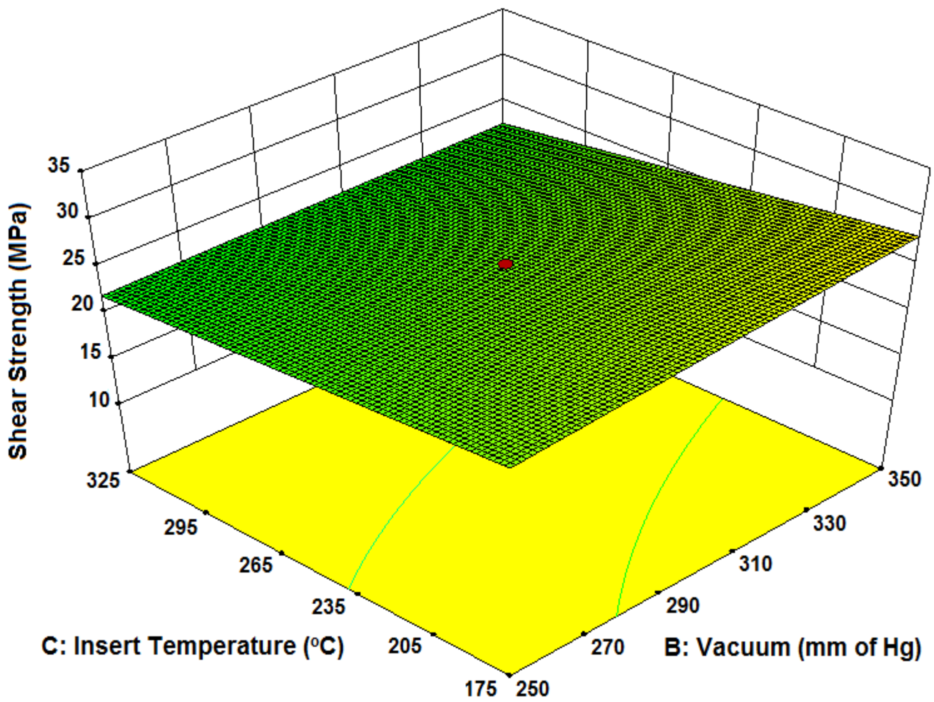

Figure 4.19 (b) Effect of insert temperature and vacuum pressure on shear strength

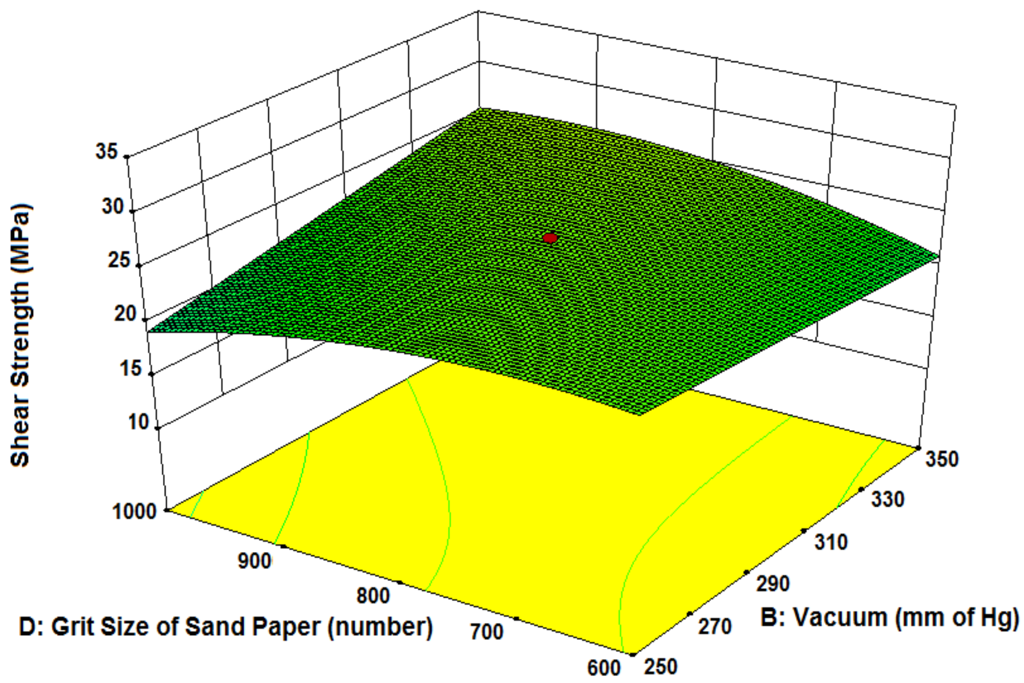

Figure 4.19 (c) Effect of grit size of sand paper and vacuum pressure on shear strength

4.7 RSM MODEL FOR IMPACT STRENGTH

The mathematical regression model created by using Design Expert software established the relationship between impact strength (response) and process parameters (input variables). The collected experimental data is used to develop this model. The regression equation in terms of actual factors obtained for impact strength of joint interface is as below:

$$IS = -54.80128 + 0.13241*PT + 0.20639*IT + 0.00977638*GS - 0.0003302*PT*VC - 0.00031606*PT*IT + 0.0000145833*IT*GS + 0.000388875*(VC)^2 - 0.00000624045*(GS)^2 \quad (4.4)$$

The results of second-order response surface quadric model fitting in the form of ANOVA, after neglecting the insignificant parameters for impact strength of compound casting, are mentioned in Table 4.6. The P-value ("Prob. > F'') less than 0.05 indicates that model terms are statistically significant at 95% confidence level. It is desirable as it indicates that the terms in model have the significant effect on the response. In the present model, pouring temperature (PT), insert temperature (IT) and grit size of sand paper (GS); interaction effect of pouring temperature and vacuum pressure (PT.VC), pouring temperature and insert temperature (PT.IT), insert temperature and grit size of sand paper (IT.GS), and second order term of vacuum pressure (VC^2) and grit size of sand paper (GS^2) have the significant effect. The rest of the terms are insignificant. The lack-of-fit is not significant relative to the pure error, as it is desired.

Table 4.6 Analysis of variance for impact strength – values of coded and real coefficients with F ratio for significant terms

Source	Sum of Squares	Degree of freedom	Mean Square	F-Value	P-Value Prob. > F	
Model	84.64	8	10.58	95.38	< 0.0001	Significant
A - PT	31.51	1	31.51	284.07	< 0.0001	
C - IT	1.76	1	1.76	15.87	0.0007	
D - GS	11.34	1	11.34	102.26	< 0.0001	
AB - PT *VC	1.27	1	1.27	11.41	0.0028	
AC - PT *IT	5.64	1	5.64	50.85	< 0.0001	
CD - IT*GS	0.77	1	0.77	6.9	0.0157	
B^2 – VC^2	28.67	1	28.67	258.44	< 0.0001	
D^2 – GS^2	1.72	1	1.72	15.53	0.0007	
Residual	2.33	21	0.11			
Lack of Fit	2	16	0.12	1.87	0.2526	Not Significant
Pure Error	0.33	5	0.067	-		
Cor Total	86.97	29	-			
Standard deviation	0.33	R-Squared			0.9732	
Mean	7.03	Adjusted R-Squared			0.9630	
Coefficient of variation%	4.74	Predicted R-Squared			0.9399	
PRESS	5.23	Adequate Precision			35.389	
Significant at 95% confidence level.						

The R^2 is the ratio of variability explained by the model to the total variability in actual data. This is used to measure the goodness of fit. The value of R^2 as unity indicates the best result in terms of model. The calculated value of R^2 (0.9732) verifies that the relationship between the selected process parameters and response (impact strength) can be adequately described by the model. The adjusted R^2 value is particularly useful when comparing models with different number of terms. This comparison is, however, done in the background when model reduction is taking place. The value of adjusted R^2 (0.963) is also high, which indicates a high level of accuracy of model. The value of predicted R^2 (0.9399) indicates a reasonable agreement with that of adjusted R^2. Adequate precision compares the range of predicted values at the design points to the average prediction error. It indicates the signal to noise (S/N) ratio. The value of S/N ratio greater than 4 implies that the model is fit to proceed further. Adequate precision (35.389) indicates an adequate signal in compound casting process. At the same condition, relatively lower value of standard deviation (0.33) and coefficient of variation (4.74%) indicates better precision and reliability of the conducted experiments. The normal probability plot of the residuals (Figure 4.20) for impact strength reveals that the residuals are falling on the straight line, which means the errors are distributed normally.

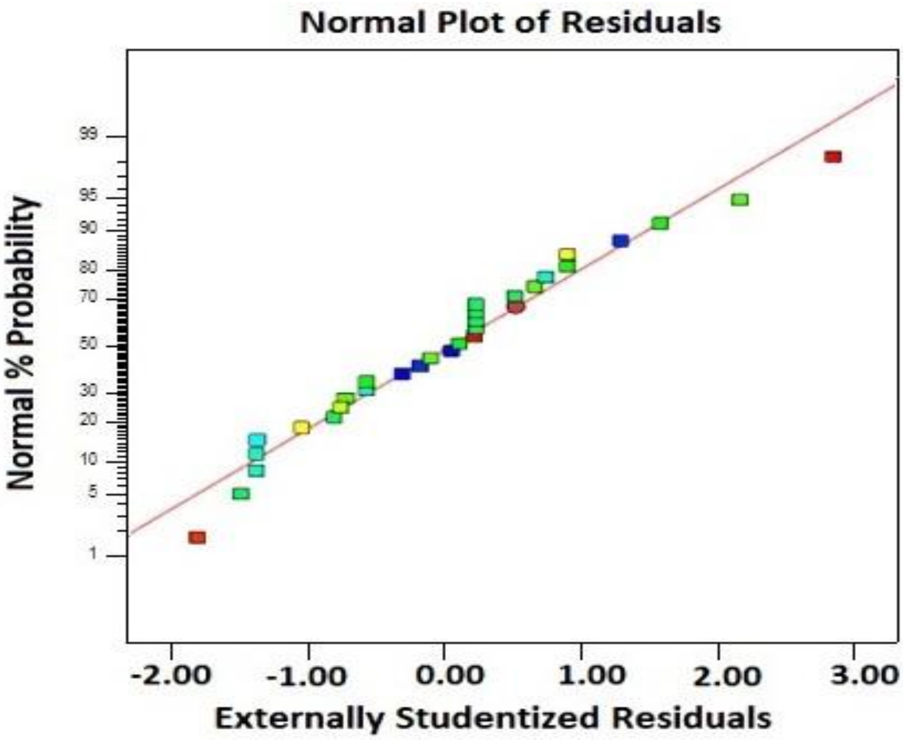

Figure 4.20 Plot of normal probability of residuals for impact strength

The experimental values of impact strength obtained by Charpy test and the regression model values obtained from Equation 4.4 are represented in Table 4.7.

Table 4.7 Impact strength values by experimentation and regression model

Exp. No.	Process Parameters				Impact Strength by Experiment (J)	Impact Strength by Regression Model (J)
	Pouring Temp. (˚C)	Vacuum Pressure (mm of Hg)	Insert Temp. (˚C)	Grit size of Sand paper (number)		
1	675	250	175	600	7.5	7.09
2	725	250	175	600	6.5	6.82
3	675	350	175	600	8	8.14
4	725	350	175	600	6	6.21
5	675	250	325	600	8	7.36
6	725	250	325	600	4.5	4.72
7	675	350	325	600	8	8.41
8	725	350	325	600	4	4.11
9	675	250	175	1000	8	8.03
10	725	250	175	1000	7.5	7.76
11	675	350	175	1000	9	9.07
12	725	350	175	1000	7.5	7.15
13	675	250	325	1000	9	9.18
14	725	250	325	1000	6.5	6.53
15	675	350	325	1000	10.5	10.22
16	725	350	325	1000	6	5.93
17	650	300	250	800	8.5	8.86
18	750	300	250	800	4.5	4.29
19	700	200	250	800	10	10.24
20	700	400	250	800	10.5	10.68
21	700	300	100	800	7	7.05
22	700	300	400	800	5.5	6.10
23	700	300	250	400	4	4.20
24	700	300	250	1200	6.5	6.95
25	700	300	250	800	6.5	6.57
26	700	300	250	800	6	6.57
27	700	300	250	800	6.5	6.57
28	700	300	250	800	6	6.57
29	700	300	250	800	6.5	6.57
30	700	300	250	800	6.5	6.57

The values of impact strength as observed at the A356/Mg joint interface, lies between 4 to 10.5 J while 6 and 10 J at base metals A356 and magnesium respectively. Figure 4.21 represents the relationship between predicted and actual value of impact strength.

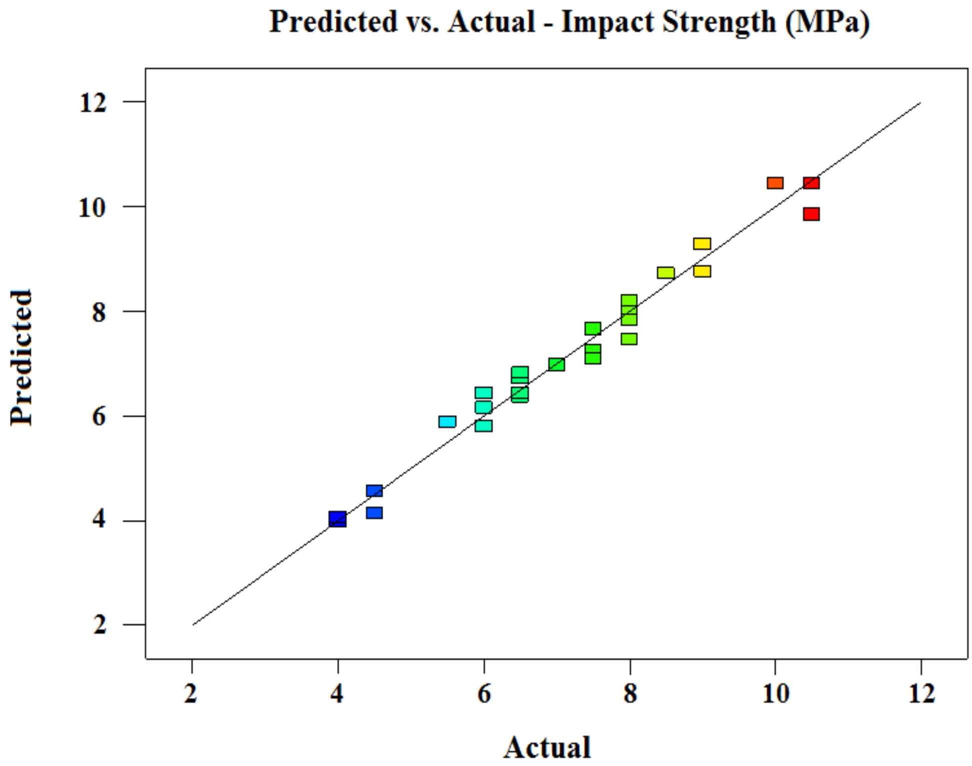

Figure 4.21 Plot of predicted vs. actual for impact strength

Comparison between experimental and regression results of impact strength is elaborated in Figure 4.22. It indicates that regression model and experimental values of impact strength follow a similar pattern. Further, the results predicted by regression model are quite closer to the experimental results. All of the above considerations indicate an excellent adequacy of the regression model. Hence, the obtained second-order mathematical model for impact strength can be regarded as significant for fitting and predicting the experimental results.

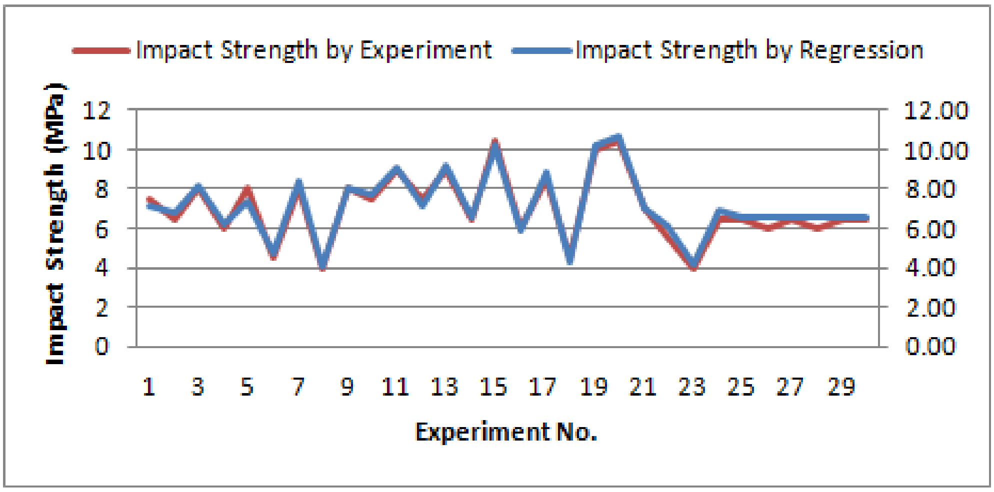

Figure 4.22 Comparison of experimental and regression model values of impact strength

4.8 EFFECT OF PROCESS PARAMETERS ON IMPACT STRENGTH

To investigate the combined effect of process parameters on impact strength of joint interface, 3D surface plots are drawn as shown in Figure 4.23 (a, b and c). It can be seen in Figure 4.23 (a and b) that increase in pouring temperature leads to decrease in the value of impact strength. This effect is much more dominating at the higher value of insert temperature as reflected in Figure 4.23 (b). Impact strength also decreased with increase in insert temperature as shown in Figure 4.23 (b and c). This is due to the fact that with the increase in pouring and insert temperature, the solidification time will increase. This results in formation of coarse grain structure which accomplished with a low value of impact strength. Similar observations have also been reported by other researchers [106]. Figure 4.23 (a) represents that impact strength is increased with increase in vacuum pressure. The increase in the degree of compaction of sand aggregates is attributed due to increase in vacuum pressure. Higher degree of compaction implies effective contact area of sand particles to be more. This results in increased solidification rate which leads to fine grain structure. Consequently, the impact strength is increased. Figure 4.23 (c) represents that with increase in grit size of sand paper, the impact strength of joint interface increases. This is due to the fact that with the increase in grit size (decrease in surface roughness of insert) better feeding of molten metal will take place at the interdendritic cavities. It implies more uniform diffusion between A356 alloy and Mg melt. This results in the improved impact strength. Similar observations have also been reported by other researchers [107].

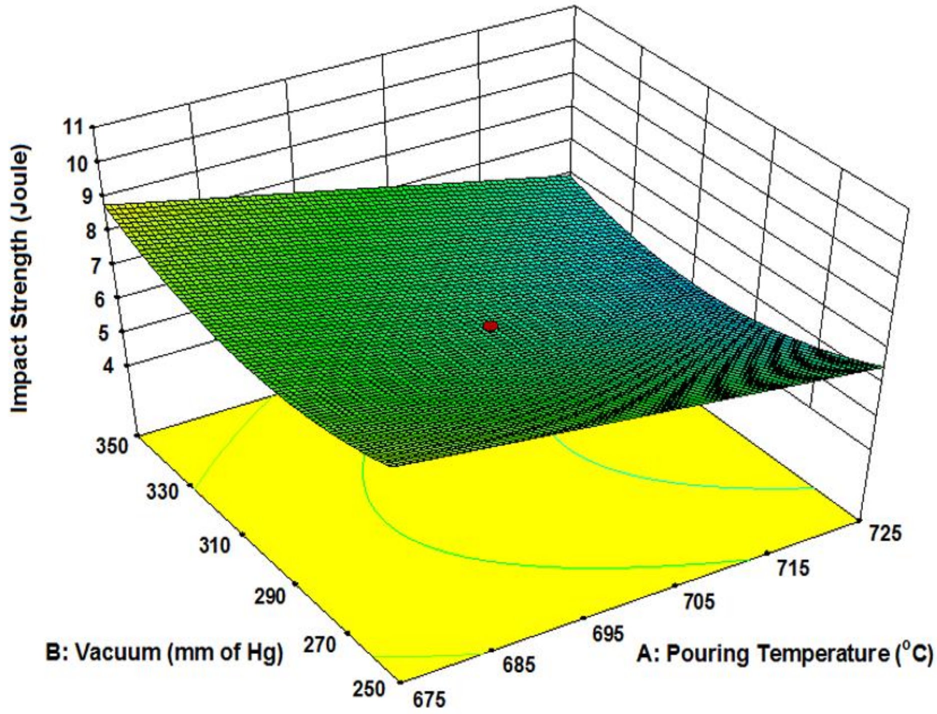

Figure 4.23 (a) Effect of vacuum pressure and pouring temperature on impact strength

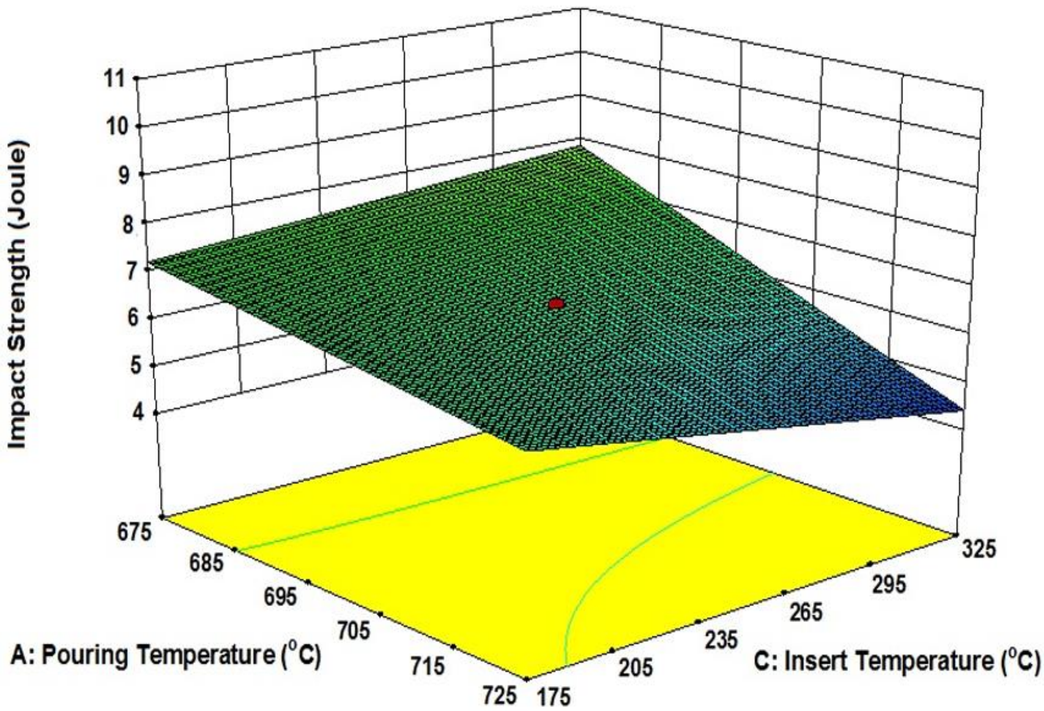

Figure 4.23 (b) Effect of pouring temperature and insert temperature on impact strength

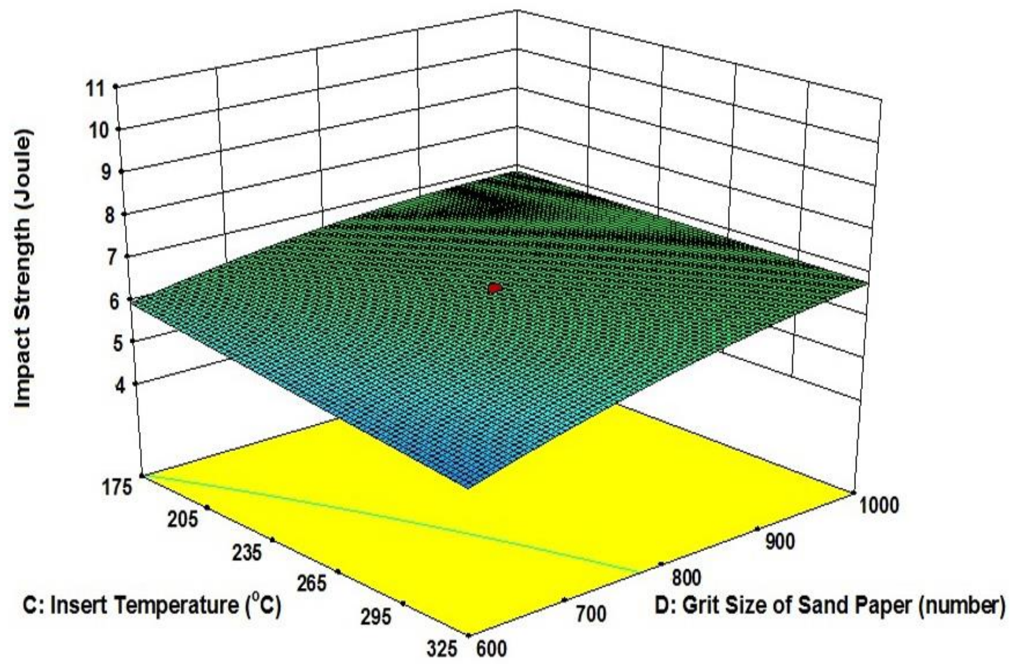

Figure 4.23 (c) Effect of insert temperature and grit size of sand paper on impact strength

4.9 RSM MODEL FOR MICROHARDNESS

Coefficients of second-order regression equation are determined from the experimental data. The final equation along with regression constants as a function of input process parameters (pouring temperature, vacuum pressure, insert temperature and grit size of sand paper) subjected to the response characteristics (microhardness) is obtained as:

$$MH = - 5984.38 + 17.3175*PT + 4.1649*VC - 0.413062*GS - 0.00536*PT*VC + 0.00050871*PT*GS + 0.0000627636*VC*IT - 0.012020*(PT)^2 - 0.000585*(VC)^2 \quad (4.5)$$

The result of the second-order response surface quadric model fitting in the form of ANOVA, after neglecting the insignificant parameters for microhardness of joint interface in compound casting, is shown in Table 4.8.

Table 4.8 Analysis of variance for microhardness – values of coded and real coefficients with F ratio for significant terms

Source	Sum of Squares	Degree of freedom	Mean Square	F Value	P Value (Prob. > F)	
Model	14141.86	8	1767.73	1305	< 0.0001	Significant
A - PT	7511.88	1	7511.88	5545.53	< 0.0001	
B - VC	167.48	1	167.48	123.64	< 0.0001	
D - GS	1917.09	1	1917.09	1415.26	< 0.0001	
AB – PT * VC	727.65	1	727.65	537.18	< 0.0001	
AD – PT * GS	110.78	1	110.78	81.78	< 0.0001	
BC – VC * IT	2090.32	1	2090.32	1543.14	< 0.0001	
A^2 – PT^2	1605.27	1	1605.27	1185.07	< 0.0001	
B^2 – VC^2	60.93	1	60.93	44.98	< 0.0001	
Residual	28.45	21	1.35			
Lack of Fit	26.51	16	1.66	4.27	0.0582	Not Significant
Pure Error	1.94	5	0.39	-		
Cor Total	14170.31	29	-			
Standard deviation	1.16	R-Squared			0.9980	
Mean	273.79	Adjusted R-Squared			0.9972	
Coefficient of variation%	0.43	Predicted R-Squared			0.9938	
PRESS	87.37	Adequate Precision			167.116	
Significant at 95% confidence level.						

The P-value (Prob. > F) less than 0.05 indicates the model terms are statistically significant at 95% confidence level. The Models F-value of 1305 implies that the model is significant. It is desirable as it indicates that the terms in model have the significant effect on the response. In the present model, pouring temperature (PT), vacuum pressure (VC) and grit size of sand paper (GS); interaction effect of pouring temperature and vacuum pressure (PT.VC), pouring temperature and grit size of sand paper (PT.GS), vacuum pressure and insert temperature (VC.IT), and second order term of pouring temperature (PT^2) and vacuum pressure (VC^2) have the significant effect. The rest of the terms are insignificant. The lack-of-fit is not significant relative to the pure error, as it is desired.

R^2 is the ratio of variability explained by the model to the total variability in the actual data. This is used to measure the goodness of fit. The value of R^2 as unity indicates the best result in terms of model. The calculated value of R^2 (0.998) verifies that the relationship between the selected process parameters and response (microhardness) can adequately be described by the model. The value of predicted R^2 (0.9938) indicates a good agreement with that of adjusted R^2 (0.9972). Adequate precision compares the range of predicted values at the design points to the average prediction error. It indicates the signal to noise (S/N) ratio. S/N ratio greater than 4 implies that the model is fit to proceed further. Adequate precision (167.116) indicates an adequate signal in compound casting process. At the same condition, a relatively lower value of coefficient of variation (0.43%) indicates better precision and reliability of the conducted experiments. The normal probability plot of the residuals as shown in Figure 4.24 for microhardness reveals that the residuals are falling on the straight line, which means the errors are distributed normally. Predicated microhardness calculated through Equation 4.5 for all thirty experiments is represented in Table 4.9.

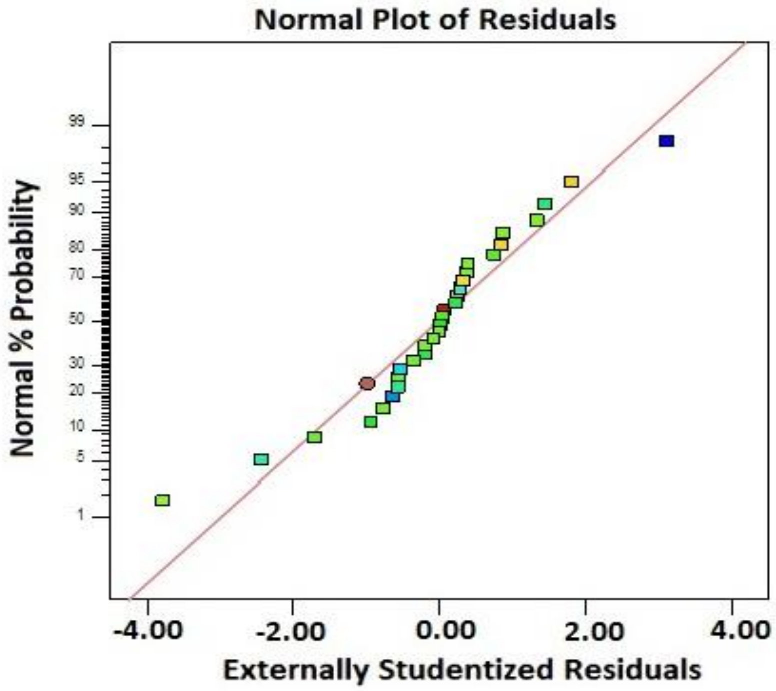

Figure 4.24 Plot of normal probability of residuals for microhardness

Table 4.9 Microhardness values by experimentation and regression model

Exp. No.	Process Parameters				Micro Hardness by Experiment (MPa)	Micro Hardness by Regression Model (MPa)
	Pouring Temp. (˚C)	Vacuum Pressure (mm of Hg)	Insert Temp. (˚C)	Grit size of Sand paper (number)		
1	675	250	175	600	303.54	298.84
2	725	250	175	600	276.86	272.98
3	675	350	175	600	300.02	319.83
4	725	350	175	600	245.36	267.17
5	675	250	325	600	281.68	301.20
6	725	250	325	600	251.23	275.33
7	675	350	325	600	322.15	323.13
8	725	350	325	600	267.06	270.46
9	675	250	175	1000	279.63	270.97
10	725	250	175	1000	263.35	255.28
11	675	350	175	1000	276.12	291.96
12	725	350	175	1000	231.86	249.47
13	675	250	325	1000	258.63	273.32
14	725	250	325	1000	240.16	257.63
15	675	350	325	1000	300.56	295.25
16	725	350	325	1000	254.79	252.76
17	650	300	250	800	284.03	292.85
18	750	300	250	800	217.56	224.50
19	700	200	250	800	269.85	274.82
20	700	400	250	800	280.13	290.93
21	700	300	100	800	279.15	285.85
22	700	300	400	800	281.41	291.50
23	700	300	250	400	299.19	311.46
24	700	300	250	1200	263.34	265.89
25	700	300	250	800	281.96	288.68
26	700	300	250	800	280.98	288.68
27	700	300	250	800	281.42	288.68
28	700	300	250	800	280.76	288.68
29	700	300	250	800	280.89	288.68
30	700	300	250	800	280.12	288.68

Figure 4.25 represents the relationship between predicted and actual value of microhardness. Comparison between experimental and predicted values of

microhardness is shown in Figure 4.26. It indicates that a similar pattern is followed by experimental and regression model values. The results predicted by regression analysis are quite closer to the experimental results. Hence, the obtained second-order mathematical model for microhardness can be regarded as significant for fitting and predicting the experimental results.

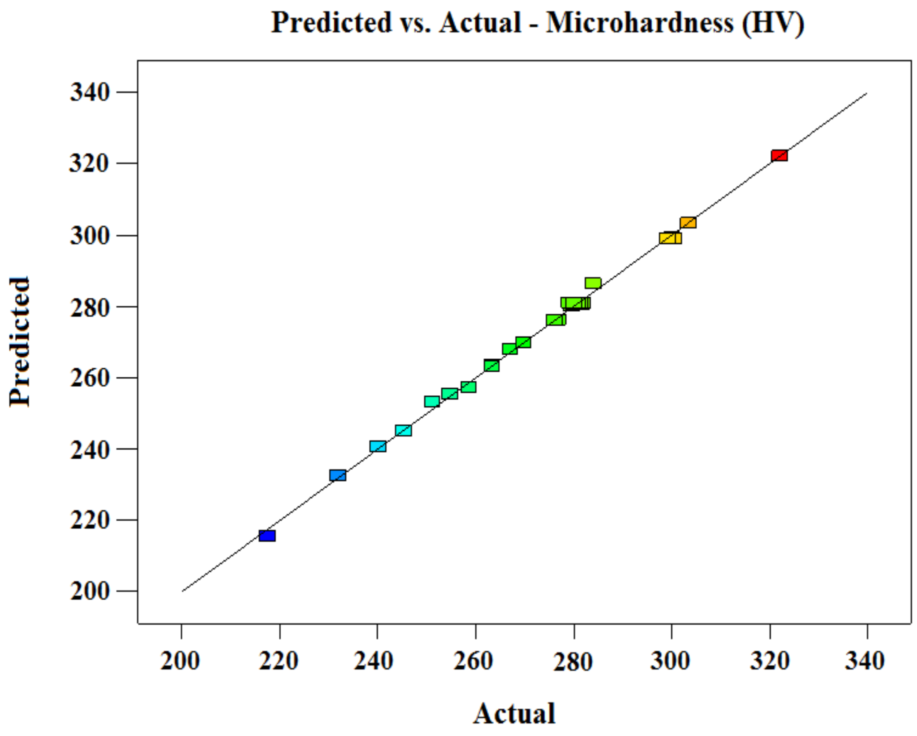

Figure 4.25 Plot of predicted vs. actual for microhardness

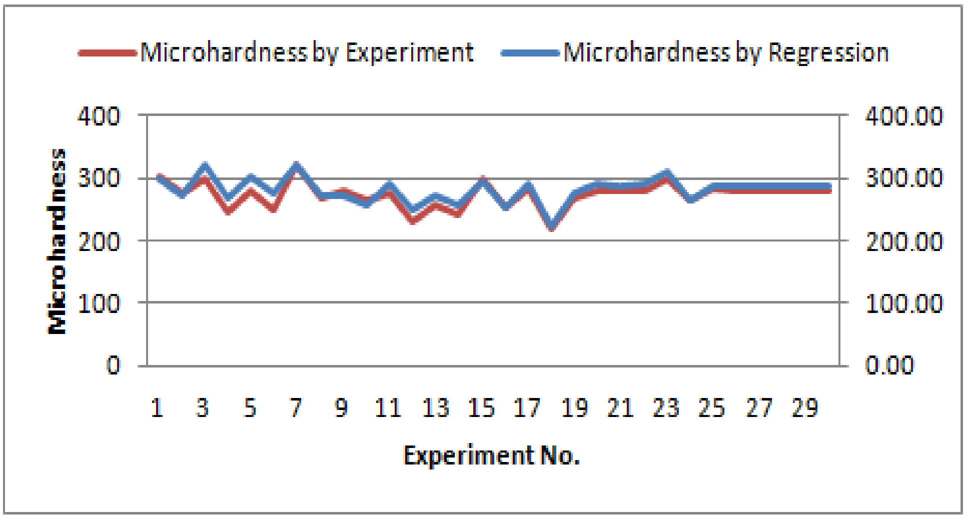

Figure 4.26 Comparison of Experimental and regression model values of microhardness

4.10 EFFECT OF PROCESS PARAMETERS ON MICROHARDNESS

Figure 4.27 (a-c) indicates the 3D surface plots which are drawn to investigate the combined effect of process parameters on microhardness of joint interface. It is observed from Figure 4.27 (a and b) that microhardness is decreased with increase in pouring temperature. This is due to the fact that as pouring temperature is increased, the solidification time will increase. This leads to the coarse grain structure. A coarse grain structure is accompanied with a low value of microhardness. Figure 4.27 (a) depicts that as the grit size of sand paper used is decreased (surface roughness of insert increased), the microhardness is increased. This may be due to the wettability behavior of solid insert and molten metal. High surface roughness of insert leads to better interaction of solid surface and molten metal. Due to which, a relatively more uniform diffusion of metals will take place. Consequently, the fine grain structure is obtained having comparatively more microhardness. Figure 4.27 (b) indicates that microhardness tends to increase with increase in vacuum pressure. The level of compaction of sand aggregates increases with increase in the degree of vacuum applied. Higher the level of compaction more will be the effective contact area of sand particles in sand aggregates. It leads to an increased cooling rate, which decreases the dendritic arm spacing [107]. Reduced dendritic arm spacing leads to the formation of fine grained structure. A fine grain structure is accomplished with high value of hardness [108-109]. Therefore, the microhardness will increase with increase in degree of vacuum. Figure 4.27 (c) indicates that there is no significant effect of insert temperature on the microhardness in presence of other acting parameters (pouring temperature, degree of vacuum and surface roughness of insert). However, at high value of insert temperature (325˚C), the microhardness increases slightly with increase in vacuum pressure whereas at the low insert temperature (175˚C), there is a little increase in microhardness with decrease in vacuum pressure. Similarly, at high vacuum pressure (350 mm of Hg), microhardness increases slightly with increase in insert temperature and at low vacuum pressure (250 mm of Hg), microhardness increase slightly with decrease in insert temperature.

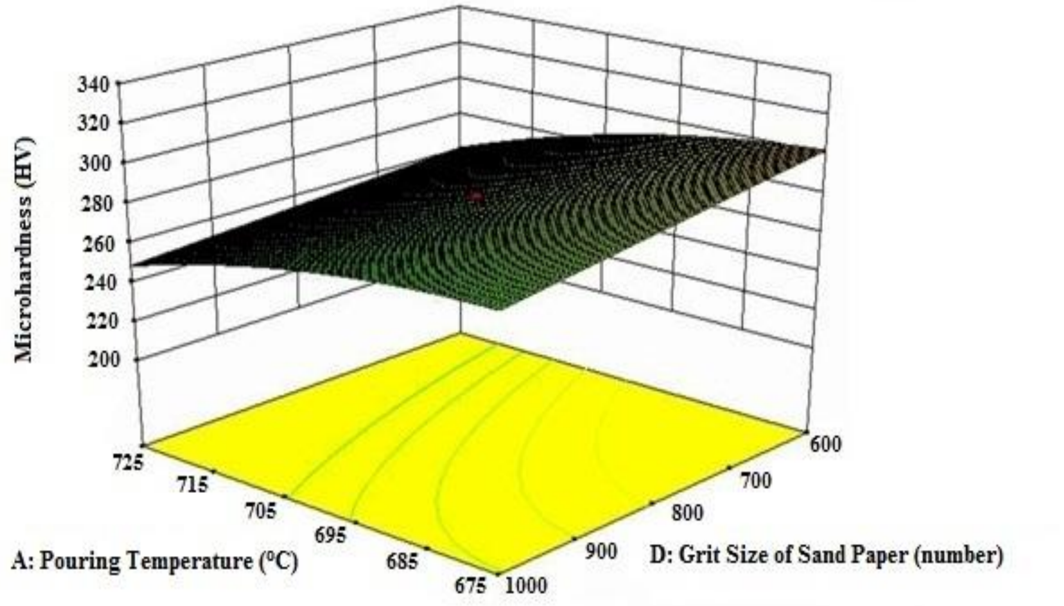

Figure 4.27 (a) Effect of pouring temperature and grit size of sand paper on microhardness.

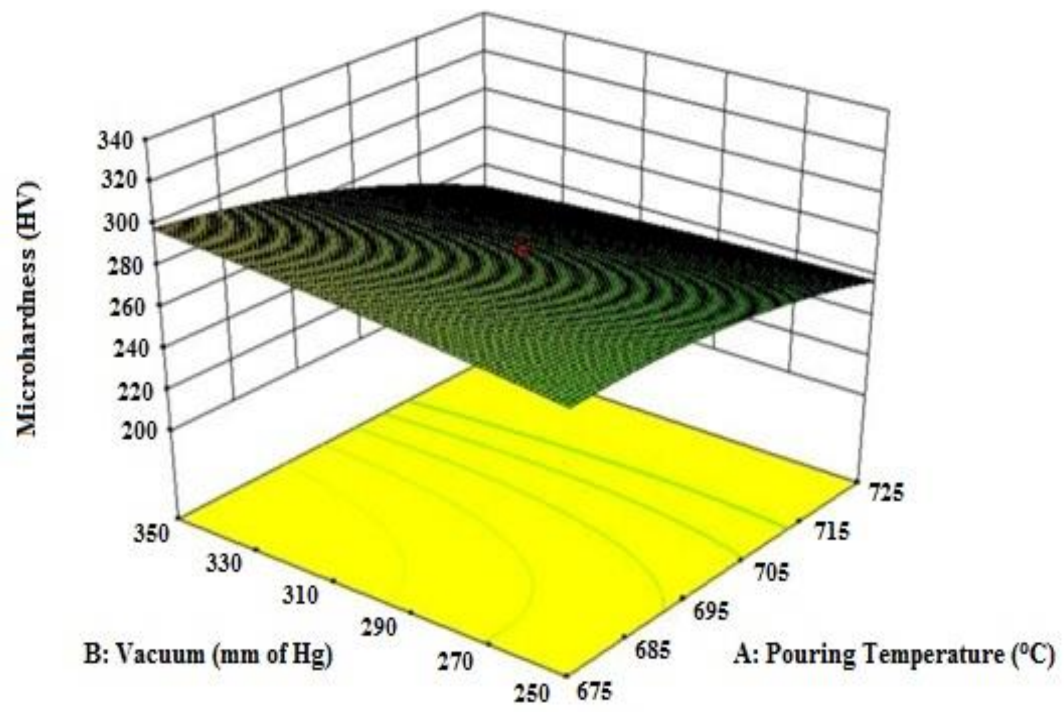

Figure 4.27 (b) Effect of pouring temperature and vacuum pressure on microhardness.

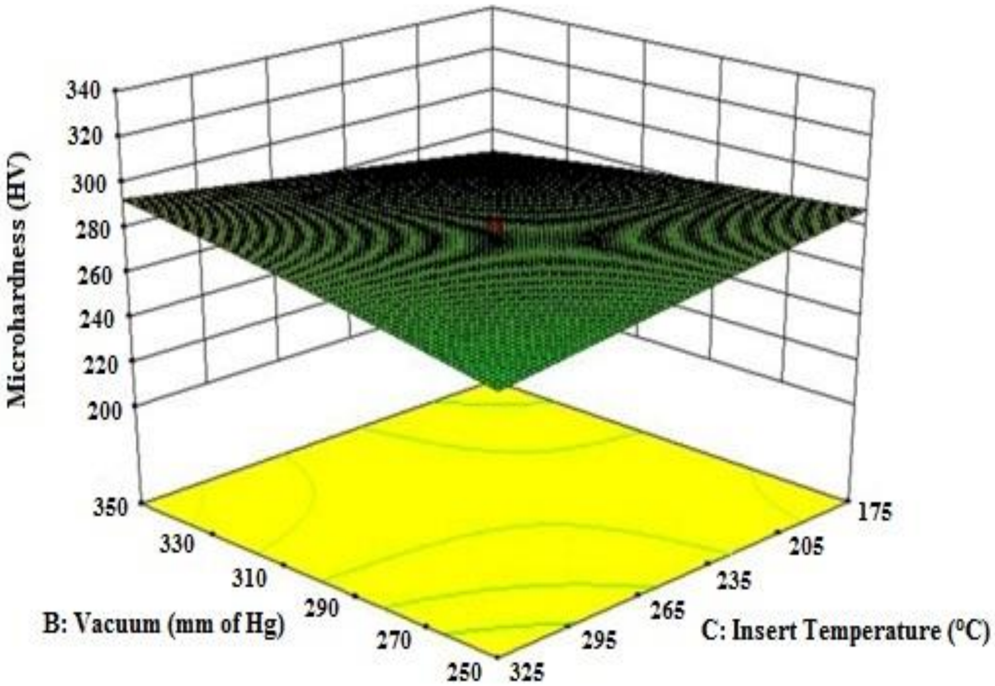

Figure 4.27 (c) Effect of vacuum pressure and insert temperature on microhardness

4.11 ANALYSIS OF MICROHARDNESS BY FRACTOGRAPHY

Microhardness at A356/Mg joint interface lies between 217.56 to 322.15 HV while 48 and 78 HV at the base metals magnesium and A356 respectively. It indicates that microhardness of joint interface is comparatively higher than the parent metals, which is consistent with other findings [57, 80, 86]. The microhardness distribution among the joint interface is shown in Figure 4.28. The microhardness at joint interface is lower on Mg side where $Mg_{17}Al_{12}$ + δ eutectic structure is formed, intermediate at middle portion where $Mg_{17}Al_{12}$ is formed and maximum at A356 side where Mg_2Al_3 is formed. As can be seen, the interfacial microhardness towards Mg side has minimum value where $Mg_{17}Al_{12}$ + δ intermetallic compound is formed. It indicates a partial ductile fracture due to its lower microhardness as shown in fractograph Figure 4.29 (a and b). The fractograph in Figure 4.29 (c) reveals the obvious cleavage planes along A356 side, a typical brittle fracture morphology without plastic deformation.

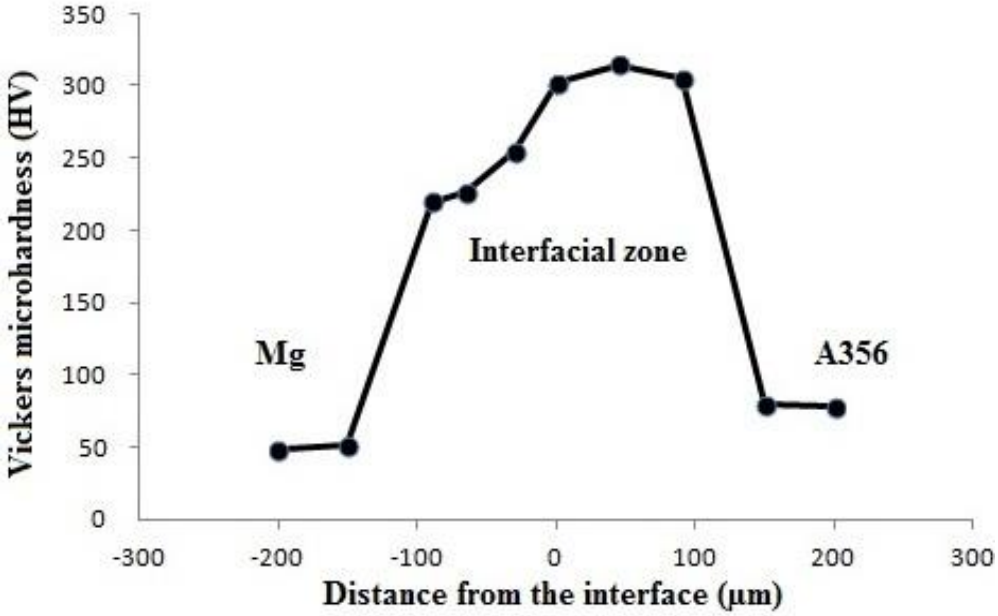

Figure 4.28 Microhardness distribution along A356/Mg joint interface

This can be explained by the fact that due to the presence of hard and brittle Mg_2Al_3 and $Mg_{17}Al_{12}$ intermetallic compounds, a large stress concentration will be generated, resulting in the crack propagation quite easily. Middle portion of interface indicates microhardness gradient where $Mg_{17}Al_{12}$ is formed as the major constituent along with $Mg_{17}Al_{12} + \delta$ eutectic structure. Figure 4.29 (d) indicates a partial ductile failure due to plastic deformation and an evidence of cleavage planes shown by arrowhead indicates the brittle fracture morphology. This type of mixed fracture morphology is obtained by the presence of hard and brittle $Mg_{17}Al_{12}$ intermetallic compound and partial ductile $Mg_{17}Al_{12} + \delta$ eutectic structure. Similar results have also been reported by other researchers [11, 81].

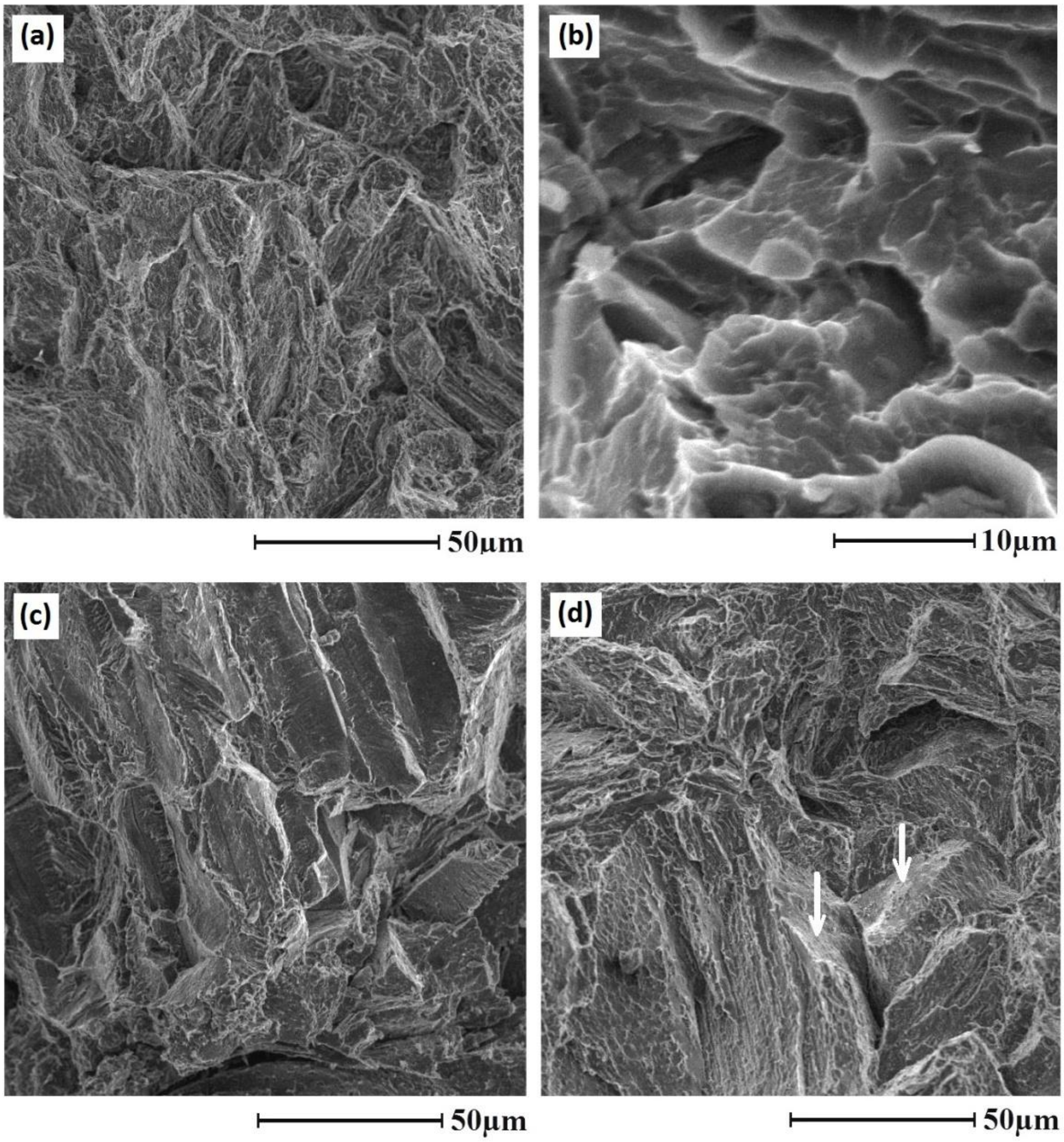

Figure 4.29 Fracture surfaces of A356/Mg joint (a, b) partial ductile fracture, (c) brittle fracture, and (d) brittle and partial ductile fracture

4.12 COMPARISON OF HARDNESS RESULTS OF VASMCC PROCESS WITH OTHER Al/Mg JOINING/WELDING PROCESSES

The interfacial microhardness of Al/Mg couples prepared by other dissimilar joining/welding methods is represented in Table 4.10. Research indicates that the maximum value of microhardness in other Al/Mg dissimilar joining processes is higher than the values obtained in the present experimental work. The microhardness value obtained at the Al/Mg interface is much higher than the base metals.

Table 4.10 Microhardness of other Al/Mg dissimilar joining/welding processes

S. No.	Joining method	Materials or Al/Mg Intermetallic Compounds	Microhardness at Joint Interface	Reference
1	Vacuum Assisted Sand Mold Compound Casting	Al alloy (A356) and pure Mg	217.56-322.15 HV	Present work Tayal et al. [97]
2	Gas Metal Arc Welding	Al alloy (A6061) and Mg alloy (AZ31B)	260-362 HV	Shang et al. [89]
3	Spot Welding	Al_3Mg_2, $Al_{12}Mg_{17}$	356.9 HV 336.5 HV	Wang et al. [90]
4	Friction Stir Welding	Al alloy (6061) and Mg alloy (NZ30K)	300 HV	Tan et al. [91]
5	Friction Stir Welding	Al alloy (AA7075) and Mg alloy (AZ31B)	390 HV	Bilgin et al. [110]
6	Friction Stir Welding	Al alloy (AA6061) and Mg alloy (AZ31B)	400 HV	Chlouk et al. [111]
7	Friction Stir Welding	Al alloy (A5052) and Mg Alloy (AZ31B)	300HV	Morishige et al. [112]
8	Diffusion welding	Al alloy (EN AW-6082), Mg Alloy (AZ31B)	240-560 HV	Dietrich et al. [113]
9	Diffusion Bonding	Al_3Mg_2 $Al_{12}Mg_{17}$	448.7 HV 443.6 HV	Zhang et al. [114]

CHAPTER 5

OPTIMIZATION OF PROCESS PARAMETERS USING DESIRABILITY ANALYSIS, GENETIC ALGORITHM AND GRAPH THEORETIC APPROACH

5.1 INTRODUCTION

This chapter presents the optimization of process parameters; pouring temperature, vacuum pressure, insert temperature and grit size of sand paper by desirability analysis and genetic algorithm subjected to the output characteristics; shear strength, impact strength and microhardness. The joint strength evaluation by graph theoretic approach is discussed in detail. Multiobjective optimization is also highlighted.

5.2 DESIRABILITY ANALYSIS

Desirability analysis is an optimization technique in which, the measured properties of each predicted response is converted into a desirability value *d*, which is dimensionless. The value of *d* lies between zero to one. Zero indicates that the response is unacceptable completely and one indicates that the response completely approaches the target value [99, 115]. In desirability analysis, numerous solutions are generated. It is being used by researchers to find out the optimal solutions.

In the present work, optimization of process parameters of VASMCC process is carried out by getting the desirability values for the shear strength, impact strength and microhardness of A356/Mg joint interface by using design-expert software.

5.3 GENETIC ALGORITHM

It is an optimization technique based on the survival of the fittest idea into a search algorithm, which provides a method of searching. Therefore, there is no need to explore every possible solution in the feasible region to obtain a good result [116-118]. GA is applied to a problem by first guessing the solutions and then combining the fittest solutions, which creates a new generation of solutions. The solutions obtained should be better than the previous generation [119-122].

In the present work, Global optimization toolbox of MATLAB (R2010a) is used to generate the optimum values of shear strength, impact strength and microhardness. The significant operating parameters in genetic algorithm are size of population, type and probability of cross over, mutation and number of iterations etc. Table 5.1 represents these parameters along with their values used for the present work.

Table 5.1 Genetic algorithm operating parameters for optimization

Parameters	Sub Parameters with values		
Population	Size-20	Type-double vector	Creation function-Use constraint dependent default
Selection	Stochastic uniform		
Crossover	Single point crossover	Crossover rate-0.8	
Mutation	Adaptive feasible		
Migration	Direction-Both		
Hybrid function	None		
Stopping criteria	Generations-100	Time limit-infinite	Fitness time-infinite
	Stall generations-50	Stall time limit-infinite	Tolerance 1e-6
Plot function	Best fitness	Best individual	

5.4 OPTIMIZATION OF PROCESS PARAMETERS FOR SHEAR STRENGTH

The designated process parameters are optimized in order to maximize the shear strength of A356/Mg joint interface. Optimization is carried out by desirability analysis and genetic algorithm.

5.4.1 Optimization for Shear Strength by Desirability Analysis

Design expert software provided the desirability values for the shear strength subjected to the process parameters as represented in Table 5.2 along with their limits and goal settings. Fifteen solutions are generated as shown in Table 5.3. The solution with higher desirability is selected in order to find the optimal value.

Table 5.2 Constraints used for desirability analysis of shear strength

Constraints Name	Goal	Lower Limit	Upper Limit	Lower Weight	Upper Weight	Importance
Pouring Temperature (°C)	In range	650	750	1	1	3
Vacuum Pressure (mm of Hg)	In range	200	400	1	1	3
Insert Temperature (°C)	In range	100	400	1	1	3
Grit Size of Sand Paper (no.)	In range	400	1200	1	1	3
Shear Strength (MPa)	Maximize	11.78	33.14	1	1	5

Table 5.3 Optimal solution for shear strength by desirability analysis

Sr. No.	Optimal Process Parameters				Optimal Shear Strength (MPa)	Desirability	Selection
	Pouring Temp. (°C)	Vacuum Pressure (mm of Hg)	Insert Temp. (°C)	Grit size of Sand paper (Number)			
1	674.93	379.46	122.68	825.46	35.99	1.00	Selected
2	670.49	364.80	161.54	923.65	34.35	1.00	
3	670.00	342.10	112.37	732.06	34.15	0.99	
4	668.34	334.97	117.69	728.74	34.08	0.98	
5	650.00	400.00	185.23	788.67	33.06	0.97	
6	654.14	200.00	100.00	400.00	32.51	0.97	
7	665.67	200.03	100.00	419.33	31.97	0.95	
8	679.78	400.00	222.41	894.74	31.73	0.93	
9	662.46	200.00	100.00	778.43	31.47	0.92	
10	665.68	400.00	233.11	1174.75	31.38	0.92	
11	650.00	200.06	165.01	433.35	30.25	0.87	
12	691.25	400.00	245.30	1030.89	30.25	0.87	
13	653.31	400.00	250.86	1158.18	30.13	0.86	
14	679.57	400.00	242.85	1200.00	29.82	0.84	
15	668.09	200.00	203.76	538.52	29.41	0.83	

The highest value of desirability is obtained as one for the shear strength as shown in ramp graph, Figure 5.1. The optimum process parameters are pouring temperature = 674.93 °C, vacuum pressure = 379.46 mm of Hg, insert temperature = 122.68 °C, and grit size of sand paper = 825.46. The optimal value of shear strength = 35.99 MPa at desirability value one.

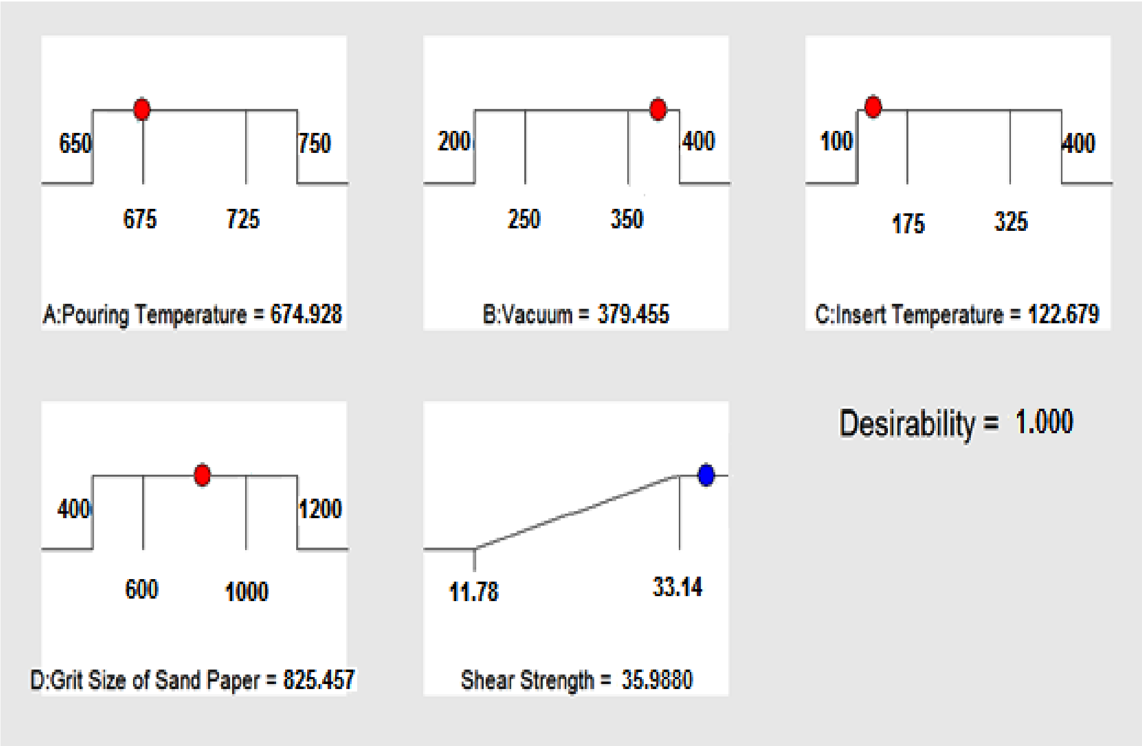

Figure 5.1 Ramp graph of optimal solution for shear strength

5.4.2 Optimization for Shear Strength by Genetic Algorithm

In order to find the optimum value of shear strength as a function of designated process parameters for VASMCC process a MATLAB function is written by using the RSM model proposed in Equation 4.3. This function is used as input for creating a fitness function for the optimization problem. The fitness function so formulated is written as:

```
function SS = shearstrengthfun(x)
```

SS = - (-769.45144 + 2.63608*x(1) - 0.148586*x(2) - 0.44473*x(3) + 0.000660667*x(1)*x(3) - 0.000152333*x(2)*x(3) + 0.000255295*x(2)*x(4) - 0.00210*x(1)^2) - 0.000046601*x(4)^2);

end (5.1)

Where x(1), x(2), x(3) and x(4) represent the process parameters; pouring temperature, vacuum pressure, insert temperature and grit size of sand paper respectively. The fitness function is marked negative as GA minimizes all the objectives by default. Actual range of process parameters is used for optimization. The selected range of process parameters to represent the boundaries of the optimization solution is as below:

$$650 \leq PT \leq 750 \tag{5.2}$$

$$200 \leq VC \leq 400 \tag{5.3}$$

$$100 \leq IT \leq 400 \tag{5.4}$$

$$400 \leq GS \leq 1200 \tag{5.5}$$

The fitness function as formulated in Equation 5.1, range of process parameters as shown in Equation 5.2 to Equation 5.5 and the GA operating parameters as indicated in Table 5.1 are considered to find the optimal solution. The optimum shear strength thus obtained is 37.85 MPa. The optimum value of process parameters, which lead the maximum shear strength, are pouring temperature = 650.01 °C, vacuum pressure = 307.45 mm of Hg, insert temperature = 100 °C and grit size of sand paper = 807.35 as shown in Figure 5.2. The optimal solution is obtained at the 69th generation as shown in Figure 5.3. The mean fitness value of shear strength is 37.84 MPa, being the best fitness as 37.85 MPa. It also indicates the best individual value for the optimal solution. The criterion for GA to stop further extension in the process to find the optimal solution is the weighted average change of fitness function value over stall a generation, the value of which is less than the function tolerance.

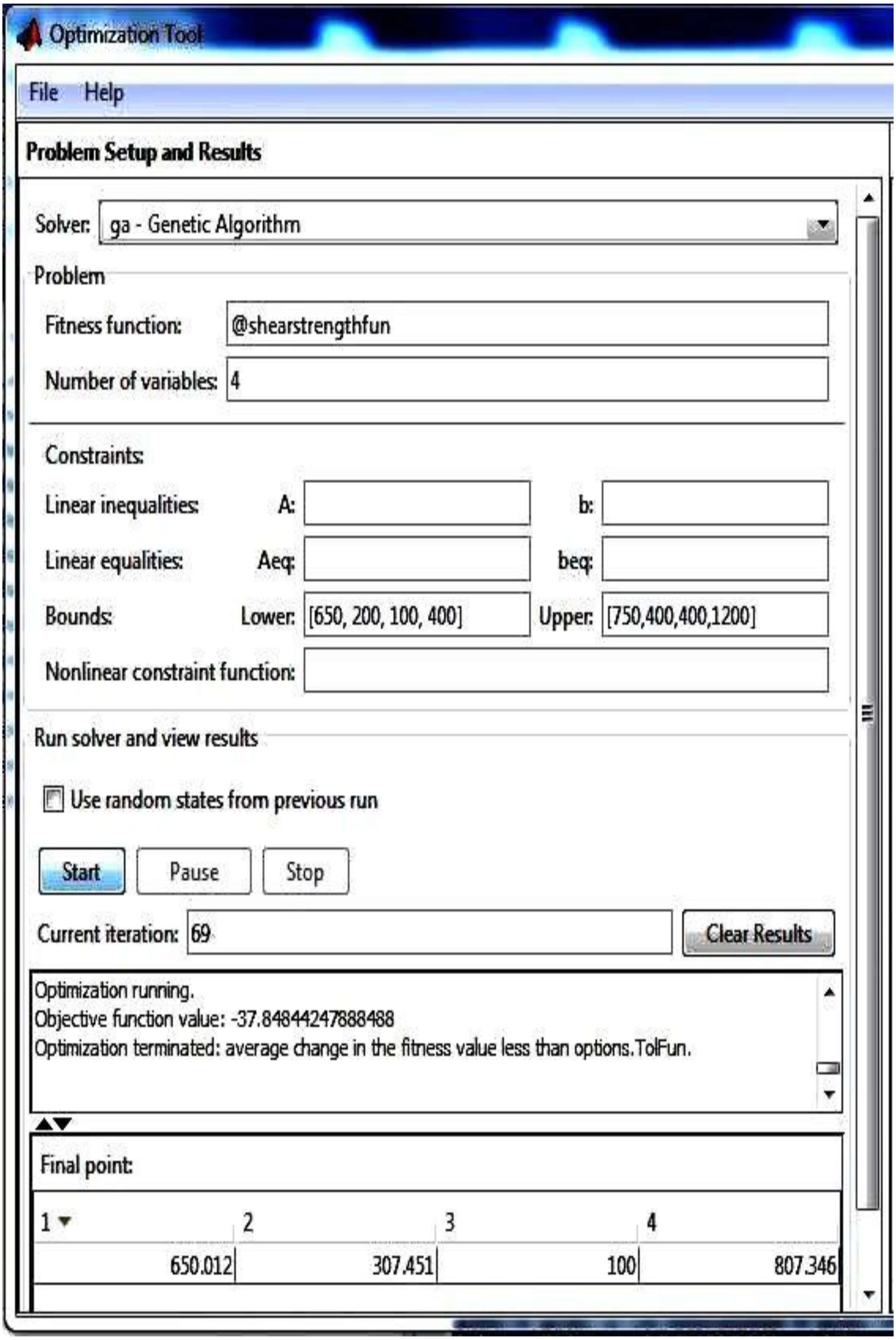

Figure 5.2 Screen shot of GA optimization for shear strength

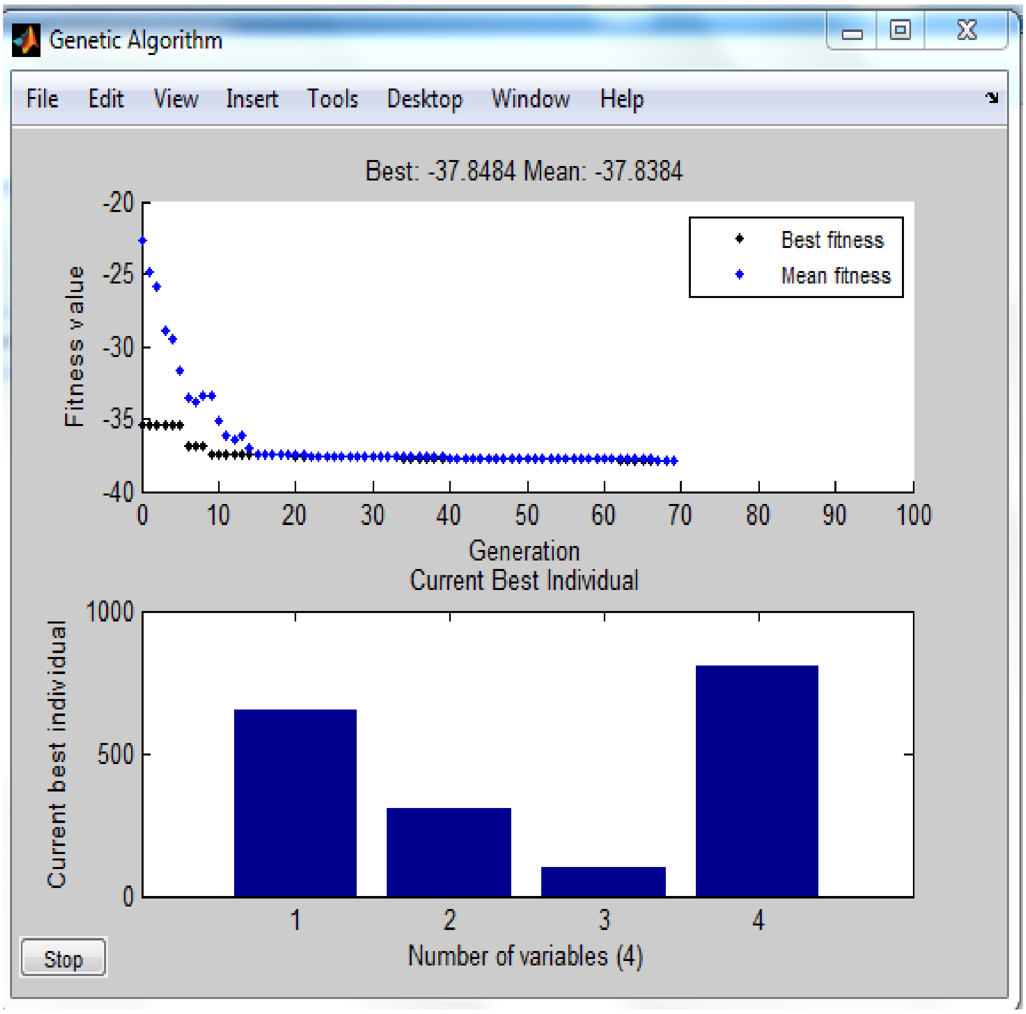

Figure 5.3 GA optimization history and best individuals for shear strength

5.4.3 Comparison of Optimization Results for Shear Strength

Optimal value of shear strength and process parameters of vacuum assisted sand mold compound casting obtained by means of experiments, regression model, desirability analysis and GA are summarized in Table 5.4. The optimum shear strength for the actual compound casting experiments, regression model, desirability analysis and genetic algorithm are 33.14, 34.73, 35.9 and 37.85 MPa respectively. It is observed that GA has given the maximum value of shear strength as compared to the result of experiments, regression model and desirability analysis. The optimal values as predicted by GA for each process parameter lies in the range of actual process parameters. So, it is stated that maximum (best) value of shear strength (37.85 MPa) can be achieved if applied to the actual compound casting process.

Table 5.4 Optimal values of shear strength along with optimal process parameters by different methods

Method	Optimal Value of Shear Strength (MPa)	Optimal Process Parameters			
		Pouring Temperature (650-750 °C)	Vacuum Pressure (200 - 400 mm of Hg)	Insert Temperature (100-400 °C)	Grit Size of Sand Paper (400-1200)
Genetic Algorithm	37.85	650.01	307.45	100.00	807.35
Desirability Analysis	35.99	674.93	379.46	122.68	825.46
Regression Model	34.73	675.00	350.00	175.00	1000.00
Experimental Method	33.14	675.00	350.00	175.00	1000.00

5.5 OPTIMIZATION OF PROCESS PARAMETERS FOR IMPACT STRENGTH

The selected process parameters are optimized in order to maximize the impact strength of A356/Mg joint interface. Optimization is carried out by desirability analysis and genetic algorithm.

5.5.1 Optimization for Impact Strength by Desirability Analysis

Desirability values for impact strength are obtained with reference to the process parameters as shown in Table 5.5 along with their limit and constraints. The solutions generated in the present analysis are shown in Table 5.6. The solution acquiring the highest value of desirability is considered as optimal solution. The highest value of desirability obtained for the impact strength is one. The optimal solution represented by ramp graph as shown in Figure 5.4. The optimal value of impact strength (11.71 J) is achieved corresponding to the highest desirability. The optimized process parameters are pouring temperature = 675.58^{o}C, vacuum pressure = 201.35 mm of Hg, insert temperature = 322.74^{o}C and grit size of sand paper = 934.15.

Table 5.5 Constraints used for desirability analysis of impact strength

Constraints Name	Goal	Lower Limit	Upper Limit	Lower Weight	Upper Weight	Importance
Pouring Temperature (°C)	In range	650	750	1	1	3
Vacuum Pressure (mm of Hg)	In range	200	400	1	1	3
Insert Temperature (°C)	In range	100	400	1	1	3
Grit Size of Sand Paper (number)	In range	400	1200	1	1	3
Impact Strength (J)	Maximize	4.00	10.50	1	1	5

Table 5.6 Optimal solution for impact strength by desirability analysis

Sr. No.	Optimal Process Parameters				Optimal Impact Strength (J)	Desirability	Selection
	Pouring Temp. (˚C)	Vacuum Pressure (mm of Hg)	Insert Temp. (˚C)	Grit Size of Sand Paper (number)			
1	675.58	201.35	322.74	934.15	11.71	1.00	Selected
2	657.14	235.22	363.77	975.03	11.29	1.00	
3	651.62	359.19	297.03	738.65	10.97	0.99	
4	667.58	200.00	164.87	741.62	10.48	0.98	
5	732.44	399.98	100.00	963.47	10.35	0.98	
6	650.00	200.00	141.42	810.66	10.30	0.97	
7	736.42	400.00	100.00	727.88	10.10	0.94	
8	749.65	200.00	192.11	694.02	10.06	0.93	
9	650.00	324.44	266.08	1200.00	9.91	0.91	
10	670.23	200.00	100.00	591.47	9.74	0.88	

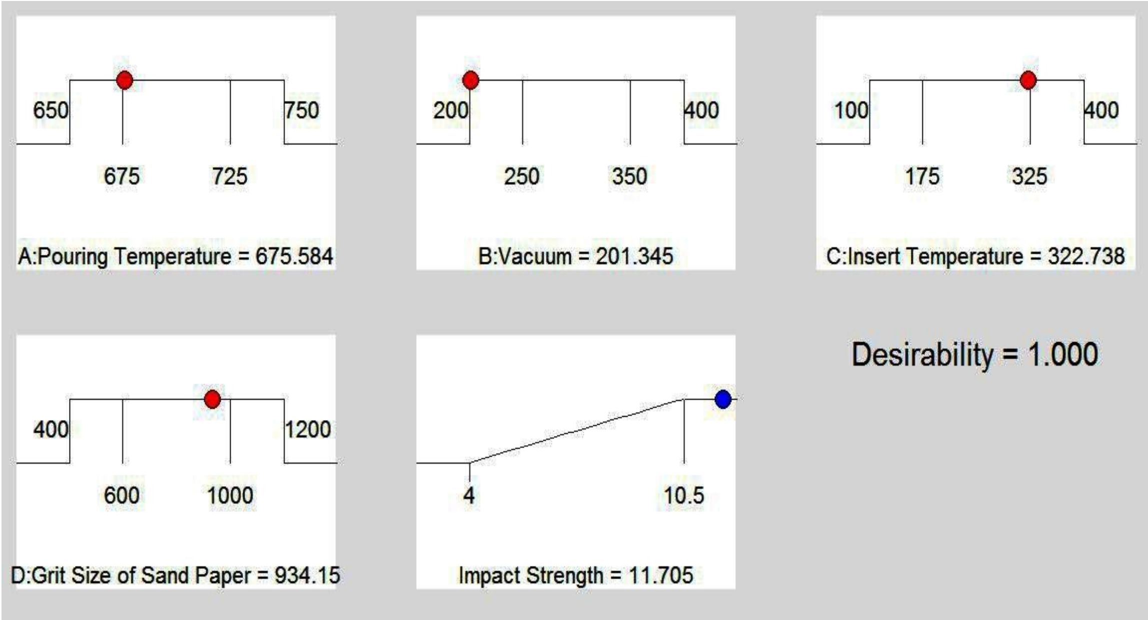

Figure 5.4 Ramp graph of optimal solution for impact strength

5.5.2 Optimization for Impact Strength by Genetic Algorithm

In the present work, Global optimization toolbox of MATLAB (R2010a) is used to generate the optimum value of impact strength. Fitness function created using the regression model (Equation 5.6) is written as:

```
function IS= impactstrengthfun(x)

IS = - (- 54.80128 + 0.13241*x(1) + 0.206039*x(3) + 0.00977638*x(4) -
     0.0003302*x(1)*x(2) - 0.00031606*x(1)*x(3) + 0.0000145833 * x(3)*x(4) +
     0.000358875*x(2)^2 - 0.00000624045*x(4)^2);

     end                                                              (5.6)
```

Where x(1), x(2), x(3) and x(4) represents the process parameters; pouring temperature, vacuum pressure, insert temperature and grit size of sand paper respectively. GA minimizes all the objectives by default. So, the fitness function is made negative to maximize the impact strength. The size of population, probability of crossover, rate of mutation and number of iterations are the important operating parameters in genetic algorithm. In order to find the solution of the current problem, fitness function as shown in Equation 5.6, GA parameters as given Table 5.1 and the range of process parameters as given in Equation 5.2 to Equation 5.5 are considered. The maximum value of impact strength thus obtained is 12.29 J corresponding to the optimal process parameters as pouring temperature = 661.13^{o}C, vacuum pressure = 200.02 mm of Hg, insert temperature = 328^{o}C and grit size of sand paper = 1187.15 as shown in Figure 5.5. The optimal solution is obtained at the 96th generation. The mean fitness value of impact strength (12.288 J) and the best individuals for optimal solution are shown in Figure 5.6.

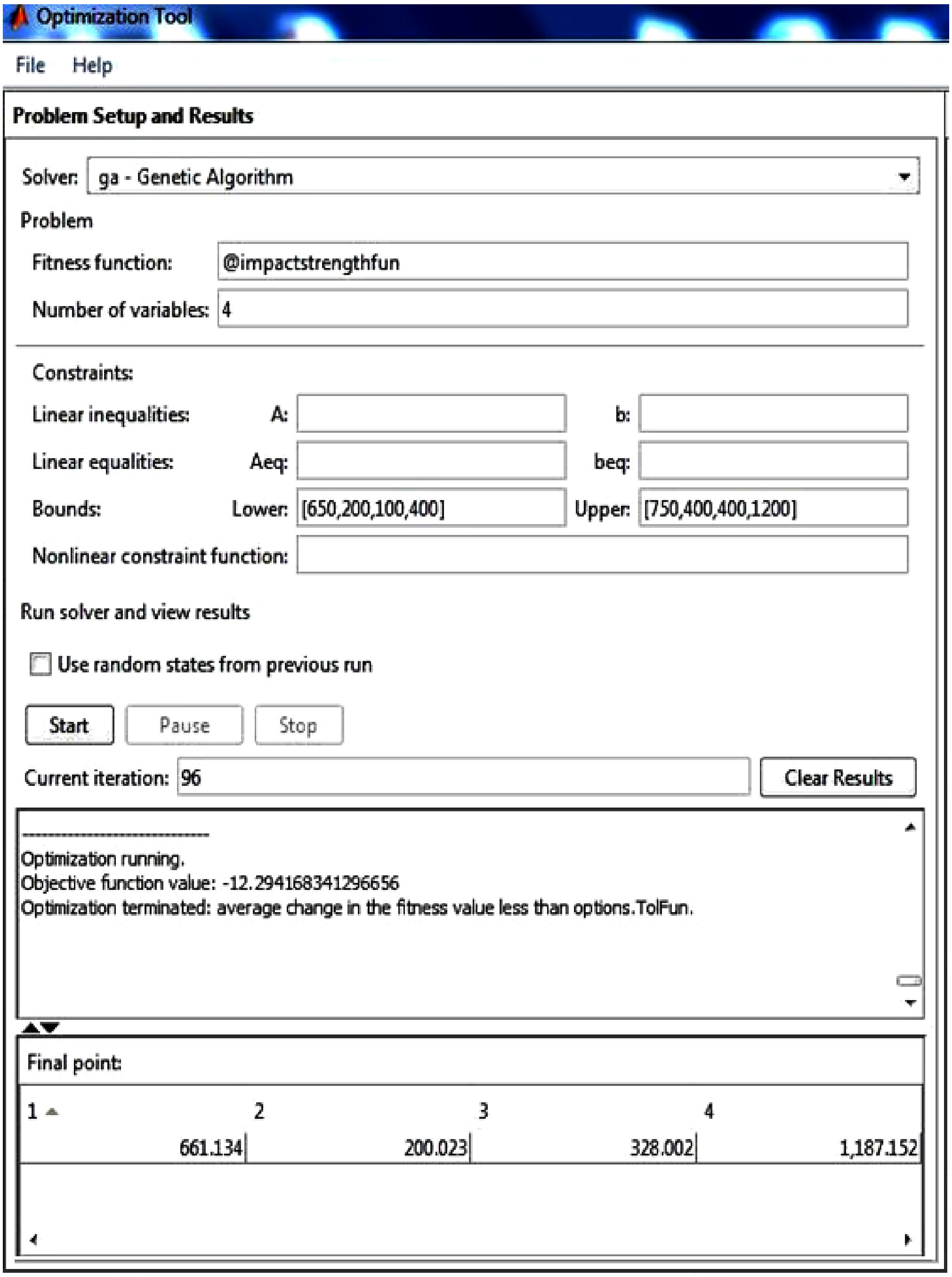

Figure 5.5 Screen shot of GA optimization for impact strength

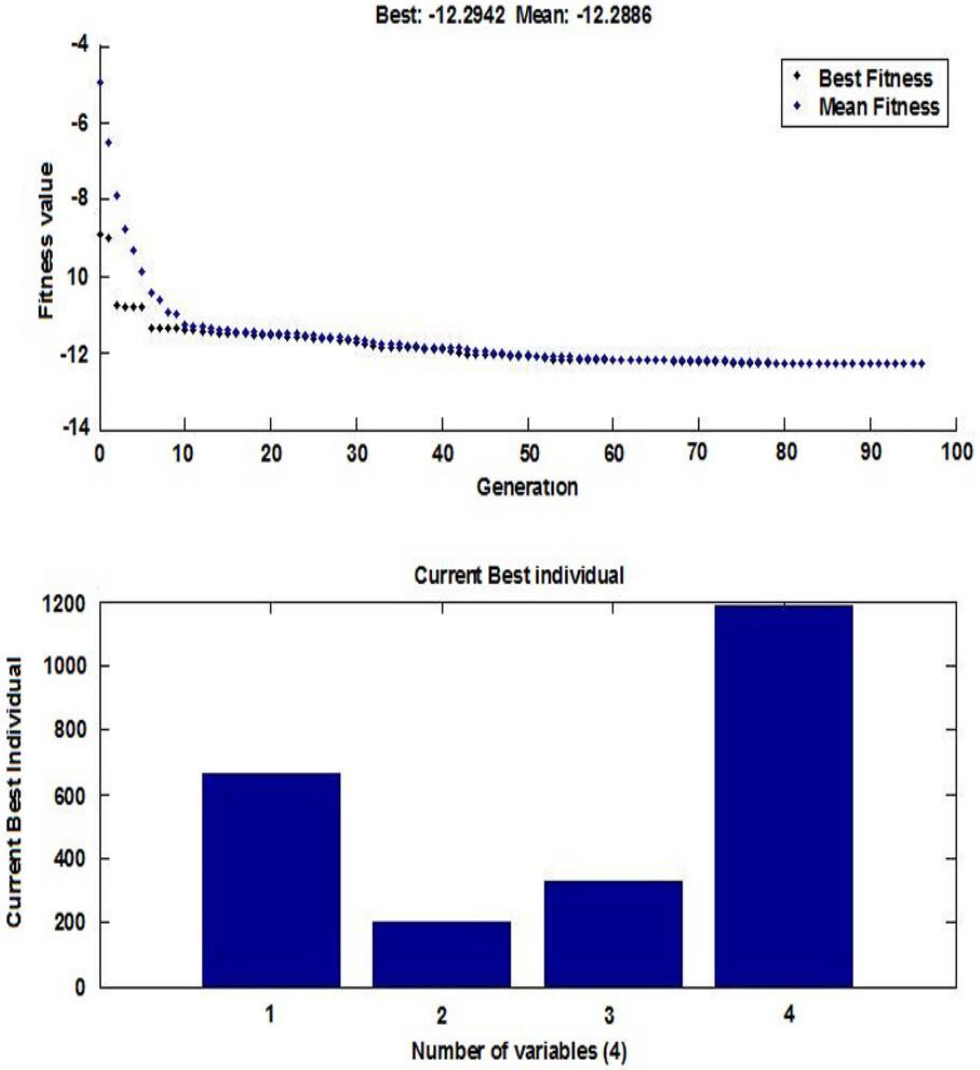

Figure 5.6 GA optimization history and best individuals for impact strength

5.5.3 Comparison of Optimization Results for Impact Strength

Optimal value of impact strength and corresponding process parameters achieved by the experimental, regression model, desirability analysis and genetic algorithm are recapitulated in Table 5.7. The maximum value of impact strength for experimental, regression model, desirability analysis and genetic algorithm are 10.5, 10.68, 11.71 and 12.29 J respectively. It reflects that GA has predicted the optimal value of impact strength having the optimal process parameters lie in their actual range.

Table 5.7 Optimal values of impact strength along with optimal process parameters by different methods

Method	Optimal Value of Impact Strength (J)	Optimal Process Parameters			
		Pouring Temperature (650-750 °C)	Vacuum Pressure (200 - 400 mm of Hg)	Insert Temperature (100-400 °C)	Grit Size of Sand Paper (400-1200)
Genetic Algorithm	12.29	661.13	200.02	328.00	1187.15
Desirability Analysis	11.71	675.58	201.35	322.74	934.15
Regression Model	10.68	700.00	400.00	250.00	800.00
Experimental Method	10.50	700.00	400.00	250.00	800.00

5.6 OPTIMIZATION OF PROCESS PARAMETERS FOR MICROHARDNESS

The designated process parameters are optimized in order to maximize the microhardness of A356/Mg joint interface. Optimization is carried out by desirability analysis and genetic algorithm.

5.6.1 Optimization for Microhardness by Desirability Analysis

Input parameters used in optimization along with their limits and goal settings are shown in Table 5.8 for microhardness. Fifteen solutions are generated for the optimization of process parameters for microhardness as shown in Table 5.9. Solution with higher desirability is chosen in order to find the optimal value. Figure 5.7 depicts the ramp graph of optimal solution obtained by desirability analysis. The highest desirability acquired in these cases is 1. Based on the criterion of maximum desirability, the optimal solution is achieved for maximizing the microhardness of A356/Mg joint interface. The optimized process parameters are pouring temperature = 663.20 ˚C, vacuum pressure = 347.38 mm of Hg, insert temperature = 295.13 ˚C and grit size of sand paper = 534.41. The optimal value of micro-hardness = 324.86 at desirability value of 1.

Table 5.8 Constraints used for desirability analysis of microhardness

Constraints Name	Goal	Lower Limit	Upper Limit	Lower Weight	Upper Weight	Importance
Pouring Temperature (°C)	In range	650	750	1	1	3
Vacuum Pressure (mm of Hg)	In range	200	400	1	1	3
Insert Temperature (°C)	In range	100	400	1	1	3
Grit Size of Sand Paper (number)	In range	400	1200	1	1	3
Microhardness (HV)	Maximize	217.56	322.15	1	1	5

Table 5.9 Optimal solution for microhardness by desirability analysis

Sr. No	Optimal Process Parameters				Optimal Micro Hardness (HV)	Desirability	Selection
	Pouring Temp. (°C)	Vacuum Pressure (mm of Hg)	Insert Temp. (˚C)	Grit size of Sand paper (number)			
1	663.20	347.38	295.13	534.41	324.86	1.00	Selected
2	717.88	200.00	100.00	434.35	321.60	1.00	
3	694.47	247.84	100.00	400.00	321.50	0.99	
4	677.58	200.00	100.00	679.84	320.07	0.98	
5	694.45	200.00	105.48	686.10	319.87	0.98	
6	691.49	200.00	100.00	737.90	319.17	0.97	
7	664.60	208.63	100.00	595.43	318.53	0.97	
8	702.70	200.00	100.00	754.94	316.97	0.95	
9	663.98	290.37	150.41	400.00	316.82	0.95	
10	697.26	200.00	100.02	802.48	315.81	0.94	
11	650.01	346.35	156.68	400.00	315.22	0.93	
12	698.63	200.00	100.11	857.66	313.11	0.91	
13	706.07	200.00	100.00	845.15	312.22	0.91	
14	677.17	292.13	323.13	400.00	310.37	0.89	
15	698.26	200.00	100.00	946.59	309.13	0.88	

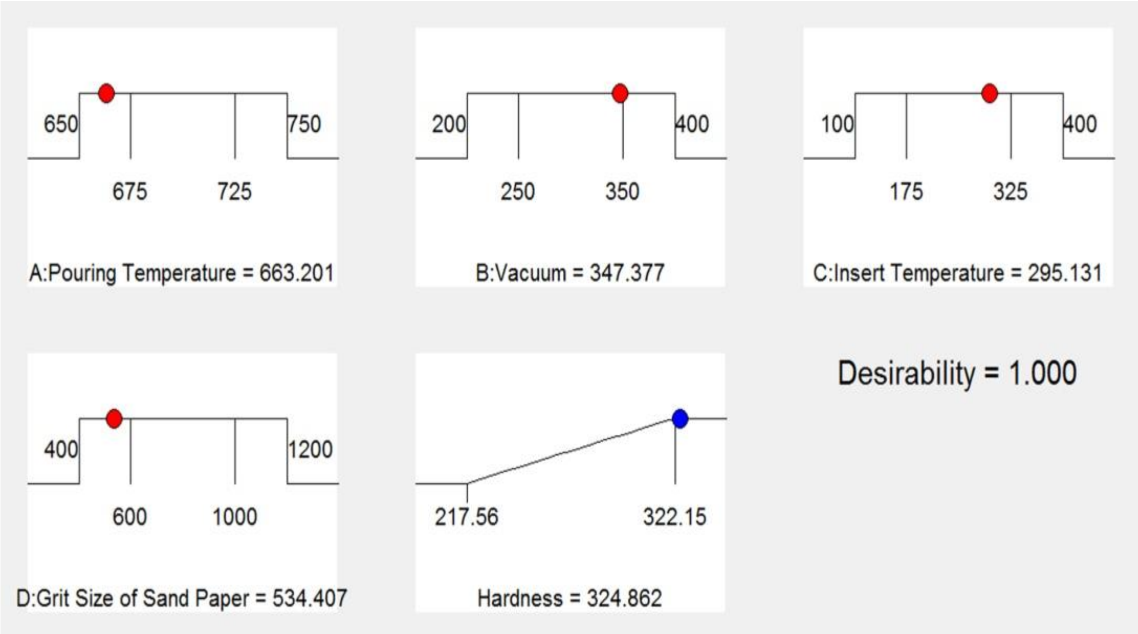

Figure 5.7 Ramp graph of optimal solution for microhardness

5.6.2 Optimization for Microhardness by Genetic Algorithm

GA Optimization for microhardness is performed by using global optimization toolbox of MATLAB (R2010a). The microhardness of joint interface is subjected to the process parameters; pouring temperature, vacuum pressure, insert temperature and grit size of sand paper used. The fitness function formulated by using RSM model Equation 5.7 is expressed as:

```
function MH= microhardnessfun(x)

MH = -(-5984.38 + 17.3175*x(1) + 4.1649*x(2) - 0.413062*x(4) - 0.00536*x(1)*x(2)
     + 0.00050871*x(1)*x(4) + 0.0000627636*x(2)*x(3) - 0.01202*x(1)^2 –
     0.000585*x(2)^2);

     end                                                                    (5.7)
```

Where x(1), x(2), x(3) and x(4) denotes the pouring temperature, vacuum pressure, insert temperature and grit size of sand paper, respectively. The fitness function is marked negative to maximize the microhardness as genetic algorithm minimizes all the objectives by default. Actual range of process parameters as mentioned in

Equation 5.2 to Equation 5.5 is utilized to obtain the effective results by GA. Significant operating parameters of GA such as size of population, probability of cross over, mutation and number of iterations, etc. is represented in Table 5.1. The optimal solution was achieved at 51^{st} iteration having the best fitness value of microhardness as 326.51 HV as shown in Figure 5.8. The process parameters, which yield the maximum microhardness are: 650.36 ˚C pouring temperature, 399.96 mm of Hg vacuum pressure, 377.59 ˚C insert temperature and 780.93 grit size of sand paper. Figure 5.9 depicts the optimization history and best individuals for microhardness

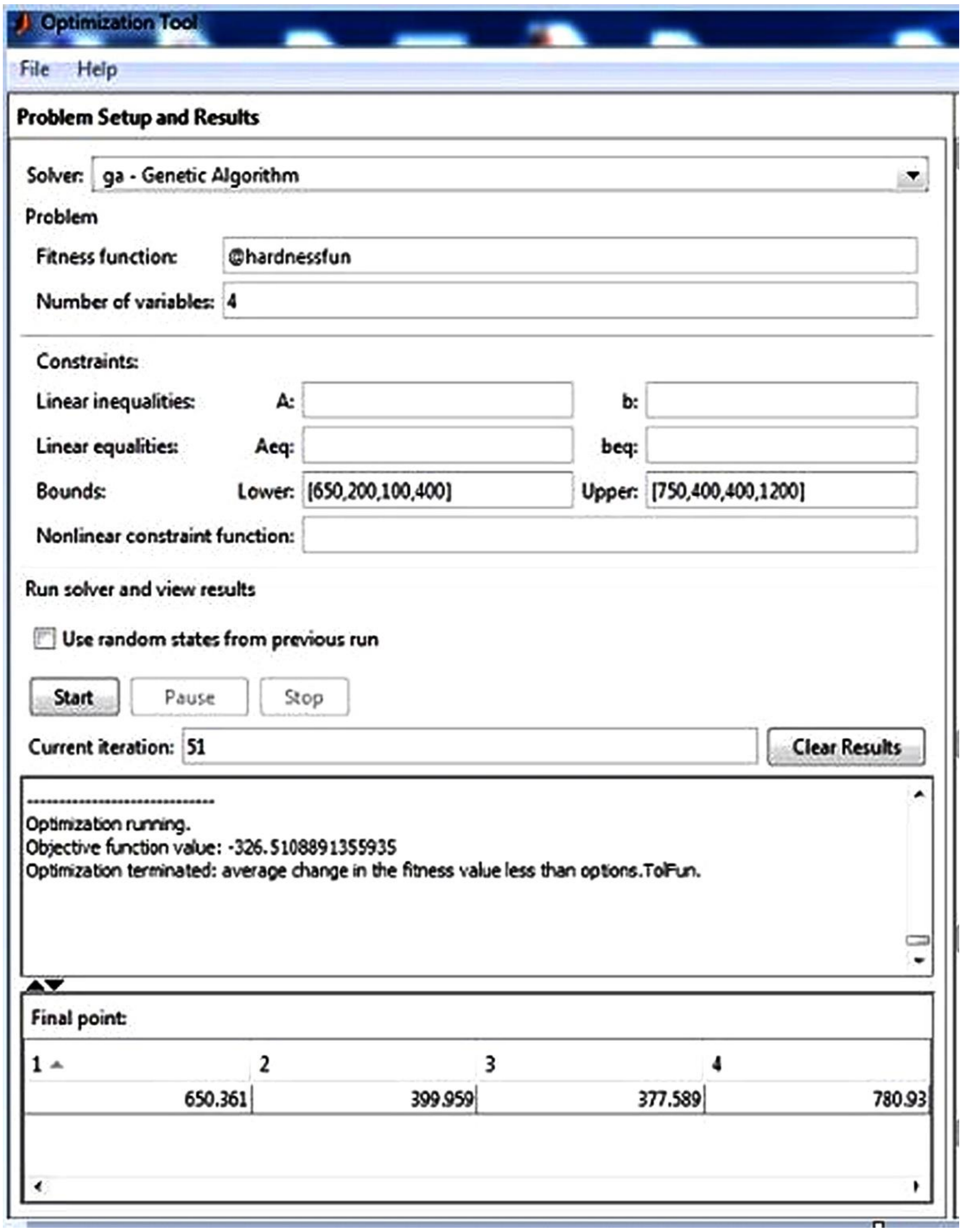

Figure 5.8 Screen shot of GA optimization for microhardness

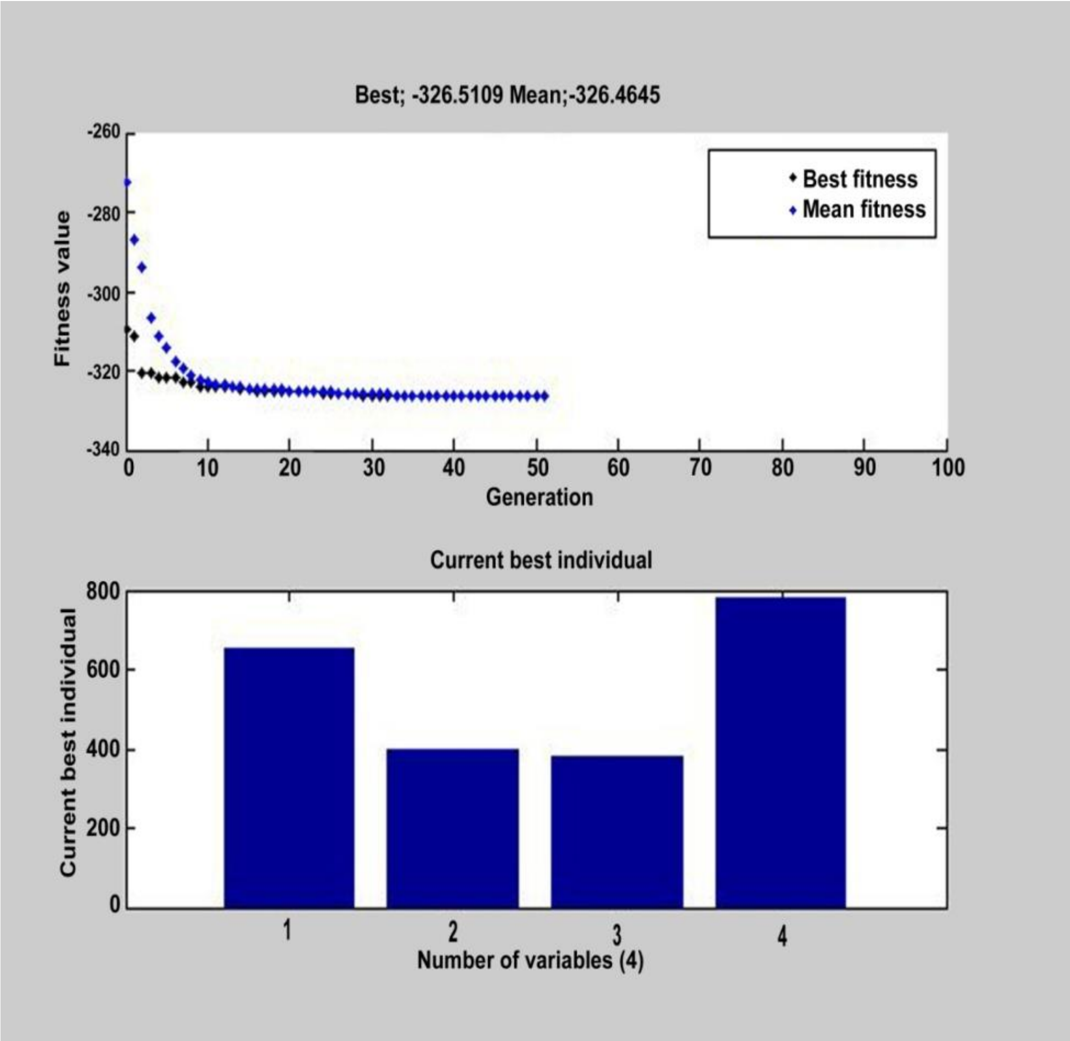

Figure 5.9 GA optimization history and best individuals for microhardness

5.6.3 Comparison of Optimization Results for Microhardness

Table 5.10 summarizes the optimal value of microhardness along with optimal process parameters of vacuum assisted sand mold compound casting process obtained by means of experimental, regression model, desirability analysis and genetic algorithm. The maximum value of microhardness is 322.15, 323.13, 324.86 and 326.51 HV for experimental, regression model, desirability analysis and genetic algorithm respectively. It is conferred that GA has given the maximum value of microhardness as compared to the other methods. The optimal values as predicted by genetic algorithm for each process parameter lies in the range of actual process parameters.

Table 5.10 Optimal values of microhardness along with optimal process parameters by different methods

Method	Optimal Value of Micro Hardness (HV)	Optimal Process Parameters			
		Pouring Temperature (650-750 °C)	Vacuum Pressure (200 - 400 mm of Hg)	Insert Temperature (100-400 °C)	Grit Size of Sand Paper (400-1200)
Genetic Algorithm	326.51	650.36	399.96	377.59	780.93
Desirability Analysis	324.86	663.20	347.38	295.13	534.41
Regression Model	323.13	675.00	350.00	325.00	600.00
Experimental Method	322.15	675.00	350.00	325.00	600.00

5.7 VALIDATION OF OPTIMIZATION RESULTS

The results obtained by optimization are validated theoretically as well as experimentally by conducting confirmation experiments.

5.7.1 Theoretical Validation

It is clear from previous section that the optimal values of shear strength, impact strength and microhardness are obtained by GA optimization. Therefore, the optimal process parameters so obtained are to be verified. In order to validate the optimal process parameters evaluated by GA; these values are transferred to the regression model Equation 5.5 to Equation 5.7. PT, VC, IT and GS are replaced by the optimal solutions of pouring temperature, vacuum pressure, insert temperature and grit size of sand paper, respectively. The equations thus formulated are written as:

$$SS = -769.45144 + 2.63608*650.012 - 0.148586*307.451 - 0.44473*100.00 + 0.000660667*650.012*100.00 - 0.000152333*307.451*100.00 + 0.000255295*307.451*807.346 - 0.00210*(650.012)^2 - 0.000046601*(807.346)^2 \quad (5.8)$$

$$= 37.86 \text{ MPa}$$

$$IS = -54.80128 + 0.13241*661.13 + 0.20639*328.0 + 0.00977638*1187.15 - 0.0003302*661.13*200.02 - 0.00031606*661.13*328.0 + 0.0000145833*328.0*1187.15 + 0.000388875*(200.02)^2 - 0.00000624045*(1187.15)^2 \quad (5.9)$$

$$= 12.28$$

$$MH = -5984.38 + 17.3175*650.36 + 4.1649*399.96 - 0.413062*780.93 - 0.00536*650.36*399.96 + 0.00050871*650.36*780.93 + 0.0000627636*399.96*377.59 - 0.01202*(650.36)^2 - 0.000585*(399.96)^2 \quad (5.10)$$

$$= 326.66 \text{ HV}$$

Equation 5.8 to Equation 5.10 predicted the shear strength = 37.86 MPa, impact strength = 12.28 J and microhardness = 326.66 HV respectively. These values are closer to the maximum fitness function value 37.85 MPa, 12.29 J and 326.51 HV as obtained by GA optimization for shear strength, impact strength and microhardness respectively.

5.7.2 Confirmation Experiments

Confirmation experiments are conducted at the optimum setting of the process parameters suggested by regression model, desirability analysis and genetic algorithm. Three experiments are conducted for each method separately. The average value of shear strength, impact strength and microhardness so obtained is represented in Table 5.11. The predicted values and the experimental values are quite close to each other and fall within the confidence interval. Therefore, the results obtained from the confirmation experiments reflect successful optimization.

Table 5.11 Comparison of optimal predicted values and confirmation experiment results

Output	Optimization Method	Optimal Process Parameters				Predicted Best Value	Confirmation Experiment Value
		Pouring Temp. (°C)	Vacuum Pressure (mm of Hg)	Insert temp (°C)	Grit size of sand paper (no.)		
Shear Strength	Genetic Algorithm	650.01	307.45	100.00	807.35	37.85	37.43
	Desirability Analysis	674.93	379.46	122.68	825.46	35.99	35.78
	Regression Model	675.00	350.00	175.00	1000.00	34.73	34.85
Impact Strength	Genetic Algorithm	661.13	200.02	328.00	1187.15	12.29	12.21
	Desirability Analysis	675.58	201.35	322.74	934.15	11.71	11.57
	Regression Model	700.00	400.00	250.00	800.00	10.68	10.50
Micro Hardness	Genetic Algorithm	650.36	399.96	377.59	780.93	326.51	326.12
	Desirability Analysis	663.20	347.38	295.13	534.41	324.86	325.22
	Regression Model	675.00	350.00	325.00	600.00	323.13	323.05

5.8 OPTIMIZATION BY GRAPH THEORETIC APPROACH

GTA is a versatile tool that has been used in various fields for the conversion of qualitative factors in quantitative terms. It enables to understand and analyze the system by recognizing system and subsystem up to its constituent level [123-129]. Mathematical modeling improves the application of this approach in comparison to other conventional approaches such as flow chart, block diagram, fish-bone diagram, etc. The mathematical model developed by GTA, considers the inheritance and relative importance/interdependencies of factors and subfactors. The inheritance refers to the participation of factor itself whereas inter-relation refers to the level of dependency among the factors [130-134]. GTA is represented in three steps; (i) digraph, (ii) matrix, and (iii) permanent function. A system is represented by a digraph (directed graph) in the form of nodes and edges. Directed edges denote inter-relation among the factors. Digraph is used to characterize a physical condition that contains different objects and their correlation. Digraph is converted into mathematical form in terms of matrix representation. The matrix form permits the use of computers to solve the complex problems. The required output/response is determined in terms of an index provided by permanent function of a matrix [135-139].

In present work, joint strength of A356/Mg couples is evaluated by GTA. Joint strength is dependent upon the mechanical properties associated with it. These properties have been considered as factors. Each property is further dependent upon four dominating process parameters, which have been considered as subfactors. Figure 5.10 represents the factors and subfactors affecting the joint strength of A356/Mg couple prepared by VASMCC process.

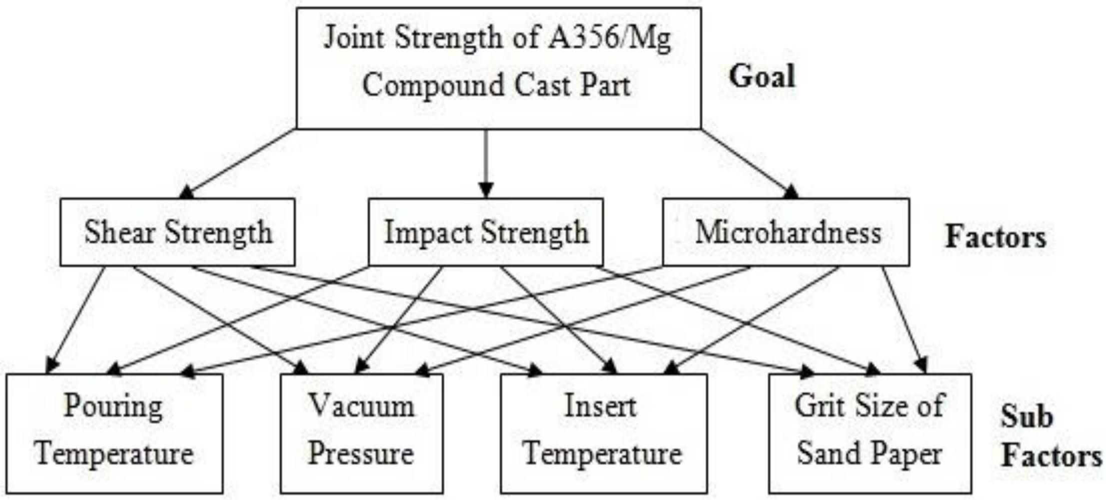

Figure 5.10 Factors and subfactors affecting joint strength of A356/Mg compound cast part

GTA is executed in three steps as follows:

5.8.1 Digraph Representation

Joint strength of A356/Mg couple is represented by a digraph consisting of a set of nodes P = R_i where i = 1, 2....N and directed edges Q = r_{ij}. Node R_i denotes the i^{th} factor affecting the joint strength and edge r_{ij} denotes the relative importance among the factors. Number of nodes (N) considered as equal to the number of factors which affect the joint strength. A directed edge (r_{ij}) is drawn from node *i* to node *j* when factor *i* have the relative importance over factor *j* or vice versa. Figure 5.11 shows a digraph for the joint strength of A356/Mg couple. The factors namely shear strength (R_1), impact strength (R_2) and microhardness (R_3), which affect the joint strength of A356/Mg couple, are considered. All these factors also affect each other in view of joint strength. So, directed edges are drawn from R_1 to R_2 and R_3, R_2 to R_1 and R_3, and from R_3 to R_1 and R_2. These factors are further dependent upon the subfactors (pouring temperature, vacuum pressure, insert temperature and grit size of sand paper used) considered for VASMCC process. The subsystem digraphs indicating relative importance/interdependencies of subfactors are shown in Figure 5.12 to Figure 5.14 for shear strength, impact strength and microhardness respectively. Superscript and subscript denotes the subsystem and subfactors affecting the subsystem respectively.

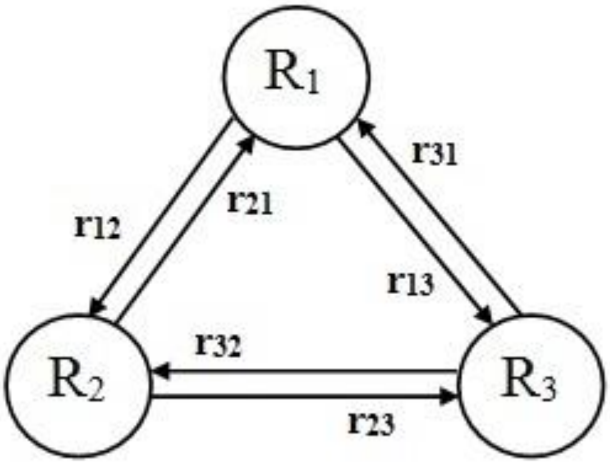

Figure 5.11 System diagraph for joint strength

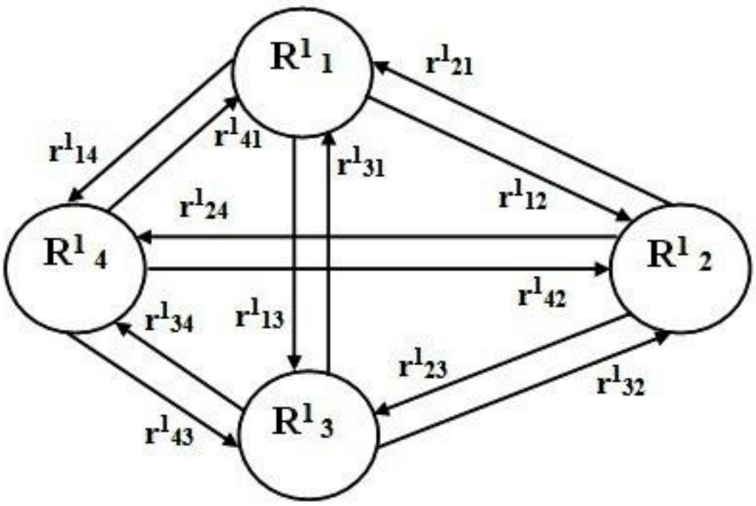

Figure 5.12 Subsystem diagraph for response R_1 (shear strength)

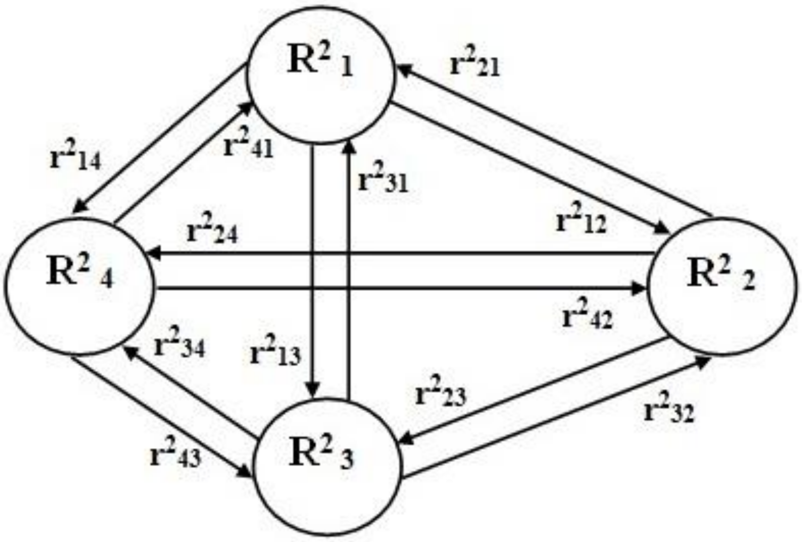

Figure 5.13 Subsystem diagraph for response R_2 (impact strength)

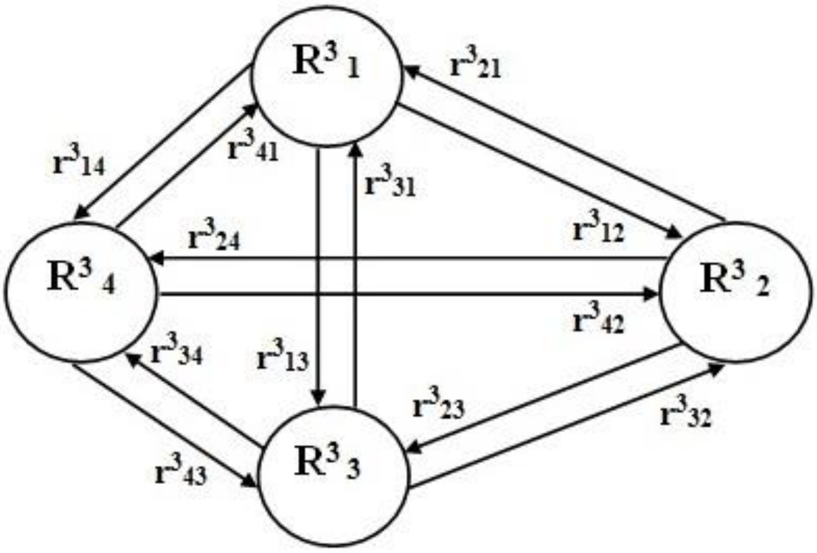

Figure 5.14 Subsystem diagraph for response R_3 (microhardness)

5.8.2 Matrix Representation

To establish a mathematical relation between joint strength and factors affecting it, the digraph is expressed in matrix form. This matrix is termed as joint strength evaluation matrix or variable permanent matrix for joint strength (VPM_{JS}). Equation 5.11 represents the matrix corresponding to joint strength evaluation digraph (Figure 5.11). The diagonal elements R_1, R_2 and R_3 represent the inheritance/impact of factors and the off-diagonal elements denote the relative importance of each factor.

$$VPM_{JS}\text{ (joint strength)} = \begin{array}{cc} \begin{matrix} R_1 & R_2 & R_3 \end{matrix} & \text{Parameters} \\ \begin{bmatrix} R_1 & r_{12} & r_{13} \\ r_{21} & R_2 & r_{23} \\ r_{31} & r_{32} & R_3 \end{bmatrix} & \begin{matrix} R_1 \\ R_2 \\ R_3 \end{matrix} \end{array} \tag{5.11}$$

Similar matrices are formulated as shown in Equation 5.12 to Equation 5.14 corresponding to the subsystem digraphs shown in Figure 5.12 to Figure 5.14.

$$VPM_{R1}\text{ (shear strength)} = \begin{array}{cc} \begin{matrix} R^1{}_1 & R^1{}_2 & R^1{}_3 & R^1{}_4 \end{matrix} & \text{Parameters} \\ \begin{bmatrix} R^1{}_1 & r^1{}_{12} & r^1{}_{13} & r^1{}_{14} \\ r^1{}_{21} & R^1{}_2 & r^1{}_{23} & r^1{}_{24} \\ r^1{}_{31} & r^1{}_{32} & R^1{}_3 & r^1{}_{34} \\ r^1{}_{41} & r^1{}_{42} & r^1{}_{43} & R^1{}_4 \end{bmatrix} & \begin{matrix} R^1{}_1 \\ R^1{}_2 \\ R^1{}_3 \\ R^1{}_4 \end{matrix} \end{array} \tag{5.12}$$

$$VPM_{R2}\text{ (impact strength)} = \begin{array}{cc} \begin{matrix} R^2{}_1 & R^2{}_2 & R^2{}_3 & R^2{}_4 \end{matrix} & \text{Parameters} \\ \begin{bmatrix} R^2{}_1 & r^2{}_{12} & r^2{}_{13} & r^2{}_{14} \\ r^2{}_{21} & R^2{}_2 & r^2{}_{23} & r^2{}_{24} \\ r^2{}_{31} & r^2{}_{32} & R^2{}_{32} & r^2{}_{34} \\ r^2{}_{41} & r^2{}_{42} & r^2{}_{43} & R^2{}_4 \end{bmatrix} & \begin{matrix} R^2{}_1 \\ R^2{}_2 \\ R^2{}_3 \\ R^2{}_4 \end{matrix} \end{array} \tag{5.13}$$

$$VPM_{R3}\text{ (microhardness)} = \begin{array}{cc} \begin{matrix} R^3{}_1 & R^3{}_2 & R^3{}_3 & R^3{}_4 \end{matrix} & \text{Parameters} \\ \begin{bmatrix} R^3{}_1 & r^3{}_{12} & r^3{}_{13} & r^3{}_{14} \\ r^3{}_{21} & R^3{}_2 & r^3{}_{23} & r^3{}_{24} \\ r^3{}_{31} & r^3{}_{32} & R^3{}_3 & r^3{}_{34} \\ r^3{}_{41} & r^3{}_{42} & r^3{}_{43} & R^3{}_4 \end{bmatrix} & \begin{matrix} R^3{}_1 \\ R^3{}_2 \\ R^3{}_3 \\ R^3{}_4 \end{matrix} \end{array} \tag{5.14}$$

In order to obtain the value of multinomial completely, numerical values are assigned to the diagonal and off diagonal elements in variable permanent matrices (Equation 5.11 to Equation 5.14). A scale of 0-10 is used to assign the values of inheritance to the factors and subfactors as per Table 5.12. The following equation is used to calculate the inheritance of subfactors:

$$\text{Scale value (inheritance)} = (X - X_{min})*10/(X_{max} - X_{min}) \tag{5.15}$$

Where, X denotes the value to be scaled, and X_{max} and X_{min} denote its maximum and minimum values respectively.

Table 5.12 Attribute Value [140]

Sr. No.	Subjective measure of an attribute	Value assigned
1	Exceptionally high	10
2	Extremely high	09
3	Very high	08
4	High	07
5	Above average	06
6	Average	05
7	Below average	04
8	Low	03
9	Very low	02
10	Extremely low	01
11	Exceptionally low	00

The perturbation diagrams generated by using design-expert software for regression models are shown in Figure 5.15 to Figure 5.17 which indicate the relationship of process parameters with joint properties; shear strength, impact strength and microhardness respectively. The inheritance of diagonal elements of subsystem matrices (Equation 5.12 to Equation 5.14) is evaluated with the help of perturbation diagrams. Table 5.13 to Table 5.15 represents the inheritance values determined by using Equation 5.15 for all levels of subfactors i.e., shear strength, impact strength and microhardness respectively.

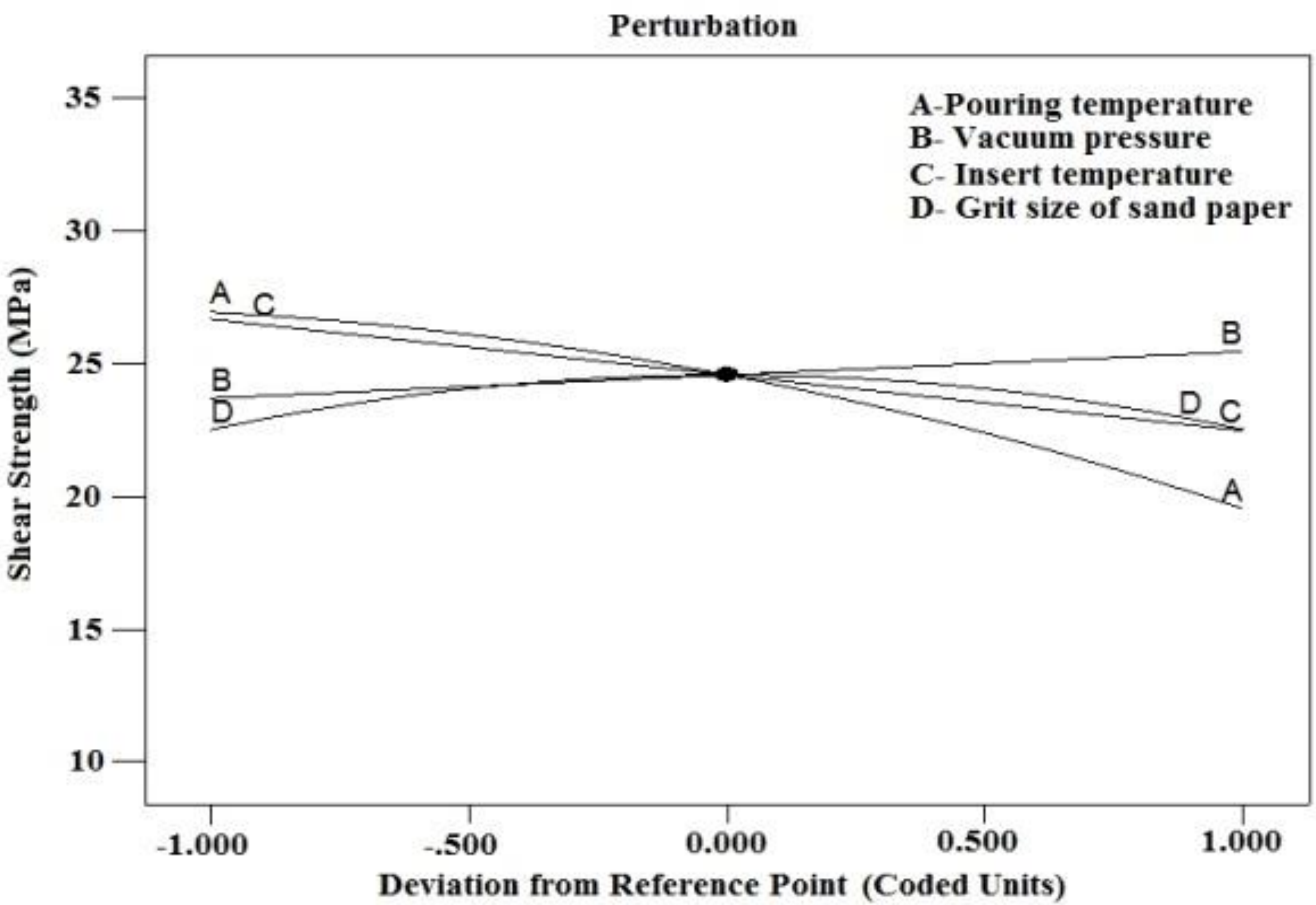

Figure 5.15 Perturbation plot for shear strength

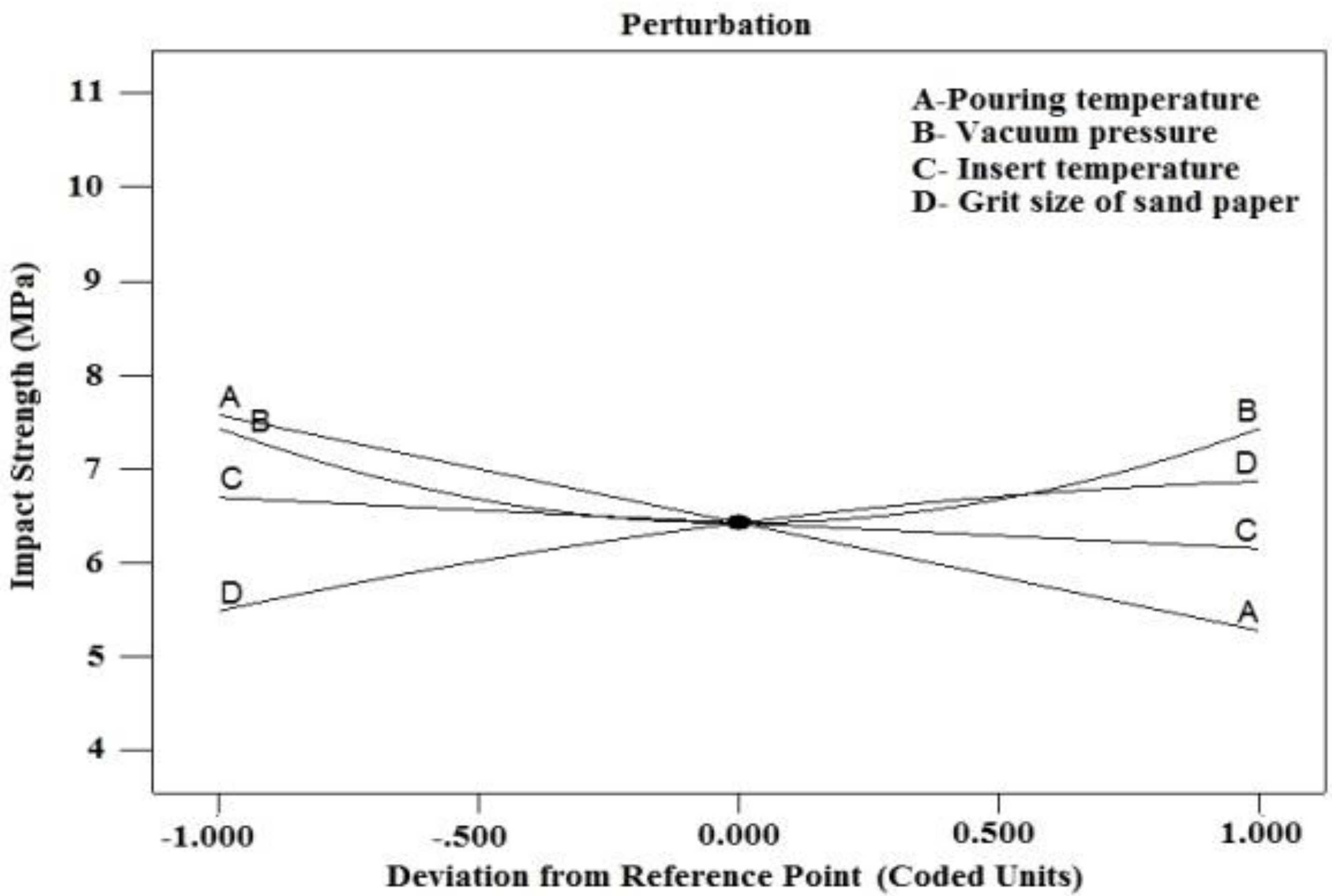

Figure 5.16 Perturbation plot for impact strength

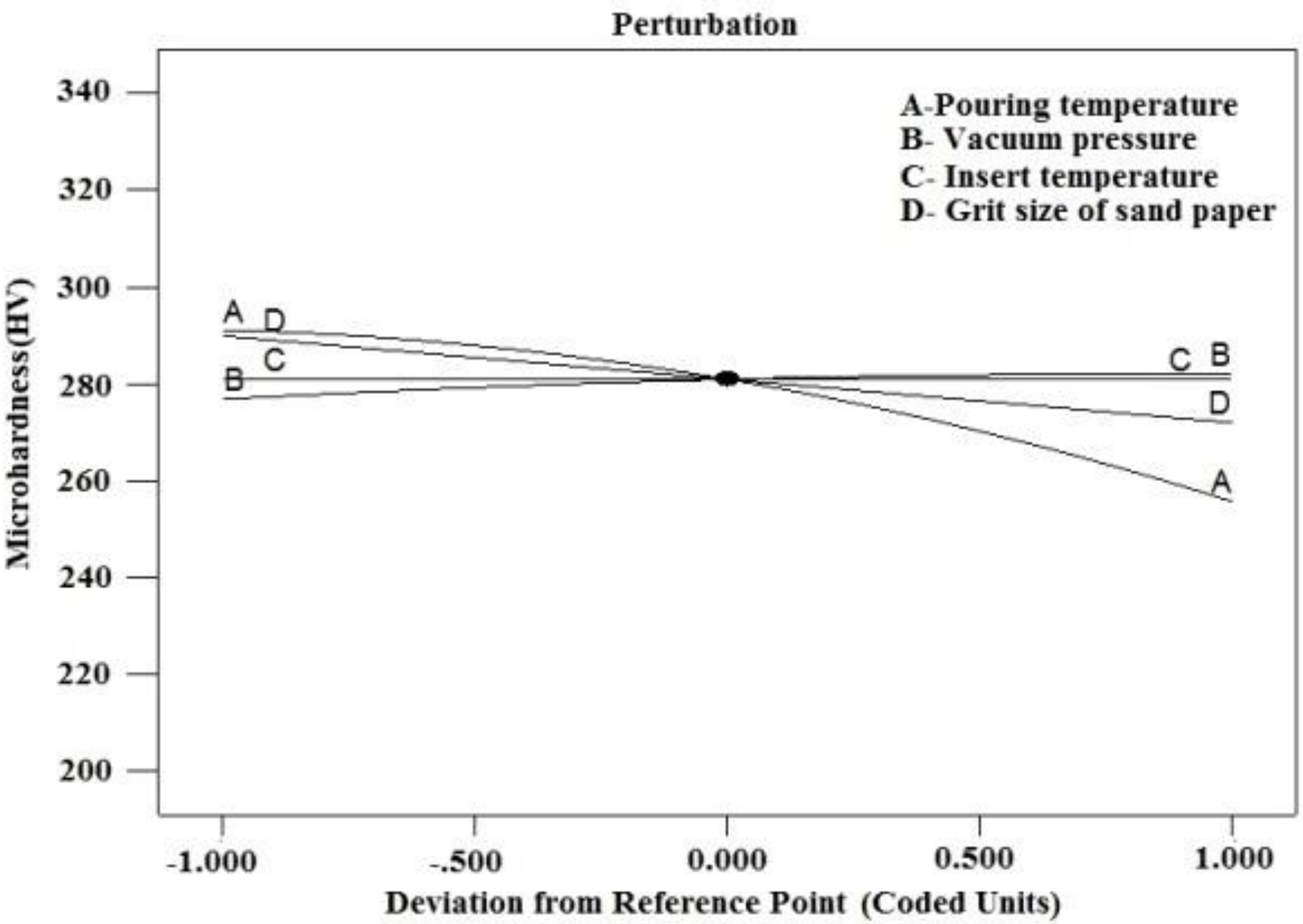

Figure 5.17 Perturbation plot for microhardness

Table 5.13 Inheritance of subfactors (diagonal elements) for shear strength

Exp. No.	Process Parameters				Inheritance			
	Pouring Temp. (˚C)	Vacuum Pressure (mm of Hg)	Insert Temp. (˚C)	Grit Size of Sand Paper (number)	Pouring Temp. (R^1_1)	Vacuum Pressure (R^1_2)	Insert Temp. (R^1_3)	Grit Size of Sand Paper (R^1_4)
1	675	250	175	600	6.7	5.7	6.5	5.7
2	725	250	175	600	5.0	5.7	6.5	5.7
3	675	350	175	600	6.7	6.2	6.5	5.7
4	725	350	175	600	5.0	6.2	6.5	5.7
5	675	250	325	600	6.7	5.7	6.5	5.7
6	725	250	325	600	5.0	5.7	6.5	5.7
7	675	350	325	600	6.7	6.2	6.5	5.7
8	725	350	325	600	5.0	6.2	6.5	5.7
9	675	250	175	1000	6.7	5.7	6.5	5.7
10	725	250	175	1000	5.0	5.7	6.5	5.7
11	675	350	175	1000	6.7	6.2	6.5	5.7
12	725	350	175	1000	5.0	6.2	6.5	5.7
13	675	250	325	1000	6.7	5.7	5.5	5.7
14	725	250	325	1000	5.0	5.7	5.5	5.7
15	675	350	325	1000	6.7	6.2	5.5	6.0
16	725	350	325	1000	5.0	6.2	5.5	6.0
17	650	300	250	800	7.1	6.0	6.0	6.0
18	750	300	250	800	3.7	6.0	6.0	6.0
19	700	200	250	800	6.0	5.5	6.0	6.0
20	700	400	250	800	6.0	6.4	6.0	6.0
21	700	300	100	800	6.0	6.0	6.9	6.0
22	700	300	400	800	6.0	6.0	5.0	6.0
23	700	300	250	400	6.0	6.0	6.0	5.1
24	700	300	250	1200	6.0	6.0	6.0	5.0
25	700	300	250	800	6.0	6.0	6.0	6.0
26	700	300	250	800	6.0	6.0	6.0	6.0
27	700	300	250	800	6.0	6.0	6.0	6.0
28	700	300	250	800	6.0	6.0	6.0	6.0
29	700	300	250	800	6.0	6.0	6.0	6.0
30	700	300	250	800	6.0	6.0	6.0	6.0

Table 5.14 Inheritance of subfactors (diagonal elements) for impact strength

Exp. No.	Process Parameters				Inheritance			
	Pouring Temp. (˚C)	Vacuum Pressure (mm of Hg)	Insert Temp. (˚C)	Grit Size of Sand Paper (number)	Pouring Temp. (R^2_1)	Vacuum Pressure (R^2_2)	Insert Temp. (R^2_3)	Grit Size of Sand Paper (R^2_4)
1	675	250	175	600	4.6	4.2	4.0	3.1
2	725	250	175	600	2.8	4.2	4.0	3.1
3	675	350	175	600	4.6	4.2	4.0	3.1
4	725	350	175	600	2.8	4.2	4.0	3.1
5	675	250	325	600	4.6	4.2	3.5	3.1
6	725	250	325	600	2.8	4.2	3.5	3.1
7	675	350	325	600	4.6	4.2	3.5	3.1
8	725	350	325	600	2.8	4.2	3.5	3.1
9	675	250	175	1000	4.6	4.2	4.0	4.2
10	725	250	175	1000	2.8	4.2	4.0	4.2
11	675	350	175	1000	4.6	4.2	4.0	4.2
12	725	350	175	1000	2.8	4.2	4.0	4.2
13	675	250	325	1000	4.6	4.2	3.5	4.2
14	725	250	325	1000	2.8	4.2	3.5	4.2
15	675	350	325	1000	4.6	4.2	3.5	4.2
16	725	350	325	1000	2.8	4.2	3.5	4.2
17	650	300	250	800	5.5	3.8	3.8	3.8
18	750	300	250	800	2.0	3.8	3.8	3.8
19	700	200	250	800	3.8	5.2	3.8	3.8
20	700	400	250	800	3.8	5.2	3.8	3.8
21	700	300	100	800	3.8	3.8	4.2	3.8
22	700	300	400	800	3.8	3.8	3.2	3.8
23	700	300	250	400	3.8	3.8	3.8	2.3
24	700	300	250	1200	3.8	3.8	3.8	4.5
25	700	300	250	800	3.8	3.8	3.8	3.8
26	700	300	250	800	3.8	3.8	3.8	3.8
27	700	300	250	800	3.8	3.8	3.8	3.8
28	700	300	250	800	3.8	3.8	3.8	3.8
29	700	300	250	800	3.8	3.8	3.8	3.8
30	700	300	250	800	3.8	3.8	3.8	3.8

Table 5.15 Inheritance of subfactors (diagonal elements) for microhardness

Exp. No.	Process Parameters				Inheritance			
	Pouring Temp. (˚C)	Vacuum Pressure (mm of Hg)	Insert Temp. (˚C)	Grit Size of Sand Paper (number)	Pouring Temp. (R^3_1)	Vacuum Pressure (R^3_2)	Insert Temp. (R^3_3)	Grit Size of Sand Paper (R^3_4)
1	675	250	175	600	6.7	5.9	6.1	6.4
2	725	250	175	600	5.0	5.9	6.1	6.4
3	675	350	175	600	6.7	6.1	6.1	6.4
4	725	350	175	600	5.0	6.1	6.1	6.4
5	675	250	325	600	6.7	5.9	6.1	6.4
6	725	250	325	600	5.0	5.9	6.1	6.4
7	675	350	325	600	6.7	6.1	6.1	5.6
8	725	350	325	600	5.0	6.1	6.1	5.6
9	675	250	175	1000	6.7	5.9	6.1	5.6
10	725	250	175	1000	5.0	5.9	6.1	5.6
11	675	350	175	1000	6.7	6.1	6.1	5.6
12	725	350	175	1000	5.0	6.1	6.1	5.6
13	675	250	325	1000	6.7	5.9	6.1	5.6
14	725	250	325	1000	5.0	5.9	6.1	5.6
15	675	350	325	1000	6.7	6.1	6.1	5.6
16	725	350	325	1000	5.0	6.1	6.1	5.6
17	650	300	250	800	7.0	6.0	6.0	6.0
18	750	300	250	800	3.6	6.0	6.0	6.0
19	700	200	250	800	6.0	5.7	6.0	6.0
20	700	400	250	800	6.0	6.2	6.0	6.0
21	700	300	100	800	6.0	6.0	6.1	6.0
22	700	300	400	800	6.0	6.0	6.1	6.0
23	700	300	250	400	6.0	6.0	6.0	6.9
24	700	300	250	1200	6.0	6.0	6.0	5.2
25	700	300	250	800	6.0	6.0	6.0	6.0
26	700	300	250	800	6.0	6.0	6.0	6.0
27	700	300	250	800	6.0	6.0	6.0	6.0
28	700	300	250	800	6.0	6.0	6.0	6.0
29	700	300	250	800	6.0	6.0	6.0	6.0
30	700	300	250	800	6.0	6.0	6.0	6.0

Comparison of an attribute *i* to the attribute *j* indicates its relative importance for a specified problem objective. If r_{ji} is the relative importance of j^{th} attribute over the i^{th} attribute, then relative importance of i^{th} attribute over j^{th} attribute can be determined as:

$$r_{ij} = 10 - r_{ji} \tag{5.16}$$

The relative importance between the factors and sub factors are assigned within a range of 0-10 based upon the experimental investigation and experts' opinion as per Table 5.16. The relative importance of process parameters (subfactors) with respect to response (factors) is represented in Table 5.17.

Table 5.16 Relative importance of attributes [140]

Sr. No.	Description	Relative Importance	
		r_{ji}	$r_{ij} = 10 - r_{ji}$
1	An attribute is exceptionally more important over the other	10	00
2	An attribute is extremely important over the other	09	01
3	An attribute is very strongly important over the other	08	02
4	An attribute is strongly more important over the other	07	03
5	An attribute is slightly more important over the other	06	04
6	Two attributes are equally important	05	05

Table 5.17 Relative importance of process parameters (subfactors) with respect to responses (factors)

Process Parameters (Subfactors)	Relative importance (Factors)		
	Shear Strength	Impact Strength	Micro-hardness
Pouring temperature over vacuum pressure (R_{12})	6	5	7
Pouring temperature over insert temperature (R_{13})	5	7	7
Pouring temperature over grit size of sand paper (R_{14})	7	6	5
Vacuum pressure over pouring temperature (R_{21})	4	5	3
Vacuum pressure over insert temperature (R_{23})	4	6	5
Vacuum pressure over grit size of sand paper (R_{24})	6	6	3
Insert temperature over pouring temperature (R_{31})	5	3	3
Insert temperature over vacuum pressure (R_{32})	6	4	5
Insert temperature over grit size of sand paper (R_{34})	7	5	3
Grit size of sand paper over pouring temperature (R_{41})	3	4	5
Grit size of sand paper over vacuum pressure (R_{42})	4	4	7
Grit size of sand paper over insert temperature (R_{43})	3	5	7

5.8.3 Permanent Representation

A unique representation for the matrices is established by anticipating their permanent function. The permanent function is similar to the determinant of a matrix with all signs positive. Permanent function for joint strength is denoted by 'per (JS)'. It is determined by developing a MATLAB program. Variable permanent matrix (VPM) for each subsystem is represented by Equation 5.17 to Equation 5.19 as per their respective digraphs. The joint strength index evaluation for experiment # 1 (Table 5.13) is illustrated below:

VPM for subsystem 1 (shear strength) is shown in Equation 5.17 by considering relative importance of subfactors (off diagonal elements) as r^1_{12}=6, r^1_{13}= 5, r^1_{14}= 7, r^1_{21}= 4, r^1_{23}= 4, r^1_{24}=6, r^1_{31}=5, r^1_{32}=6, r^1_{34}=7, r^1_{41}=3, r^1_{42}= 4, r^1_{43}=3 (Table 5.17). The inheritance is taken from Table 5.13 as R^1_1=6.7, R^1_2=5.7, R^1_3=6.5 and R^1_4= 5.7.

$$
VPM_{R1} \text{ (shear strength)} = \begin{array}{c} R^1{}_1 \quad R^1{}_2 \quad R^1{}_3 \quad R^1{}_4 \\ \begin{bmatrix} 6.7 & 6 & 5 & 7 \\ 4 & 5.7 & 4 & 6 \\ 5 & 6 & 6.5 & 7 \\ 3 & 4 & 3 & 5.7 \end{bmatrix} \end{array} \begin{array}{l} \text{Parameters} \\ R^1{}_1 \\ R^1{}_2 \\ R^1{}_3 \\ R^1{}_4 \end{array} \qquad (5.17)
$$

The permanent function for the shear strength (shear strength index), per (R_1) = 16943.

The variable permanent matrix subsystem 2 (impact strength) is written in Equation 5.18 by considering the relative importance of subfactors as r^2_{12}=5, r^2_{13}= 7, r^2_{14}= 6, r^2_{21}= 5, r^2_{23}= 6, r^2_{24}=6, r^2_{31}=3, r^2_{32}=4, r^2_{34}=5, r^2_{41}=4, r^2_{42}= 4, r^2_{43}=5 (Table 5.17). The inheritance is taken from Table 5.14 as R^2_1=4.6, R^2_2=4.2, R^2_3=4.0 and R^2_4= 3.1.

$$
VPM_{R2} \text{ (impact strength)} = \begin{array}{c} R^2{}_1 \quad R^2{}_2 \quad R^2{}_3 \quad R^2{}_4 \\ \begin{bmatrix} 4.6 & 5 & 7 & 6 \\ 5 & 4.2 & 6 & 6 \\ 3 & 4 & 4.0 & 5 \\ 4 & 4 & 5 & 3.1 \end{bmatrix} \end{array} \begin{array}{l} \text{Parameters} \\ R^2{}_1 \\ R^2{}_2 \\ R^2{}_3 \\ R^2{}_4 \end{array} \qquad (5.18)
$$

The permanent function for the impact strength (impact strength index), per (R_2) =11395.

VPM for subsystem 3 (microhardness) is shown in Equation 5.19 by considering relative importance of subfactors (off diagonal elements) as r^3_{12}=7, r^3_{13}= 7, r^3_{14}= 5, r^3_{21}= 3, r^3_{23}= 5, r^3_{24}=3, r^3_{31}=3, r^3_{32}=5, r^3_{34}=3, r^3_{41}=5, r^3_{42}= 7, r^3_{43}=7 (Table 5.17). The inheritance is taken from Table 5.15 as R^3_1=6.7, R^3_2=5.9, R^3_3=6.1 and R^3_4= 6.4.

$$VPM_{R3}\,(\text{microhardness}) = \begin{array}{c} \begin{matrix} R^3{}_1 & R^3{}_2 & R^3{}_3 & R^3{}_4 \end{matrix} \\ \begin{bmatrix} 6.7 & 7 & 7 & 5 \\ 3 & 5.9 & 5 & 3 \\ 3 & 5 & 6.1 & 3 \\ 5 & 7 & 7 & 6.4 \end{bmatrix} \end{array} \begin{array}{l} \text{Parameters} \\ R^3{}_1 \\ R^3{}_2 \\ R^3{}_3 \\ R^3{}_4 \end{array} \qquad (5.19)$$

The permanent function for the microhardness (microhardness index), per (R_3) = 16576.

VPM for joint strength index is shown in Equation 5.20. The index values of shear strength, impact strength and microhardness constitute diagonal elements of this matrix. Off diagonal elements are taken as r_{12}=7, r_{13}=5, r_{21}=3, r_{23}=4, r_{31}=5, r_{32}=6 on the basis of experimental investigation and experts' opinion.

$$VPM_{JS}\,(\text{joint strength}) = R = \begin{array}{c} \begin{matrix} R_1 & R_2 & R_3 \end{matrix} \\ \begin{bmatrix} 16943 & 7 & 5 \\ 3 & 11395 & 4 \\ 5 & 6 & 16576 \end{bmatrix} \end{array} \begin{array}{l} \text{Parameters} \\ R_1 \\ R_2 \\ R_3 \end{array} \qquad (5.20)$$

The permanent function for joint strength (joint strength index), per (JS) = 3.20E12.

Joint strength index calculated for all thirty experiments are represented in Table 5.18. The shear strength index = 16943, impact strength index = 11395 and microhardness index = 16576 indicate that shear strength has maximum influence on joint strength followed by microhardness and impact strength (shear strength > microhardness > impact strength) for experiment # 1.

Table 5.18 Index values of subsystems and system

Exp. No.	Sub Factors				Factors/Subsystem			System
	Pouring Temp. (˚C)	Vacuum Pressure (mm of Hg)	Insert Temp. (˚C)	Grit Size of Sand Paper (number)	Shear Strength Index per (R_1)	Impact Strength Index per (R_2)	Micro-hardness Index per (R_3)	Joint Strength Index per(JS)
1	675	250	175	600	16943	11395	16576	3.20E+12
2	725	250	175	600	15509	10374	15127	2.43E+12
3	675	350	175	600	17382	11395	16756	3.32E+12
4	725	350	175	600	15899	10374	15287	2.52E+12
5	675	250	325	600	16943	11101	16576	3.18E+12
6	725	250	325	600	15509	10113	15127	2.37E+12
7	675	350	325	600	17382	11101	16050	3.08E+12
8	725	350	325	600	15899	10113	14665	2.38E+12
9	675	250	175	1000	16943	12061	15880	3.25E+12
10	725	250	175	1000	15509	10959	14514	2.47E+12
11	675	350	175	1000	17382	12061	16050	3.37E+12
12	725	350	175	1000	15899	10959	14665	2.56E+12
13	675	250	325	1000	16088	11743	15880	3.00E+12
14	725	250	325	1000	14750	10678	14514	2.27E+12
15	675	350	325	1000	16772	11743	16050	3.16E+12
16	725	350	325	1000	15360	10678	14665	2.41E+12
17	650	300	250	800	17391	11977	16477	3.43E+12
18	750	300	250	800	14501	9974	13662	1.98E+12
19	700	200	250	800	16042	11776	15401	2.91E+12
20	700	400	250	800	16787	11776	15815	3.13E+12
21	700	300	100	800	17221	11233	15732	3.04E+12
22	700	300	400	800	15606	10661	15732	2.62E+12
23	700	300	250	400	15651	10178	16394	2.61E+12
24	700	300	250	1200	15562	11390	14987	2.66E+12
25	700	300	250	800	16456	11004	15649	2.83E+12
26	700	300	250	800	16456	11004	15649	2.83E+12
27	700	300	250	800	16456	11004	15649	2.83E+12
28	700	300	250	800	16456	11004	15649	2.83E+12
29	700	300	250	800	16456	11004	15649	2.83E+12
30	700	300	250	800	16456	11004	15649	2.83E+12

Results obtained for other experiments indicate similar observations. Joint strength index is dependent upon the index value of factors R_1, R_2 and R_3. Different combinations of subfactors imply different index values of these factors. A subsystem with higher index value indicates the greater influence on joint strength. In Table 5.18 the highest joint strength index (3.43E12) corresponds to the experiment # 17. This combination of factors and corresponding subfactors will produce the highest value of joint strength. The optimal process parameters at this value are 650 °C pouring temperature, 300 mm of Hg vacuum pressure, 250 °C insert temperature and 800 grit size of sand paper.

5.9 MULTIOBJECTIVE OPTIMIZATION

Multiobjective optimization provides the solutions of multiple criteria decision making problems. It provides the optimal solutions to the problems which are subjected to two of more objective functions simultaneously. The objective functions are usually in confliction with each other. A solution that maximizes one of the objectives might deteriorate another one. Therefore, a single optimal solution is not feasible. There are multiple optimal solutions which refer to the various tradeoffs between the objective functions [141-144]. Multiobjective optimization is functional in numerous fields including logistic, economics, science, engineering and technology where optimal decisions are looked-for in the occurrence of tradeoffs between two or more conflicting objectives. In the present work, multiobjective optimization is carried out by choosing two or more responses simultaneously. Following combination of objective functions are considered for this purpose:

- Combination of shear strength and impact strength
- Combination of impact strength and microhardness
- Combination of microhardness and shear strength
- Combination of shear strength, impact strength and microhardness

Multiobjective optimization is executed by desirability analysis and genetic algorithm.

5.9.1 Multiobjective Optimization for Combination of Shear Strength and Impact Strength by Desirability Analysis

Desirability values for combination of shear strength and impact strength are obtained with reference to the limits and constraints of process parameters as shown in Table 5.19. The solutions generated are represented in Table 5.20. The solution acquiring the highest value of desirability is considered as optimal solution. In this case, the number of solutions have the highest desirability value i.e., unity. It provides the optimal values which depend upon both the output variables. Sometime objectives may not be improved without trailing at least one of the objectives. Therefore, several combinations of optimal solution are provided in multiobjective optimization. Figure 5.18 represents the ramp graph of first optimal solution having maximum value of shear strength as 35.72 MPa and impact strength as 11.42 J that has been achieved corresponding to the desirability value of 1. The optimal process parameters as pouring temperature = 682.51 ^{o}C, vacuum pressure = 398.03 mm of Hg, insert temperature = 156.52 ^{o}C and grit size of sand paper = 1055.28 at these values.

Table 5.19 Constraints used in desirability analysis for multiobjective optimization of shear strength and impact strength

Constraints Name	Goal	Lower Limit	Upper Limit	Lower Weight	Upper Weight	Importance
Pouring Temperature (°C)	In range	650	750	1	1	3
Vacuum Pressure (mm of Hg)	In range	200	400	1	1	3
Insert Temperature (°C)	In range	100	400	1	1	3
Grit Size of Sand Paper (number)	In range	400	1200	1	1	3
Shear Strength (MPa)	Maximize	11.78	33.14	1	1	5
Impact Strength (J)	Maximize	4.00	10.50	1	1	5

Table 5.20 Multiobjective optimization of shear strength and impact strength by desirability analysis

No.	Optimal Process Parameters				Optimal Response		Desirability
	Pouring Temp. (˚C)	Vacuum Pressure (mm of Hg)	Insert Temp. (˚C)	Grit size of Sand paper (number)	Shear Strength (MPa)	Impact Strength (J)	
1	682.51	398.03	156.52	1055.28	35.72	11.42	1.00
2	651.36	397.22	131.48	722.15	35.26	11.95	1.00
3	660.37	392.82	168.05	1121.64	35.84	11.88	1.00
4	680.97	397.40	128.38	848.00	36.02	11.30	1.00
5	684.61	399.05	105.66	827.32	36.36	11.26	1.00
6	670.32	391.37	131.21	772.20	35.38	11.01	1.00
7	651.36	397.22	131.48	722.15	35.26	11.95	0.99
8	674.89	399.88	101.42	712.01	35.17	11.34	0.97
9	652.09	394.38	169.61	827.18	34.92	12.35	0.96
10	661.63	399.56	120.47	693.42	34.71	11.69	0.96
11	682.88	399.92	103.70	793.29	34.06	11.33	0.92
12	664.51	386.81	182.31	1080.15	34.58	11.46	0.90
13	662.34	387.21	209.80	1009.08	33.24	11.94	0.89
14	676.23	400.00	219.22	1200.00	31.40	10.96	0.87
15	669.70	200.00	100.00	678.73	32.28	10.78	0.87

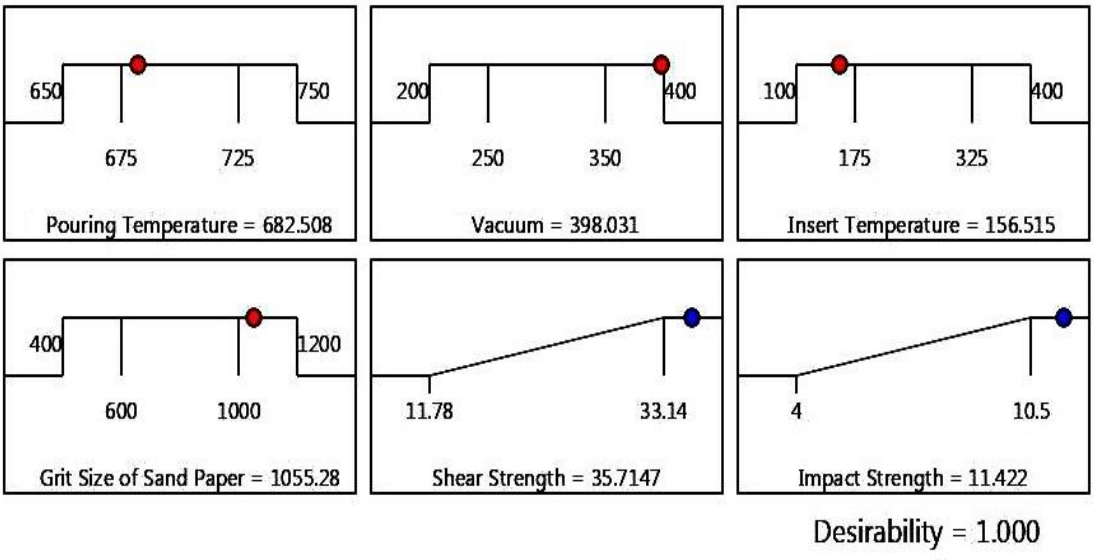

Figure 5.18 Ramp graph of optimal solution for shear and impact strength

5.9.2 Multiobjective Optimization for Combination of Shear Strength and Impact Strength by Genetic Algorithm

The GA multiobjective optimization is done by using MATLAB R2010a software. Global optimization toolbox is used for generating the optimum value of shear strength and impact strength as a function of designated process parameters for VASMCC process.

A MATLAB function is written by using the developed RSM models for shear strength and impact strength (Equation 4.3 and Equation 4.4). This function is called as input for creating a fitness function for the optimization problem. The fitness function so formulated is written as:

```
function R= shearstrengthimpactstrengthfun(x)
R(1) = - (-769.45144 + 2.63608*x(1) - 0.148586*x(2) - 0.44473*x(3) +
        0.000660667*x(1)*x(3) - 0.000152333*x(2)*x(3) +
        0.000255295*x(2)*x(4) - 0.00210*x(1)^2) - 0.000046601*x(4)^2);
R(2) = - (- 54.80128 + 0.13241*x(1) + 0.206039*x(3) + 0.00977638*x(4) -
        0.0003302*x(1)*x(2) - 0.00031606*x(1)*x(3) + 0.0000145833 * x(3)*x(4)
        + 0.000358875*x(2)^2 - 0.00000624045*x(4)^2);
end                                                                    (5.21)
```

Where, x(1), x(2), x(3) and x(4) symbolize the pouring temperature, vacuum pressure, insert temperature and grit size of sand paper respectively. The fitness function is marked negative as GA deals with minimization of objectives by default. The multiobjective optimization is carried out by using the fitness function formulated in Equation 5.21, subjected to the designated process parameters (Equation 5.2 to Equation 5.5) and GA operating parameters for multiobjective optimization as represented in Table 5.21. In multiobjective optimization problems, no single solution exists that simultaneously optimizes all the objectives. In that case, there exist a number of optimal solutions which are represented by the pareto front. It shows the tradeoff between the two objective functions [145-146]. Figure 5.19 depicts the pareto front of the optimal solutions for shear strength and impact strength.

Table 5.21 Genetic algorithm parameters for multiobjective optimization

Parameters	Sub Parameters with values		
Population	Size-15 x No. of variables	Type-double vector	Creation function-Constraint dependent default
Selection	Tournament		
Crossover	Single point crossover	Crossover rate-0.8	
Mutation	Adaptive feasible		
Stopping criteria	Generations-200 x No. of variables	Time limit-Infinite	Fitness time-Infinite
	Stall generations-50	Stall time limit-Infinite	Tolerance 1e-4
Plot function	Pareto front		

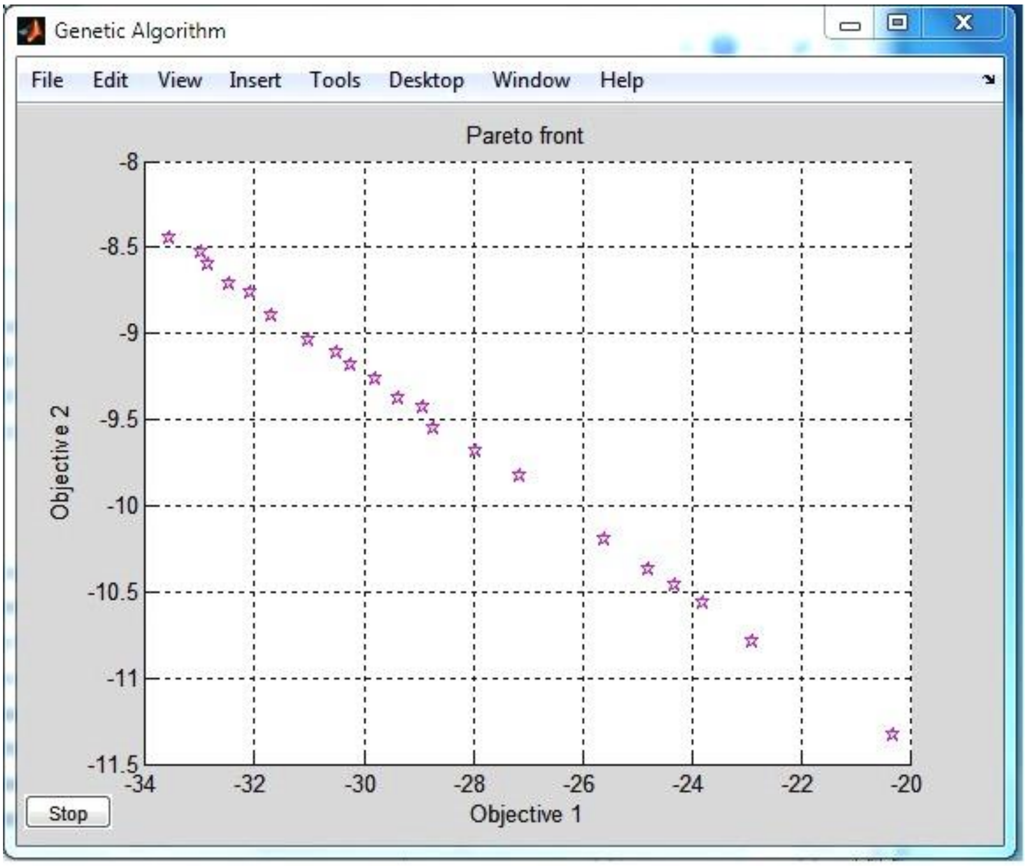

Objective 1 - Shear strength   Objective 2 - Impact strength

Figure 5.19 Pareto front of GA multiobjective optimization for shear strength and impact strength

The results of the optimization are shown in Table 5.22. It depicts optimal values of both the objective functions and the process variables. Screen shot of this multiobjective optimization is shown in Figure 5.20.

Table 5.22 Optimal process parameters corresponding to optimal value of fitness function for GA multiobjective optimization of shear strength and impact strength

Index	Optimal Process Parameters				Optimal Fitness Function	
	Pouring Temp. (˚C)	Vacuum Pressure (mm of Hg)	Insert Temp. (˚C)	Grit size of Sand paper (number)	Shear Strength (MPa)	Impact Strength (J)
1	650.80	399.86	161.33	1075.39	-32.47	-8.71
2	650.20	399.94	321.29	1073.99	-20.31	-11.34
3	651.47	400.00	147.01	1080.40	-33.55	-8.45
4	651.47	399.94	208.52	1077.41	-28.91	-9.42
5	650.83	399.91	190.94	1076.97	-30.23	-9.18
6	650.21	399.93	287.39	1073.97	-22.89	-10.78
7	650.48	399.93	171.48	1075.49	-31.71	-8.89
8	651.17	399.97	187.67	1076.28	-30.48	-9.11
9	650.65	399.95	275.75	1075.86	-23.81	-10.56
10	650.96	399.92	231.72	1075.56	-27.15	-9.83
11	652.15	399.97	154.23	1077.93	-32.99	-8.53
12	651.19	399.98	197.01	1078.82	-29.79	-9.26
13	650.45	399.94	180.77	1074.89	-31.00	-9.04
14	651.36	399.91	156.13	1075.64	-32.85	-8.60
15	650.37	399.91	262.59	1075.78	-24.78	-10.37
16	650.70	399.95	202.37	1076.16	-29.37	-9.38
17	650.73	399.98	221.29	1074.93	-27.94	-9.68
18	650.21	399.94	210.90	1075.37	-28.71	-9.55
19	650.49	399.96	252.21	1077.43	-25.59	-10.19
20	651.33	399.98	166.43	1078.89	-32.09	-8.76

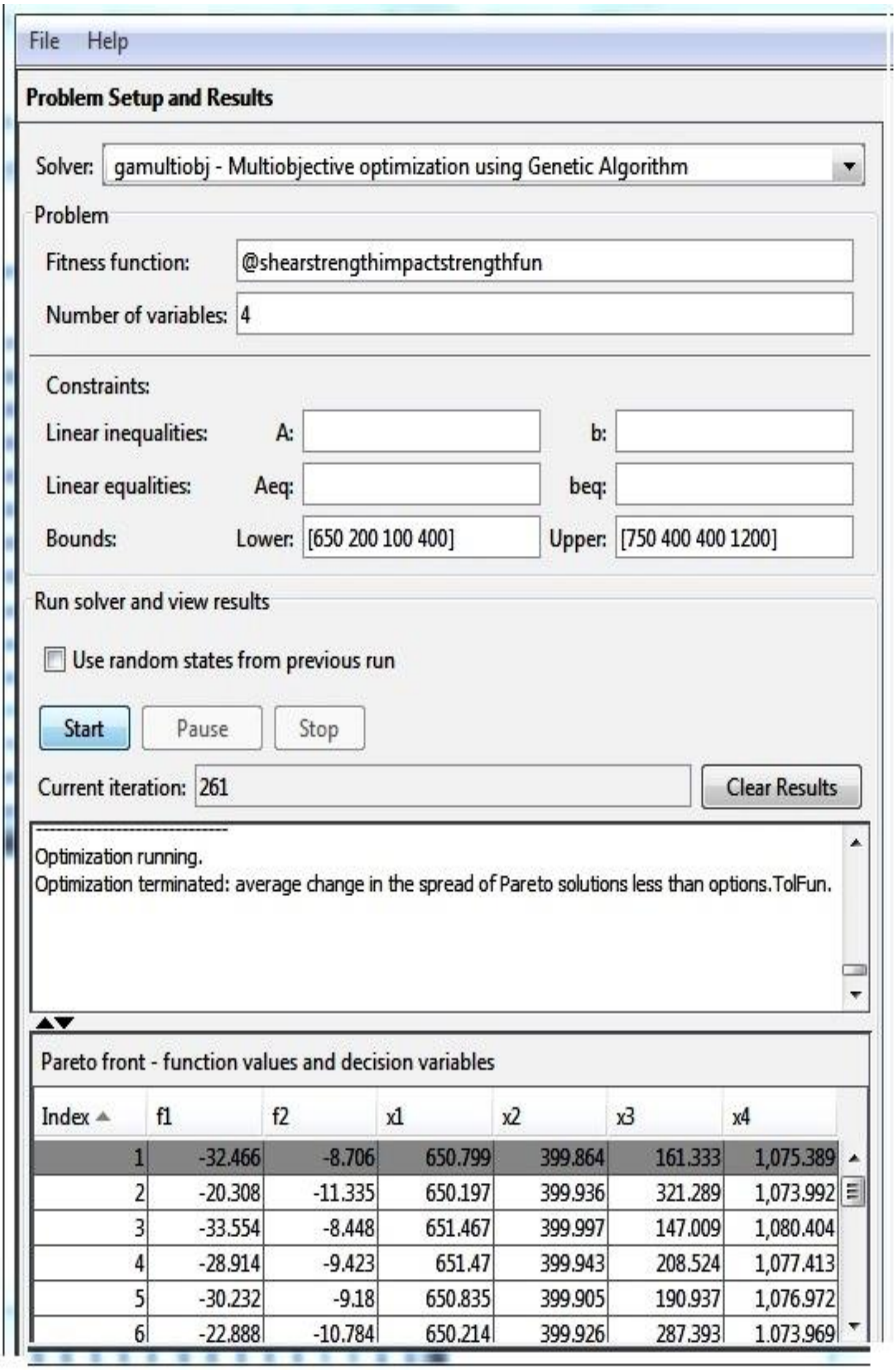

Figure 5.20 Screen shot of GA multiobjective optimization for shear strength and impact strength

5.9.3 Multiobjective Optimization for Combination of Impact Strength and Microhardness by Desirability Analysis

Input parameters used in multiobjective optimization for combination of impact strength and microhardness are shown in Table 5.23 along with their limits and goal settings. Fifteen solutions are generated as represented in Table 5.24. Solution with higher desirability is selected as the optimal solution. The highest desirability acquired in these cases is 1. A number of optimal solutions are obtained in this case. Ramp graph of first optimal solution is shown in Figure 5.21. The optimal process parameters are pouring temperature = 659.24 ˚C, vacuum pressure = 383.43 mm of Hg, insert temperature = 285.41 ˚C and grit size of sand paper = 690.86 for the optimal value of impact strength = 11.68 J and microhardness = 324.75 HV at the desirability value of 1.

Table 5.23 Constraints used in desirability analysis for multiobjective optimization of impact strength and microhardness

Constraints Name	Goal	Lower Limit	Upper Limit	Lower Weight	Upper Weight	Importance
Pouring Temperature (°C)	In range	650	750	1	1	3
Vacuum Pressure (mm of Hg)	In range	200	400	1	1	3
Insert Temperature (°C)	In range	100	400	1	1	3
Grit Size of Sand Paper (number)	In range	400	1200	1	1	3
Impact Strength (J)	Maximize	4.00	10.50	1	1	5
Microhardness (HV)	Maximize	217.56	322.15	1	1	5

Table 5.24 Multiobjective optimization of impact strength and microhardness by desirability analysis

No.	Optimal Process Parameters				Optimal Response		Desirability
	Pouring Temp. (˚C)	Vacuum Pressure (mm of Hg)	Insert Temp. (˚C)	Grit size of Sand Paper (number)	Impact Strength (J)	Micro Hardness (HV)	
1	659.24	383.43	285.41	690.86	11.68	324.75	1.00
2	684.99	398.35	342.90	791.94	11.40	324.65	1.00
3	660.03	384.88	274.00	632.48	11.33	325.85	1.00
4	685.17	393.80	385.88	995.96	11.93	324.70	1.00
5	657.03	364.57	355.49	694.21	11.15	323.78	0.99
6	660.98	393.66	260.43	526.35	11.11	322.98	0.98
7	670.31	398.58	395.63	1198.32	12.14	322.14	0.98
8	676.98	394.15	396.13	888.44	12.51	321.28	0.97
9	660.27	376.08	297.86	658.49	10.97	320.44	0.97
10	675.97	396.76	313.73	738.65	11.77	320.52	0.94
11	704.46	200.00	100.00	694.20	10.89	319.05	0.92
12	704.05	200.00	100.00	688.83	10.87	319.41	0.92
13	703.96	200.00	100.01	700.99	10.90	318.92	0.91
14	704.67	200.00	100.00	703.66	10.92	318.58	0.88
15	704.31	200.00	100.00	677.01	10.84	319.83	0.87

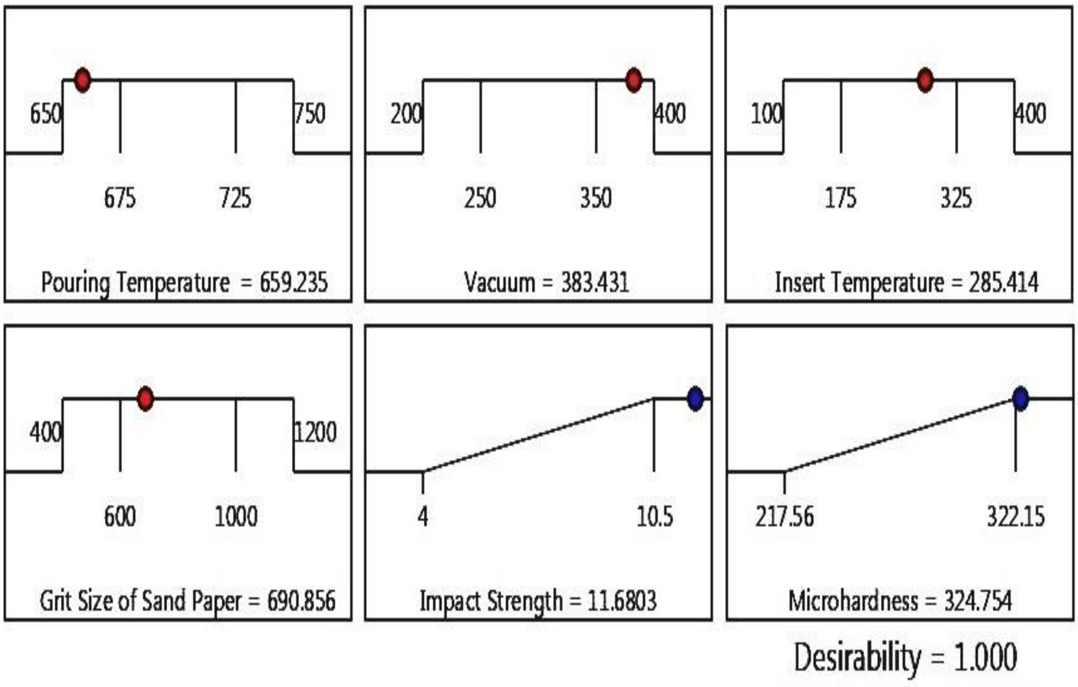

Figure 5.21 Ramp graph of optimal solution for impact strength and microhardness

5.9.4 Multiobjective Optimization for Combination of Impact Strength and Microhardness by Genetic Algorithm

In this case, a MATLAB function is formulated by using the developed RSM models for impact strength and microhardness (Equation 4.4 and Equation 4.5). This function has participated as fitness function for the multiobjective optimization. The fitness function is as below:

```
function R= impactstrengthmicrohardnessfun(x)
 R(1) = - (- 54.80128 + 0.13241*x(1) + 0.206039*x(3) + 0.00977638*x(4) -
          0.0003302*x(1)*x(2) - 0.00031606*x(1)*x(3) + 0.0000145833 * x(3)*x(4)
          + 0.000358875*x(2)^2 - 0.00000624045*x(4)^2);
 R(2) = - (-5984.38 + 17.3175*x(1) + 4.1649*x(2) - 0.413062*x(4) -
          0.00536*x(1)*x(2) + 0.00050871*x(1)*x(4) + 0.0000627636*x(2)*x(3) -
          0.01202*x(1)^2 – 0.000585*x(2)^2);
 end                                                              (5.22)
```

Where, x(1), x(2), x(3) and x(4) denote the pouring temperature, vacuum pressure, insert temperature and grit size of sand paper respectively. The multiobjective optimization is carried out by using this fitness function subject to the designated process parameters (Equation 5.2 to Equation 5.5) by considering the GA operating parameters from Table 5.21. The pareto front of the optimal solutions for impact strength and microhardness is depicted in Figure 5.22. The optimal results showing the compromise between two fitness functions are represented in Table 5.25. Screen shot of this multiobjective optimization is shown in Figure 5.23.

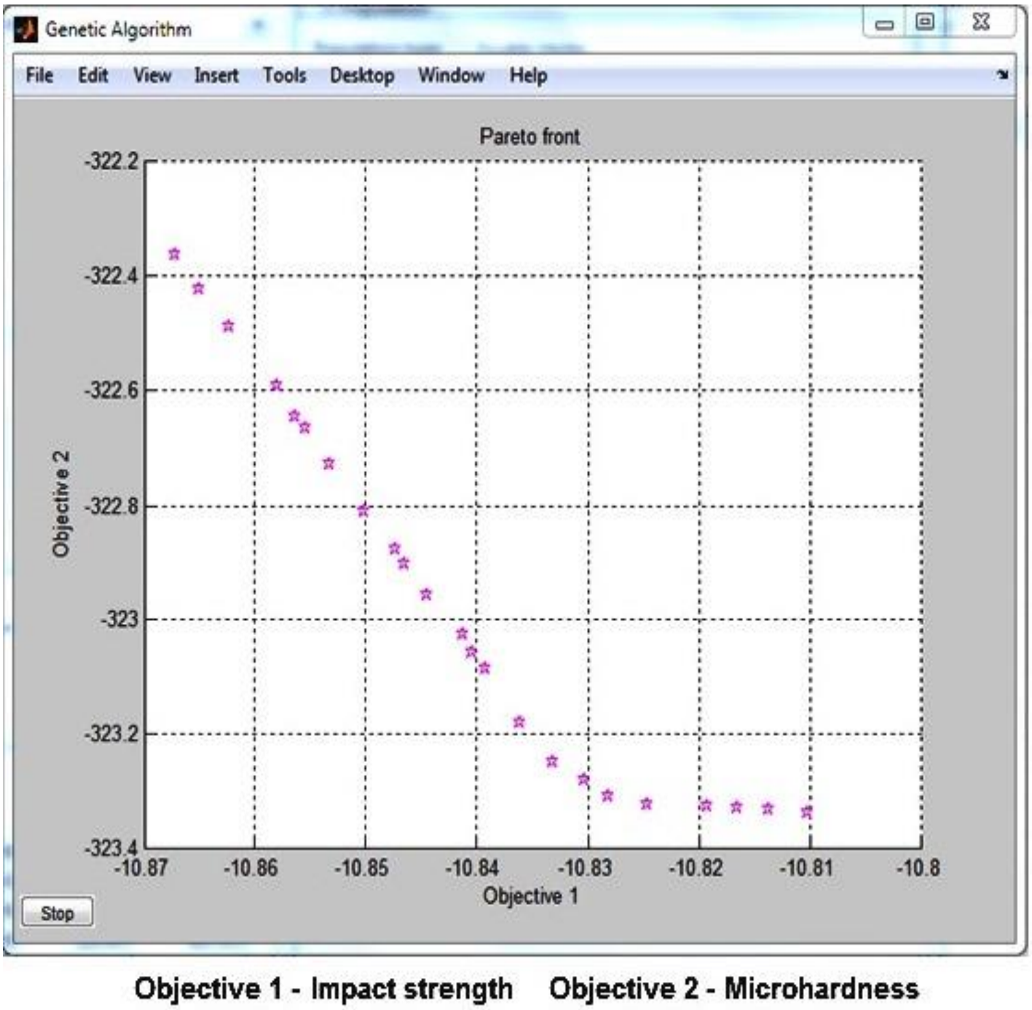

Figure 5.22 Pareto front of GA multiobjective optimization for impact strength and microhardness

Table 5.25 Optimal process parameters corresponding to optimal value of fitness function for GA multiobjective optimization of impact strength and microhardness

Index	Optimal Process Parameters				Optimal Fitness Function	
	Pouring Temp. (˚C)	Vacuum Pressure (mm of Hg)	Insert Temp. (˚C)	Grit size of Sand paper (number)	Impact Strength (J)	Microhardness (HV)
1	650.00	400.00	330.09	862.80	-10.85	-322.87
2	650.01	400.00	318.92	862.97	-10.87	-322.36
3	650.01	400.00	339.64	859.53	-10.82	-323.33
4	650.00	400.00	328.70	862.92	-10.85	-322.81
5	650.00	400.00	338.20	862.77	-10.83	-323.25
6	650.02	400.00	339.66	860.29	-10.82	-323.33
7	650.01	400.00	330.66	862.87	-10.85	-322.90
8	650.01	400.00	338.85	862.41	-10.83	-323.28
9	650.00	400.00	331.85	862.86	-10.84	-322.96
10	650.00	400.00	334.67	862.82	-10.84	-323.08
11	650.01	400.00	321.65	862.93	-10.86	-322.49
12	650.01	400.00	339.66	861.52	-10.82	-323.32
13	650.01	400.00	320.27	862.97	-10.87	-322.42
14	650.01	400.00	318.92	862.97	-10.87	-322.36
15	650.02	400.00	339.65	858.89	-10.81	-323.33
16	650.01	400.00	334.01	862.82	-10.84	-323.05
17	650.01	400.00	323.88	862.89	-10.86	-322.59
18	650.00	400.00	336.68	862.88	-10.84	-323.18
19	650.01	400.00	325.09	862.95	-10.86	-322.64
20	650.00	400.00	326.91	862.92	-10.85	-322.73

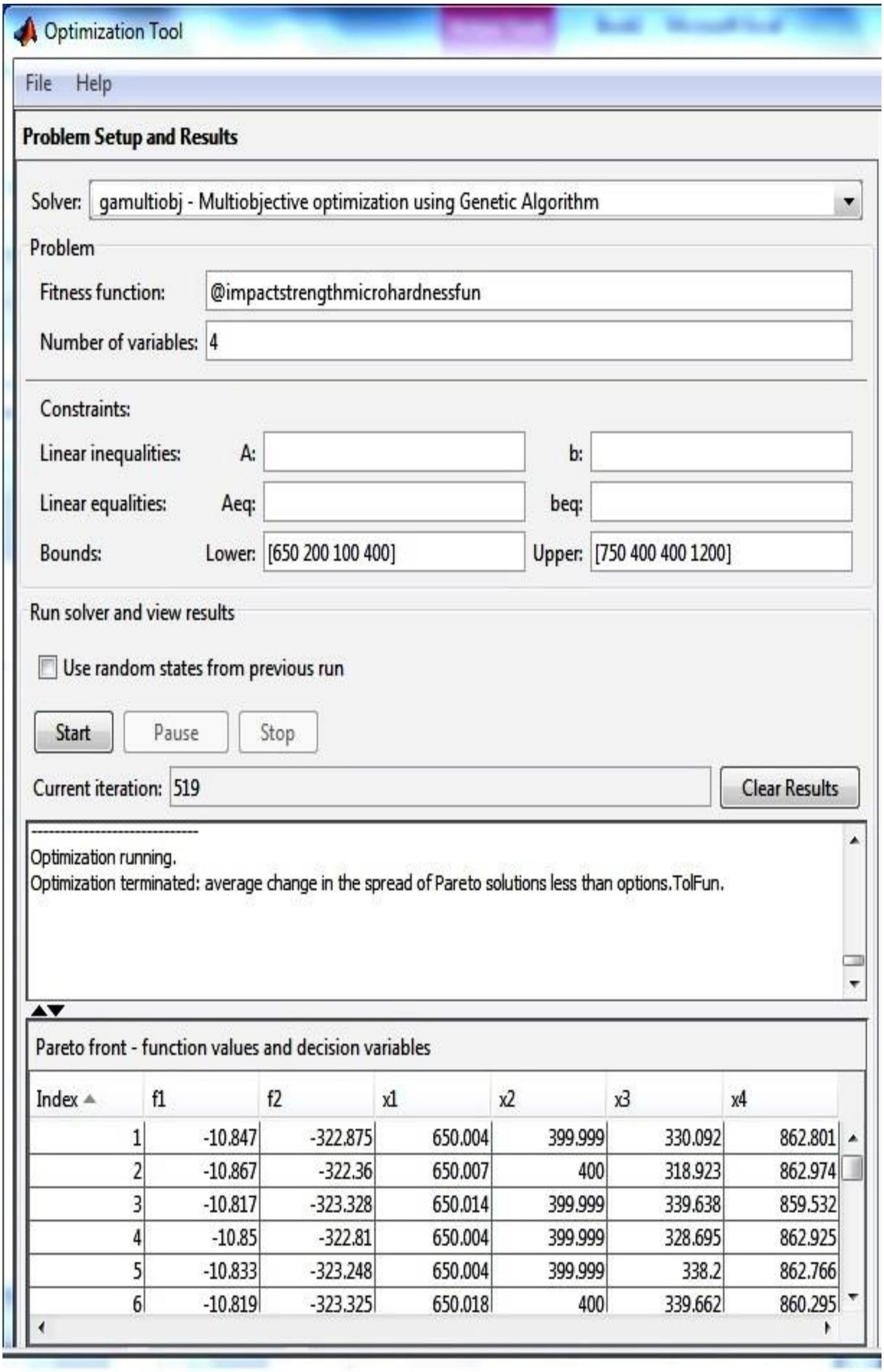

Figure 5.23 Screen shot of GA multiobjective optimization for shear strength and impact strength

5.9.5 Multiobjective Optimization for Combination of Microhardness and Shear Strength by Desirability Analysis

Desirability values for the combination of microhardness and shear strength have been obtained by design-expert software, subjected to the process parameters as represented in Table 5.26 along with their limits and goal settings. The solutions thus generated are shown in Table 5.27. Solution with higher desirability is considered as optimal solution. The highest desirability obtained is one for this combination. The ramp graph in Figure 5.24 indicates the first optimum solution. The optimal process parameters are pouring temperature = 660.25 °C, vacuum pressure = 202.06 mm of Hg, insert temperature = 100.21 °C, and grit size of sand paper = 480.17 for the optimal value of microhardness = 324.02 HV and shear strength = 33.17 MPa at the desirability value of one.

Table 5.26 Constraints used in desirability analysis for multiobjective optimization of microhardness and shear strength

Constraints Name	Goal	Lower Limit	Upper Limit	Lower Weight	Upper Weight	Importance
Pouring Temperature (°C)	In range	650	750	1	1	3
Vacuum Pressure (mm of Hg)	In range	200	400	1	1	3
Insert Temperature (°C)	In range	100	400	1	1	3
Grit Size of Sand Paper (number)	In range	400	1200	1	1	3
Microhardness (HV)	Maximize	217.56	322.15	1	1	5
Shear strength (MPa)	Maximize	11.78	33.14	1	1	5

Table 5.27 Multiobjective optimization of microhardness and shear strength by desirability analysis

No.	Optimal Process Parameters				Optimal Response		Desirability
	Pouring Temp. (˚C)	Vacuum Pressure (mm of Hg)	Insert Temp. (˚C)	Grit size of Sand paper (number)	Micro Hardness (HV)	Shear Strength (MPa)	
1	660.25	202.06	100.21	480.17	324.02	33.17	1.00
2	664.55	200.17	100.01	512.39	324.61	33.14	1.00
3	658.99	201.39	100.03	474.32	323.72	33.23	1.00
4	657.66	202.73	100.28	463.39	323.42	33.14	1.00
5	656.90	206.65	100.18	470.85	322.21	33.15	0.99
6	652.15	200.00	100.00	426.94	322.15	33.05	0.99
7	663.31	200.00	105.85	512.68	322.15	33.05	0.98
8	663.49	200.00	100.00	481.70	326.01	32.99	0.97
9	663.70	200.01	100.00	483.66	326.00	32.99	0.97
10	663.88	200.00	100.00	485.45	325.98	32.99	0.95
11	663.54	200.00	100.00	482.94	325.96	33.00	0.95
12	658.85	215.18	100.00	481.12	322.15	32.87	0.95
13	200.00	100.00	439.52	325.77	32.89	0.99	0.94
14	650.82	200.00	100.00	411.73	322.15	32.86	0.93
15	650.03	200.00	100.40	428.40	320.21	33.14	0.92

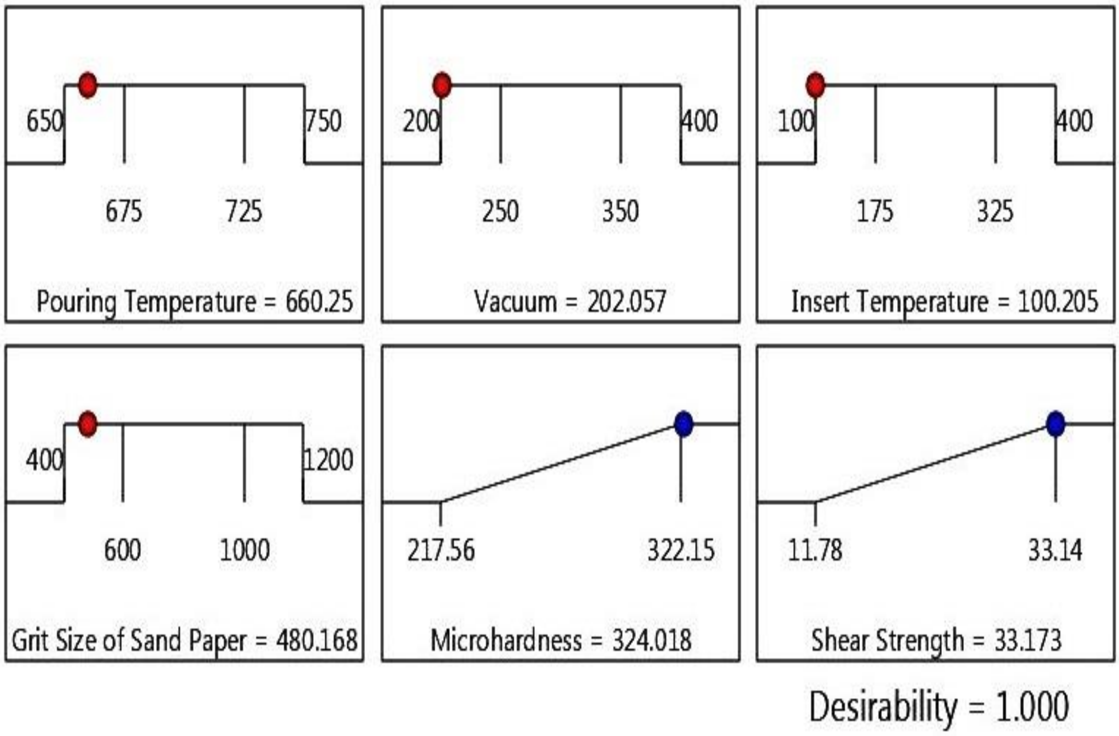

Figure 5.24 Ramp graph of optimal solution for microhardness and shear strength

5.9.6 Multiobjective Optimization for Combination of Microhardness and Shear Strength by Genetic Algorithm

The fitness function for the multiobjective optimization of microhardness and shear strength is developed by using their RSM models (Equation 4.5 and Equation 4.3). The fitness function so formulated is written as:

```
function R= microhardnessshearstrengthfun(x)
R(1) = - (-5984.38 + 17.3175*x(1) + 4.1649*x(2) - 0.413062*x(4) -
       0.00536*x(1)*x(2) + 0.00050871*x(1)*x(4) + 0.0000627636*x(2)*x(3) -
       0.01202*x(1)^2 – 0.000585*x(2)^2);
R(2) = - (-769.45144 + 2.63608*x(1) - 0.148586*x(2) - 0.44473*x(3) +
       0.000660667*x(1)*x(3) - 0.000152333*x(2)*x(3) +
       0.000255295*x(2)*x(4) - 0.00210*x(1)^2) - 0.000046601*x(4)^2);
end                                                                (5.23)
```

Where, x(1), x(2), x(3) and x(4) designate the pouring temperature, vacuum pressure, insert temperature and grit size of sand paper respectively. The fitness function is marked negative to maximize the objectives as genetic algorithm minimizes all the objectives by default. Actual range of process parameters as mentioned in Equation 5.2 to Equation 5.5 is utilized to obtain the effective results. Significant operating parameters of GA multiobjective optimization are considered as per Table 5.21.

A number of optimal solutions are obtained as a result of tradeoff between two fitness functions. Pareto front (Figure 5.25) embodies the optimal distribution of microhardness and shear strength with respect to each other. The optimal value of both the objective functions and corresponding process parameters which yields these values is represented in Table 5.28. Screen shot of this multiobjective optimization is shown in Figure 5.26.

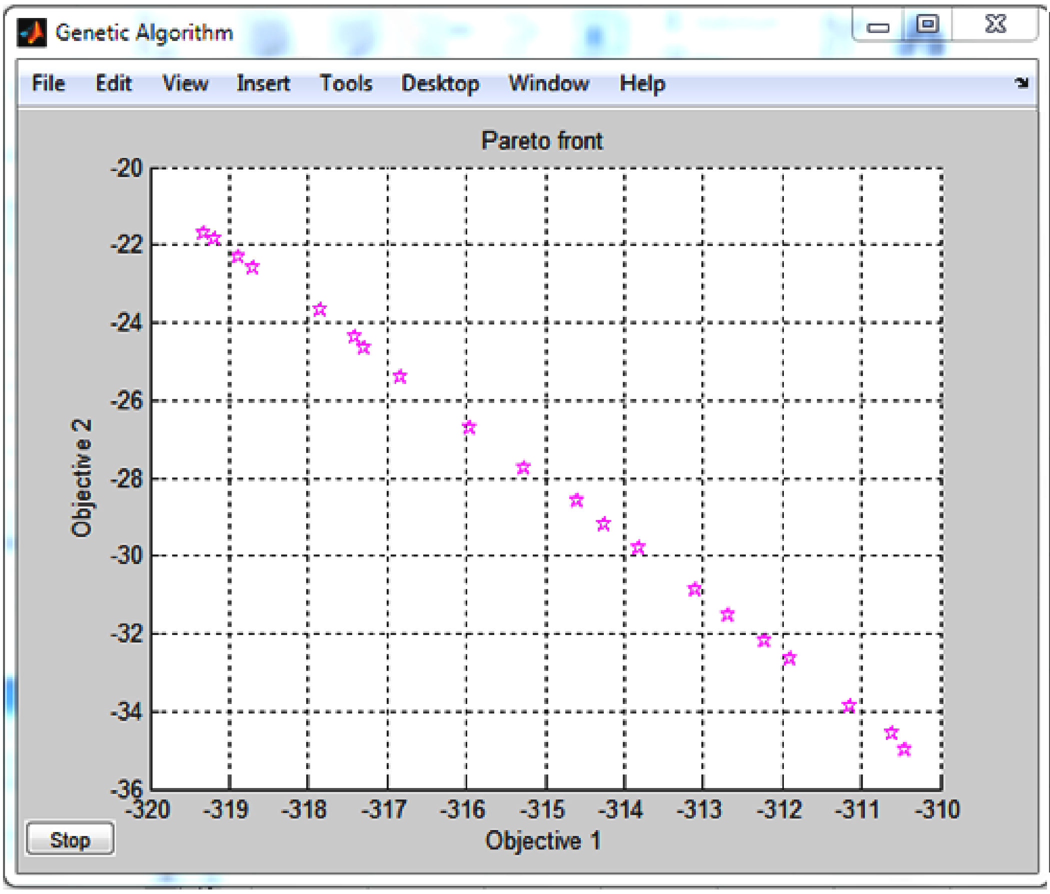

Objective 1 - Microhardness Objective 2 - Shear strength

Figure 5.25 Pareto front of GA multiobjective optimization for microhardness and shear strength

Table 5.28 Optimal process parameters corresponding to optimal value of fitness function for GA multiobjective optimization of microhardness and shear strength

Index	Optimal Process Parameters				Optimal Fitness Function	
	Pouring Temp. (˚C)	Vacuum Pressure (mm of Hg)	Insert Temp. (˚C)	Grit size of Sand paper (number)	Microhardness (HV)	Shear Strength (MPa)
1	661.00	394.22	129.85	1046.04	-310.45	-35.01
2	661.13	394.34	325.46	1044.62	-319.31	-21.70
3	661.25	393.93	223.78	1045.35	-314.60	-28.59
4	661.18	394.21	281.69	1044.75	-317.29	-24.67
5	661.03	394.05	214.72	1045.60	-314.26	-29.21
6	661.01	393.69	135.55	1045.88	-310.61	-34.57
7	661.15	393.99	205.82	1045.60	-313.82	-29.81
8	661.11	393.95	170.60	1045.38	-312.22	-32.20
9	661.10	394.23	236.58	1045.31	-315.27	-27.74
10	661.12	394.22	312.14	1044.82	-318.69	-22.60
11	661.14	393.81	164.07	1045.90	-311.90	-32.63
12	661.15	394.26	322.97	1045.06	-319.18	-21.87
13	661.12	393.76	295.80	1045.31	-317.86	-23.68
14	661.05	393.95	146.38	1045.74	-311.14	-33.85
15	661.17	394.14	180.53	1045.58	-312.69	-31.54
16	661.16	394.28	271.09	1044.73	-316.83	-25.40
17	661.08	393.90	190.11	1045.59	-313.11	-30.87
18	661.00	394.22	129.85	1046.04	-310.45	-35.01
19	661.26	393.93	285.88	1045.08	-317.41	-24.37
20	661.14	394.28	316.24	1044.69	-318.88	-22.33

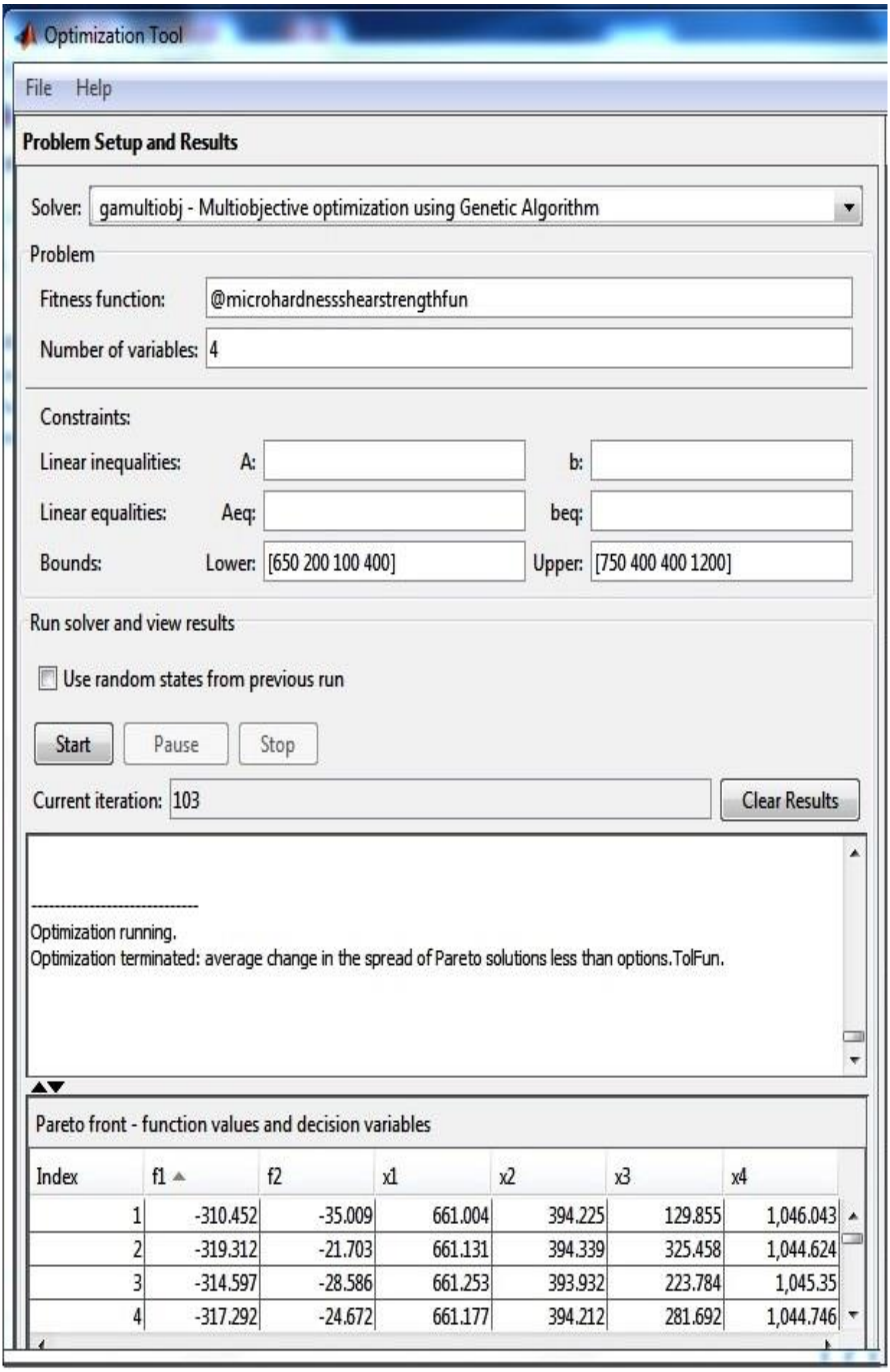

Figure 5.26 Screen shot of GA multiobjective optimization for shear strength and impact strength

5.9.7 Multiobjective Optimization for Combination of Shear Strength, Impact Strength and Microhardness by Desirability Analysis

In this case, desirability values are determined for all the output characteristics i.e., shear strength, impact strength and microhardness simultaneously. The limits of process parameters and constraints used for output variables are represented in Table 5.29. Solutions generated by this analysis are shown in Table 5.30. It specifies that highest value of desirability acquired in these cases is 0.96. The ramp graph of optimal solution as shown in Figure 5.27 that indicates the maximum value of shear strength = 31.77 MPa, impact strength = 10.04 J and microhardness = 322.15 corresponding to this desirability value. The optimal process parameters are pouring temperature = 676.28 ^{o}C, vacuum pressure = 200.00 mm of Hg, insert temperature = 100.00 ^{o}C and grit size of sand paper = 636.14 at these values.

Table 5.29 Constraints used in desirability analysis for multiobjective optimization of shear strength, impact strength and microhardness

Constraints Name	Goal	Lower Limit	Upper Limit	Lower Weight	Upper Weight	Importance
Pouring Temperature (°C)	In range	650	750	1	1	3
Vacuum Pressure (mm of Hg)	In range	200	400	1	1	3
Insert Temperature (°C)	In range	100	400	1	1	3
Grit Size of Sand Paper (number)	In range	400	1200	1	1	3
Shear strength (MPa)	Maximize	11.78	33.14	1	1	5
Impact strength (J)	Maximize	4.00	10.50	1	1	5
Microhardness (HV)	Maximize	217.56	322.15	1	1	5

Table 5.30 Multiobjective optimization of shear strength, impact strength and microhardness by desirability analysis

No.	Optimal Process Parameters				Optimal Response			Desirability
	Pouring Temp. (˚C)	Vacuum Pressure (mm of Hg)	Insert Temp. (˚C)	Grit size of Sand paper (number)	Shear Strength (MPa)	Impact Strength (J)	Micro-hardness (HV)	
1	676.28	200.00	100.00	636.14	31.77	10.04	322.15	0.96
2	672.14	205.00	100.00	610.67	31.96	9.38	322.10	0.95
3	673.44	200.00	101.01	619.19	32.25	9.92	321.65	0.95
4	676.70	200.86	100.52	637.89	31.70	10.06	322.18	0.94
5	686.47	203.12	100.00	656.95	29.91	10.35	323.04	0.94
6	665.69	200.00	109.96	530.07	32.79	9.40	321.08	0.93
7	664.27	200.28	100.00	508.71	33.14	9.21	324.69	0.92
8	660.75	200.00	107.81	507.21	33.14	9.18	320.39	0.92
9	663.70	205.08	100.46	656.25	33.14	9.45	314.38	0.92
10	692.65	200.01	100.00	706.43	28.13	10.64	320.68	0.91
11	654.65	400.00	225.41	862.80	31.69	13.45	300.44	0.90
12	665.01	400.00	281.33	912.90	28.75	13.43	311.75	0.89
13	650.00	391.45	133.55	661.15	33.06	11.32	288.31	0.88
14	677.80	211.40	100.00	595.57	31.63	9.13	322.90	0.88
15	691.52	200.00	136.63	450.13	27.73	9.37	322.15	0.84

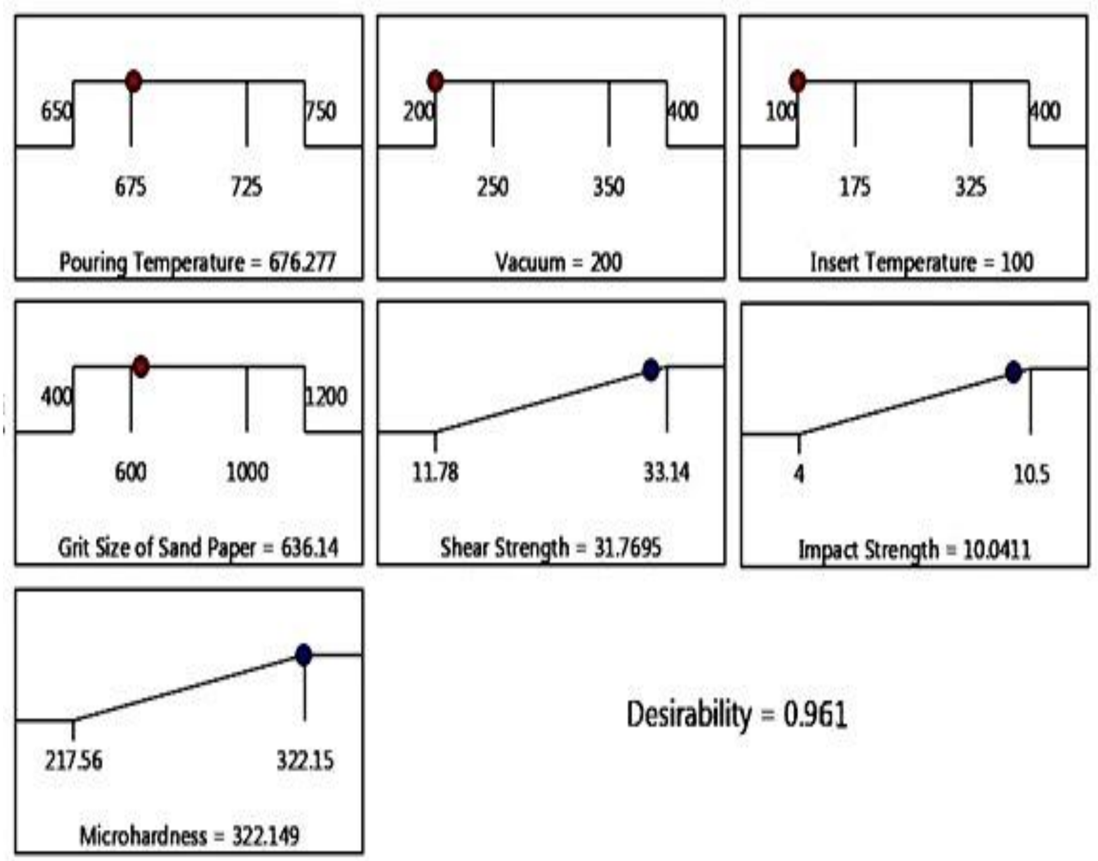

Figure 5.27 Ramp graph of optimal solution for shear strength, impact strength and microhardness

5.9.8 Multiobjective Optimization for Combination of Shear Strength, Impact Strength and Microhardness by Genetic Algorithm

In this case, multiobjective optimization is executed by considering all the three objective functions simultaneously. Fitness function is formulated by using the developed RSM models for shear strength, impact strength and microhardness (Equation 5.5 to Equation 5.7). It is expressed as:

function R= shearstrengthimpactstrengthmicrohardnessfun(x)

R(1) = - (-769.45144 + 2.63608*x(1) - 0.148586*x(2) - 0.44473*x(3) + 0.000660667*x(1)*x(3) - 0.000152333*x(2)*x(3) + 0.000255295*x(2)*x(4) - 0.00210*x(1)^2) - 0.000046601*x(4)^2);

R(2) = - (- 54.80128 + 0.13241*x(1) + 0.206039*x(3) + 0.00977638*x(4) - 0.0003302*x(1)*x(2) - 0.00031606*x(1)*x(3) + 0.0000145833 * x(3)*x(4) + 0.000358875*x(2)^2 - 0.00000624045*x(4)^2);

$$R(3) = -(-5984.38 + 17.3175*x(1) + 4.1649*x(2) - 0.413062*x(4) - 0.00536*x(1)*x(2) + 0.00050871*x(1)*x(4) + 0.0000627636*x(2)*x(3) - 0.01202*x(1)^2 - 0.000585*x(2)^2);$$

end (5.24)

Where, x(1), x(2), x(3) and x(4) designate the pouring temperature, vacuum pressure, insert temperature and grit size of sand paper respectively. Multiobjective optimization is carried out by using this fitness function subjected to the designated process parameters (Equation 5.2 to Equation 5.5). There exist a number of optimal solutions due to tradeoff between the objective functions. Table 5.31 represents the result of optimization in terms of optimal values of all the objective function and their corresponding process parameters.

Table 5.31 Optimal process parameters corresponding to optimal value of fitness function for GA multiobjective optimization of shear strength, impact strength and microhardness

Index	Optimal Process Parameters				Optimal Fitness Function		
	Pouring Temp. (˚C)	Vacuum Pressure (mm of Hg)	Insert Temp. (˚C)	Grit size of Sand paper (number)	Shear Strength (MPa)	Impact Strength (J)	Micro-hardness (HV)
1	650.01	397.66	374.20	1074.06	-32.51	-10.23	-321.08
2	651.56	397.34	118.56	1061.73	-32.89	-11.98	-300.69
3	657.08	372.84	129.40	522.94	-31.12	-12.02	-322.92
4	650.96	393.56	235.66	1106.64	-36.23	-10.78	-318.45
5	650.71	396.63	133.10	773.88	-36.35	-09.95	-320.15
6	650.52	395.02	359.89	471.07	-30.56	-11.26	-309.28
7	657.59	384.13	155.33	686.69	-24.85	-11.27	-323.58
8	656.53	379.53	124.52	641.91	-32.20	-10.54	-319.15
9	650.28	396.89	359.15	957.95	-29.45	-09.12	-312.80
10	656.59	394.34	344.59	478.85	-25.36	-12.23	-308.19
11	650.55	395.13	359.81	471.05	-28.45	-10.45	-306.86
12	651.90	384.83	163.43	570.93	-35.42	-11.16	-302.97
13	653.46	392.78	357.59	963.00	-18.58	-11.23	-311.69
14	653.78	374.86	141.24	579.24	-28.73	-08.84	-299.45
15	655.18	394.11	238.81	509.28	-29.64	-11.95	-310.43

It is not very often that there exists an ideal solution which provides the best result for every aspect of a problem. A lot of effort is applied to develop the methods which provide better ways for making decisions where tradeoffs are unavoidable. Multiobjective optimization provides a number of optimal solutions, by which one can make focused tradeoffs within the given set of parameters. In the present work, a range of optimal solutions are obtained by multiobjective optimization for the possible combinations of shear strength, impact strength and microhardness. It provides the optimal process parameters suitable for producing the A356/Mg couples of desired properties. The effective utilization of these process parameters further depends upon the applications and requirement of desired characteristics of joint interface.

CHAPTER 6

CONCLUSION AND SCOPE FOR FUTURE WORK

6.1 INTRODUCTION

This chapter concludes the present research work along with its significant contribution to the industrial applications dealing with dissimilar joining by compound casting. Scope for the future work is spelt out.

6.2 CONCLUSIONS

In the present work, dissimilar light materials, A356 alloy and pure magnesium are joined by vacuum assisted sand mold compound casting process. Mechanism of interface formation, micro-structural characteristics and mechanical properties of the joint interface are investigated. Optimization of significant process parameters; pouring temperature, vacuum pressure, insert temperature and surface roughness of insert in terms of grit size of sand paper used, has been carried out with reference to the mechanical properties; shear strength, impact strength and microhardness of joint interface. Optimization is accomplished by response surface methodology, desirability analysis and genetic algorithm. Graph theoretic approach is used to evaluate the impact of mechanical properties on joint strength**.** Multiobjective optimization is also executed by using DA and GA to predict the optimal process parameters by choosing two or more output characteristics simultaneously. The following conclusions are drawn:

6.2.1 A356/Mg Joint Interface

- A uniform joint interface is observed.
- Joint formation is diffusion controlled.
- The interfacial microstructure of A356/Mg joint is composed of three distinct layers containing Mg_2Al_3 on aluminium side, $Mg_{17}Al_{12}$ +δ eutectic structure on magnesium side and $Mg_{17}Al_{12}$ as middle layer.
- Mg_2Si particles are formed due to the interaction of magnesium with silicon present in A356 and dispersed throughout the interface.

6.2.2 Shear Strength of A356/Mg Joint Interface

- Shear strength of joint interface lies between 11.78 to 33.14 MPa.
- PT, VC and IT; interaction effect of PT and IT, VC and IT and VC and GS; and second order terms of PT and GS have the significant effect on shear strength.
- Shear strength at the joint interface decreased by increasing the pouring and insert temperature and decreasing the vacuum pressure.
- The optimum process parameters by desirability are pouring temperature = 674.93 °C, vacuum pressure = 379.46 mm of Hg, insert temperature = 122.68 °C and grit size of sand paper = 825.46 at an optimal value of shear strength = 35.99 MPa.
- The optimal process parameters predicted by GA corresponding to the best shear strength value of 37.85 MPa are 650.01°C pouring temperature, 307.45 mm of Hg vacuum pressure, 100°C insert temperature and 807.35 as grit size of sand paper used.
- Shear strength increased by 4.80, 8.60 and 14.21 % by regression model, desirability analysis and GA respectively with respect to the experimental results.

6.2.3 Impact Strength of A356/Mg Joint Interface

- Impact strength of joint interface lies between 4 to 10.5 J, while 6 and 10 J at base materials A356 and magnesium respectively.
- PT, IT and GS; interaction effect of PT and VC, PT and IT, IT and GS; and second order terms of VC and GS have the significant effect on impact strength.
- Impact strength of joint interface increased by decreasing the pouring and insert temperature whereas it decreased by decreasing the vacuum pressure and grit size of sand paper.
- The optimal value of impact strength 11.71 J achieved corresponding to the highest desirability with optimum process parameters as pouring temperature = 675.58^{o}C, vacuum pressure = 201.35 mm of Hg, insert temperature = 322.74^{o}C and grit size of sand paper = 934.15.

- Best value of impact strength 12.29 J obtained by GA optimization at 661.13^{o}C pouring temperature, 200.02 mm of Hg vacuum pressure, 328^{o}C insert temperature and 1187.15 as grit size of sand paper.
- Impact strength increased by 1.72, 11.52 and 17.05% by regression model, desirability analysis and GA respectively with respect to the experimental results.

6.2.4 Microhardness of A356/Mg Joint Interface

- Microhardness of joint interface lies between 217.56 to 322.15 HV while 48 and 78 HV at base metals magnesium and A356 respectively.
- Mg_2Al_3 revealed highest microhardness followed by $Mg_{17}Al_{12}$ and $Mg_{17}Al_{12}$ + δ eutectic structure.
- Brittle and partial ductile fracture morphology observed on A356 and Mg side respectively. The middle portion indicated mixed brittle and partial ductile fracture morphology.
- PT, VC and GS; interaction effect of PT and VC, PT and GS and VC and IT; and second order terms of PT and VC have the significant effect on microhardness.
- Microhardness of joint interface decreased with increase in pouring temperature and grit size of sand paper used, whereas it increased with increase in vacuum pressure.
- Optimal process parameters by desirability are PT = 663.20 ˚C, VC = 347.38 mm of Hg, IT = 295.13 ˚C and GS = 534.41 for the optimal value of microhardness = 324.86 HV.
- The optimal process parameters predicted by GA corresponding to the best microhardness value (326.86 HV) are 650.36 ˚C pouring temperature, 399.96 mm of Hg vacuum pressure, 377.59 ˚C insert temperature and 780.93 as grit size of sand paper used.
- Microhardness of joint interface increased by 0.30, 0.84 and 1.35% by regression model, desirability analysis and GA respectively with respect to the experimental results.

6.2.5 RSM Model and Optimization of Process Parameters

- Second-order regression model developed in RSM for shear strength, impact strength and microhardness of joint interface, validated the accuracy and reliability of experimental results.
- GA proves an effective approach in finding the better solution in terms of optimal value of shear strength, impact strength and microhardness.
- The optimal process parameters obtained by GA fall within the range of process parameters employed in present experimental work.

6.2.6 Joint Strength Evaluation by GTA

- The shear strength index = 16943, impact strength index = 11395 and microhardness index = 16576 indicate that shear strength has maximum influence on joint strength followed by microhardness and impact strength (Shear strength>Microhardness>Impact strength).
- Different combinations of factors and subfactors imply different index values. The highest joint strength index (3.43E12) corresponds to the experiment number 17. The optimal process parameters at this value are 650°C pouring temperature, 300 mm of Hg vacuum pressure, 250°C insert temperature and 800 grit size of sand paper used.
- Graph theory proves to be an appropriate approach in estimating the impact of process parameters on vacuum assisted sand mold compound casting process.

6.2.7 Multiobjective Optimization

- A range of optimal solutions are obtained by multiobjective optimization for the possible combinations of shear strength, impact strength and microhardness.
- Multiobjective optimization provides the optimal process parameters suitable for producing the A356/Mg couples of desired properties by choosing two or more output characteristics simultaneously.

6.3 CONTRIBUTION

The present work has suggested a relatively newer process of joining of lightweight structures. It benefits the vehicle construction and aerospace industry in particular by providing the solutions which saves as much weight as possible while fulfilling identical or even greater requirements of a part, and which can be produced at low cost. Optimization of process parameters of VASMCC process has predicted better solutions that could be employed at shop floor effectively and efficiently.

6.4 SCOPE FOR FUTURE WORK

Present work has analyzed and optimized the process parameters for A356/Mg joint produced by vacuum assisted sand mold compound casting process.

- Further, attempts can be made to join other lightweight materials by compound casting process.
- Optimization of process parameters other than that used in this study can be carried out.
- Analysis and modeling of intermetallic compounds' growth and joint formation phenomenon in compound casting process can be investigated.
- Further, investigation on lost foam compound casting process can be carried out.

REFERENCES

[1] L. Wang, R. Lett, S. Felicelli, J. Berry, J. Jordon, and D. Penrod, "Microstructure and performance of four casting processes for magnesium alloy AZ91," in *International Journal of Metalcasting*, Vol. 5, No. 4, 2011, pp. 37-46.

[2] R. Lumley, N. Deeva, and M. Gershenzon, "An evaluation of quality parameters for high pressure die castings," in *International Journal of Metalcasting*, Vol. 5, No. 3, 2011, 37-56.

[3] A. A. Luo, "Magnesium casting technology for structural applications," in *Journal of Magnesium and Alloys*, Vol. 1, No. 1, 2013, pp. 2-22.

[4] M. J. Fernandus, T. Senthilkumar, V. Balasubramanian, and S. Rajakumar, "Optimizing diffusion bonding parameters in AA6061-T6 aluminum and AZ80 magnesium alloy dissimilar joints," in *Journal of Materials Engineering and Performance*, Vol. 21, No. 11, 2012, pp. 2303-2315.

[5] P. Senthil and K. S. Amirthagadeswaran, "Experimental study and squeeze casting process optimization for high quality AC2A aluminium alloy castings," in *Arabian Journal for Science and Engineering*, Vol. 39, No. 3, 2014, pp. 2215-2225.

[6] D. S. Kumar, C. T. Sasanka, K. Ravindra, and K. N. S. Suman, "Magnesium and its alloys in automotive applications-A review," in *American Journal of Materials Science and Technology*, Vol. 4, No. 1, 2015, pp. 12-30.

[7] K. R. Gopi, H. S. Nayaka, and S. Sahu, "Microstructural evolution and strengthening of AM90 magnesium alloy processed by ECAP," *Arabian Journal for Science and Engineering*, Vol. 42, No. 11, 2017, pp. 4635-4647.

[8] M. Paramsothy, N. Srikanth, and M. Gupta, "Solidification processed Mg/Al bimetal macrocomposite: Microstructure and mechanical properties," in *Journal of Alloys and Compounds*, Vol. 461, No. 1-2, 2008, pp. 200-208.

[9] M. K. Kulekci, "Magnesium and its alloys applications in automotive industry," in *International Journal of Advanced Manufacturing Technology*, Vol. 39, No. 9, 2008, pp. 851-865.

[10] K. J. M. Papis, "Processing strategies in light metal compound casting," Sc. D. Dissertation, in *ETH Zurich University of Science and Technology, Switzerland*, 2009.

[11] E. Hajjari, M. Divandari, S. H. Razavi, S. M. Emami, T. Homma, and S. Kamado, "Dissimilar joining of Al/Mg light metals by compound casting process," in *Journal of Material Science*, Vol. 46, No. 20, 2011, pp. 6491-6499.

[12] K. J. M. Papis, J. F. Loeffler, and P. J. Uggowitzer, "Light metal compound casting," in *Science in China Series E: Technological Sciences*, Vol. 52, No. 1, 2009, pp. 46-51.

[13] L. Liu, D. Ren, and F. Liu, 'A review of dissimilar welding techniques for magnesium alloys to aluminum alloys," in *Materials*, Vol. 7, No. 5, 2014, pp. 3735-3757.

[14] V. K. Patel, D. L. Chen, and S. D. Bhole, "Dissimilar ultrasonic spot welding of Mg-Al and Mg-highstrength low alloy steel," in *Theoretical & Applied Mechanics Letters*, Vol. 4, No. 4, 2014, pp. 1-8.

[15] G. Cam and G. Ipekoglu, "Recent developments in joining of aluminum alloys," in *International Journal of Advanced Manufacturing Technology*, Vol. 91, No. 5-8, 2017, pp. 1851-1866.

[16] L. Liu, H. Wang, G. Song, and J. Ye, "Microstructure characteristics and mechanical properties of laser weld bonding of magnesium alloy to aluminium alloy," in *Journal of Materials Science*, Vol. 42, No. 2, 2007, pp. 565–572.

[17] R. Borrisutthekul, Y. Miyashita, and Y. Mutoh, “Dissimilar material laser welding between magnesium alloy AZ31B and aluminium alloy A5052-O,” in *Science and Technology of Advanced Materials*, Vol. 6, No 2, 2005, pp. 199-204.

[18] J. Yang, Z. Yu, Y. Li, H. Zhang, and N. Zhou, “Laser welding/brazing of 5182 aluminium alloy to ZEK100 magnesium alloy using a nickel interlayer,” in *Science and Technology of Welding and Joining*, Vol. 23, No. 7, 2018, pp 543-550.

[19] M. R. Islam, M. Ishak, L. H. Shah, S. R. A. Idris, and C. Meric, “Dissimilar welding of A7075-T651 and AZ31B alloys by gas metal arc plug welding method,” in *International Journal of Advanced Manufacturing Technology*, Vol. 88, No. 9-12, 2017, pp. 2773-2783.

[20] A. Kostka, R. S. Coelho, J. D. Santos, and A. R. Pyzalla, “Microstructure of friction stir welding of aluminium alloy to magnesium alloy,” in *Scripta Materialia*, Vol. 60, No. 11, 2009, pp. 953-956.

[21] H. K Sharma, K. Bhatt, K. Shah, and U. Joshi, “Experimental analysis of friction stir welding of dissimilar alloys AA6061 and Mg AZ31 using circular butt joint geometry,” in *Procedia Technology*, Vol. 23, 2016, pp. 566-572.

[22] V. Paradiso, F. Rubino, P. Carlone, and G. S. Palazzo, “Magnesium and aluminium alloys dissimilar joining by friction stir welding,” in *Procedia Engineering*, Vol. 183, 2017, pp. 239-244.

[23] J. Verma, R. V. Taiwade, C. Reddy, and R. K. Khatirkar, “Effect of friction stir welding process parameters on Mg-AZ31B/Al-AA6061 joints,” in *Materials and Manufacturing Processes*, Vol. 33, No. 3, 2018, pp. 308-314.

[24] J. Wang, L. Yajiang, and H. Wanqun, “Interface microstructure and diffusion kinetics in diffusion bonded Mg/Al joint,” in *Reaction Kinetics and Catalysis Letters*, Vol. 95, No. 1, 2008, 71-79.

[25] L. Peng, L. Yajiang, G. Haoran, and W. Juan, “Investigation of interfacial structure of Mg/Al vacuum diffusion-bonded joint,” in *Vacuum*, Vol. 80, No. 5, 2006, pp. 395-399.

[26] S. Scharf, E. Riedel, N. Stein, and R. Baehr, “Fe–Al/AlSi compound casting based on a targeted oxide removal,” in *Journal of Materials Processing Technology*, Vol. 248, 2017, pp. 31-38.

[27] W. Jianga, Z. Fan, and C. Li, “Improved steel/aluminum bonding in bimetallic castings by a compound casting process,” in *Journal of Materials Processing Technology*, Vol. 226, 2015, pp. 25-31.

[28] M. Rubner, M. Gunzl, C. Korner, and R. F. Singer, “Aluminium-aluminium compound fabrication by high pressure die casting,” in *Materials Science and Engineering A*, Vol. 528, No. 22-23, 2011, pp. 7024-7029.

[29] K. J. M. Papis, B. Hallstedt, J. F. Loffler, and P. J. Uggowitzer, “Interface formation in aluminium-aluminium compound casting,” in *Acta Materialia*, Vol. 56, No. 13, 2008, pp. 3036-3043.

[30] K. J. M. Papis, J. F. Loffler, and P. J. Uggowitzer, “Interface formation between liquid and solid Mg alloys-An approach to continuously metallurgic joining of magnesium parts,” in *Materials Science and Engineering A*, Vol. 527, No. 9, 2010, pp. 2274-2279.

[31] E. Hajjari , M. Divandari, S. H. Razavi, S. M. Emami, and S. Kamado, “Estimation of the transient interfacial heat flux between substrate/melt at the initiation of magnesium solidification on aluminum substrates using the lumped capacitance method,” in *Applied Surface Science*, Vol. 257, No. 11, 2011, pp. 5077-5082.

[32] S. Manasijevic, R. Radisa, Z. Z. Brodarac, N. Dolic, and M. Djurdjevic, “AI-Fin bond in aluminum piston alloy & austenitic cast iron insert,” in *International Journal of Metalcasting*, Vol. 9, No. 4, 2015, pp. 27-32.

[33] M. Pintore, T. Mittler, W. Volk, O. Starykov, and B. Tonn, "Experimental investigations on the influence of the thermal conditions during composite casting on the microstructure of Cu-Al bilayer compounds," in *International Journal of Metalcasting*, Vol. 12, No. 1, 2017, pp. 79-88.

[34] M. Akbarifar and M. Divandari, "On the interface characteristics of compound cast Al/Brass bimetals." in *International Journal of Metalcasting*, Vol. 11, No. 3, 2017, pp. 506-512.

[35] M. S. Kenevisi, S. M. M. Khoie, and M. Alaei, "Microstructural evaluation and mechanical properties of the diffusion bonded Al/Ti alloys joint," *in Mechanics of Materials*, Vol. 64, 2013, pp. 69–75.

[36] W. Jiang , G. Li, Y. Wu, X. Liu, and Z. Fan, "Effect of heat treatment on bonding strength of aluminum/steel bimetal produced by a compound casting," in *Journal of Materials Processing Technology*, Vol. 258, 2018, pp. 239-250.

[37] J. Ho, C. B. Lin, and C. H. Liu, "Effect of continuous cooling heat treatment on interface characteristics of S45C/copper compound casting," in *Journal of Materials Science*, Vol. 39, No. 7, 2004, pp. 2473-2480.

[38] J. Wang, K. Ma, H. Peng, C. Wu, and X. Su, "Study on Fe–Al layers of Fe/(Zn-11%Al-3%Mg-0.2%Si) solid–liquid diffusion couples," in *Materials and Manufacturing Processes*, Vol. 31, No. 11, 2017, pp. 1290-1295.

[39] M. S. Peronnet, E. Guiot, F. Bosselet, O. Dezellus, D. Rouby, and J. C. Viala, "Local reinforcement of magnesium base castings with mild steel inserts," in *Materials Science and Engineering A*, Vol. 445-446, 2007, pp. 296-301.

[40] http://www.foundry-planet.com/fileadmin/redakteur/pdf-dateien/technical-reports/euroLiteVerbundguss_V1_GB.pdf

[41] J. C. Viala, M. Peronnet, F. Barbeau, F. Bosselet, and J. Bouix, “Interface chemistry in aluminium alloy castings reinforced with iron base inserts,” in *Composites Part A: Applied Science and Manufacturing*, Vol. 33, No. 10, 2002, pp. 1417-1420.

[42] M. Kluting and C. Landerl, “The new BMW inline six-cylinder spark-ignition engine: Concept and construction,” in *MTZ Worldwide*, Vol. 65, No. 11, 2004, pp. 2-5.

[43] W. Kiefer, N. Klauer, M. Krauss, W. Mahrle, and E. Schunemann, “The new BMW inline six-cylinder spark ignition engine: Thermodynamics and functional properties,” *in MTZ Worldwide*, Vol. 65, No. 12, 2004, pp. 22-25.

[44] W. Hua, “Study on bimetal compound casting technology of hammers,” *in Advanced Materials Research*, Vol. 535-537, 2012, pp. 566-570.

[45] https://kunskapsformedlingen.se/en/projects/compound-casting-for-lightweight-applications-with-optimized-properties/

[46] F. B. Andreas, L. Christian, F Andreas, and W. Johann, “The new BMW inline six-cylinder composite Mg/Al crankcase,” *in IMA Annual World Magnesium Conference*, Vol. 62, 2005, pp. 49-58.

[47] https://skysun-truckparts.en.made-in-china.com/product/CqHmyNYxnsTc/China-Auto-Spare-Parts-Shock-Mounting-48609-0d050-Mount-for-Toyota.html

[48] https://www.lmrkartstore.com/collections/otk/bearing-carriers

[49] https://www.indiamart.com/geartechengineers-chennai/gearbox-spare-parts.html

[50] https://www.bmwblog.com/2008/12/31/bmw-m3s-32-liter-straight-six-engine-comes-to-an-end/

[51] http://www.e90post.com/forums/attachment.php?attachmentid=466157&d=1292458586

[52] https://www.mountuneusa.com/Ford-Lotus-Twin-Cam-Engine-Block-M-6010-16L-p/m-6010-16l.htm

[53] S. Tavassoli, M. Abbasi, and R. Tahavvori, "Investigating Formation of Intermetallics in Compound Casting of Al/Cu Bimetals," in *Journal of Advanced Materials in Engineering*, Vol. 35, No. 2, 2016, pp. 115-129.

[54] M. Akbarifar and M. Divandari, "Study of Al/cast iron interface and graphite behavior," in *Journal of Mining and Metallurgy Section B: Metallurgy*, Vol. 53, No. 1, 2017, pp. 53-59.

[55] T. Liu, Q. Wang, P. Liu, J. Sun, X. Yin, and Q. Wang, "Microstructure and mechanical properties of overcast aluminum joints," in *Transactions of Nonferrous Metals Society of China*, Vol. 25, No. 4, 2015, pp. 1064−1072.

[56] E. Hajjari, M. Divandari, S. H. Razavi, T. Homma, and S. Kamado, "Intermetallic compounds and antiphase domains in Al/Mg compound casting," in *Intermetallics*, Vol. 23, 2012, pp. 182-186.

[57] S. M. Emami, M. Divandari, H. Arabi, and E. Hajjari, "Effect of melt-to-solid insert volume ratio on Mg/Al dissimilar metals bonding," in *Journal of Materials Engineering and Performance*, Vol. 22, No. 1, 2013, pp. 123-130.

[58] R. Mola, T. Bucki, and A. Dziadon, "Effects of the pouring temperature on the formation of the bonding zone between AZ91 and AlSi17 in the compound casting process," in *IOP Conference Series: Materials Science and Engineering*, Vol. 179, 2017, pp. 1-6.

[59] Q. S. Ren, C. Z. Zhao, Z. B. Li, and H. X. Zhang, "Microstructure and mechanical properties of Mg/Al bimetallic composite fabricated by compound casting," in *Materials Research Innovations*, Vol. 19, No. 4, 2015, pp. S73-S78.

[60] H. Zhang, Y. Chen, and A. A. Luo, "Improved interfacial bonding in magnesium/aluminum overcasting systems by aluminum surface

treatments," in *Metallurgical and Materials Transactions B*, Vol. 45, No 6, 2014, pp. 2495-2503.

[61] G. R. Zare, M. Divandariand, and H. Arabi, "Investigation on interface of Al/Cu couples in compound casting," in *Materials Science and Technology*, Vol. 29, No. 2, 2013, pp. 190-196.

[62] M. Akbarifar and M. Divandari, "Interface characterization of Al/cast iron composite," in *Journal of Science and Technology of Composites*, Vol. 3, No. 3, 2016, pp. 261-268.

[63] M. Salimi, M. Malekan, B. Nami, and H. Hoseiny, "Microstructure characteristics and mechanical properties of the interface layer of coated steel insert-aluminum bimetals," in *Journal of Materials Research*, Vol. 32, No. 4, 2017, pp. 874-882.

[64] C. B. Lin and J. S. Ho, "The effect of continuous cooling heat treatment on interface properties of SK3/Copper compound casting," in *Journal of Materials Engineering and Performance,* Vol. 09, No. 1, 2000, pp. 81-87.

[65] J. Feng, B. Ye, L. Zuo, Q. Wang, Q. Wang, H. Jiang, and W. Ding, "Bonding of aluminum alloys in compound casting," in *Metallurgical and Materials Transactions A*, Vol. 48, No. 10, 2017, pp. 4632-4644.

[66] E. Hajjari, M. Divandari, S. H. Razavi, T. Homma, and S. Kamado, "Microstructure characteristics and mechanical properties of Al 413/Mg joint in compound casting process," in *Metallurgical and Materials Transactions A*, Vol. 43, No. 12, 2012, pp. 4667-4677.

[67] Y. Liu, Y. Chen, and C. Yang, "A study on atomic diffusion behaviours in an Al-Mg compound casting process," in *AIP Advances*, Vol. 5, 2015, pp. 1-13.

[68] W. Jiang, F. Guan, G. Li, H. Jiang, J. Zhu, and Z. Fan, "Processing of Al/Cu bimetal via a novel compound casting method," in *Materials and Manufacturing Processes*, Vol. 34, No. 9, 2019, pp. 1016-1025.

[69] O. Dezellus, B. Digonnet, M. S. Peronnet, F. Bosselet, D. Rouby, and J. C. Viala, “Mechanical testing of steel/aluminium-silicon interfaces by pushout,” in *International Journal of Adhesion & Adhesives*, Vol. 27, No 5, 2007, pp. 417-421.

[70] A. Bouayad, C. H. Gerometta, A. Belkebir, and A. Ambari, “Kinetic interactions between solid iron and molten aluminium,” in *Materials Science and Engineering A*, Vol. 363, No. 1-2, 2003, pp. 53-61.

[71] O. Dezellus, L. Milani, F. Bosselet, M. S. Peronnet, D. Rouby, and J. Viala, “Mechanical testing of titanium/aluminium–silicon interfaces by push-out,” in *Journal of Material Science*, Vol. 43, No. 6, 2008, pp. 1749-1756.

[72] K. N. Zhao, J. C. Liu, X. Y. Nie, Y. Li, H. X. Li, Q. Du, L. Z. Zhuang, and J. S. Zhang, “Interface Formation in magnesium-magnesium bimetal composites fabricated by insert molding method,” in *Materials and Design*, Vol. 91, 2016, pp. 122-131.

[73] H. Li, X. Nie, Z. He, K. Zhao, Q. Du, J. Zhang, and L. Zhuang, “Interfacial microstructure and mechanical properties of Ti-6Al-4V/Al7050 joints fabricated using the insert molding method,” *in International Journal of Minerals, Metallurgy and Materials*, Vol. 24, No. 12, 2017, pp. 1412-1423.

[74] X. Y. Nie, Z. KangNing, L. Hongxiang, Q. Du, J. S. Zhang, and L. Zhuang, “Comparisons of interface microstructure and mechanical behavior between Ti/Al and Ti-6Al-4V/Al bimetallic composites,” in *China Foundry*, Vol. 12, No. 1, 2015, pp. 1-8.

[75] O. Dezellus, M. Zhe, F. Bosselet, D. Rouby, and J. C. Viala, “Mechanical testing of titanium/aluminium–silicon interface: Effect of T6 heat treatment,” in *Materials Science and Engineering A*, Vol. 528, No. 6, 2011, pp. 2795-2803.

[76] V. I. Dybkov, "Interaction of 18Cr-10Ni stainless steel with liquid aluminium," in *Journal of Materials Science*, Vol. 25, No. 8, 1990, pp. 3615-3633.

[77] K. Barmak and V. I. Dybkov, "Interaction of iron-chromium alloys containing 10 and 25 mass% chromium with liquid aluminium," in *Journal of Materials Science*, Vol. 39, No. 13, 2004, pp. 4219- 4230.

[78] V. I. Dybkov, "Interaction of iron-nickel alloys with liquid aluminium: Dissolution kinetics," in *Journal of Materials Science,* Vol. 28, No. 23, 1993, pp. 6371-6380.

[79] V. I. Dybkov, "Interaction of iron-nickel alloys with liquid aluminium: Formation of intermetallics," in *Journal of Materials Science*, Vol. 35, No. 7, 2000, pp. 1729-1736.

[80] W. Jiang, Z. Fan, G. Li, L. Yang, and X. Liu, "Effects of melt-to-solid insert volume ratio on the microstructures and mechanical properties of Al/Mg bimetallic castings produced by lost foam casting," in *Metallurgical and Materials Transactions A*, Vol. 47, No. 12, 2016, pp. 6487-6497.

[81] G. Li, W. Jiang, Z. Fan, Z. Jiang, X. Liu, and F. Liu, "Effects of pouring temperature on microstructure, mechanical properties, and fracture behavior of Al/Mg bimetallic composites produced by lost foam casting process," in *International Journal of Advanced Manufacturing Technology,* Vol. 91, No. 1-4, 2017, pp. 1355-1368.

[82] M. Divandari and A. R. V. Golpayegani, "Study of Al/Cu rich phases formed in A356 alloy by inserting Cu wire in pattern in LFC process," in *Materials and Design*, Vol. 30, No. 8, 2009, pp. 3279-3285.

[83] C. Dongfeng, D. Xuanpu, and F. Zitian, "Effects of parameters on formation and microstructure of surface composite layer prepared by lost foam casting technique," in *Journal of Wuhan University of Technology: Materials Science Edition*, Vol. 27, No. 1, 2012, pp. 82-87.

[84] M. M. Hejazi, M. Divandari, and E. Taghaddos, “Effect of copper insert on the microstructure of gray iron produced via lost foam casting,” in *Materials and Design*, Vol. 30, No. 4, 2009, pp. 1085-1092.

[85] S. Fan, W. Jiang, G. Li, J. Mo, and Z. Fan, “Fabrication and microstructure evolution of Al/Mg bimetal using a near-net forming process,” in *Materials and Manufacturing Processes*, Vol. 32, No. 12, 2017, pp. 1391-1397.

[86] S. M. Emami, M. Divandari, E. Hajjari, and H. Arabi, “Comparison between conventional and lost foam compound casting of Al/Mg light metals,” in *International Journal of Cast Metals Research*, Vol. 26, No. 1, 2013, pp. 43-50.

[87] R. K. Tayal, S. Kumar, A. Mondal, and S. Jambhale, “Experimental investigation and parametric optimization of AA6063/AA6351 alloys bimetallic prepared by vacuum-assisted lost foam compound casting process,” in *International Journal of Metalcasting,* 2019, https:// DOI 10.1007/s40962-019-00349-6.

[88] G. Li, W. Jiang, W. Yang, Z. Jiang, F. Guan, H. Jiang, and Z. Fan, “New insights into the characterization and formation of the interface of A356/AZ91D bimetallic composites fabricated by compound casting,” in *Metallurgical and Materials Transactions* A, Vol. 50, No. 2, 2019, pp. 1076-1090.

[89] J. Shang, K. Wang, Q. Zhou, D. Zhang, J. Huang, and G. Li, “Microstructure characteristics and mechanical properties of cold metal transfer welding Mg/Al dissimilar metals,” in *Materials and Design*, Vol. 34, 2012, pp. 559-565.

[90] Y. Wang, B. Zubaidy, and P. B. Prangnell, “The effectiveness of Al-Si coatings for preventing interfacial reaction in Al-Mg dissimilar metal welding, in *Metallurgical and Materials Transactions A*, Vol. 49, No. 1, 2018, pp. 162-176.

[91] S. Tan, F. Zheng, J. Chen, J. Han, Y. Wu, and L. Peng, "Effects of process parameters on microstructure and mechanical properties of friction stir lap linear welded 6061 aluminum alloy to NZ30K magnesium alloy," in *Journal of Magnesium and Alloys*, Vol. 5, No. 1, 2017, pp. 56-63.

[92] B. Mvola, P. Kah, and J. Martikainen, "Welding of dissimilar non-ferrous metals by GMAW processes," *in International Journal of Mechanical and Materials Engineering*, Vol. 9, No. 21, 2014, pp. 1-11.

[93] G. Peng, Q. Yan, J. Hu, P. Chen, Z. Chen, and T. Zhang, "Effect of forced air cooling on the microstructures, tensile strength, and hardness distribution of dissimilar friction stir welded AA5A06-AA6061 joints," in *Metals*, Vol. 9, No. 3, 2019, pp. 304-312.

[94] S. Chen, H. Zhang, X. Jiang, T. Yuan, Y. Han, and X. Li, "Mechanical properties of electric assisted friction stir welded 2219 aluminum alloy," in *Journal of Manufacturing Processes*, Vol. 44, 2019, pp. 197-206.

[95] R. K. Tayal, S. Kumar, and V. Singh, "Experimental investigation and optimization of process parameters for shear strength of compound cast bimetallic joints," in *Transactions of the Indian Institute Metals*, Vol. 77, No. 9, 2018, pp. 2173-2183.

[96] R. K. Tayal, S. Kumar, and V. Singh, "Experimental investigation and optimization of process parameters for impact strength of compound cast bimetallic joints," in *International Journal of Metalcasting*, Vol. 12, No 3, 2018, pp. 498-513.

[97] R. K. Tayal, S. Kumar, V. Singh, and R. Garg, "Characterization and microhardness evaluation of A356/Mg joint produced by vacuum-assisted sand mold compound casting process," in *International Journal of Metalcasting*, Vol. 13, No 2, 2019, pp. 392-406.

[98] H. Zhang, Y. Chen, and A. A. Luo, “A novel aluminium surface treatment for improved bonding in magnesium/aluminium bimetallic casting,” in *Scripta Materialia*, Vol. 86, No. 1, 2014, pp. 52-55.

[99] D. C. Montgomery, *Design and analysis of experiments*, 8th ed. New Delhi, India: Wiley India Private Limited, 2014.

[100] B. Singh, J. Kumar, and S. Kumar, “Influences of process parameters on MRR improvement in simple and powder-mixed EDM of AA6061/10%SiC composite,” in *Materials and Manufacturing Processes*, Vol. 30, No. 3, 2015, pp. 303-312.

[101] P. S. Vishnu and S. Joseph, “Optimization of friction welding parameters for joining medium carbon steels using response surface methodology,” in *International Journal of Engineering Research & Technology*, Vol. 3, No. 10, 2014, pp. 338-345.

[102] B. S. Reddy, J. S. Kumar, and K. V. K. Reddy, “Optimization of surface roughness in CNC end milling using response surface methodology and genetic algorithm,” in *International Journal of Engineering, Science and Technology*, Vol. 3, No. 8, 2011, pp. 102-109.

[103] B. Singh, J. Kumar, and S. Kumar, “Experimental investigation on surface characteristics in powder-mixed electro discharge machining of AA6061/10%SiC composite,” in *Materials and Manufacturing Processes*, Vol. 29, No. 3, 2014, pp. 287-297.

[104] S. Kumar, P. Kumar, and H. S. Shan, “Effect of process parameters on the solidification time of al-7%si alloy castings produced by VAEPC process,” In *Materials and Manufacturing Processes*, Vol. 22, No. 7-8, 2007, pp. 879-886.

[105] A. Farzadi, M. Bahmani, and D. F. Haghshenas, “Optimization of operational parameters in friction stir welding of AA7075-T6 aluminum alloy using response surface method,” in *Arabian Journal for Science and Engineering*, Vol. 42, No. 11, 2017, pp. 4905-4916.

[106] S. Kumar, P. Kumar, and H. S. Shan, "Effect of process parameters on impact strength of Al-7%Si alloy castings produced by VAEPC process," in *International Journal of Advanced Manufacturing Technology*, Vol. 38, No. 5-6, 2008, pp. 586-593.

[107] S. Kumar, P. Kumar, and H. S. Shan, "Optimization of tensile properties of evaporative pattern casting process through Taguchi's method," in *Journal of Materials Processing Technology*, Vol. 204, No. 1-3, 2008, pp. 59-69.

[108] S M. Sadrossadat and S. Johansson "The effects of solidification conditions and heat treatment on the microstructure and mechanical properties of EN-AC 44400 alloy." in *Materials Science Forum*, Vol. 649, 2010, pp. 505-510.

[109] B. R. Jinugu and N. M. Inampudi, "Microstructure, SDAS and mechanical properties of A356 alloy castings made in sand and granulated blast furnace slag moulds," in *Archives of Foundry Engineering*, Vol. 17, No. 1, 2017, pp. 179-191.

[110] M. Bilgin, S. Karabulut, and A. Ozdemir, "Effect of preheating and dry ice cooling on dissimilar friction stir welding of AA7075-T6 and AZ31B, in *Journal of Polytechnic*, 2018, DOI: 10.2339/politeknik.42 6649.

[111] Z. G. E. Chlouk, G. Ayoub, G. T. Kridli, and R. F. Hamade, "Intermetallic compound formation in Al/Mg friction stir welded (FSW) butt joints," in *Proceedings of the ASME 2014 International Mechanical Engineering Congress & Exposition*, Vol. 14, 2014, pp. 1-6.

[112] T. Morishige, A. Kawaguchi, M. Tsujikawa, M. Hino, T. Hirata, and K. Higashi, "Dissimilar welding of Al and Mg alloys by FSW," in *Materials Transactions*, Vol. 49, No. 5, 2008, pp. 1129-1131.

[113] D. Dietrich, D. Nickel, M. Krause, T. Lampke, M. P. Coleman, and V. Randle, "Formation of intermetallic phases in diffusion-welded joints

of aluminium and magnesium alloys," in *Journal of Material Science*, Vol. 46, No. 2, 2011, pp. 357-364.

[114] M. X. Zhang, H. Huang, K. Spencer, and Y. N. Shi, "Nanomechanics of Mg–Al intermetallic compounds," in *Surface & Coatings Technology*, Vol. 204, No. 14, 2010, pp. 2118-2122.

[115] R. K. Bhushan, S. Kumar, and S. Das, "GA approach for optimization of surface roughness parameters in machining of al alloy SiC particle composite," in *Journal of Materials Engineering and Performance*, Vol. 21, No. 8, 2012, pp. 1676-1686.

[116] M. Mitchell, *An introduction to genetic algorithm,* India: Printice Hall of India, 2005.

[117] K. Deb, *Multi-objective optimization using evolutionary algorithms*, New Delhi, India: Wiley India Private Limited, 2013.

[118] R. Malhotra, N. Singh, and Y. Singh, "Genetic algorithms: Concepts, design for optimization of process controllers," in *Computer and Information Science*, Vol. 4, No. 2, 2011, pp. 39-54.

[119] A. Jameel, M. Minhat, and M. Nizam, "Using genetic algorithm to optimize machining parameters in turning operation: A review," in *International Journal of Scientific and Research Publications*, Vol. 3, No. 5, 2013, pp. 1-6.

[120] W. M. Aly, "A new approach for classifier model selection and tuning using logistic regression and genetic algorithms," in *Arabian Journal for Science and Engineering*, Vol. 41, No. 12, 2016, pp. 5195-5204.

[121] H. Ganesan and G. Mohankumar, "Optimization of machining techniques in CNC turning centre using genetic algorithm," in *Arabian Journal for Science and Engineering*, Vol. 38, No. 6, 2013, pp. 1529-1538.

[122] K. Deb, *Optimization for engineering design - Algorithms and examples*, New Delhi, India: Prentice Hall of India, 2012.

[123] T. Raj and R. Attri, "Quantifying barriers to implementing Total Quality Management (TQM)," in *European Journal of Industrial Engineering*, Vol. 4, No. 3, 2010, pp. 308-335.

[124] K. Jangra, S. Grover, F. T. S. Chan, and A. Aggarwal, "Digraph and matrix method to evaluate the machinability of tungsten carbide composite with wire EDM," in *International Journal of Advanced Manufacturing Technology,* Vol. 56, No. 9-12, 2011, pp. 959-974.

[125] V. Paramasivam, V. Senthil, and N. R. Ramasamy, "Decision making in equipment selection: an integrated approach with digraph and matrix approach, AHP and ANP," in *International Journal of Advanced Manufacturing Technology,* Vol. 54, No. 9-12, 2011, pp. 1233-1244.

[126] N. K. Geetha and P. Sekar, "Graph theory matrix approach – A review," in *Indian Journal of Science and Technology,* Vol. 9, No. 16, 2016, pp. 1-4.

[127] R. K. Garg, V. P. Agrawal, and V. K. Gupta, "Selection of power plants by evaluation and comparison using graph theoretical methodology," in *International Journal of Electrical Power and Energy Systems*, Vol. 28, No. 6, 2006, pp. 429-435.

[128] R. V. Rao, "A decision-making framework model for evaluating flexible manufacturing systems using digraph and matrix methods," in *International Journal of Advanced Manufacturing Technology,* Vol. 30, No. 11-12, 2006, pp. 1101-1110.

[129] K. Jangra, S. Grover, and A. Aggarwal, "Digraph and matrix method for the performance evaluation of carbide compacting die manufactured by wire EDM," in *International Journal of Advanced Manufacturing Technology,* Vol. 54, No. 5-8, 2011, pp. 579-591.

[130] N. Vashisth and M. Gupta, "Performance analysis of CNC milling machine using graph theory," in *International Journal of Innovative Research in Science & Technology*, Vol. 1, No. 12, 2015, pp. 359-368.

[131] I. R. Mcdonald and S. P. Ogorman, “Graph theoretic techniques in the theory of classical fluids,” in *International Journal of Physics and Chemistry of Liquids*, Vol. 8, No. 2, 1978, pp. 57-98.

[132] M. Singh, I. A. Khan, and S. Grover, “Selection of manufacturing process using graph theoretic approach,” in *International Journal of System Assurance Engineering and Management,* Vol. 2, No. 4, 2011, pp. 301-311.

[133] W. Y. Zhang, S. B. Tor, and G. A. Britton, “A graph and matrix representation scheme for functional design of mechanical products,” in *International Journal of Advanced Manufacturing Technology,* Vol. 25, No. 3-4, 2005, pp. 221-232.

[134] J. Dou, X. Dai, and Z. Meng, “Graph theory-based approach to optimize single-product flow-line configurations of RMS,” in *International Journal of Advanced Manufacturing Technology*, Vol. 41, No. 9-10, 2009, pp. 916-931.

[135] V. Malhotra, T. Raj, and A. Arora, “Evaluation of barriers affecting reconfigurable manufacturing systems with graph theory and matrix approach,” in *Materials and Manufacturing processes*, Vol. 27, No. 1, 2012, pp. 88-94.

[136] S. V. N. Rao and N. Viswanadham, “Fault diagnosis in dynamical systems: a graph theoretic approach,” in *International Journal of Systems Science*, Vol. 18, No. 4, 1987, pp. 687-695.

[137] S. K. Mukhopadhyay, K. R. Babu, and K. V. V. Sai, “Modified hamiltonian chain: A graph theoretic approach to group technology,” in *International Journal of Production Research*, Vol. 38, No. 11, 2000, pp. 2459-2470.

[138] E. G. Kavilal, S. P. Venkatesan, and J. Sanket, "An integrated interpretive structural modeling and a graph-theoretic approach for measuring the supply chain complexity in the Indian automotive

industry," in *Journal of Manufacturing Technology Management*, Vol. 29, No. 3, 2018, pp. 478-514.

[139] N. D. Chakladar, R. Das, and S. Chakraborty, "A digraph-based expert system for non-traditional machining processes selection," in *International Journal of Advanced Manufacturing Technology*, Vol. 43, No. 3-4, 2009, pp. 226-237.

[140] R.V. Rao, *Decision making in the manufacturing environment: Using graph theory and fuzzy multiple attribute decision making methods*, Springer-Verlag London: Springer Series in Advanced Manufacturing, 2007.

[141] R. Q. Sardinas, M. R. Santana, and E. A. Brindis, "Genetic algorithm-based multi-objective optimization of cutting parameters in turning processes," in *Engineering Applications of Artificial Intelligence*, Vol. 19, No. 2, 2006, pp. 127-133.

[142] R. Khalil, D. Stockton, P. S. Kang, and L. M. Mukhongo, "A multi-objective optimization approach using genetic algorithms for quick response to effects of variability in flow manufacturing," in *International Journal of Advanced Computer Science and Applications*, Vol. 3, No. 9, 2012, pp. 12-17.

[143] P. C. Padhi, S. S. Mahapatra, S. N. Yadav, and D. K. Tripathy, "Multi-objective optimization of wire electrical discharge machining (WEDM) process parameters using weighted sum genetic algorithm approach," in *Journal of Advanced Manufacturing Systems*, Vol. 15, No. 2, 2016, pp. 85-100.

[144] G. C. M. Patel , P. Krishna, P. R. Vundavilli, and M. B. Parappagoudar, "Multi-objective optimization of squeeze casting process using genetic algorithm and particle swarm optimization," in *Archives of Foundry Engineering*, Vol. 16, No. 3, 2016, pp. 172-186.

[145] I. Giagkiozis and P. J. Fleming, “Methods for multi-objective optimization: An analysis,” in *Information Sciences*, Vol. 293, 2015, pp. 1-16.

[146] S. Deshpande, L. T. Watson, and R. A. Canfield, “Pareto front approximation using a hybrid approach,” in *Procedia Computer Science*, Vol. 18, 2013, pp. 521-530.

APPENDIX-I

CALCULATION FOR JOINT STRENGTH INDEX

Experiment No. 2

$$\text{VPM}_{R1}\text{ (shear strength)} = \begin{array}{c} \begin{array}{cccc} R^1{}_1 & R^1{}_2 & R^1{}_3 & R^1{}_4 \end{array} \\ \begin{bmatrix} 5.0 & 6 & 5 & 7 \\ 4 & 5.7 & 4 & 6 \\ 5 & 6 & 6.5 & 7 \\ 3 & 4 & 3 & 5.7 \end{bmatrix} \end{array} \begin{array}{l} \text{Parameters} \\ R^1{}_1 \\ R^1{}_2 \\ R^1{}_3 \\ R^1{}_4 \end{array}$$

The permanent function for the shear strength (shear strength index), per (R_1) = 15509.

$$\text{VPM}_{R2}\text{ (impact strength)} = \begin{array}{c} \begin{array}{cccc} R^2{}_1 & R^2{}_2 & R^2{}_3 & R^2{}_4 \end{array} \\ \begin{bmatrix} 2.8 & 5 & 7 & 6 \\ 5 & 4.2 & 6 & 6 \\ 3 & 4 & 4.0 & 5 \\ 4 & 4 & 5 & 3.1 \end{bmatrix} \end{array} \begin{array}{l} \text{Parameters} \\ R^2{}_1 \\ R^2{}_2 \\ R^2{}_3 \\ R^2{}_4 \end{array}$$

The permanent function for the impact strength (impact strength index), per (R_2) =10374.

$$\text{VPM}_{R3}\text{ (microhardness)} = \begin{array}{c} \begin{array}{cccc} R^3{}_1 & R^3{}_2 & R^3{}_3 & R^3{}_4 \end{array} \\ \begin{bmatrix} 5.0 & 7 & 7 & 5 \\ 3 & 5.9 & 5 & 3 \\ 3 & 5 & 6.1 & 3 \\ 5 & 7 & 7 & 6.4 \end{bmatrix} \end{array} \begin{array}{l} \text{Parameters} \\ R^3{}_1 \\ R^3{}_2 \\ R^3{}_3 \\ R^3{}_4 \end{array}$$

The permanent function for the microhardness (microhardness index), per (R_3) = 15127.

$$
\begin{array}{l} \\ \text{VPM}_{JS}\text{ (joint strength) } = R = \end{array}
\begin{array}{c}
\begin{array}{cccc} R_1 & R_2 & R_3 \end{array} \\
\begin{bmatrix} 15509 & 7 & 5 \\ 3 & 10374 & 4 \\ 5 & 6 & 15127 \end{bmatrix}
\end{array}
\begin{array}{l} \text{Parameters} \\ R_1 \\ R_2 \\ R_3 \end{array}
$$

The permanent function for joint strength (joint strength index), per (JS) = 2.43E12.

Experiment No. 3

$$
\text{VPM}_{R1}\text{ (shear strength)} =
\begin{array}{c}
\begin{array}{cccc} R^1{}_1 & R^1{}_2 & R^1{}_3 & R^1{}_4 \end{array} \\
\begin{bmatrix} 6.7 & 6 & 5 & 7 \\ 4 & 6.2 & 4 & 6 \\ 5 & 6 & 6.5 & 7 \\ 3 & 4 & 3 & 5.7 \end{bmatrix}
\end{array}
\begin{array}{l} \text{Parameters} \\ R^1{}_1 \\ R^1{}_2 \\ R^1{}_3 \\ R^1{}_4 \end{array}
$$

The permanent function for the shear strength (shear strength index), per (R_1) = 17382.

$$
\text{VPM}_{R2}\text{ (impact strength)} =
\begin{array}{c}
\begin{array}{cccc} R^2{}_1 & R^2{}_2 & R^2{}_3 & R^2{}_4 \end{array} \\
\begin{bmatrix} 4.6 & 5 & 7 & 6 \\ 5 & 4.2 & 6 & 6 \\ 3 & 4 & 4.0 & 5 \\ 4 & 4 & 5 & 3.1 \end{bmatrix}
\end{array}
\begin{array}{l} \text{Parameters} \\ R^2{}_1 \\ R^2{}_2 \\ R^2{}_3 \\ R^2{}_4 \end{array}
$$

The permanent function for the impact strength (impact strength index), per (R_2) =11395.

$$
\text{VPM}_{R3}\text{ (microhardness)} =
\begin{array}{c}
\begin{array}{cccc} R^3{}_1 & R^3{}_2 & R^3{}_3 & R^3{}_4 \end{array} \\
\begin{bmatrix} 6.7 & 7 & 7 & 5 \\ 3 & 6.1 & 5 & 3 \\ 3 & 5 & 6.1 & 3 \\ 5 & 7 & 7 & 6.4 \end{bmatrix}
\end{array}
\begin{array}{l} \text{Parameters} \\ R^3{}_1 \\ R^3{}_2 \\ R^3{}_3 \\ R^3{}_4 \end{array}
$$

The permanent function for the microhardness (microhardness index), per (R_3) = 16756.

$$\text{VPM}_{JS}\text{ (joint strength) } = R = \begin{array}{c} \\ R_1 \\ R_2 \\ R_3 \end{array}\!\!\begin{array}{c} \begin{array}{cccc} R_1 & R_2 & R_3 & \text{Parameters} \end{array} \\ \end{array}$$

$$\begin{array}{cccc} R_1 & R_2 & R_3 & \text{Parameters} \\ \left[\begin{array}{c} 17382 \\ 3 \\ 5 \end{array}\right. & \begin{array}{c} 7 \\ 11395 \\ 6 \end{array} & \left.\begin{array}{c} 5 \\ 4 \\ 16756 \end{array}\right] & \begin{array}{c} R_1 \\ R_2 \\ R_3 \end{array} \end{array}$$

The permanent function for joint strength (joint strength index), per (JS) = 3.32E12.

Experiment No. 4

$$\text{VPM}_{R1}\text{ (shear strength)} = \begin{array}{ccccc} R^1{}_1 & R^1{}_2 & R^1{}_3 & R^1{}_4 & \text{Parameters} \\ \left[\begin{array}{c} 5.0 \\ 4 \\ 5 \\ 3 \end{array}\right. & \begin{array}{c} 6 \\ 6.2 \\ 6 \\ 4 \end{array} & \begin{array}{c} 5 \\ 4 \\ 6.5 \\ 3 \end{array} & \left.\begin{array}{c} 7 \\ 6 \\ 7 \\ 5.7 \end{array}\right] & \begin{array}{c} R^1{}_1 \\ R^1{}_2 \\ R^1{}_3 \\ R^1{}_4 \end{array} \end{array}$$

The permanent function for the shear strength (shear strength index), per (R_1) = 15899.

$$\text{VPM}_{R2}\text{ (impact strength)} = \begin{array}{ccccc} R^2{}_1 & R^2{}_2 & R^2{}_3 & R^2{}_4 & \text{Parameters} \\ \left[\begin{array}{c} 2.8 \\ 5 \\ 3 \\ 4 \end{array}\right. & \begin{array}{c} 5 \\ 4.2 \\ 4 \\ 4 \end{array} & \begin{array}{c} 7 \\ 6 \\ 4.0 \\ 5 \end{array} & \left.\begin{array}{c} 6 \\ 6 \\ 5 \\ 3.1 \end{array}\right] & \begin{array}{c} R^2{}_1 \\ R^2{}_2 \\ R^2{}_3 \\ R^2{}_4 \end{array} \end{array}$$

The permanent function for the impact strength (impact strength index), per (R_2) =10374.

$$\text{VPM}_{R3}\text{ (microhardness)} = \begin{array}{ccccc} R^3{}_1 & R^3{}_2 & R^3{}_3 & R^3{}_4 & \text{Parameters} \\ \left[\begin{array}{c} 5.0 \\ 3 \\ 3 \\ 5 \end{array}\right. & \begin{array}{c} 7 \\ 6.1 \\ 5 \\ 7 \end{array} & \begin{array}{c} 7 \\ 5 \\ 6.1 \\ 7 \end{array} & \left.\begin{array}{c} 5 \\ 3 \\ 3 \\ 6.4 \end{array}\right] & \begin{array}{c} R^3{}_1 \\ R^3{}_2 \\ R^3{}_3 \\ R^3{}_4 \end{array} \end{array}$$

The permanent function for the microhardness (microhardness index), per (R_3) = 15287.

$$\text{VPM}_{JS}\text{ (joint strength) } = R = \begin{array}{c} \begin{array}{ccc} R_1 & R_2 & R_3 \end{array} \\ \begin{bmatrix} 15899 & 7 & 5 \\ 3 & 10374 & 4 \\ 5 & 6 & 15287 \end{bmatrix} \end{array} \begin{array}{l} \text{Parameters} \\ R_1 \\ R_2 \\ R_3 \end{array}$$

The permanent function for joint strength (joint strength index), per (JS) = 2.52E12.

Experiment No. 5

$$\text{VPM}_{R1}\text{ (shear strength) } = \begin{array}{c} \begin{array}{cccc} R^1{}_1 & R^1{}_2 & R^1{}_3 & R^1{}_4 \end{array} \\ \begin{bmatrix} 6.7 & 6 & 5 & 7 \\ 4 & 5.7 & 4 & 6 \\ 5 & 6 & 6.5 & 7 \\ 3 & 4 & 3 & 5.7 \end{bmatrix} \end{array} \begin{array}{l} \text{Parameters} \\ R^1{}_1 \\ R^1{}_2 \\ R^1{}_3 \\ R^1{}_4 \end{array}$$

The permanent function for the shear strength (shear strength index), per (R_1) = 16943.

$$\text{VPM}_{R2}\text{ (impact strength) } = \begin{array}{c} \begin{array}{cccc} R^2{}_1 & R^2{}_2 & R^2{}_3 & R^2{}_4 \end{array} \\ \begin{bmatrix} 4.6 & 5 & 7 & 6 \\ 5 & 4.2 & 6 & 6 \\ 3 & 4 & 3.5 & 5 \\ 4 & 4 & 5 & 3.1 \end{bmatrix} \end{array} \begin{array}{l} \text{Parameters} \\ R^2{}_1 \\ R^2{}_2 \\ R^2{}_3 \\ R^2{}_4 \end{array}$$

The permanent function for the impact strength (impact strength index), per (R_2) =11101.

$$\text{VPM}_{R3}\text{ (microhardness) } = \begin{array}{c} \begin{array}{cccc} R^3{}_1 & R^3{}_2 & R^3{}_3 & R^3{}_4 \end{array} \\ \begin{bmatrix} 6.7 & 7 & 7 & 5 \\ 3 & 5.9 & 5 & 3 \\ 3 & 5 & 6.1 & 3 \\ 5 & 7 & 7 & 6.4 \end{bmatrix} \end{array} \begin{array}{l} \text{Parameters} \\ R^3{}_1 \\ R^3{}_2 \\ R^3{}_3 \\ R^3{}_4 \end{array}$$

The permanent function for the microhardness (microhardness index), per (R_3) = 16576.

$$\mathrm{VPM_{JS}}\text{ (joint strength) } = R = \begin{array}{c} \\ \\ \\ \\ \end{array}\begin{array}{ccc|c} R_1 & R_2 & R_3 & \text{Parameters} \\ \end{array}$$

$$\mathrm{VPM_{JS}}\text{ (joint strength) } = R = \begin{array}{cl} \begin{array}{ccc} R_1 & R_2 & R_3 \end{array} & \text{Parameters} \\ \begin{bmatrix} 16943 & 7 & 5 \\ 3 & 11101 & 4 \\ 5 & 6 & 16576 \end{bmatrix} & \begin{array}{c} R_1 \\ R_2 \\ R_3 \end{array} \end{array}$$

The permanent function for joint strength (joint strength index), per (JS) = 3.18E12.

Experiment No. 6

$$\mathrm{VPM_{R1}}\text{ (shear strength) } = \begin{array}{cl} \begin{array}{cccc} R^1{}_1 & R^1{}_2 & R^1{}_3 & R^1{}_4 \end{array} & \text{Parameters} \\ \begin{bmatrix} 5.0 & 6 & 5 & 7 \\ 4 & 5.7 & 4 & 6 \\ 5 & 6 & 6.5 & 7 \\ 3 & 4 & 3 & 5.7 \end{bmatrix} & \begin{array}{c} R^1{}_1 \\ R^1{}_2 \\ R^1{}_3 \\ R^1{}_4 \end{array} \end{array}$$

The permanent function for the shear strength (shear strength index), per (R_1) = 15509.

$$\mathrm{VPM_{R2}}\text{ (impact strength) } = \begin{array}{cl} \begin{array}{cccc} R^2{}_1 & R^2{}_2 & R^2{}_3 & R^2{}_4 \end{array} & \text{Parameters} \\ \begin{bmatrix} 2.8 & 5 & 7 & 6 \\ 5 & 4.2 & 6 & 6 \\ 3 & 4 & 3.5 & 5 \\ 4 & 4 & 5 & 3.1 \end{bmatrix} & \begin{array}{c} R^2{}_1 \\ R^2{}_2 \\ R^2{}_3 \\ R^2{}_4 \end{array} \end{array}$$

The permanent function for the impact strength (impact strength index), per (R_2) =10113.

$$\mathrm{VPM_{R3}}\text{ (microhardness) } = \begin{array}{cl} \begin{array}{cccc} R^3{}_1 & R^3{}_2 & R^3{}_3 & R^3{}_4 \end{array} & \text{Parameters} \\ \begin{bmatrix} 5.0 & 7 & 7 & 5 \\ 3 & 5.9 & 5 & 3 \\ 3 & 5 & 6.1 & 3 \\ 5 & 7 & 7 & 6.4 \end{bmatrix} & \begin{array}{c} R^3{}_1 \\ R^3{}_2 \\ R^3{}_3 \\ R^3{}_4 \end{array} \end{array}$$

The permanent function for the microhardness (microhardness index), per (R_3) = 15127.

$$\text{VPM}_{JS}\text{ (joint strength) } = R = \begin{array}{cccc} R_1 & R_2 & R_3 & \text{Parameters} \\ \left[\begin{array}{c} 15509 \\ 3 \\ 5 \end{array}\right. & \begin{array}{c} 7 \\ 10113 \\ 6 \end{array} & \left.\begin{array}{c} 5 \\ 4 \\ 15127 \end{array}\right] & \begin{array}{c} R_1 \\ R_2 \\ R_3 \end{array} \end{array}$$

The permanent function for joint strength (joint strength index), per (JS) = 2.37E12.

Experiment No. 7

$$\text{VPM}_{R1}\text{ (shear strength) } = \begin{array}{ccccc} R^1{}_1 & R^1{}_2 & R^1{}_3 & R^1{}_4 & \text{Parameters} \\ \left[\begin{array}{c} 6.7 \\ 4 \\ 5 \\ 3 \end{array}\right. & \begin{array}{c} 6 \\ 6.2 \\ 6 \\ 4 \end{array} & \begin{array}{c} 5 \\ 4 \\ 6.5 \\ 3 \end{array} & \left.\begin{array}{c} 7 \\ 6 \\ 7 \\ 5.7 \end{array}\right] & \begin{array}{c} R^1{}_1 \\ R^1{}_2 \\ R^1{}_3 \\ R^1{}_4 \end{array} \end{array}$$

The permanent function for the shear strength (shear strength index), per (R_1) = 17382.

$$\text{VPM}_{R2}\text{ (impact strength) } = \begin{array}{ccccc} R^2{}_1 & R^2{}_2 & R^2{}_3 & R^2{}_4 & \text{Parameters} \\ \left[\begin{array}{c} 4.6 \\ 5 \\ 3 \\ 4 \end{array}\right. & \begin{array}{c} 5 \\ 4.2 \\ 4 \\ 4 \end{array} & \begin{array}{c} 7 \\ 6 \\ 3.5 \\ 5 \end{array} & \left.\begin{array}{c} 6 \\ 6 \\ 5 \\ 3.1 \end{array}\right] & \begin{array}{c} R^2{}_1 \\ R^2{}_2 \\ R^2{}_3 \\ R^2{}_4 \end{array} \end{array}$$

The permanent function for the impact strength (impact strength index), per (R_2) =11101.

$$\text{VPM}_{R3}\text{ (microhardness) } = \begin{array}{ccccc} R^3{}_1 & R^3{}_2 & R^3{}_3 & R^3{}_4 & \text{Parameters} \\ \left[\begin{array}{c} 6.7 \\ 3 \\ 3 \\ 5 \end{array}\right. & \begin{array}{c} 7 \\ 6.1 \\ 5 \\ 7 \end{array} & \begin{array}{c} 7 \\ 5 \\ 6.1 \\ 7 \end{array} & \left.\begin{array}{c} 5 \\ 3 \\ 3 \\ 5.6 \end{array}\right] & \begin{array}{c} R^3{}_1 \\ R^3{}_2 \\ R^3{}_3 \\ R^3{}_4 \end{array} \end{array}$$

The permanent function for the microhardness (microhardness index), per (R_3) = 16050.

$$\mathrm{VPM}_{JS}\text{ (joint strength) } = R = \begin{array}{cccc} R_1 & R_2 & R_3 & \text{Parameters} \\ \left[\begin{array}{ccc} 17382 & 7 & 5 \\ 3 & 11101 & 4 \\ 5 & 6 & 16050 \end{array}\right. & & \left.\right] & \begin{array}{c} R_1 \\ R_2 \\ R_3 \end{array} \end{array}$$

The permanent function for joint strength (joint strength index), per (JS) = 3.08E12.

Experiment No. 8

$$\mathrm{VPM}_{R1}\text{ (shear strength) } = \begin{array}{cc} \begin{array}{cccc} R^1{}_1 & R^1{}_2 & R^1{}_3 & R^1{}_4 \end{array} & \text{Parameters} \\ \begin{bmatrix} 5.0 & 6 & 5 & 7 \\ 4 & 6.2 & 4 & 6 \\ 5 & 6 & 6.5 & 7 \\ 3 & 4 & 3 & 5.7 \end{bmatrix} & \begin{array}{c} R^1{}_1 \\ R^1{}_2 \\ R^1{}_3 \\ R^1{}_4 \end{array} \end{array}$$

The permanent function for the shear strength (shear strength index), per (R_1) = 15899.

$$\mathrm{VPM}_{R2}\text{ (impact strength) } = \begin{array}{cc} \begin{array}{cccc} R^2{}_1 & R^2{}_2 & R^2{}_3 & R^2{}_4 \end{array} & \text{Parameters} \\ \begin{bmatrix} 2.8 & 5 & 7 & 6 \\ 5 & 4.2 & 6 & 6 \\ 3 & 4 & 3.5 & 5 \\ 4 & 4 & 5 & 3.1 \end{bmatrix} & \begin{array}{c} R^2{}_1 \\ R^2{}_2 \\ R^2{}_3 \\ R^2{}_4 \end{array} \end{array}$$

The permanent function for the impact strength (impact strength index), per (R_2) =10113.

$$\mathrm{VPM}_{R3}\text{ (microhardness) } = \begin{array}{cc} \begin{array}{cccc} R^3{}_1 & R^3{}_2 & R^3{}_3 & R^3{}_4 \end{array} & \text{Parameters} \\ \begin{bmatrix} 5.0 & 7 & 7 & 5 \\ 3 & 6.1 & 5 & 3 \\ 3 & 5 & 6.1 & 3 \\ 5 & 7 & 7 & 5.6 \end{bmatrix} & \begin{array}{c} R^3{}_1 \\ R^3{}_2 \\ R^3{}_3 \\ R^3{}_4 \end{array} \end{array}$$

The permanent function for the microhardness (microhardness index), per (R_3) = 14665.

$$\mathrm{VPM_{JS}}\ \text{(joint strength)} = R = \begin{array}{c} \\ \\ \\ \end{array}\begin{array}{cccc} R_1 & R_2 & R_3 & \text{Parameters} \\ \left[\begin{array}{ccc} 15899 & 7 & 5 \\ 3 & 10113 & 4 \\ 5 & 6 & 14665 \end{array}\right] & & & \begin{array}{c} R_1 \\ R_2 \\ R_3 \end{array} \end{array}$$

The permanent function for joint strength (joint strength index), per (JS) = 2.38E12.

Experiment No. 9

$$\mathrm{VPM_{R1}}\ \text{(shear strength)} = \begin{array}{cc} \begin{array}{cccc} R^1{}_1 & R^1{}_2 & R^1{}_3 & R^1{}_4 \end{array} & \text{Parameters} \\ \left[\begin{array}{cccc} 6.7 & 6 & 5 & 7 \\ 4 & 5.7 & 4 & 6 \\ 5 & 6 & 6.5 & 7 \\ 3 & 4 & 3 & 5.7 \end{array}\right] & \begin{array}{c} R^1{}_1 \\ R^1{}_2 \\ R^1{}_3 \\ R^1{}_4 \end{array} \end{array}$$

The permanent function for the shear strength (shear strength index), per (R_1) = 16943.

$$\mathrm{VPM_{R2}}\ \text{(impact strength)} = \begin{array}{cc} \begin{array}{cccc} R^2{}_1 & R^2{}_2 & R^2{}_3 & R^2{}_4 \end{array} & \text{Parameters} \\ \left[\begin{array}{cccc} 4.6 & 5 & 7 & 6 \\ 5 & 4.2 & 6 & 6 \\ 3 & 4 & 4.0 & 5 \\ 4 & 4 & 5 & 4.2 \end{array}\right] & \begin{array}{c} R^2{}_1 \\ R^2{}_2 \\ R^2{}_3 \\ R^2{}_4 \end{array} \end{array}$$

The permanent function for the impact strength (impact strength index), per (R_2) =12061.

$$\mathrm{VPM_{R3}}\ \text{(microhardness)} = \begin{array}{cc} \begin{array}{cccc} R^3{}_1 & R^3{}_2 & R^3{}_3 & R^3{}_4 \end{array} & \text{Parameters} \\ \left[\begin{array}{cccc} 6.7 & 7 & 7 & 5 \\ 3 & 5.9 & 5 & 3 \\ 3 & 5 & 6.1 & 3 \\ 5 & 7 & 7 & 5.6 \end{array}\right] & \begin{array}{c} R^3{}_1 \\ R^3{}_2 \\ R^3{}_3 \\ R^3{}_4 \end{array} \end{array}$$

The permanent function for the microhardness (microhardness index), per (R_3) = 15880.

$$VPM_{JS}\text{ (joint strength) } = R = \begin{array}{c} \\ \\ \\ \end{array}\begin{array}{ccc|c} R_1 & R_2 & R_3 & \text{Parameters} \end{array}$$

$$\begin{array}{c@{}c} \begin{bmatrix} 16943 & 7 & 5 \\ 3 & 12061 & 4 \\ 5 & 6 & 15880 \end{bmatrix} & \begin{array}{c} R_1 \\ R_2 \\ R_3 \end{array} \end{array}$$

The permanent function for joint strength (joint strength index), per (JS) = 3.25E12.

Experiment No. 10

$$VPM_{R1}\text{ (shear strength)} = \begin{array}{cc} \begin{array}{cccc} R^1{}_1 & R^1{}_2 & R^1{}_3 & R^1{}_4 \end{array} & \text{Parameters} \\ \begin{bmatrix} 5.0 & 6 & 5 & 7 \\ 4 & 5.7 & 4 & 6 \\ 5 & 6 & 6.5 & 7 \\ 3 & 4 & 3 & 5.7 \end{bmatrix} & \begin{array}{c} R^1{}_1 \\ R^1{}_2 \\ R^1{}_3 \\ R^1{}_4 \end{array} \end{array}$$

The permanent function for the shear strength (shear strength index), per (R_1) = 15509.

$$VPM_{R2}\text{ (impact strength)} = \begin{array}{cc} \begin{array}{cccc} R^2{}_1 & R^2{}_2 & R^2{}_3 & R^2{}_4 \end{array} & \text{Parameters} \\ \begin{bmatrix} 2.8 & 5 & 7 & 6 \\ 5 & 4.2 & 6 & 6 \\ 3 & 4 & 4.0 & 5 \\ 4 & 4 & 5 & 4.2 \end{bmatrix} & \begin{array}{c} R^2{}_1 \\ R^2{}_2 \\ R^2{}_3 \\ R^2{}_4 \end{array} \end{array}$$

The permanent function for the impact strength (impact strength index), per (R_2) =10959.

$$VPM_{R3}\text{ (microhardness)} = \begin{array}{cc} \begin{array}{cccc} R^3{}_1 & R^3{}_2 & R^3{}_3 & R^3{}_4 \end{array} & \text{Parameters} \\ \begin{bmatrix} 5.0 & 7 & 7 & 5 \\ 3 & 5.9 & 5 & 3 \\ 3 & 5 & 6.1 & 3 \\ 5 & 7 & 7 & 5.6 \end{bmatrix} & \begin{array}{c} R^3{}_1 \\ R^3{}_2 \\ R^3{}_3 \\ R^3{}_4 \end{array} \end{array}$$

The permanent function for the microhardness (microhardness index), per (R_3) = 14514.

$$
\mathrm{VPM_{JS}}\ \text{(joint strength)} = R = \begin{array}{c} \\ \\ \\ \end{array}
\begin{array}{cccc}
R_1 & R_2 & R_3 & \text{Parameters} \\
\end{array}
$$

$$
\begin{array}{c|ccc|c}
 & R_1 & R_2 & R_3 & \text{Parameters} \\
\hline
 & 15509 & 7 & 5 & R_1 \\
\mathrm{VPM_{JS}}\ \text{(joint strength)} = R = & 3 & 10959 & 4 & R_2 \\
 & 5 & 6 & 14514 & R_3
\end{array}
$$

The permanent function for joint strength (joint strength index), per (JS) = 2.47E12.

Experiment No. 11

$$
\mathrm{VPM_{R1}}\ \text{(shear strength)} =
\begin{array}{c}
\begin{array}{cccc} R^1{}_1 & R^1{}_2 & R^1{}_3 & R^1{}_4 \end{array} \\
\begin{bmatrix}
6.7 & 6 & 5 & 7 \\
4 & 6.2 & 4 & 6 \\
5 & 6 & 6.5 & 7 \\
3 & 4 & 3 & 5.7
\end{bmatrix}
\end{array}
\begin{array}{l}
\text{Parameters} \\
R^1{}_1 \\
R^1{}_2 \\
R^1{}_3 \\
R^1{}_4
\end{array}
$$

The permanent function for the shear strength (shear strength index), per (R_1) = 17382.

$$
\mathrm{VPM_{R2}}\ \text{(impact strength)} =
\begin{array}{c}
\begin{array}{cccc} R^2{}_1 & R^2{}_2 & R^2{}_3 & R^2{}_4 \end{array} \\
\begin{bmatrix}
4.6 & 5 & 7 & 6 \\
5 & 4.2 & 6 & 6 \\
3 & 4 & 4.0 & 5 \\
4 & 4 & 5 & 4.2
\end{bmatrix}
\end{array}
\begin{array}{l}
\text{Parameters} \\
R^2{}_1 \\
R^2{}_2 \\
R^2{}_3 \\
R^2{}_4
\end{array}
$$

The permanent function for the impact strength (impact strength index), per (R_2) =12061.

$$
\mathrm{VPM_{R3}}\ \text{(microhardness)} =
\begin{array}{c}
\begin{array}{cccc} R^3{}_1 & R^3{}_2 & R^3{}_3 & R^3{}_4 \end{array} \\
\begin{bmatrix}
6.7 & 7 & 7 & 5 \\
3 & 6.1 & 5 & 3 \\
3 & 5 & 6.1 & 3 \\
5 & 7 & 7 & 5.6
\end{bmatrix}
\end{array}
\begin{array}{l}
\text{Parameters} \\
R^3{}_1 \\
R^3{}_2 \\
R^3{}_3 \\
R^3{}_4
\end{array}
$$

The permanent function for the microhardness (microhardness index), per (R_3) = 16050.

$$\text{VPM}_{JS}\text{ (joint strength) } = R = \begin{array}{c} \begin{array}{ccc} R_1 & R_2 & R_3 \end{array} \\ \begin{bmatrix} 17382 & 7 & 5 \\ 3 & 12061 & 4 \\ 5 & 6 & 16050 \end{bmatrix} \end{array} \begin{array}{l} \text{Parameters} \\ R_1 \\ R_2 \\ R_3 \end{array}$$

The permanent function for joint strength (joint strength index), per (JS) = 3.37E12.

Experiment No. 12

$$\text{VPM}_{R1}\text{ (shear strength) } = \begin{array}{c} \begin{array}{cccc} R^1{}_1 & R^1{}_2 & R^1{}_3 & R^1{}_4 \end{array} \\ \begin{bmatrix} 5.0 & 6 & 5 & 7 \\ 4 & 6.2 & 4 & 6 \\ 5 & 6 & 6.5 & 7 \\ 3 & 4 & 3 & 5.7 \end{bmatrix} \end{array} \begin{array}{l} \text{Parameters} \\ R^1{}_1 \\ R^1{}_2 \\ R^1{}_3 \\ R^1{}_4 \end{array}$$

The permanent function for the shear strength (shear strength index), per (R_1) = 15899.

$$\text{VPM}_{R2}\text{ (impact strength) } = \begin{array}{c} \begin{array}{cccc} R^2{}_1 & R^2{}_2 & R^2{}_3 & R^2{}_4 \end{array} \\ \begin{bmatrix} 2.8 & 5 & 7 & 6 \\ 5 & 4.2 & 6 & 6 \\ 3 & 4 & 4.0 & 5 \\ 4 & 4 & 5 & 4.2 \end{bmatrix} \end{array} \begin{array}{l} \text{Parameters} \\ R^2{}_1 \\ R^2{}_2 \\ R^2{}_3 \\ R^2{}_4 \end{array}$$

The permanent function for the impact strength (impact strength index), per (R_2) =10959.

$$\text{VPM}_{R3}\text{ (microhardness) } = \begin{array}{c} \begin{array}{cccc} R^3{}_1 & R^3{}_2 & R^3{}_3 & R^3{}_4 \end{array} \\ \begin{bmatrix} 5.0 & 7 & 7 & 5 \\ 3 & 6.1 & 5 & 3 \\ 3 & 5 & 6.1 & 3 \\ 5 & 7 & 7 & 5.6 \end{bmatrix} \end{array} \begin{array}{l} \text{Parameters} \\ R^3{}_1 \\ R^3{}_2 \\ R^3{}_3 \\ R^3{}_4 \end{array}$$

The permanent function for the microhardness (microhardness index), per (R_3) = 14665.

$$\text{VPM}_{JS}\text{ (joint strength) } = R = \begin{array}{c} \\ \\ \\ \\ \end{array}\begin{array}{cccc} R_1 & R_2 & R_3 & \text{Parameters} \\ \left[\begin{array}{ccc} 15899 & 7 & 5 \\ 3 & 10959 & 4 \\ 5 & 6 & 14665 \end{array}\right. & & \left.\right] & \begin{array}{c} R_1 \\ R_2 \\ R_3 \end{array} \end{array}$$

The permanent function for joint strength (joint strength index), per (JS) = 2.56E12.

Experiment No. 13

$$\text{VPM}_{R1}\text{ (shear strength)} = \begin{array}{cc} \begin{array}{cccc} R^1{}_1 & R^1{}_2 & R^1{}_3 & R^1{}_4 \end{array} & \text{Parameters} \\ \begin{bmatrix} 6.7 & 6 & 5 & 7 \\ 4 & 5.7 & 4 & 6 \\ 5 & 6 & 5.5 & 7 \\ 3 & 4 & 3 & 5.7 \end{bmatrix} & \begin{array}{c} R^1{}_1 \\ R^1{}_2 \\ R^1{}_3 \\ R^1{}_4 \end{array} \end{array}$$

The permanent function for the shear strength (shear strength index), per (R_1) = 16088.

$$\text{VPM}_{R2}\text{ (impact strength)} = \begin{array}{cc} \begin{array}{cccc} R^2{}_1 & R^2{}_2 & R^2{}_3 & R^2{}_4 \end{array} & \text{Parameters} \\ \begin{bmatrix} 4.6 & 5 & 7 & 6 \\ 5 & 4.2 & 6 & 6 \\ 3 & 4 & 3.5 & 5 \\ 4 & 4 & 5 & 4.2 \end{bmatrix} & \begin{array}{c} R^2{}_1 \\ R^2{}_2 \\ R^2{}_3 \\ R^2{}_4 \end{array} \end{array}$$

The permanent function for the impact strength (impact strength index), per (R_2) =11743.

$$\text{VPM}_{R3}\text{ (microhardness)} = \begin{array}{cc} \begin{array}{cccc} R^3{}_1 & R^3{}_2 & R^3{}_3 & R^3{}_4 \end{array} & \text{Parameters} \\ \begin{bmatrix} 6.7 & 7 & 7 & 5 \\ 3 & 5.9 & 5 & 3 \\ 3 & 5 & 6.1 & 3 \\ 5 & 7 & 7 & 5.6 \end{bmatrix} & \begin{array}{c} R^3{}_1 \\ R^3{}_2 \\ R^3{}_3 \\ R^3{}_4 \end{array} \end{array}$$

The permanent function for the microhardness (microhardness index), per (R_3) = 15880.

$$\text{VPM}_{JS}\text{ (joint strength) } = R = \begin{array}{c} \\ \\ \\ \end{array}\begin{array}{cccc} R_1 & R_2 & R_3 & \text{Parameters} \\ \end{array}$$

$$\begin{array}{c|ccc|c} & R_1 & R_2 & R_3 & \text{Parameters} \\ & 16088 & 7 & 5 & R_1 \\ \text{VPM}_{JS}\text{ (joint strength) } = R = & 3 & 11743 & 4 & R_2 \\ & 5 & 6 & 15880 & R_3 \end{array}$$

The permanent function for joint strength (joint strength index), per (JS) = 3.00E12.

Experiment No. 14

$$\text{VPM}_{R1}\text{ (shear strength) } = \begin{array}{cccc|l} R^1{}_1 & R^1{}_2 & R^1{}_3 & R^1{}_4 & \text{Parameters} \end{array}$$

$$\begin{array}{l} \\ \text{VPM}_{R1}\text{ (shear strength) } = \end{array} \begin{array}{c} R^1{}_1 \quad R^1{}_2 \quad R^1{}_3 \quad R^1{}_4 \\ \begin{bmatrix} 5.0 & 6 & 5 & 7 \\ 4 & 5.7 & 4 & 6 \\ 5 & 6 & 5.5 & 7 \\ 3 & 4 & 3 & 5.7 \end{bmatrix} \end{array} \begin{array}{l} \text{Parameters} \\ R^1{}_1 \\ R^1{}_2 \\ R^1{}_3 \\ R^1{}_4 \end{array}$$

The permanent function for the shear strength (shear strength index), per (R_1) = 14750.

$$\text{VPM}_{R2}\text{ (impact strength) } = \begin{array}{c} R^2{}_1 \quad R^2{}_2 \quad R^2{}_3 \quad R^2{}_4 \\ \begin{bmatrix} 2.8 & 5 & 7 & 6 \\ 5 & 4.2 & 6 & 6 \\ 3 & 4 & 3.5 & 5 \\ 4 & 4 & 5 & 4.2 \end{bmatrix} \end{array} \begin{array}{l} \text{Parameters} \\ R^2{}_1 \\ R^2{}_2 \\ R^2{}_3 \\ R^2{}_4 \end{array}$$

The permanent function for the impact strength (impact strength index), per (R_2) =10678.

$$\text{VPM}_{R3}\text{ (microhardness) } = \begin{array}{c} R^3{}_1 \quad R^3{}_2 \quad R^3{}_3 \quad R^3{}_4 \\ \begin{bmatrix} 5.0 & 7 & 7 & 5 \\ 3 & 5.9 & 5 & 3 \\ 3 & 5 & 6.1 & 3 \\ 5 & 7 & 7 & 5.6 \end{bmatrix} \end{array} \begin{array}{l} \text{Parameters} \\ R^3{}_1 \\ R^3{}_2 \\ R^3{}_3 \\ R^3{}_4 \end{array}$$

The permanent function for the microhardness (microhardness index), per (R_3) = 14514.

$$
\text{VPM}_{JS}\text{ (joint strength) } = R = \begin{array}{c}
\begin{array}{ccc} R_1 & R_2 & R_3 \end{array} \\
\begin{bmatrix} 14750 & 7 & 5 \\ 3 & 10678 & 4 \\ 5 & 6 & 14514 \end{bmatrix}
\end{array}
\begin{array}{l} \text{Parameters} \\ R_1 \\ R_2 \\ R_3 \end{array}
$$

The permanent function for joint strength (joint strength index), per (JS) = 2.27E12.

Experiment No. 15

$$
\text{VPM}_{R1}\text{ (shear strength) } = \begin{array}{c}
\begin{array}{cccc} R^1{}_1 & R^1{}_2 & R^1{}_3 & R^1{}_4 \end{array} \\
\begin{bmatrix} 6.7 & 6 & 5 & 7 \\ 4 & 6.2 & 4 & 6 \\ 5 & 6 & 5.5 & 7 \\ 3 & 4 & 3 & 6.0 \end{bmatrix}
\end{array}
\begin{array}{l} \text{Parameters} \\ R^1{}_1 \\ R^1{}_2 \\ R^1{}_3 \\ R^1{}_4 \end{array}
$$

The permanent function for the shear strength (shear strength index), per (R_1) = 16772.

$$
\text{VPM}_{R2}\text{ (impact strength) } = \begin{array}{c}
\begin{array}{cccc} R^2{}_1 & R^2{}_2 & R^2{}_3 & R^2{}_4 \end{array} \\
\begin{bmatrix} 4.6 & 5 & 7 & 6 \\ 5 & 4.2 & 6 & 6 \\ 3 & 4 & 3.5 & 5 \\ 4 & 4 & 5 & 4.2 \end{bmatrix}
\end{array}
\begin{array}{l} \text{Parameters} \\ R^2{}_1 \\ R^2{}_2 \\ R^2{}_3 \\ R^2{}_4 \end{array}
$$

The permanent function for the impact strength (impact strength index), per (R_2) =11743.

$$
\text{VPM}_{R3}\text{ (microhardness) } = \begin{array}{c}
\begin{array}{cccc} R^3{}_1 & R^3{}_2 & R^3{}_3 & R^3{}_4 \end{array} \\
\begin{bmatrix} 6.7 & 7 & 7 & 5 \\ 3 & 6.1 & 5 & 3 \\ 3 & 5 & 6.1 & 3 \\ 5 & 7 & 7 & 5.6 \end{bmatrix}
\end{array}
\begin{array}{l} \text{Parameters} \\ R^3{}_1 \\ R^3{}_2 \\ R^3{}_3 \\ R^3{}_4 \end{array}
$$

The permanent function for the microhardness (microhardness index), per (R_3) = 16050.

$$
\text{VPM}_{JS}\ \text{(joint strength)} = R = \begin{array}{c} \\ \\ \\ \\ \end{array}
\begin{array}{c}
\begin{array}{ccc} R_1 & R_2 & R_3 \end{array} \\
\begin{bmatrix} 16772 & 7 & 5 \\ 3 & 11743 & 4 \\ 5 & 6 & 16050 \end{bmatrix}
\end{array}
\begin{array}{l} \text{Parameters} \\ R_1 \\ R_2 \\ R_3 \end{array}
$$

The permanent function for joint strength (joint strength index), per (JS) = 3.16E12.

Experiment No. 16

$$
\text{VPM}_{R1}\ \text{(shear strength)} =
\begin{array}{c}
\begin{array}{cccc} R^1{}_1 & R^1{}_2 & R^1{}_3 & R^1{}_4 \end{array} \\
\begin{bmatrix} 5.0 & 6 & 5 & 7 \\ 4 & 6.2 & 4 & 6 \\ 5 & 6 & 5.5 & 7 \\ 3 & 4 & 3 & 6.0 \end{bmatrix}
\end{array}
\begin{array}{l} \text{Parameters} \\ R^1{}_1 \\ R^1{}_2 \\ R^1{}_3 \\ R^1{}_4 \end{array}
$$

The permanent function for the shear strength (shear strength index), per (R_1) = 15360.

$$
\text{VPM}_{R2}\ \text{(impact strength)} =
\begin{array}{c}
\begin{array}{cccc} R^2{}_1 & R^2{}_2 & R^2{}_3 & R^2{}_4 \end{array} \\
\begin{bmatrix} 2.8 & 5 & 7 & 6 \\ 5 & 4.2 & 6 & 6 \\ 3 & 4 & 3.5 & 5 \\ 4 & 4 & 5 & 4.2 \end{bmatrix}
\end{array}
\begin{array}{l} \text{Parameters} \\ R^2{}_1 \\ R^2{}_2 \\ R^2{}_3 \\ R^2{}_4 \end{array}
$$

The permanent function for the impact strength (impact strength index), per (R_2) =10678.

$$
\text{VPM}_{R3}\ \text{(microhardness)} =
\begin{array}{c}
\begin{array}{cccc} R^3{}_1 & R^3{}_2 & R^3{}_3 & R^3{}_4 \end{array} \\
\begin{bmatrix} 5.0 & 7 & 7 & 5 \\ 3 & 6.1 & 5 & 3 \\ 3 & 5 & 6.1 & 3 \\ 5 & 7 & 7 & 5.6 \end{bmatrix}
\end{array}
\begin{array}{l} \text{Parameters} \\ R^3{}_1 \\ R^3{}_2 \\ R^3{}_3 \\ R^3{}_4 \end{array}
$$

The permanent function for the microhardness (microhardness index), per (R_3) = 14665.

$$
\begin{array}{l}
 \\
\text{VPM}_{JS}\,\text{(joint strength)} = R =
\end{array}
\begin{array}{cccc}
R_1 & R_2 & R_3 & \text{Parameters} \\
\left[\begin{array}{ccc} 15360 & 7 & 5 \\ 3 & 10678 & 4 \\ 5 & 6 & 14665 \end{array}\right] & & & \begin{array}{c} R_1 \\ R_2 \\ R_3 \end{array}
\end{array}
$$

The permanent function for joint strength (joint strength index), per (JS) = 2.41E12.

Experiment No. 17

$$
\text{VPM}_{R1}\,\text{(shear strength)} =
\begin{array}{cc}
\begin{array}{cccc} R^1{}_1 & R^1{}_2 & R^1{}_3 & R^1{}_4 \end{array} & \text{Parameters} \\
\left[\begin{array}{cccc} 7.1 & 6 & 5 & 7 \\ 4 & 6.0 & 4 & 6 \\ 5 & 6 & 6.0 & 7 \\ 3 & 4 & 3 & 6.0 \end{array}\right] & \begin{array}{c} R^1{}_1 \\ R^1{}_2 \\ R^1{}_3 \\ R^1{}_4 \end{array}
\end{array}
$$

The permanent function for the shear strength (shear strength index), per (R_1) = 17391.

$$
\text{VPM}_{R2}\,\text{(impact strength)} =
\begin{array}{cc}
\begin{array}{cccc} R^2{}_1 & R^2{}_2 & R^2{}_3 & R^2{}_4 \end{array} & \text{Parameters} \\
\left[\begin{array}{cccc} 5.5 & 5 & 7 & 6 \\ 5 & 3.8 & 6 & 6 \\ 3 & 4 & 3.8 & 5 \\ 4 & 4 & 5 & 3.8 \end{array}\right] & \begin{array}{c} R^2{}_1 \\ R^2{}_2 \\ R^2{}_3 \\ R^2{}_4 \end{array}
\end{array}
$$

The permanent function for the impact strength (impact strength index), per (R_2) =11977.

$$
\text{VPM}_{R3}\,\text{(microhardness)} =
\begin{array}{cc}
\begin{array}{cccc} R^3{}_1 & R^3{}_2 & R^3{}_3 & R^3{}_4 \end{array} & \text{Parameters} \\
\left[\begin{array}{cccc} 7.0 & 7 & 7 & 5 \\ 3 & 6.0 & 5 & 3 \\ 3 & 5 & 6.0 & 3 \\ 5 & 7 & 7 & 6.0 \end{array}\right] & \begin{array}{c} R^3{}_1 \\ R^3{}_2 \\ R^3{}_3 \\ R^3{}_4 \end{array}
\end{array}
$$

The permanent function for the microhardness (microhardness index), per (R_3) = 16477.

$$\text{VPM}_{JS} \text{ (joint strength) } = R = \begin{array}{c} \\ \\ \\ \\ \end{array}\begin{array}{cccc} R_1 & R_2 & R_3 & \text{Parameters} \\ \left[\begin{array}{c} 17391 \\ 3 \\ 5 \end{array}\right. & \begin{array}{c} 7 \\ 11977 \\ 6 \end{array} & \left.\begin{array}{c} 5 \\ 4 \\ 16477 \end{array}\right] & \begin{array}{c} R_1 \\ R_2 \\ R_3 \end{array} \end{array}$$

The permanent function for joint strength (joint strength index), per (JS) = 3.43E12.

Experiment No. 18

$$\text{VPM}_{R1} \text{ (shear strength) } = \begin{array}{c|c} \begin{array}{cccc} R^1{}_1 & R^1{}_2 & R^1{}_3 & R^1{}_4 \end{array} & \text{Parameters} \\ \begin{bmatrix} 3.7 & 6 & 5 & 7 \\ 4 & 6.0 & 4 & 6 \\ 5 & 6 & 6.0 & 7 \\ 3 & 4 & 3 & 6.0 \end{bmatrix} & \begin{array}{c} R^1{}_1 \\ R^1{}_2 \\ R^1{}_3 \\ R^1{}_4 \end{array} \end{array}$$

The permanent function for the shear strength (shear strength index), per (R_1) = 14501.

$$\text{VPM}_{R2} \text{ (impact strength) } = \begin{array}{cc} \begin{array}{cccc} R^2{}_1 & R^2{}_2 & R^2{}_3 & R^2{}_4 \end{array} & \text{Parameters} \\ \begin{bmatrix} 2.0 & 5 & 7 & 6 \\ 5 & 3.8 & 6 & 6 \\ 3 & 4 & 3.8 & 5 \\ 4 & 4 & 5 & 3.8 \end{bmatrix} & \begin{array}{c} R^2{}_1 \\ R^2{}_2 \\ R^2{}_3 \\ R^2{}_4 \end{array} \end{array}$$

The permanent function for the impact strength (impact strength index), per (R_2) =9974.

$$\text{VPM}_{R3} \text{ (microhardness) } = \begin{array}{cc} \begin{array}{cccc} R^3{}_1 & R^3{}_2 & R^3{}_3 & R^3{}_4 \end{array} & \text{Parameters} \\ \begin{bmatrix} 3.6 & 7 & 7 & 5 \\ 3 & 6.0 & 5 & 3 \\ 3 & 5 & 6.0 & 3 \\ 5 & 7 & 7 & 6.0 \end{bmatrix} & \begin{array}{c} R^3{}_1 \\ R^3{}_2 \\ R^3{}_3 \\ R^3{}_4 \end{array} \end{array}$$

The permanent function for the microhardness (microhardness index), per (R_3) = 13662.

$$
\begin{array}{l}
\\
VPM_{JS}\ \text{(joint strength)} = R = \\
\\
\end{array}
\begin{array}{c}
\begin{array}{ccc} R_1 & R_2 & R_3 \end{array} \\
\begin{bmatrix} 14501 & 7 & 5 \\ 3 & 9974 & 4 \\ 5 & 6 & 13662 \end{bmatrix}
\end{array}
\begin{array}{l} \text{Parameters} \\ R_1 \\ R_2 \\ R_3 \end{array}
$$

The permanent function for joint strength (joint strength index), per (JS) = 1.98E12.

Experiment No. 19

$$
VPM_{R1}\ \text{(shear strength)} =
\begin{array}{c}
\begin{array}{cccc} R^1{}_1 & R^1{}_2 & R^1{}_3 & R^1{}_4 \end{array} \\
\begin{bmatrix} 6.0 & 6 & 5 & 7 \\ 4 & 5.5 & 4 & 6 \\ 5 & 6 & 6.0 & 7 \\ 3 & 4 & 3 & 6.0 \end{bmatrix}
\end{array}
\begin{array}{l} \text{Parameters} \\ R^1{}_1 \\ R^1{}_2 \\ R^1{}_3 \\ R^1{}_4 \end{array}
$$

The permanent function for the shear strength (shear strength index), per (R_1) = 16042.

$$
VPM_{R2}\ \text{(impact strength)} =
\begin{array}{c}
\begin{array}{cccc} R^2{}_1 & R^2{}_2 & R^2{}_3 & R^2{}_4 \end{array} \\
\begin{bmatrix} 3.8 & 5 & 7 & 6 \\ 5 & 5.2 & 6 & 6 \\ 3 & 4 & 3.8 & 5 \\ 4 & 4 & 5 & 3.8 \end{bmatrix}
\end{array}
\begin{array}{l} \text{Parameters} \\ R^2{}_1 \\ R^2{}_2 \\ R^2{}_3 \\ R^2{}_4 \end{array}
$$

The permanent function for the impact strength (impact strength index), per (R_2) =11776.

$$
VPM_{R3}\ \text{(microhardness)} =
\begin{array}{c}
\begin{array}{cccc} R^3{}_1 & R^3{}_2 & R^3{}_3 & R^3{}_4 \end{array} \\
\begin{bmatrix} 6.0 & 7 & 7 & 5 \\ 3 & 5.7 & 5 & 3 \\ 3 & 5 & 6.0 & 3 \\ 5 & 7 & 7 & 6.0 \end{bmatrix}
\end{array}
\begin{array}{l} \text{Parameters} \\ R^3{}_1 \\ R^3{}_2 \\ R^3{}_3 \\ R^3{}_4 \end{array}
$$

The permanent function for the microhardness (microhardness index), per (R_3) = 15401.

$$\text{VPM}_{JS}\text{ (joint strength) } = R = \begin{array}{c} \begin{array}{ccc} R_1 & R_2 & R_3 \end{array} \\ \begin{bmatrix} 16042 & 7 & 5 \\ 3 & 11776 & 4 \\ 5 & 6 & 15401 \end{bmatrix} \end{array} \begin{array}{l} \text{Parameters} \\ R_1 \\ R_2 \\ R_3 \end{array}$$

The permanent function for joint strength (joint strength index), per (JS) = 2.91E12.

Experiment No. 20

$$\text{VPM}_{R1}\text{ (shear strength) } = \begin{array}{c} \begin{array}{cccc} R^1{}_1 & R^1{}_2 & R^1{}_3 & R^1{}_4 \end{array} \\ \begin{bmatrix} 6.0 & 6 & 5 & 7 \\ 4 & 6.4 & 4 & 6 \\ 5 & 6 & 6.0 & 7 \\ 3 & 4 & 3 & 6.0 \end{bmatrix} \end{array} \begin{array}{l} \text{Parameters} \\ R^1{}_1 \\ R^1{}_2 \\ R^1{}_3 \\ R^1{}_4 \end{array}$$

The permanent function for the shear strength (shear strength index), per (R_1) = 16787.

$$\text{VPM}_{R2}\text{ (impact strength) } = \begin{array}{c} \begin{array}{cccc} R^2{}_1 & R^2{}_2 & R^2{}_3 & R^2{}_4 \end{array} \\ \begin{bmatrix} 3.8 & 5 & 7 & 6 \\ 5 & 5.2 & 6 & 6 \\ 3 & 4 & 3.8 & 5 \\ 4 & 4 & 5 & 3.8 \end{bmatrix} \end{array} \begin{array}{l} \text{Parameters} \\ R^2{}_1 \\ R^2{}_2 \\ R^2{}_3 \\ R^2{}_4 \end{array}$$

The permanent function for the impact strength (impact strength index), per (R_2) =11776.

$$\text{VPM}_{R3}\text{ (microhardness) } = \begin{array}{c} \begin{array}{cccc} R^3{}_1 & R^3{}_2 & R^3{}_3 & R^3{}_4 \end{array} \\ \begin{bmatrix} 6.0 & 7 & 7 & 5 \\ 3 & 6.2 & 5 & 3 \\ 3 & 5 & 6.0 & 3 \\ 5 & 7 & 7 & 6.0 \end{bmatrix} \end{array} \begin{array}{l} \text{Parameters} \\ R^3{}_1 \\ R^3{}_2 \\ R^3{}_3 \\ R^3{}_4 \end{array}$$

The permanent function for the microhardness (microhardness index), per (R_3) = 15815.

$$\begin{array}{l c c c l} & R_1 & R_2 & R_3 & \text{Parameters} \\ \text{VPM}_{JS}\text{ (joint strength) } = R = & \multicolumn{3}{c}{\left[\begin{array}{ccc} 16787 & 7 & 5 \\ 3 & 11776 & 4 \\ 5 & 6 & 15815 \end{array}\right]} & \begin{array}{l} R_1 \\ R_2 \\ R_3 \end{array} \end{array}$$

The permanent function for joint strength (joint strength index), per (JS) = 3.13E12.

Experiment No. 21

$$\begin{array}{l c c c c l} & R^1{}_1 & R^1{}_2 & R^1{}_3 & R^1{}_4 & \text{Parameters} \\ \text{VPM}_{R1}\text{ (shear strength)} = & \multicolumn{4}{c}{\left[\begin{array}{cccc} 6.0 & 6 & 5 & 7 \\ 4 & 6.0 & 4 & 6 \\ 5 & 6 & 6.9 & 7 \\ 3 & 4 & 3 & 6.0 \end{array}\right]} & \begin{array}{l} R^1{}_1 \\ R^1{}_2 \\ R^1{}_3 \\ R^1{}_4 \end{array} \end{array}$$

The permanent function for the shear strength (shear strength index), per (R_1) = 17221.

$$\begin{array}{l c c c c l} & R^2{}_1 & R^2{}_2 & R^2{}_3 & R^2{}_4 & \text{Parameters} \\ \text{VPM}_{R2}\text{ (impact strength)} = & \multicolumn{4}{c}{\left[\begin{array}{cccc} 3.8 & 5 & 7 & 6 \\ 5 & 3.8 & 6 & 6 \\ 3 & 4 & 4.2 & 5 \\ 4 & 4 & 5 & 3.8 \end{array}\right]} & \begin{array}{l} R^2{}_1 \\ R^2{}_2 \\ R^2{}_3 \\ R^2{}_4 \end{array} \end{array}$$

The permanent function for the impact strength (impact strength index), per (R_2) =11233.

$$\begin{array}{l c c c c l} & R^3{}_1 & R^3{}_2 & R^3{}_3 & R^3{}_4 & \text{Parameters} \\ \text{VPM}_{R3}\text{ (microhardness)} = & \multicolumn{4}{c}{\left[\begin{array}{cccc} 6.0 & 7 & 7 & 5 \\ 3 & 6.0 & 5 & 3 \\ 3 & 5 & 6.1 & 3 \\ 5 & 7 & 7 & 6.0 \end{array}\right]} & \begin{array}{l} R^3{}_1 \\ R^3{}_2 \\ R^3{}_3 \\ R^3{}_4 \end{array} \end{array}$$

The permanent function for the microhardness (microhardness index), per (R_3) = 15732.

$$
VPM_{JS}\text{ (joint strength) } = R = \begin{array}{cccc} R_1 & R_2 & R_3 & \text{Parameters} \\ \left[\begin{array}{ccc} 17221 & 7 & 5 \\ 3 & 11233 & 4 \\ 5 & 6 & 15732 \end{array}\right] & & & \begin{array}{c} R_1 \\ R_2 \\ R_3 \end{array} \end{array}
$$

The permanent function for joint strength (joint strength index), per (JS) = 3.04E12.

Experiment No. 22

$$
VPM_{R1}\text{ (shear strength) } = \begin{array}{cc} \begin{array}{cccc} R^1{}_1 & R^1{}_2 & R^1{}_3 & R^1{}_4 \end{array} & \text{Parameters} \\ \left[\begin{array}{cccc} 6.0 & 6 & 5 & 7 \\ 4 & 6.0 & 4 & 6 \\ 5 & 6 & 5.0 & 7 \\ 3 & 4 & 3 & 6.0 \end{array}\right] & \begin{array}{c} R^1{}_1 \\ R^1{}_2 \\ R^1{}_3 \\ R^1{}_4 \end{array} \end{array}
$$

The permanent function for the shear strength (shear strength index), per (R_1) = 15606.

$$
VPM_{R2}\text{ (impact strength) } = \begin{array}{cc} \begin{array}{cccc} R^2{}_1 & R^2{}_2 & R^2{}_3 & R^2{}_4 \end{array} & \text{Parameters} \\ \left[\begin{array}{cccc} 3.8 & 5 & 7 & 6 \\ 5 & 3.8 & 6 & 6 \\ 3 & 4 & 3.2 & 5 \\ 4 & 4 & 5 & 3.8 \end{array}\right] & \begin{array}{c} R^2{}_1 \\ R^2{}_2 \\ R^2{}_3 \\ R^2{}_4 \end{array} \end{array}
$$

The permanent function for the impact strength (impact strength index), per (R_2) =10661.

$$
VPM_{R3}\text{ (microhardness) } = \begin{array}{cc} \begin{array}{cccc} R^3{}_1 & R^3{}_2 & R^3{}_3 & R^3{}_4 \end{array} & \text{Parameters} \\ \left[\begin{array}{cccc} 6.0 & 7 & 7 & 5 \\ 3 & 6.0 & 5 & 3 \\ 3 & 5 & 6.1 & 3 \\ 5 & 7 & 7 & 6.0 \end{array}\right] & \begin{array}{c} R^3{}_1 \\ R^3{}_2 \\ R^3{}_3 \\ R^3{}_4 \end{array} \end{array}
$$

The permanent function for the microhardness (microhardness index), per (R_3) = 15732.

$$\mathrm{VPM}_{JS}\ \text{(joint strength)} = R = \begin{array}{cc} \begin{array}{ccc} R_1 & R_2 & R_3 \end{array} & \text{Parameters} \\ \begin{bmatrix} 15606 & 7 & 5 \\ 3 & 10661 & 4 \\ 5 & 6 & 15732 \end{bmatrix} & \begin{array}{c} R_1 \\ R_2 \\ R_3 \end{array} \end{array}$$

The permanent function for joint strength (joint strength index), per (JS) = 2.62E12.

Experiment No. 23

$$\mathrm{VPM}_{R1}\ \text{(shear strength)} = \begin{array}{cc} \begin{array}{cccc} R^1{}_1 & R^1{}_2 & R^1{}_3 & R^1{}_4 \end{array} & \text{Parameters} \\ \begin{bmatrix} 6.0 & 6 & 5 & 7 \\ 4 & 6.0 & 4 & 6 \\ 5 & 6 & 6.0 & 7 \\ 3 & 4 & 3 & 5.1 \end{bmatrix} & \begin{array}{c} R^1{}_1 \\ R^1{}_2 \\ R^1{}_3 \\ R^1{}_4 \end{array} \end{array}$$

The permanent function for the shear strength (shear strength index), per (R_1) = 15651.

$$\mathrm{VPM}_{R2}\ \text{(impact strength)} = \begin{array}{cc} \begin{array}{cccc} R^2{}_1 & R^2{}_2 & R^2{}_3 & R^2{}_4 \end{array} & \text{Parameters} \\ \begin{bmatrix} 3.8 & 5 & 7 & 6 \\ 5 & 3.8 & 6 & 6 \\ 3 & 4 & 3.8 & 5 \\ 4 & 4 & 5 & 2.3 \end{bmatrix} & \begin{array}{c} R^2{}_1 \\ R^2{}_2 \\ R^2{}_3 \\ R^2{}_4 \end{array} \end{array}$$

The permanent function for the impact strength (impact strength index), per (R_2) =10178.

$$\mathrm{VPM}_{R3}\ \text{(microhardness)} = \begin{array}{cc} \begin{array}{cccc} R^3{}_1 & R^3{}_2 & R^3{}_3 & R^3{}_4 \end{array} & \text{Parameters} \\ \begin{bmatrix} 6.0 & 7 & 7 & 5 \\ 3 & 6.0 & 5 & 3 \\ 3 & 5 & 6.0 & 3 \\ 5 & 7 & 7 & 6.9 \end{bmatrix} & \begin{array}{c} R^3{}_1 \\ R^3{}_2 \\ R^3{}_3 \\ R^3{}_4 \end{array} \end{array}$$

The permanent function for the microhardness (microhardness index), per (R_3) = 16394.

$$\text{VPM}_{JS}\text{ (joint strength) } = R = \begin{array}{c c} \begin{array}{ccc} R_1 & R_2 & R_3 \end{array} & \text{Parameters} \\ \begin{bmatrix} 15651 & 7 & 5 \\ 3 & 10178 & 4 \\ 5 & 6 & 16394 \end{bmatrix} & \begin{array}{c} R_1 \\ R_2 \\ R_3 \end{array} \end{array}$$

The permanent function for joint strength (joint strength index), per (JS) = 2.61E12.

Experiment No. 24

$$\text{VPM}_{R1}\text{ (shear strength) } = \begin{array}{c c} \begin{array}{cccc} R^1{}_1 & R^1{}_2 & R^1{}_3 & R^1{}_4 \end{array} & \text{Parameters} \\ \begin{bmatrix} 6.0 & 6 & 5 & 7 \\ 4 & 6.0 & 4 & 6 \\ 5 & 6 & 6.0 & 7 \\ 3 & 4 & 3 & 5.0 \end{bmatrix} & \begin{array}{c} R^1{}_1 \\ R^1{}_2 \\ R^1{}_3 \\ R^1{}_4 \end{array} \end{array}$$

The permanent function for the shear strength (shear strength index), per (R_1) = 15562.

$$\text{VPM}_{R2}\text{ (impact strength) } = \begin{array}{c c} \begin{array}{cccc} R^2{}_1 & R^2{}_2 & R^2{}_3 & R^2{}_4 \end{array} & \text{Parameters} \\ \begin{bmatrix} 3.8 & 5 & 7 & 6 \\ 5 & 3.8 & 6 & 6 \\ 3 & 4 & 3.8 & 5 \\ 4 & 4 & 5 & 4.5 \end{bmatrix} & \begin{array}{c} R^2{}_1 \\ R^2{}_2 \\ R^2{}_3 \\ R^2{}_4 \end{array} \end{array}$$

The permanent function for the impact strength (impact strength index), per (R_2) =11390.

$$\text{VPM}_{R3}\text{ (microhardness) } = \begin{array}{c c} \begin{array}{cccc} R^3{}_1 & R^3{}_2 & R^3{}_3 & R^3{}_4 \end{array} & \text{Parameters} \\ \begin{bmatrix} 6.0 & 7 & 7 & 5 \\ 3 & 6.0 & 5 & 3 \\ 3 & 5 & 6.0 & 3 \\ 5 & 7 & 7 & 5.2 \end{bmatrix} & \begin{array}{c} R^3{}_1 \\ R^3{}_2 \\ R^3{}_3 \\ R^3{}_4 \end{array} \end{array}$$

The permanent function for the microhardness (microhardness index), per (R_3) = 14987.

$$\text{VPM}_{JS}\text{ (joint strength) } = R = \begin{array}{cccc} R_1 & R_2 & R_3 & \text{Parameters} \\ \left[\begin{array}{ccc} 15562 & 7 & 5 \\ 3 & 11390 & 4 \\ 5 & 6 & 14987 \end{array}\right] & & & \begin{array}{c} R_1 \\ R_2 \\ R_3 \end{array} \end{array}$$

The permanent function for joint strength (joint strength index), per (JS) = 2.66E12.

Experiment No. 25 to 30

$$\text{VPM}_{R1}\text{ (shear strength) } = \begin{array}{cc} \begin{array}{cccc} R^1{}_1 & R^1{}_2 & R^1{}_3 & R^1{}_4 \end{array} & \text{Parameters} \\ \left[\begin{array}{cccc} 6.0 & 6 & 5 & 7 \\ 4 & 6.0 & 4 & 6 \\ 5 & 6 & 6.0 & 7 \\ 3 & 4 & 3 & 6.0 \end{array}\right] & \begin{array}{c} R^1{}_1 \\ R^1{}_2 \\ R^1{}_3 \\ R^1{}_4 \end{array} \end{array}$$

The permanent function for the shear strength (shear strength index), per (R_1) = 16456.

$$\text{VPM}_{R2}\text{ (impact strength) } = \begin{array}{cc} \begin{array}{cccc} R^2{}_1 & R^2{}_2 & R^2{}_3 & R^2{}_4 \end{array} & \text{Parameters} \\ \left[\begin{array}{cccc} 3.8 & 5 & 7 & 6 \\ 5 & 3.8 & 6 & 6 \\ 3 & 4 & 3.8 & 5 \\ 4 & 4 & 5 & 3.8 \end{array}\right] & \begin{array}{c} R^2{}_1 \\ R^2{}_2 \\ R^2{}_3 \\ R^2{}_4 \end{array} \end{array}$$

The permanent function for the impact strength (impact strength index), per (R_2) =11004.

$$\text{VPM}_{R3}\text{ (microhardness) } = \begin{array}{cc} \begin{array}{cccc} R^3{}_1 & R^3{}_2 & R^3{}_3 & R^3{}_4 \end{array} & \text{Parameters} \\ \left[\begin{array}{cccc} 6.0 & 7 & 7 & 5 \\ 3 & 6.0 & 5 & 3 \\ 3 & 5 & 6.0 & 3 \\ 5 & 7 & 7 & 6.0 \end{array}\right] & \begin{array}{c} R^3{}_1 \\ R^3{}_2 \\ R^3{}_3 \\ R^3{}_4 \end{array} \end{array}$$

The permanent function for the microhardness (microhardness index), per (R_3) = 15649.

$$
\mathrm{VPM}_{JS}\text{ (joint strength) } = R = \begin{array}{c} \\ \\ \\ \end{array}
\begin{array}{cccc}
R_1 & R_2 & R_3 & \text{Parameters} \\
\left[\begin{array}{ccc} 16456 & 7 & 5 \\ 3 & 11004 & 4 \\ 5 & 6 & 15649 \end{array}\right. & & \left.\right] & \begin{array}{c} R_1 \\ R_2 \\ R_3 \end{array}
\end{array}
$$

The permanent function for joint strength (joint strength index), per (JS) = 2.83E12.

APPENDIX-II

RSM MODEL

In order to make an appropriate approximating model between the independent variables, $X_{1,}X_{2,}$ - - - - - - - X_n and response *Y*, the relationship is expressed as:

$$Y = f\left(X_{1,}X_{2,} \text{- - - - - - - -} X_n\right) + \varepsilon \tag{1}$$

In the above equation, response *Y* is unknown and ε indicates the other sources of variability.

$$E(y) = \hat{Y} = E\left[f\left(X_{1,}X_{2,} \text{- - - - - - - -} X_n\right)\right] + E(\varepsilon) = f\left(X_{1,}X_{2,} \text{- - - - - - - -} X_n\right) \tag{2}$$

Where X_1, X_2, ...,X_n are the natural parameters. The response function written in terms of coded parameters as f (X_1, X_2…, Xn), is known as the response surface. Usually, in RSM, the relationship between the independent parameters and response function is unknown; therefore, the first step is to search a proper approximation for the true functional relationship between the set of independent parameters and Y. In RSM, a second order model is adopted usually [102-103].

In the present study, the approximation of response function has been anticipated by fitting a quadratic model i.e., a second order polynomial regression model. This model is written as [104-105]:

$$Y = \beta_0 + \sum_{j=1}^{k} \beta_j X_j + \sum_{j=1}^{k} \beta_{jj} X_j^2 + \sum_{i<} \sum_{j=2}^{k} \beta_{jj} X_i X_j + \varepsilon \tag{3}$$

Where, X_j represents the values of j^{th} process parameter. Term β is the regression coefficients and ε indicates the experimental errors. Regression model coefficients can be determined by the experimental design techniques. Second order response surface can perfectly be achieved by the central composite design.

BRIEF PROFILE OF THE RESEARCH SCHOLAR

Rajender Kumar completed his B. Tech. Mechanical Engineering in First Division with Honors from Kuruksherta University, Kurukshetra in 2002. He has obtained his Master degree of Engineering in Manufacturing Technology with First Division from National Institute of Technical Teachers' Training and Research, Chandigarh (Panjab University, Chandigarh) in 2010. Presently, he is working as a Lecturer (Mechanical Engineering) at Government Polytechnic, Sirsa, under Technical Education Department, Haryana. He has 17 years of teaching experience.

LIST OF PUBLICATIONS OUT OF THESIS

LIST OF PUBLISHED PAPERS (JOURNAL)

S. No.	Title of the paper along with volume, Issue No, year of publication	Publisher/ Journal	Impact Factor	Refereed or Non-Refereed	Whether you paid any money or not for publication	Remarks
1	Experimental Investigation and Optimization of Process Parameters for Impact Strength of Compound Cast Bimetallic Joints Volume-12, Issue-3, 2018, Pages 498-513 DOI 10.1007/s40962-017-0190-3	Springer International Journal of Metalcasting	1.033	Refereed	No	SCI Journal
2	Experimental Investigation and Optimization of Process Parameters for Shear Strength of Compound Cast Bimetallic Joints Volume-71, Issue-9, 2018, Pages 2173-2183 DOI: 10.1007/s12666-018-1349-1	Springer Transactions of the Indian Institute of Metals	1.176	Refereed	No	SCI Journal
3	Characterization and Microhardness Evaluation of A356/Mg Joint Produced by Vacuum-Assisted Sand Mold Compound Casting Process Volume-13, Issue-2, 2019, Pages 392-406 DOI 10.1007/s40962-018-0264-x	Springer International Journal of Metalcasting	1.033	Refereed	No	SCI Journal

S. No.	Title of the paper along with volume, Issue No, year of publication	Publisher/ Journal	Impact Factor	Refereed or Non-Refereed	Whether you paid any money or not for publication	Remarks
4	Experimental Investigation and Evaluation of Joint Strength of A356/Mg Bimetallic Fabricated Using Compound Casting Process Volume-13, Issue-3, 2019, Pages 686-699 DOI: 10.1007/s40962-018-0288-2	Springer International Journal of Metalcasting	1.033	Refereed	No	SCI Journal

LIST OF PUBLISHED PAPERS (CONFERENCE)

S. No.	Title of the paper along with volume, Issue No, year of publication	Publisher	Impact factor	Refereed or Non-Refereed	Whether you paid any money or not for publication	Remarks
5	Compound Casting- A Literature Review ISBN-978-93-5087-574-2 19-20 Oct, 2012 Pages 501-5010	Proceedings of the National Conference on Trends and Advances in Mechanical Engineering, YMCAUST, Faridabad, Haryana	-	Refereed	No	